RIGA TECHNICAL UNIVERSITY

Aleksandrs Bubovičs

MULTILEVEL CONVERTERS FOR BATTERY INTERFACING

Doctoral Thesis

RTU Press
Riga 2025

RIGA TECHNICAL UNIVERSITY
Faculty of Computer Science, Information Technology and Energy
Institute of Industrial Electronics, Electrical Engineering and Energy

Aleksandrs Bubovičs
Doctoral Student of Study Programme "Computerised Control of Electrical Technologies"

MULTILEVEL CONVERTERS FOR BATTERY INTERFACING

Doctoral Thesis

Scientific supervisor
Professor Dr. sc. ing.
ILYA A. GALKIN

RTU Press
Riga 2025

Bubovičs, A. Multilevel Battery Interface Converter. Doctoral Thesis. Riga: RTU Press, 2025. 224 p.

Published in accordance with the decision of the Promotion Council "P-14" of 14 March 2025, Minutes No. 04030-9.12/5.

Doctoral thesis was supported by the EU Recovery and Resilience Facility within Project No 5.2.1.1.i.0/2/24/I/CFLA/003 "Implementation of consolidation and management changes at Riga Technical University, Liepaja University, Rezekne Academy of Technology, Latvian Maritime Academy and Liepaja Maritime College for the progress towards excellence in higher education, science and innovation" academic career doctoral grant (ID 1015).

Cover picture generated by *openAI DALL-E/ChatGPT 4.0*.

DOCTORAL THESIS PROPOSED TO RIGA TECHNICAL UNIVERSITY FOR THE PROMOTION TO THE SCIENTIFIC DEGREE OF DOCTOR OF SCIENCE

To be granted the scientific degree of Doctor of Science (Ph. D.), the present Doctoral Thesis has been submitted for the defence at the open meeting of RTU Promotion Council on 30 May 2025 at 14.00 in the Conference Hall of RTU Conference and Sports Centre "Ronīši", Klapkalnciems, Engure County.

OFFICIAL REVIEWERS

Associate Professor *Dr. sc. ing. Janis Zakis*,
Riga Technical University

Associate Professor *Ph. D. Carlos Roncero-Clemente*,
University of Extremadura, Spain

Senior Lecturer *Ph. D. Indrek Roasto*,
Tallinn University of Technology, Estonia

DECLARATION OF ACADEMIC INTEGRITY

I hereby declare that the Doctoral Thesis submitted for the review to Riga Technical University for the promotion to the scientific degree of Doctor of Science (Ph. D.) is my own. I confirm that this Doctoral Thesis had not been submitted to any other university for the promotion to a scientific degree.

Aleksandrs Bubovičs ……. (signature)
Date: ……

The Doctoral Thesis has been prepared as a thematically united collection of scientific publications. The Doctoral Thesis has been written in English. It consists of an Introduction; 5 Chapters; Conclusion; 49 figures; 5 tables; 11 appendices; the total number of pages is 70 not including appendices. The Bibliography contains 104 titles.

CONTENTS

INTRODUCTION

Motivation and background

Nowadays, electrochemical Battery Energy Storages (BES or just batteries) are considered as the most available, reliable and practical storage of electrical energy for a broad range of applications. Batteries are used in such applications as light electrical vehicles, personal mobility vehicles including rehabilitation equipment, portable electronics (for example, laptops, tablets etc.), portable household equipment and handy tools (like vacuum cleaners, robot vacuum cleaners, grass cutting robots, cutting/drilling tools etc.), energy storage systems for power supply needs, as well as in various other applications. The battery interface converter is a necessary part of the configuration. It connects the battery to the load and is needed because even if the voltages of the battery and load are generally comparable, the battery voltage is not constant and depends on various factors, first of all, on State of Charge (SOC) and State of Health (SOH). There also exist AC loads, for example, AC motors/generators and the AC grid. In this case, voltages and currents should be continuously driven as needed by application, having the requested amplitude, frequency, phase of the waveforms and, sometimes, their harmonic content.

The first big group of converters that can link batteries and AC loads includes non-isolated schemes, which in general can be divided into single-stage (efficient only in one operation point) and two-stage converters (with a wider efficient range of operation). In turn, the second big group of battery interfaces includes isolated schemes, which are two-stage by definition. Most of these topologies can serve only as a battery interface, but are not suitable for balancing, which can be considered a disadvantage.

Multilevel converters can be brought forward as the third specific big group of interface schemes, capable of linking batteries and AC loads. The multilevel converters are topologically compatible with batteries that typically consist of several sequentially connected cells. Among all multilevel converter topologies, those with independent sources have one extra advantage of natural (without extra circuits) battery balancing and, therefore, have large potential in applications with batteries. They, however, have certain drawbacks, such as a large number of active and uncontrollable semiconductor switches that increase with the number of levels, leading to higher conduction losses and more complex control. For this reason, finding and implementing classical multilevel topology modifications, which reduce switch count while keeping all the advantages of the topology, would be important. It would improve the parameters of the multilevel converters, extend their use in battery systems and expand the use of these storages.

Main hypothesis and objectives

Hypothesis

Combining an unfolding circuit with a series of independent voltage sources, connected according to a multilevel structure, thus forming a battery interface converter, gives the ability to reduce the switch count and overall losses of the converter, keeping, at the same time, the advantages of the original parts.

Aim and Objectives

The aim of the Thesis is to analyze existing multilevel converter topologies and to propose new configurations that are more advantageous in terms of efficiency and control complexity, multilevel battery interface converters, while keeping the advantages of classical multilevel structures. The objectives of the Thesis, therefore, were set as follows:

1. To analyze multilevel converter topologies and their operating principles, in order to identify their disadvantages and outline improvement opportunities.
2. To analyze the topologies of unfolding circuits and their applications.
3. To synthesize battery interface converter(s) as a combination of an unfolding circuit with a multilevel structure with independent sources.
4. To analyze the obtained battery interface converter, made of the above-mentioned parts, applying hybrid (level and pulse width) modulation.

Research methods and tools

The main research method within the Thesis is data collection and analysis. The data are obtained mostly from experiments, partly from mathematical and computer simulations, but sometimes (mostly in the Introduction) from the existing information sources.

MS Excel and *Matlab* have been used for calculations, mathematical modelling, data processing and representation of obtained results. *Matlab-Simulink* was used for modelling and simulations, and *LTspice* was used for preliminary simulations. *Altium Designer* was used as a main tool for PCB design, on rare occasions, *EasyEDA* and *KiCad EDA* were used.

For testing, debugging and experimental verification in laboratory conditions, a variety of laboratory equipment has been used, specially adapted for each experiment that was held: oscilloscopes (*RIGOL DS4012, Tektronix TDS 1024B-EDU*), power supply units (*TTi EX752M, EA-PS 8032-10 T*), thermal camera (*Fluke Ti450*), various multimeters, power analyzer (*PPA5530*). Also, for debugging in certain stages, a digital oscilloscope, a waveform generator, and the logic analyzer *Analog Discovery* was used.

Several microcontrollers from the C2000 family (*F28027 and F28379D*) have been used, as well as the *RP2040* microcontroller. *Code Composer Studio, Pycharm* and *Matlab* plugin for the C2000 microcontroller family were used to program and debug microcontrollers.

Scientific novelty

1. Several new configurations of multilevel converters with independent sources were proposed, including a novel configuration of multilevel converters with independent sources, unfolding circuit and fluent regulation.
2. A method of source balancing within one sine period in multilevel converters with independent sources during discharge has been proposed.
3. A novel system and method for transmitting power between DC and AC sources has been proposed; an application for patent LVP2023000064 was submitted on 12 July 2023.
4. A novel adjustable LED lamp single-inductor multiple-output driver has been proposed; an application for patent LVP2023000103 was submitted on 27 October 2023.

Practical implementation

Research results have been implemented in several national and international research projects:

1. European Regional Development Fund (ERDF) project, within the contract No. 1.1.1.1/16/A/147 “Research and Development of Electrical, Information and Material Technologies for Low Speed Rehabilitation Vehicles for Disabled People”.
2. Baltic Research Program project, funded by the European Economic Area and Norway, 2014–2021, financial mechanisms within the contract EMP474 “Optimised Residential Battery Energy Storage Systems (ORBES)” of the first (Estonian) call of this program.
3. Latvian Council of Science project “Enhanced Thermal Management of Electric Drives in Orthopaedic Rehabilitation Vehicles for their Better Reliability and Functionality”, project No. lzp-2020/2-0390.
4. European Regional Development Fund project in the frame of the contract No. 1.1.1.1/20/A/079 “Research and Development of Two-Phase Thermal Systems Installed in Lighting Equipment for its Functional Improvement” of its Latvian measure 1.1.1.1 “Industry-Driven Research”.

Approbation of research results

In total, the author of the Thesis has 29 publications and two patents. Of them, nine publications, two Latvian patents and two unpublished papers are directly related to the topic of the Doctoral Thesis.

I. I. A. Galkin, A. Blinov, M. Vorobyov, **A. Bubovich,** R. Saltanovs, D. Peftitsis, Interface Converters for Residential Battery Energy Storage Systems: Practices, Difficulties and Prospects. Energies 2021, 14, 3365. https://doi.org/10.3390/en14123365

II. **A. Bubovich**, M. Vorobyov, I. Galkin, A. Blinov, and A. Giannakis, "Overview of Bidirectional Unfolding Converters for Battery Energy Storage Systems," 2022 IEEE 13th International Symposium on Power Electronics for Distributed Generation

Systems (PEDG), Kiel, Germany, 2022, pp. 1–7, doi: 10.1109/PEDG54999.2022.9923093.

III. Unpublished paper "Multilevel Unfolding Converter with Independent Sources: Proof of Concept", will be submitted to MDPI Energies by May 2025.

IV. Unpublished paper "Evaluation of Smooth Waveform Regulation in Multilevel Converters with Unfolding Stage", submitted to AIEEE 2025 conference

V. **A. Bubovich**, V. Parinova, I. Galkin, and A. Giannakis, "Initial Evaluation of Multilevel Converter with Unfolding Stage and Voltage Regulators for applications in BESSs," 2022 18th Biennial Baltic Electronics Conference (BEC), Tallinn, Estonia, 2022, pp. 1–5, doi: 10.1109/BEC56180.2022.9935611.

VI. **A. Bubovich**, M. Vorobyov, I. Galkin, and T. Dovudon, "Quality Evaluation of Jointly Used Modular Multilevel Converters and Battery Energy Storages," 2021 International Conference on Electrical Drives & Power Electronics (EDPE), 2021, pp. 144–151, doi: 10.1109/EDPE53134.2021.9604102

VII. **A. Bubovich**, M. Vorobyov, A. Blinov, and D. Peftitsis, "Peculiarities of Multilevel Power Electronic Converters for Interfacing Battery Energy Storages with AC Loads," 2020 IEEE 8th Workshop on Advances in Information, Electronic and Electrical Engineering (AIEEE), 2021, pp. 1–4, doi: 10.1109/AIEEE51419.2021.9435798

VIII. **A. Bubovich**, M. Vorobyov, and A. Giannakis, "Initial Evaluation of a Multilevel Inverter with Unfolding Stage for BESS Applications," 2021 IEEE 9th Workshop on Advances in Information, Electronic and Electrical Engineering (AIEEE), 2021, pp. 1–4, doi: 10.1109/AIEEE54188.2021.9670386.

IX. **A. Bubovich**, I. Galkin, "Evaluation of Optimal Switching of Modular Multilevel Inverter with Independent Voltage Sources". In: 2020 IEEE 61st International Scientific Conference on Power and Electrical Engineering of Riga Technical University (RTUCON 2020): Conference Proceedings, Latvia, Riga, 5–7 November 2020. Piscataway: IEEE, 2020, pp.1–4.

X. O. Tetervenoks, I. Galkin, **A. Bubovich,** Considerations on Practical Implementation of Current Source Mode Single-Inductor Multiple-Output LED Driver. Electronics 2024, 13, 54. https://doi.org/10.3390/electronics13010054

XI. I. A. Galkin, R. Saltanovs, **A**. **Bubovich,** A. Blinov, D. Peftitsis, Considerations on Combining Unfolding Inverters with Partial Power Regulators in Battery–Grid Interface Converters. Energies 2024, 17, 893. https://doi.org/10.3390/en17040893

XII. R. Saltanovs, I. Galkins, **A. Bubovičs**, A. Blinov, D. Peftitsis, SYSTEM AND METHOD FOR TRANSMITTING POWER BETWEEN DC AND AC SOURCES. Latvian patent application LVP2023000064, Patent application date 12.07.2023.

XIII. O. Tetervenoks, I. Galkins, **A. Bubovičs**, Adjustable LED Lamp Single Inductor Multiple Output Driver. Latvian patent application LVP2023000103, Patent application date 27.10.2023.

Publications related to Doctoral Thesis, which were not included in summary of Doctoral Thesis:

1. **A. Bubovich**, I. Galkin, "Evaluation of Multilevel Inverter with Unfolding Stage and Voltage Regulators for BESS Applications". In: Proceedings of the 21st International Symposium "Topical Problems in the Field of Electrical and Power Engineering" and "Doctoral School of Energy and Geotechnology III", Estonia, Pärnu, 15–18 June 2022. Tallinn: TalTech, 2022, pp. 57–58. ISBN 978-9949-83-859-2
2. **A. Bubovich**, "Use of Multilevel Converters in Light Vehicles of Orthopedic Rehabilitation," 2021 IEEE 62nd International Scientific Conference on Power and Electrical Engineering of Riga Technical University (RTUCON), 2021, pp. 1–4, doi: 10.1109/RTUCON53541.2021.9711728
3. **A. Bubovich**, "Evaluation of Opportunities of Balanced Discharge of Batteries in Cost Effective Assisting Powered Wheelchair". In: Proceedings of the 19th International Symposium "Topical Problems in the Field of Electrical and Power Engineering" and "Doctoral School of Energy and Geotechnology III", Estonia, Tartu, 14–17 January 2020. Tallinn: TalTech, 2020, pp. 135–136. ISBN 978-9949-83-518-8
4. **A. Bubovich**, "Evaluation of opportunities of balanced discharge of batteries in cost effective assisting powered wheelchair", 2019 IEEE 60th International Scientific Conference on Power and Electrical Engineering of Riga Technical University (RTUCON 2019), Riga, 2019.

ABBREVIATIONS

ADC Analog-to-Digital Converter
AEV All-Electric Vehicles
BES Battery Energy Storage
BESS Battery Energy Storage System
CCS Constant Current Source
CR Current Regulator
CSM Current Source Mode
DAB Dual Active Bridge
EMC Electromagnetic Compatibility
FET Field Effect Transistor
HFHD High Frequency Harmonic Distortion
IC Integrated Circuit
LA Lead-Acid *(battery technology)*
LED Light Emitting Diode
LFHD Low Frequency Harmonic Distortion
LR Light flux Regulator
MCU Microcontroller Unit
MDS Maximal Duration of Switching
MLC Multilevel Converter
MOSFET Metal Oxide Semiconductor Field Effect Transistor
PEV Plug-in Electric Vehicle
PFC Power Factor Correction
PV Photovoltaic
PWM Pulse Width Modulation
RFB Redox Flow Battery
RGB Red, Green and Blue *(additive color model)*
SEPIC Single-Ended Primary Inductor Converter
SIMO Single Inductor Multiple Output
SLLS Segmented LED Light Source
SOC State of Charge
SOH State of Health
THD Total Harmonic Distortion
UF Unfolding Frontend
VSI Voltage Source Inverter
VRB Vanadium Redox Battery
ZCS Zero Current Switching
ZVS Zero Voltage Switching

1. APPLICATION OF BATTERIES IN MODERN TECHNOLOGIES

Author's publications I [1] and II [2] are related to Chapter 1.

1.1. Development of electrochemical energy storages

The most intensive development of electrochemical energy storage systems has taken place since the late 20th century and is still progressing. The demand for portable electrical devices, vehicular technologies and energy systems is constantly growing, and because of that, technologies of already known battery electrochemistries have been "polished" and new battery technologies have been introduced into the market. Nowadays, the most significant battery technologies are advanced lead-acid (LA), nickel-oxyhydroxide (NiMH), sodium-sulfur (NaS), various kinds of Li-ion batteries, as well as redox flow batteries (RFBs), in particular, vanadium redox batteries (VRBs) [3], [4].

LA technology, the oldest among others, is the cheapest and also has quite high efficiency. However, the main drawbacks of this technology are that LA batteries have rather low specific energy and comparably low charge-discharge cycles (i.e. lifetime). Historically, the next successive NiMH technology (replacement for NiCd) is characterized by average specific power and has a low charge-discharge efficiency (approximately 65 %). The NaS batteries have quite high specific energy, energy efficiency and lifetime (90 % and 4000 cycles, respectively [4]). However, the main drawback of NaS batteries is quite high operation temperature, which means that they require heating. This fact makes the application of these batteries impractical in many cases. Nowadays, the fastest-developing battery technology is the Li-Ion. Li-Ion batteries have high specific energy, specific power, lifetime (up to 10,000 cycles), energy efficiency (up to 95 %), achieved at a reasonable price, making the technology very applicable in portable electronics, all-electric vehicles, household energy systems and even in energy distribution grids [5]. However, specific parameters of Li-Ion batteries depend on the corresponding chemistry, and all advantages are typically not concentrated in one device. Finally, RFBs, in particular VRBs, are the batteries that utilize a reduction-oxidation reaction between two liquids, which occurs through a membrane. The liquids are pumped to the membrane, which makes RFBs similar to fuel cells, where the liquids are chemically restorable. The main advantage of these batteries is their potentially infinite lifetime. Lastly, it must be mentioned that modern batteries are not just a series connection of galvanic cells. They often include electronics for balancing, management and protection, as well as chargers in some cases. Therefore, these batteries can be considered as complex complete energy units for immediate use [6]–[8]. Figure 1.1 shows the comparison between different commercially available batteries.

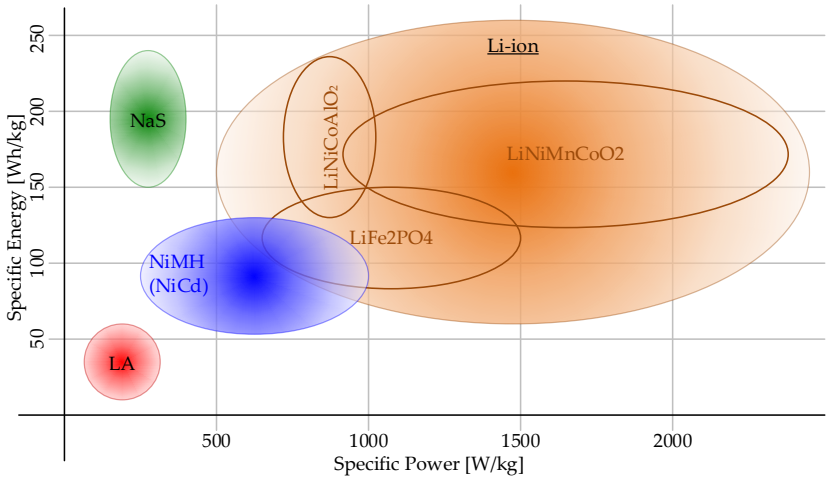

Fig. 1.1. Specific energy and specific power of the commercially available batteries

1.2. Motivation for use of batteries

With the development of electronic technologies, portable electronic devices have been rapidly growing over the past decades. The primary motivation of this growth is that portable electronic appliances are widely used in our daily life, from low power appliances, for example, flashlights, TV remote controls, scales, watches, to more power-consuming devices, for example, laptops, tablets, robot vacuum cleaners, etc.

Application of batteries in transport

One of the recent global societal and legislative tendencies on the national and international levels is the request to reduce the consumption of fossil fuels and to increase the efficiency of energy consumption [9], [10]. Among other areas, this involves vehicular technologies as well. Regarding ground vehicles, this initiative means wider use of plug-in electric vehicles (PEVs) or all-electric vehicles (AEVs) and hybrid ones, equally in the public and private sectors. In [11], [12], the availability of cost-effective batteries of several hundred volts for the main electrochemical energy storage of PEV is reported. Papers [13]–[16] consider these PEV storage systems valuable enough to be a part of the energy supply grid. Further development of the BESs makes their use possible in larger ground vehicles, first of all, in public transport [17], [18].

Better BESs are also required for water vehicles, first of all, for smaller auxiliary vehicles – boats, yachts, water buses, etc. For example, in [19], the electrification of the water buses in Venice is considered a successful example of BES use in water transport. At the same time, with regard to bigger ships and vessels, the role of BESs differs with time. While earlier configurations of marine energy systems utilize high voltage batteries for stabilizing the traditional onboard AC grid and power smoothing [20], [21], modern systems also take into account the possibility of all-electric propulsion of the ship [21], [22].

Finally, the most advanced BESs are applicable in aircraft. The traditional electrical supply of an aircraft combines an AC and DC grid. Better performance of the applied batteries leads to a better quality of the 28 V DC grid [23], [24]. At the same time, top BES technologies allow the production of extremely light batteries that enable all-electric aircraft [25].

Application of batteries in power and energy supply.

The request to reduce fossil fuel consumption [9], [10] regards also power distribution and supply networks. For the power and energy supply systems, this means that the burning of fossil fuels must be substituted with renewable energy generation. In turn, the main properties of renewable energy generation are as follows:

- Uneven generation profile – regardless of the kind, the renewable energy sources typically do not provide constant power. In particular, the generation of PV panels depends on solar irradiation and varies with the daytime, cloudiness, season, location of PV and solar activity. The generation of wind turbines depends on the wind strength, which is unique for its location, season and occasional weather fluctuation. The generation of hydro and wave turbines depends on the amount of water, which is a long-term function of seasonal and global weather changes.
- A variety of power ratings and types of energy sources exist even within the same group. For example, the power of PV depends on the local properties and financial abilities of a particular household.
- Variety of allocation of the renewable energy sources – depending on the particular economic conditions and policy of the energy operator, these sources may be allocated differently.

Altogether, this makes renewable energy generation less stable and reliable. This, as well as several other problems [26]–[31], can be solved with the help of Battery Energy Storage Systems (BESSs). In the distribution grids, the functions of the dedicated BESS are similar but more specified. Price compensation now can be considered as a complete function of energy trading, smoothening of power generation regards not only renewables, but smoothening of consumed power at this level saves the capacity of distribution equipment. Additionally, BESS in distribution grids may perform grid service functions: grid black restart, as well as voltage and frequency regulation [27], [32]. The choice of BESS parameters is a subject of multiple factors [33]: standards, power losses, voltage of the majority of available PEVs, compatibility with pure resistive loads.

The market of commercially available BESSs, especially residential BESSs is dynamic, with both large and small companies continuously entering and leaving the market. Depending on the configuration, commercially available BESSs can be either with only AC coupling (does not depend on the availability of alternative energy sources, for example, solar farm), with only DC coupling (complementing alternative energy sources) and AC/DC coupling (with hybrid inverter and availability to connect additional DC sources and loads). Figure 1.2. shows examples of BESS coupling.

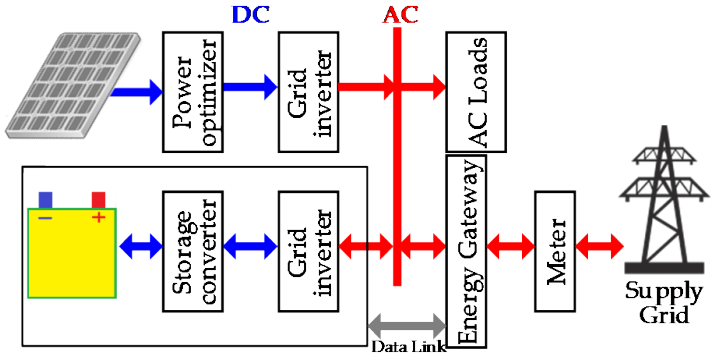

(a)

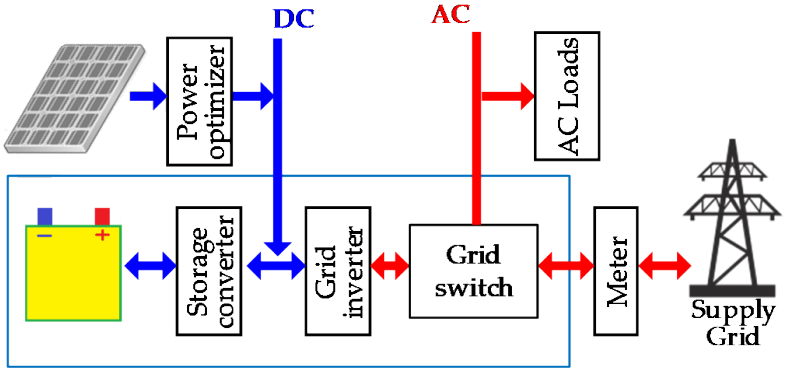

(b)

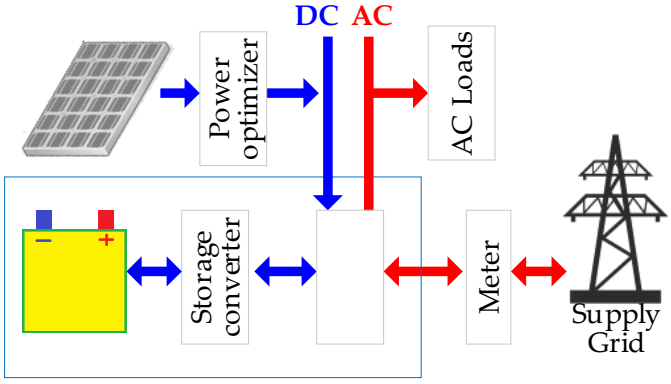

(c)

Fig. 1.2. BESS coupling: (a) AC coupling, (b) DC coupling, (c) AC/DC coupling

Brief overview and comparison of commercially available BESSs for general use and use with renewable energy sources are shown in Table 1.1.

Table 1.1.

Overview of commercially available BESS for general use.

BESS manufacturer/model	Maximal Energy Capacity [kWh]	Charge/Discharge BES Power [kW]	Battery Voltage [V]	Coupling
Tesla PowerWall 3 [34]	13.5	5 / 11.5	52	AC/DC
Tesla PowerWall 2 [35]	13.5	5	50	AC
Tesla PowerWall+ [36]	13.5	5	50	DC
Sonnen Batterie 10 [37]	5 - 22	4.6	48	AC
Sonnen Batterie Hybrid 9.53 [38]	5 - 15	2.5 - 3.3	48	DC
PowerVault P4 [39]	8 - 24	4.8	48	AC
Puredrive Storage II AC 5/10 kWh [40]	5 - 10	5	50	AC
Duracell Dura5 battery + Dura-I inverter [41], [42]	5.12	3	48	AC/DC
Enphase Encharge 3 [43]	3.5	1.3	67	AC
Enphase Encharge 10 [44]	10.5	3.8		
Eaton xStorage [45]	4.2 - 10	3.6 - 6	90	AC/DC
Samsung SDI All in One 3 [46]	3.6	4.6	60	AC/DC
Varta Pulse / Pulse Neo 3 [47]	3.3	1.6 / 1.4	50	AC
Victron Energy EasySolar-II [48]	External battery	1.9 – 3.7 / 2.4 - 4	24 - 50	DC
Solax Hybrid X3 + T-BAT-SYS-HV-(5.8 - 23) [49], [50]	Stackable - up to 23 (4 modules)	4 - 16.1	115.2 (for T-BAT H 5.8) - 460.8 (for T-BAT H 23)	AC/DC
SolarEdge Home Hub Inverter + BAT-10K1P [51], [52]	9.7	5	400	AC/DC
AlphaESS SMILE-T10-HV [53]	8.2 - 49.2	10	256	AC
BSLBATT MatchBox HVS (Stackable) [54]	10.64 - 37.27	7.2 (for HVS2) - 25 (for HVS7) / 9.2 - 32	204.8 (for HVS2) - 716.8 (for HVS7)	AC/DC
ETEKWARE EIH175 [55]	17.92	18	358.4	AC/DC
Sunny Boy Storage [56]	External battery	3.7/5/6	360	AC
FoxESS Stackable AIO [57]	4.92 – 29.52	5.5/3.6 – 16.5/12.1	360	AC/DC

The majority of commercially available residential BESSs are low-voltage, utilizing batteries with voltage equal to 48 – 50 V, meaning that to achieve higher power these systems are dealing with relatively high-currents. Considering that technical information on these products in most cases is limited to general specifications and technical datasheets, particular power electronic converter topologies utilized in these systems are not known. However, it can be assumed that connection to AC grid in these cases would require rather complex interface converter with a transformer for the voltage step-up.

Comparing with the research presented in 2021 [1], the number of BESSs utilizing higher voltage batteries has increased. Power electronic converter in this case can be non-isolated, because of the difference between input and output voltage is not considerable.

Also, the number of systems having AC\DC coupling has increased, meaning that BESS manufacturers provide the possibility of creating self-sufficient energy systems at household level by combining BESS with renewable energy sources. In this scenario energy supply would be taken from the grid only at peak of consumption. This possibility allows to increase stability of energy supply which is important in remote areas.

1.3. Configurations of battery interface converters

In all applications, described in Section 1.2, the battery interface converter is an essential part. The choice of the converter topology is mainly dependent on the configuration of the battery and the load. Figure 1.2 shows possible configurations of batteries and loads.

Considering the configuration of the battery and load, the topology of the interface converter should be chosen. Taking into account that, especially with application in power and energy supply, the battery should not only be charged but also discharged, it is reasonable to narrow the variety of battery interface converters to bidirectional ones.

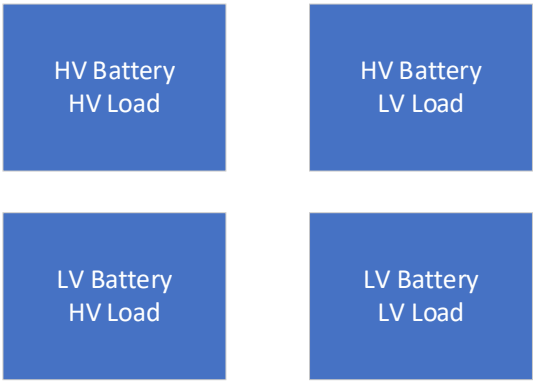

Fig. 1.3. Possible configurations of batteries and loads

If the voltage of the battery and the load are close to each other, a non-isolated topology can be chosen. However, the main disadvantage of this type of converter is that it operates at maximal efficiency only at one point. Also, there are single-stage converters and two-stage converters. Two-stage converters allow for increasing the efficient operation range of non-

isolated converters. If the battery and load have different voltage ratings, then isolated topologies can be chosen. An example of such a topology is Dual Active Bridge (DAB). Table 1.2 represents bidirectional converters with examples, characteristics of BES and peculiarities.

Table 1.2.

Bidirectional battery interface converters.

Bidirectional converter		**Characteristics of BES**	**Peculiarities**
Non-isolated topologies	Non-inverting buck-boost converter	Low voltage Low to medium power	Easier voltage regulation. Higher maximal efficiency, however, small range of higher efficiency.
	Ćuk, SEPIC, Zeta	Low voltage Low power	
Isolated topologies	DAB converter	Low to medium voltage Low to medium power	Soft switching capability Galvanic isolation
Multilevel topologies	Multilevel converter with independent sources	Low to high voltage Low to high power	Natural battery balancing capability. Sophisticated control.

2. ANALYSIS OF MULTILEVEL CONVERTER CLASSICAL TOPOLOGIES

Author's publications I [1], VII [58] and IX [59] are related to Chapter 2.

Multilevel converters (MLC) can be considered as a specific kind of single-stage inverters, processing energy in separate cells of a battery. In contrast to the topologies mentioned in Section 1.3, which always deal with the same DC voltage or with the entire battery, MLCs form their output of DC voltage that may have several levels, obtained directly from the battery. The advantages of multilevel converters are lower harmonic distortion, switching losses and electromagnetic interference [60]. There are three main topologies of MLCs: neutral point clamped multilevel converter (also known as diode clamped multilevel converter), multilevel converter with flying capacitors and multilevel converters with independent sources.

Output waveforms of MLCs can be either level-modulated (output waveforms are stepped and formed only by adding/removing voltage levels to the output waveform) or PWM modulated.

In the literature, there are multiple versions of the term *level* definition in MLCs. There is a version where all possible voltage levels are taken into account (positive, negative and 0 V). Another version of the term *level* is when only positive voltage levels and 0 V are considered. Hereinafter, the term *level* implies all positive voltage levels, not including 0 V.

The output phase voltage waveform in the case of level modulation for one phase cascade with s levels can be described with the help of the Fourier transform:

$$V(\omega t) = \frac{4V_g}{\pi} \sum_n [\cos(n\alpha_1) + \cos(n\alpha_2) + ... + \cos(n\alpha_s)] \cdot \frac{\sin(n\omega t)}{n} \tag{2.1}$$

where: V_g – source input voltage;

ω – angular frequency;

$\alpha_1, \alpha_2, ..., \alpha_s$ - level conducting angles.

Level conducting angles can be chosen in such a way that total harmonic distortion is minimal. If sinewave with phase angle φ equal to 0 radians, amplitude is equal to 1 V and frequency f = 1 Hz is examined as reference signal for single level voltage source inverter (VSI), or simply full transistor bridge, and instead of radians on x-axis of a plot time in seconds is taken (see Fig. 2.1 (a)), then instead of conducting angle θ there is conducting time t_{sw}. Considering that a sinewave is symmetrical, only one quarter of the sinewave should be examined. As shown in Fig. 2.1 (a), during time period from 0 to T/4, there is one commutation time (or level switching time), in Fig. 2.1 (a), it is denominated as t_{sw}. If a line $t = t_{sw}$ is drawn, then there are two areas: $S1$ and $S2$, that show the displacement of the generated output voltage by a 3-level multilevel inverter with independent sources from the reference sinewave. Areas $S1$ and $S2$ can be calculated by Equations (2.2) and (2.3):

$$S_1 = \iint_{S_1} dtdV = \int_0^{t_x} dt \int_0^{\sin(\omega t)} dV \tag{2.2}$$

$$S_2 = \iint_{S_2} dtdV = \int_{t_x}^{T/4} dt \int_{\sin(\omega t)}^{1} dV \tag{2.3}$$

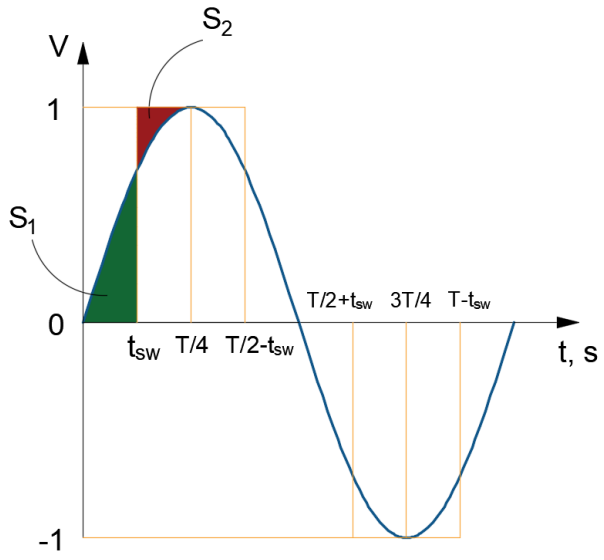

(a)

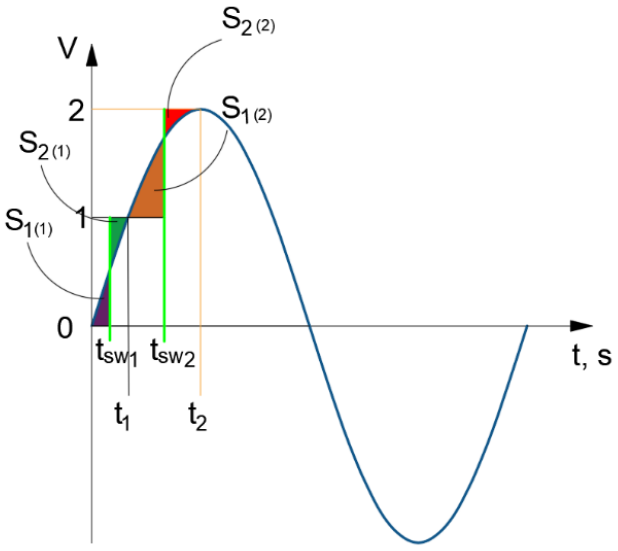

(b)

Fig. 2.1. Reference sinewave for: (a) VSI, (b) 2-level MLC.

In order to have minimal THD, the sum of areas $S_1 + S_2$ should be minimal, and the only parameter that can be changed in this case to make changes in S_1 and S_2 is the switching time. The same principles of calculation are applicable when the level count is different (2, 3, 4, 5, etc.); the only thing that changes is the borders of the y-axis. It is convenient to use a reference sinewave with amplitude 2 for 2-level MLC, with amplitude 3 for 3-level MLC, etc. In Fig. 2.1 (b), the reference signal for the 2-level multilevel inverter is shown.

Evaluation of performance of multilevel converter with independent sources was performed using MATLAB-Simulink models. As it was previously said, there are two ways of MLC operation – with PWM modulation and without PWM modulation (level modulation). Evaluation of performance was made for 3 cases: PWM modulation with 2 kHz and 5 kHz modulation frequencies and with level modulation. Simulations were performed for MLC with independent sources, however, the results are extrapolatable on other MLC topologies.

Figure 2.2. shows output phase voltage of single level VSI with PWM modulation frequency equal to 5 kHz, Figure 2.3. shows output phase voltage single level VSI without PWM modulation.

Figure 2.4. shows the harmonic distribution of phase voltage for single level MLC with modulation frequency equal to 5 kHz, Figure 2.5. shows harmonics of output phase voltage with modulation frequency 2 kHz and Figure 2.6. shows harmonics for output phase voltage without PWM.

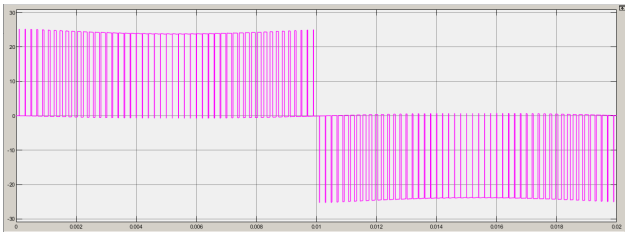

Fig. 2.2. Output phase voltage of single level VSI with PWM 5 kHz modulation frequency

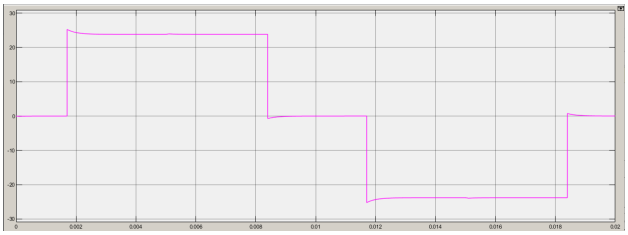

Fig. 2.3. Output phase voltage of single level VSI without PWM modulation.

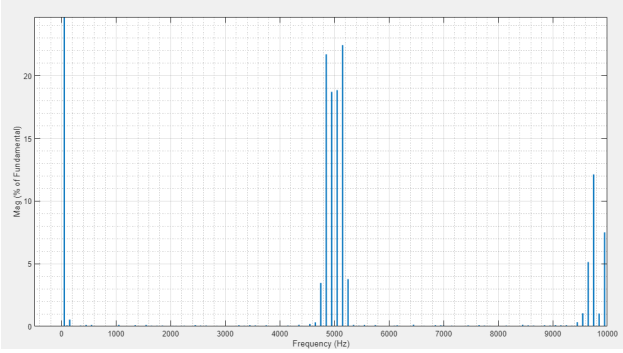

Fig. 2.4. Harmonics of phase voltage for single level VSI with modulation frequency equal to 5 kHz

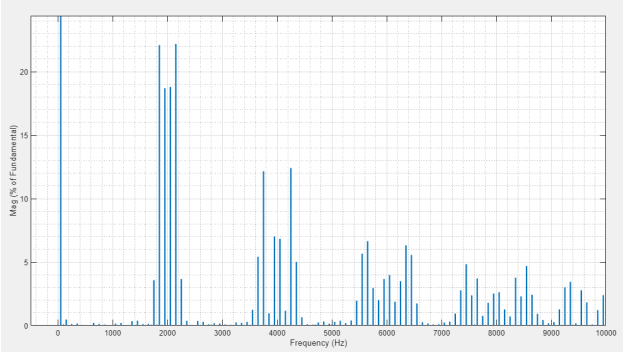

Fig. 2.5. Harmonics of phase voltage for single level VSI with modulation frequency equal to 2 kHz

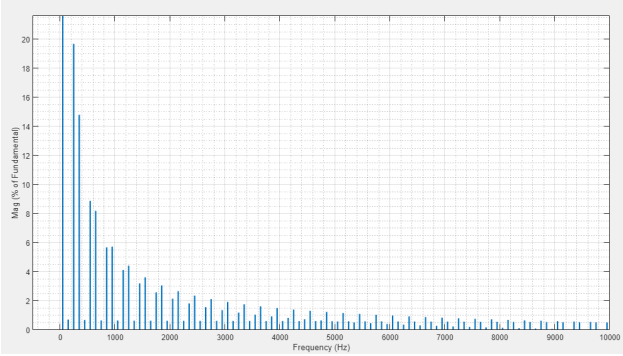

Fig. 2.6. Harmonics of phase voltage for single level VSI without PWM.

From Figures 2.4. – 2.6. it can be seen, that the modulation frequency is affecting the purity of the output waveform and the THD. For 5 kHz modulation frequency the greatest impact gives exactly harmonics close to switching frequency and harmonics that are the multiplications of the modulation frequency. The same situation is in cases with 2 kHz modulation frequency. In case when PWM is not used, it is seen that harmonic decomposition is proportional.

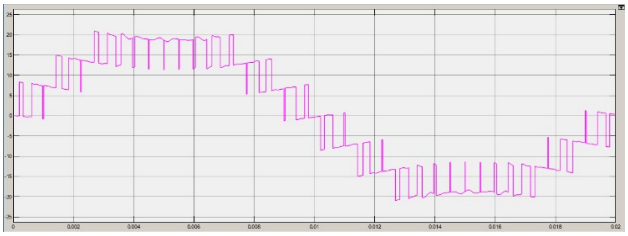

Fig. 2.7. Output phase voltage of 3-level MLC with independent sources with PWM modulation frequency equal to 2 kHz.

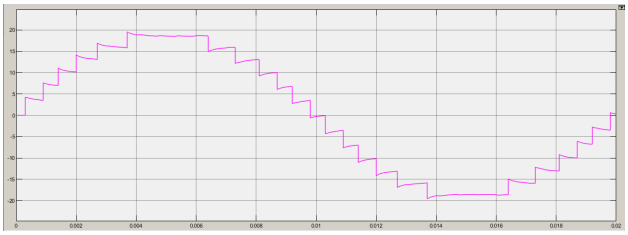

Fig. 2.8. Output phase voltage of 6-level MLC with independent sources without PWM modulation

The results are shown at Figures 2.9. – 2.11. for two-level MLC, Figures 2.12. – 2.14. for three-level MLC, and Figure 2.15. – 2.17. – for six-level MLC.

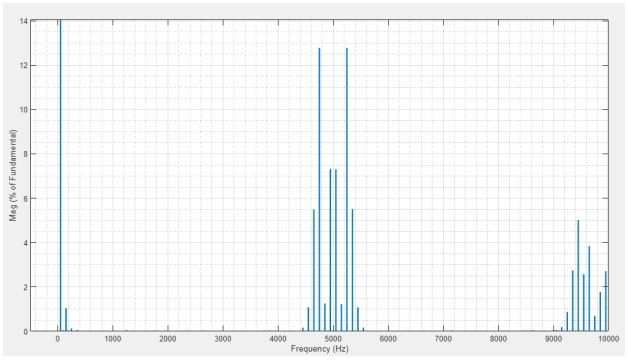

Fig. 2.9. Harmonics of phase voltage for 2-level MLC with modulation frequency equal to 5 kHz.

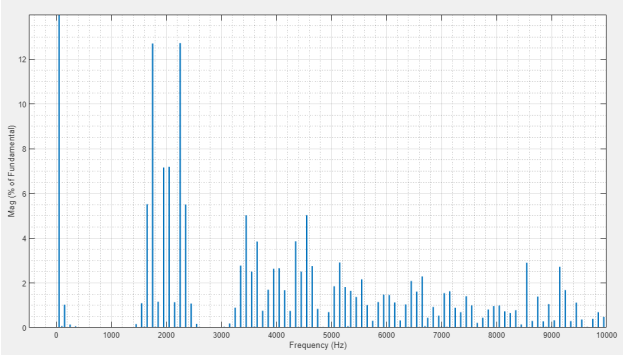

Fig. 2.10. Harmonics of phase voltage for 2-level MLC with modulation frequency equal to 2 kHz.

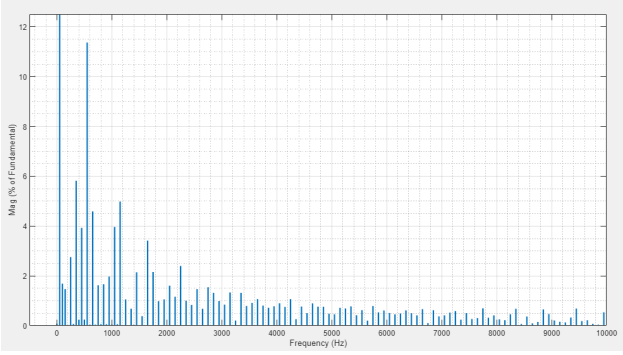

Fig. 2.11. Harmonics of phase voltage for 2-level MLC without PWM modulation.

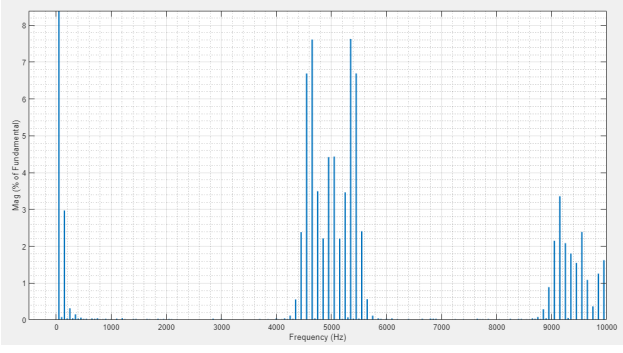

Fig. 2.12. Harmonics of phase voltage for 3-level MLC with modulation frequency equal to 5 kHz.

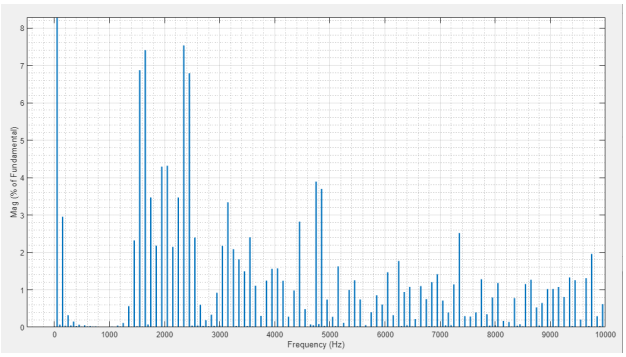

Fig. 2.13. Harmonics of phase voltage for 3-level MLC with modulation frequency equal to 2 kHz.

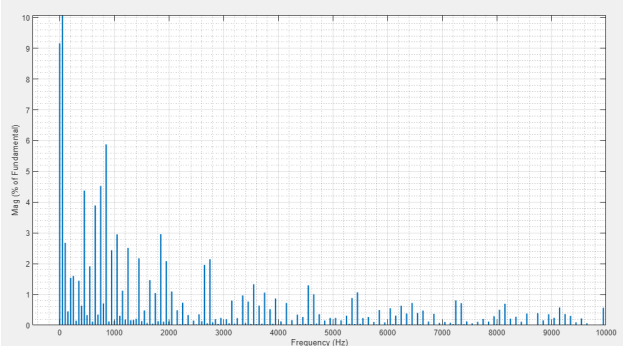

Fig. 2.14. Harmonics of phase voltage for 3-level MLC without PWM modulation.

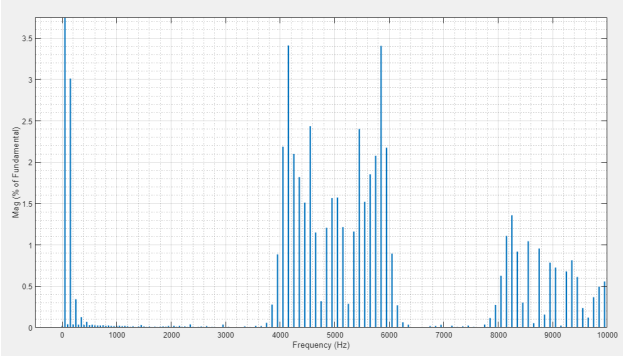

Fig. 2.15. Harmonics of phase voltage for 6-level MLC with modulation frequency equal to 5 kHz.

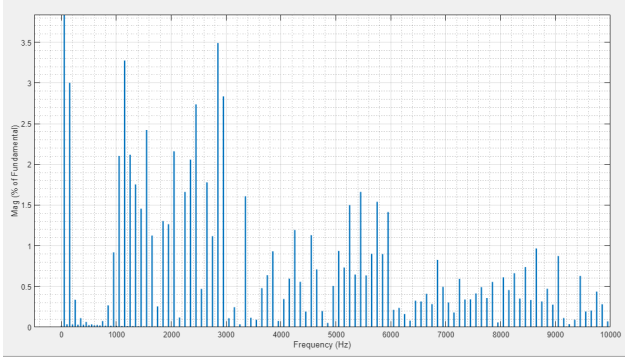

Fig. 2.16. Harmonics of phase voltage for 6-level MLC with modulation frequency equal to 2 kHz.

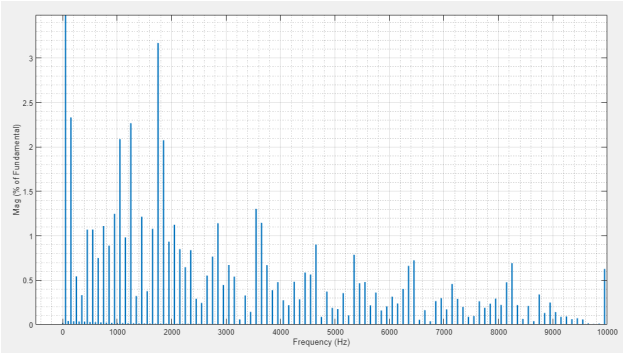

Fig. 2.17. Harmonics of phase voltage for 6-level MLC without PWM modulation.

Same as with simulations of VSI, in all cases with PWM modulation it can be seen, that modulation frequency is affecting the output voltage. This effect is seen at Figures 2.9., 2.12. and 2.15., when modulation frequency is chosen to be 5 kHz. For output voltage frequency 50 Hz (50 Hz is fundamental frequency), the 5 kHz and harmonics that are multiples of 5 kHz have great effect. This effect is less noticeable for 2 kHz modulation frequency, however, this effect can also be seen. In case, when PWM is not used, it is seen (Figures 2.11., 2.14. and 2.17.) that the harmonic distribution is more proportional.

Table 2.1. shows the THD of output voltages for all modulated cases. It can be seen that THD of output voltage waveforms when PWM is not used is lower, than in all cases, when PWM is used. However, it can be said that exactly the modulation frequency of PWM is increasing distortion, making THD larger in cases when PWM is used to form output voltage. In the Table I for cases, when PWM is used, THD is divided to Low Frequency Harmonic Distortion (LFHD) – Harmonic Distortion, that appears for frequencies $f = (0, \frac{1}{2} f_{\text{mod}}]$ and

High Frequency Harmonic Distortion (HFHD), that appears for frequencies $f > \frac{1}{2} f_{\text{mod}}$ (where f_{mod} - modulation frequency).

Table 2.1.

THD of output phase voltages of MLCs with independent sources.

	Modulation frequency 2 kHz			Modulation frequency 5 kHz			THD without PWM
	THD	LFHD	HFHD	THD	LFHD	HFHD	
Single-level VSI	54.46%	0.60%	53.86%	54.35%	0.66%	53.69%	31.44%
2-level MLC	28.67%	1.05%	27.62%	29.16%	1.06%	28.10%	18.50%
3-level MLC	22.17%	2.97%	19.20%	22.43%	3.00%	19.43%	13.78%
6-level MLC	11.59%	3.17%	8.42%	11.73%	3.04%	8.69%	7.97%

From Table 2.1. it can be seen, that despite the fact, that THD of output voltage waveforms is larger when PWM is used, it can also be said, that exactly higher harmonics (larger, than the half of modulation frequency) are giving that impact to THD. It means that output voltages can be filtered in order to reduce this negative impact. In cases, when PWM is not used, harmonic distribution is proportional, which means that even with output filter THD of output voltage will not decrease so significantly, then in case of when PWM is used.

By increasing level count of the MLC, it is possible to decrease THD, however, it means, that converter will have higher conduction losses – larger switch count will be opened more time, than in case of lower level count. By implementing PWM + filtering output voltages it is also possible to reduce THD significantly, however, PWM implementation will result in an increase of switching losses.

2.1. Neutral point clamped multilevel converters

Neutral point clamped MLCs were first introduced in 1981 by A. Nabae, I. Takashi, and H. Akagi [61]. To separate the DC voltage into different levels, capacitors are used. The voltage across each switch is limited to the voltage of a capacitor by means of the diode. The main advantage of this topology is quite high efficiency compared to other topologies. However, there are some disadvantages: the number of power diodes is quadratically related to the level count, which makes this topology quite difficult to use when a large number of levels is needed [62]. Another disadvantage of the topology is that charge balancing in capacitors is needed. Figure 2.18 (a) shows diode neutral point clamped multilevel converter. The use of neutral point clamped converters in the energy storage system is described in [63]. Paper [64] describes the use of a neutral point clamped converter in the AC part of the BESS grid-connected system.

The neutral point clamped multilevel converter has one subtype – active neutral point clamped multilevel converter, shown in Fig. 2.18 (b). The main advantage of this topology –

additional switches – gives the ability to distribute power losses more evenly between switches. Also, it is possible to provide a 0 V level by different paths. Paper [65] shows the use of neutral point clamped and active neutral point clamped converters in battery energy storage systems.

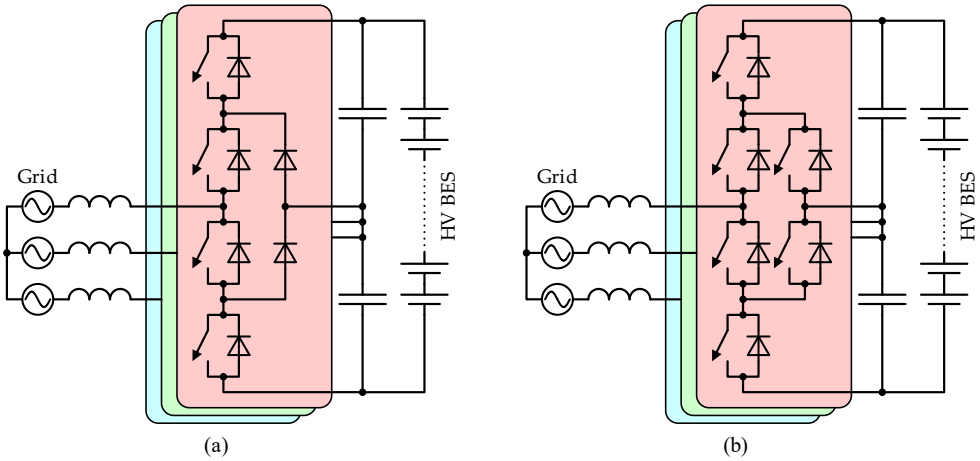

Fig. 2.18. Neutral point clamped MLCs: (a) three phase diode clamped MLC, (b) three phase active neutral point clamped MLC.

2.2. Multilevel converters with flying capacitors

MLC with flying capacitors was introduced by Thierry A. Meynard and Henri Foch in 1992 [66]. The main difference between neutral point clamped MLC and MLC with flying capacitors is that instead of clamping diodes, capacitors are used, forming a ladder structure, where the voltage of one capacitor leg is different from that of the other capacitor leg for one phase. Figure 2.19 shows the MLC with flying capacitors.

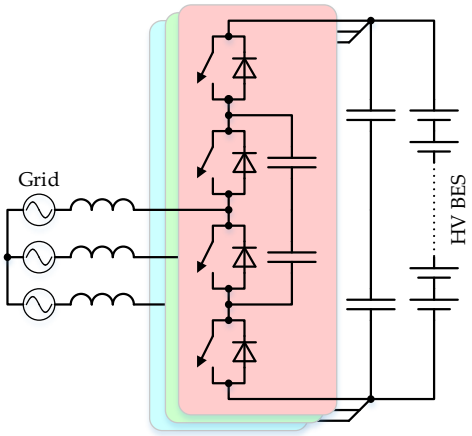

Fig. 2.19. Three phase flying capacitor MLC.

This topology has one advantage – if a number of levels allows that, the necessary amplitude output voltage can be synthesized with multiple switch combinations. Similar to the diode-clamped topology, the main disadvantage of the MLC with flying capacitors is the large number of used capacitors, which makes the practical implementation of this solution larger in terms of packaging.

2.3. Multilevel converters with independent sources

In case of MLCs with independent sources, one phase cascade consists of several single-phase full bridge converters connected in series; the inputs for full bridge converters are separate (independent) DC sources [67]. Considering that DC sources are independent, this makes this topology advantageous in terms of using it with batteries. DC sources can be charged and discharged more evenly – DC sources are separate and can be turned on and off independently. This fact makes this classical MLC topology more advantageous than the others – battery balancing in this case can be performed naturally. An additional advantage of topology is the modular implementation, which makes the manufacturing process of the converter cheaper.

Figure 2.20 shows a structural schematic of a three-phase MLC with independent sources. Each transistor H-bridge can generate three output voltages: $+V_g$ (switches Q1 and Q4 are turned on), 0 V (switches Q1 and Q2 or Q3 and Q4 are turned on) and $-V_g$ (switches Q2 and Q3 are turned on).

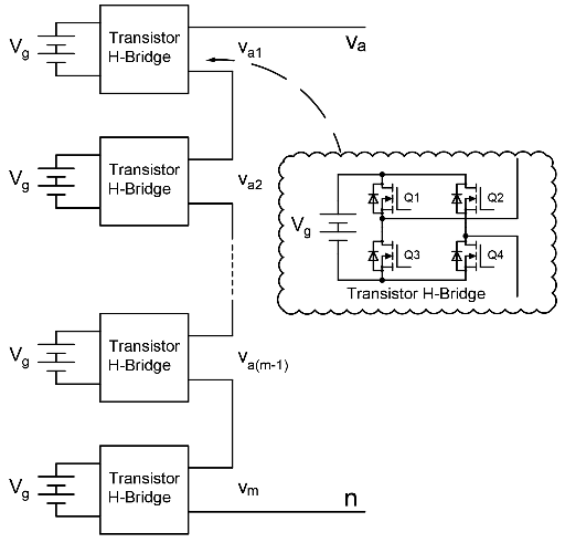

Fig. 2.20. Single phase MLC with independent sources.

As was previously mentioned, the main advantage of the topology is the ability of independent operation of series-connected sub-modules, which allows for balancing batteries used as sub-module sources.

The State of Charge (SOC) of a battery can be expressed as a percentage of the remaining capacity of the battery (the available or "real" capacity) of the maximal (initial) capacity of a battery [68]:

$$SOC = \frac{\text{Real capacity}}{\text{Initial capacity}} \tag{2.4}$$

If submodules operate without source balancing, and sources are connected to the output depending on the position, then activation of modules will look it is shown at Figure 2.21.(a).

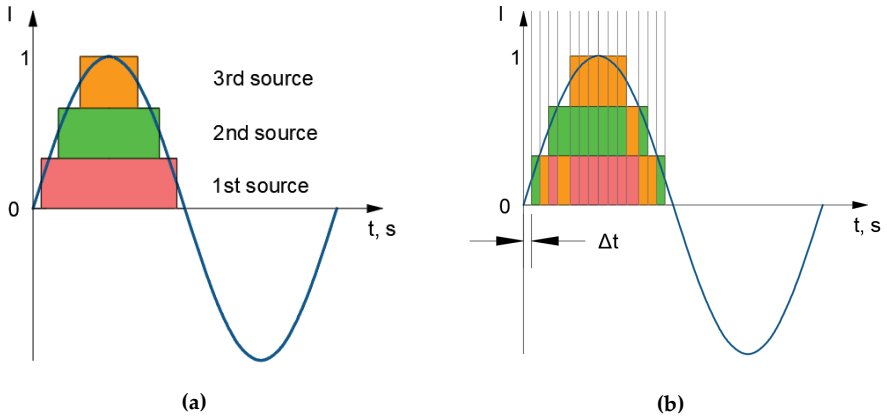

Fig. 2.21. Current waveform formation of MLC with independent sources: (a) unbalanced, (b) with proposed balancing algorithm.

If sub-modules are operated in such a way, it will cause uneven discharge of sources. To improve the discharge, a balancing algorithm of MLC with independent sources was proposed.

In case of three-phase MLC with independent sources, let the SOC_a, SOC_b and SOC_c be the mean value of the state of charge of all batteries connected as sources to H-bridges of one phase cascade (a, b and c phases respectively). For m-level MLC with independent sources, these can be defined as:

$$\begin{aligned} SOC_a &= \frac{1}{m}\sum_{i=1}^{m} SOC_{a,i} \\ SOC_b &= \frac{1}{m}\sum_{i=1}^{m} SOC_{b,i} \\ SOC_c &= \frac{1}{m}\sum_{i=1}^{m} SOC_{c,i} \end{aligned} \tag{2.5}$$

If the time is divided by periods of time Δt, then for each Δt consumed, the amount of charge can be calculated for each battery by multiplying the current by the Δt, and, therefore, the matrix with the real state of charge of the batteries can be calculated. The example of a 3-level MLC with independent sources will look like this:

$$SOC = \begin{pmatrix} SOC_{a1} & SOC_{b1} & SOC_{c1} \\ SOC_{a2} & SOC_{b2} & SOC_{c2} \\ SOC_{a3} & SOC_{b3} & SOC_{c3} \end{pmatrix} \tag{2.6}$$

If in one period for each Δt the SOC of all batteries is calculated, then turned on batteries can be swapped in such a manner that batteries with larger SOC are utilized more frequently, as is shown in Figure 2.21 (b). During each period Δt, matrix of differences between real values of SOC and the mean values of SOC for each phase ΔSOC should be calculated:

$$\Delta SOC = \begin{pmatrix} SOC_a - SOC_{a1} & SOC_b - SOC_{b1} & SOC_c - SOC_{c1} \\ SOC_a - SOC_{a2} & SOC_b - SOC_{b2} & SOC_c - SOC_{c2} \\ SOC_a - SOC_{a3} & SOC_b - SOC_{b3} & SOC_c - SOC_{c3} \end{pmatrix} \tag{2.7}$$

ΔSOC should be kept minimal, which would result in submodule "swapping", and such estimation is performed during each Δt. For evaluation, a *Matlab-Simulink* model of a 3-level MLC with independent sources was developed (see Fig. 2.22).

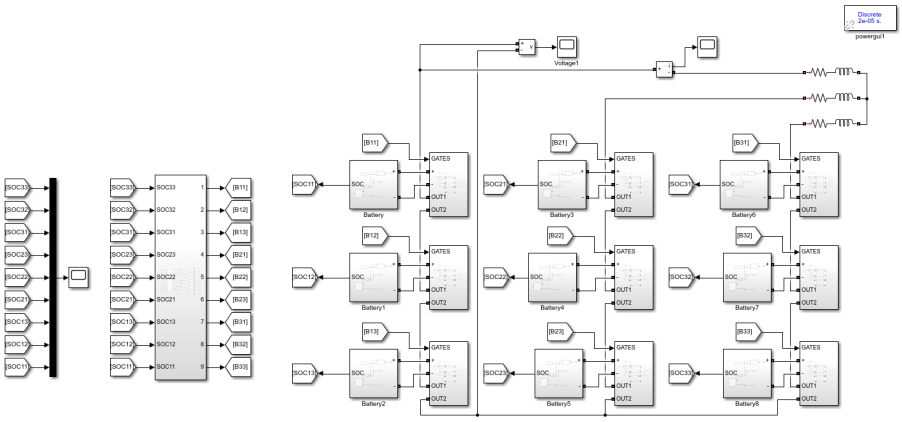

Fig. 2.22. Simulink model of 3-level MLC with independent sources.

Evaluation results are shown in Fig. 2.23. Without a balancing algorithm, batteries are discharged unevenly, which is shown in Fig. 2.23 (a). In turn, when the algorithm is implemented, SOC waveforms form one straight line, which means that batteries are discharged evenly, which is shown in Fig. 2.23 (b).

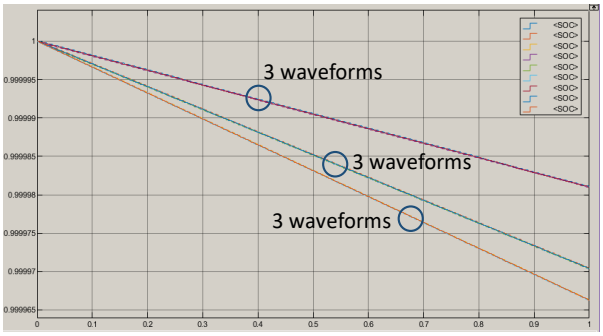

(a)

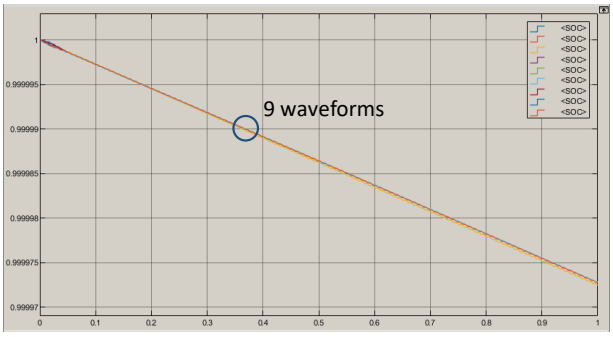

(b)

Fig. 2.23. SOC of batteries of 3-level MLC with independent sources: (a) unbalanced, (b) with balancing algorithm.

3. ANALYSIS OF UNFOLDING CIRCUIT APPLICATION IN POWER ELECTRONIC CONVERTERS

Author's publications II [2] and XI [69] and patent XII are related to Chapter 3.

Considering application of converters in power and energy supply and with AC loads, inverter (DC-AC converter) should be used. Speaking about two stage inverters, there are two alternatives of DC-AC stage operation. Figure 3.1. shows these two alternatives.

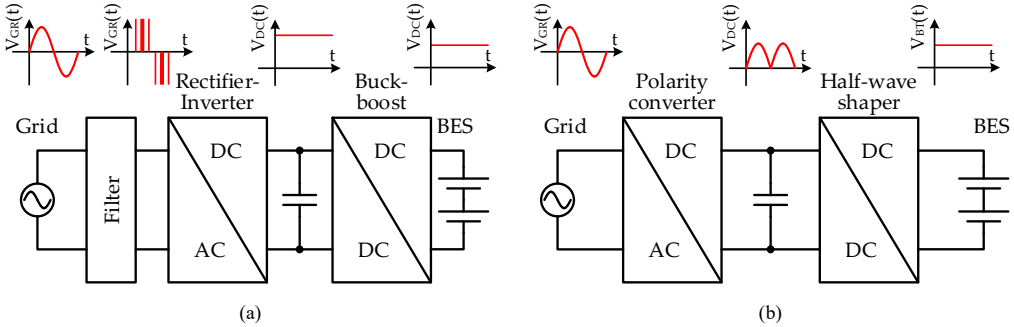

Fig. 3.1. Single phase MLC with independent sources.

Figure 3.1 (a) shows the case when the AC-DC stage (frontend) operates in pulse mode, modulating the grid voltage according to the phase of the grid voltage and the required grid current, while the DC-DC stage provides a stabilized voltage in the DC-link at all operation points of the battery. This case also has another advantage – stable DC-link voltage allows integration of other DC sources and loads.

Figure 3.1 (b) shows a different operation mode of the frontend. In this case, the DC-DC stage forms unipolar sine half-waves in the DC-link (forming so-called *virtual* or *quasi-DC-link*), and the frontend applies formed half-waves to the grid with the correct polarity. In this case, the frontend does not operate in a real switch-mode, but commutates half-waves at grid frequency. This commutator is called an *unfolding circuit* (or simply *unfolder*).

Application of the unfolding circuit as a part of a two-stage converter gives the ability to reduce the overall losses of the converter. It is known that the largest source of losses of a transistor is the commutation losses. If an unfolding circuit is applied, then commutation losses of the frontend are minimal and in some cases can even be neglected.

The unfolding frontend is composed of a commutation matrix, switching at grid frequency, and an inductance coil that serves as a current forming element and which can be allocated at the DC or AC port of the frontend. Figure 3.2 shows both options of unfolding frontend.

When the coil is allocated at the AC port (as shown in Fig. 3.2 (a)), the first contact of the coil is fixed at the grid, while the second contact is connected through the commutation matrix to the DC-link. Then the coil operates with alternating sine current and voltage. Since the voltage in the grid must be in line with the grid current formed in the coil, the voltage in the coil must have a +/–90° shift. Therefore, the voltage at the first end of the coil (at the AC port of the commutation matrix) must be slightly leading for battery loading mode, or lagging for

battery charging mode and slightly higher, compared with the grid voltage on the second end of the coil. This means that the commutation matrix must be a four-quadrant converter, capable of conducting current in both directions at both polarities of the voltage.

Voltages and currents of current forming inductor with inductor allocation at the AC port are shown in Figure 3.3.

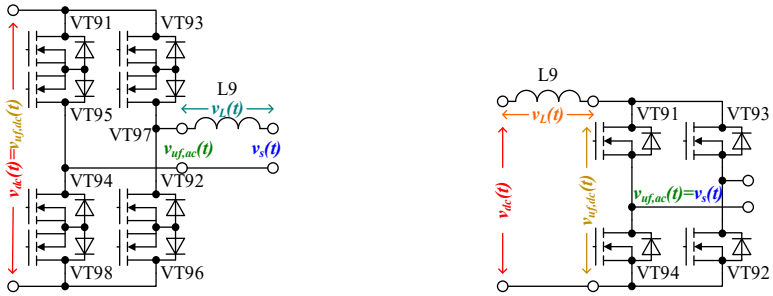

Fig. 3.2. Configurations of unfolding frontend: (a) with current forming coil at AC port, (b) with current forming coil at DC port.

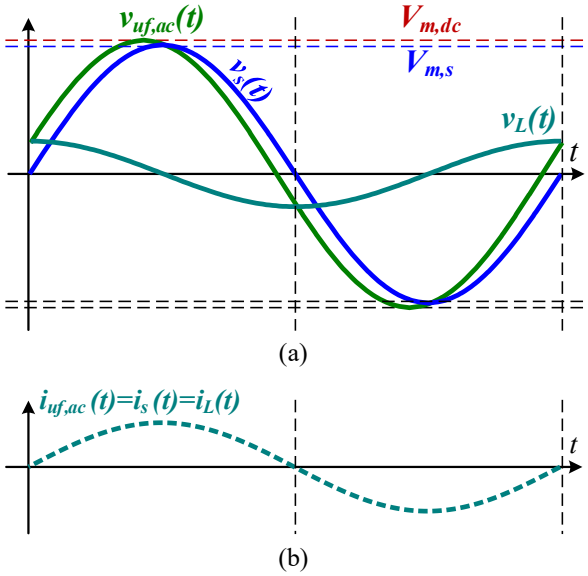

Fig. 3.3. Operation of current forming inductor at AC port of unfolding frontend (for battery loading mode): (a) voltages, (b) currents

Alternative allocation of the current limiting and forming inductance coil is at the the DC port of the commutation matrix. Then, the first end of the coil is attached to the DC-link voltage, but at the second end, the matrix forms a semi-sinusoidal grid voltage. Then the voltage over the coil is semi-sinusoidal with a 90° shift. With such a configuration, the polarity of the voltage

at the AC port of the frontend always corresponds to the polarity of the current. Therefore, the commutation matrix may be a common transistor H-bridge, shown in Figure 3.2 (b).

Voltages and currents of inductor with inductor allocation at DC port of the unfolding circuit are shown in Figure 3.4.

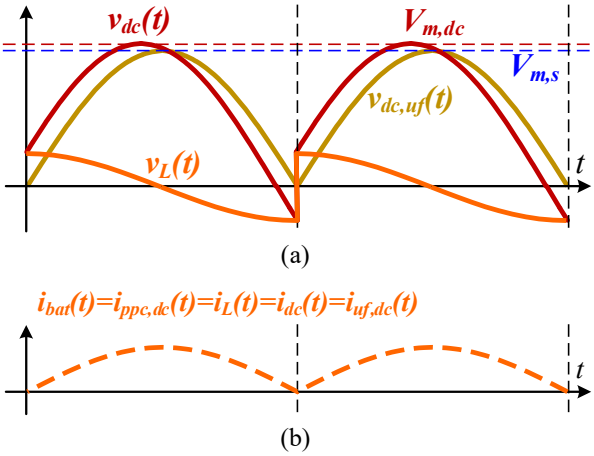

Fig. 3.4. Operation of current forming inductor at DC port of unfolding frontend (for battery loading mode): (a) voltages, (b) currents

Also, despite the fact that majority of converters that are utilizing explicit unfolding circuits as grid frontend, there is another configuration, utilizing unfolding circuit as a part of converter structure, meaning, that unfolding circuit is integrated into the converter. Difference between integrated and explicit unfolding stage is shown in Figure 3.5.

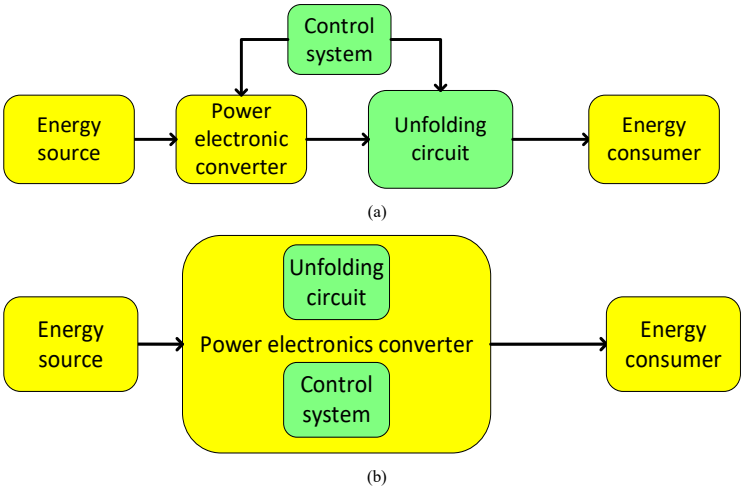

Fig. 3.5. Structure of unfolding converter: (a) with separated unfolding circuit, (b) with integrated unfolding circuit.

3.1. Non-isolated topologies

A number of DC-DC choppers for two-stage converters with unfolding circuit exist. The major part deals with unidirectional applications like PV systems. However, the review of these systems is important for further understanding of the operation of bi-directional choppers.

Papers [70], [71], [72] propose buck-boost choppers in grid-connected PV systems. The combination of buck and boost operation modes combined with unfolding circuit gives the ability of voltage regulation to match the value of grid voltage.

Paper [73] shows the simulation of model predictive control of buck-boost converter with unfolding circuit. Papers [74], [75] also describe the application of converters with unfolding circuits in PV systems. In [74] the combination of buck converter and unfolding circuit is implemented in the form of low-profile microinverter. Paper [75] focuses on the high-gain operation of boost converter, tied with full-bridge unfolding circuit. In addition, this unfolding circuit is working in partial sine-form PWM when voltage has to be stepped down.

An example of buck-boost topology with integrated unfolding circuit (Aalborg Inverter) is described in [76], [77], [78]. Reference [79] describes the implementation of isolated Ćuk converter with unfolding circuit as differential power processor for aircraft application. In this case the unfolding circuit gives the ability of four-quadrant operation of converter and reduces the worst-case processed power. Paper [80] describes the evaluation of inverter topology based on a buck converter and unfolding circuit within Google's "Little Box Challenge". The major advantage of the topology is the reduction of volume and complexity of the system. Figure 3.6. shows 3 configurations of non-isolated topologies with unfolding frontend.

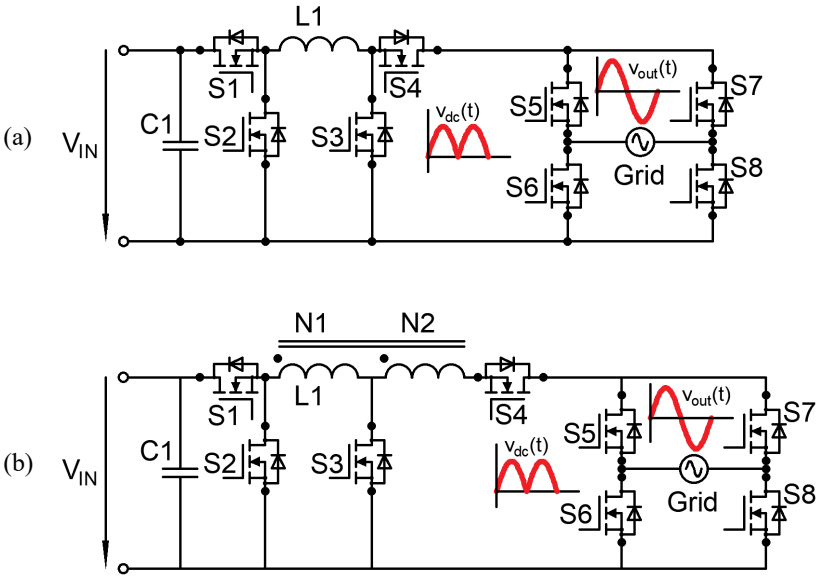

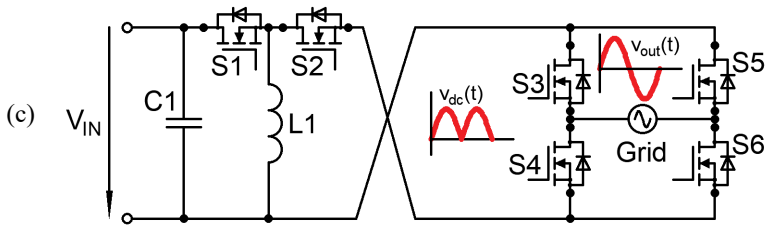

Fig. 3.6. Non-isolated topologies with unfolding circuits: (a) single inductor buck-boost converter with unfolding circuit, (b) tapped inductor buck-boost converter with unfolding circuit, (c) single inductor twisted buck boost converter with unfolding circuit.

3.2. Isolated topologies

A particular configuration is based on dual active bridge (DAB). Typically, the DAB is connected with power factor correction (PFC) rectifier through intermediate DC link. DAB gives the ability of bidirectional energy flow, which perfectly fits the requirements of BESS [81], [82].

Most commonly, DAB contains two full bridges, a series inductor and a high frequency (HF) isolation transformer (Fig. 3.4.) [81]–[89]. The main advantage of the DAB topology is easy implementable zero-voltage switching (ZVS), which decreases power losses of the converter.

There are two main types of DAB converters: current-fed and voltage-fed. The voltage-fed DAB converters are implemented in various applications, where bidirectional power flow is needed. One of the simplest control methods of the voltage-fed DAB converters is phase shift control [90]–[92]. With phase shift control, both H-bridges of DAB operate with the same duty cycle. In this case, power is controlled by phase shift between the sides of DAB converter [93]. Combining the phase shift with PWM enables minimizing the losses of the converter and also extends the operation range, when ZVS can be provided [94], [95]. Papers [96], [97] describe series resonant DAB converter. An LC circuit is added at the primary side of the transformer to provide series-resonance. By adding series resonant circuit to the topology, it is possible to achieve ZCS (zero current switching) operation of the DAB converter. Figure 3.7. shows three of the above-described configurations of DAB converter.

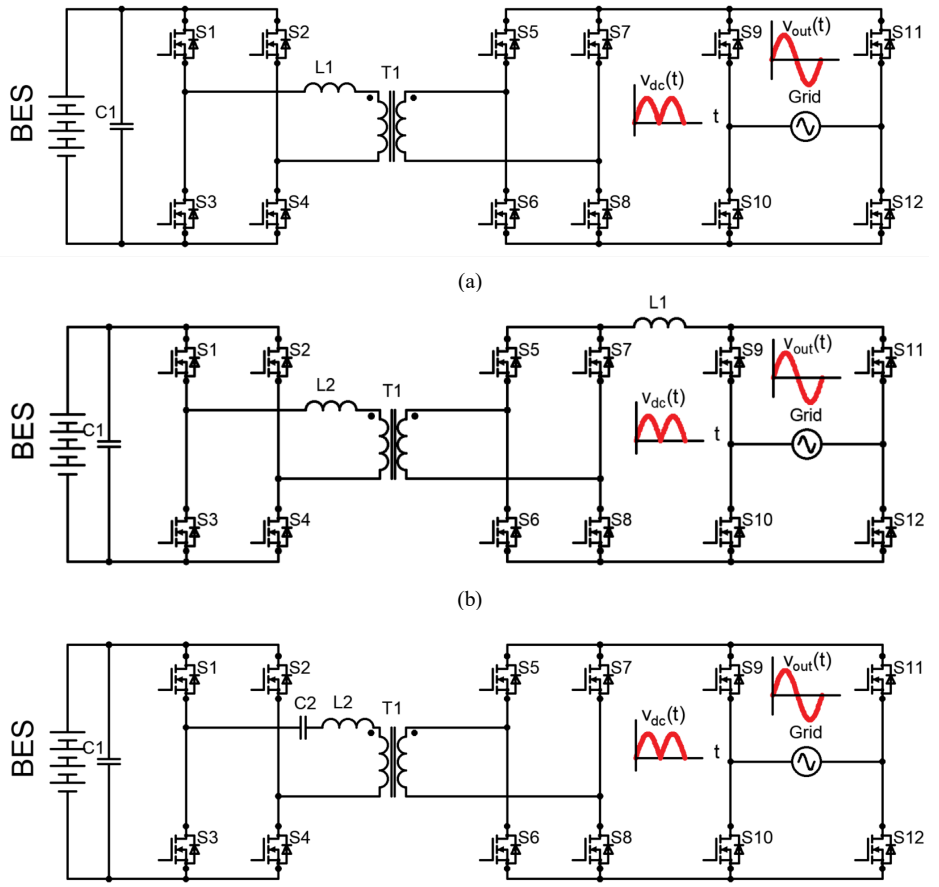

Fig. 3.7. Isolated topologies with unfolding circuits: (a) voltage-fed DAB; (b) current-fed DAB (c) series resonant DAB

3.3. Partial power converters

Partial power converter (PPC) links the input and the output of the system. While one part of the energy from the source goes directly to the load, PPC processes only the necessary reminder. Figure 3.8. shows the difference between full power converter and PPC.

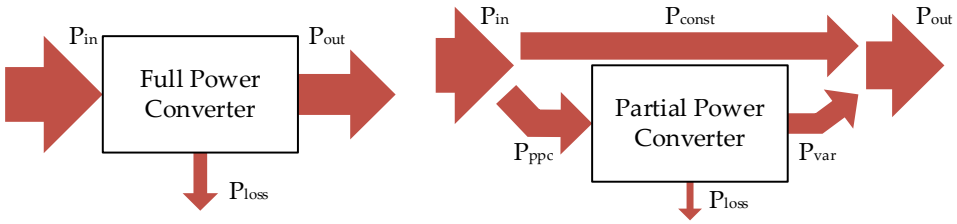

(a) (b)

Fig. 3.8. Difference between full power and partial power converters: (a) energy distribution in full power converter, (b) energy distribution in partial power converter.

One of the possible configurations of combining PPC with unfolding grid frontend consists of isolated bidirectional PPC capable of generating bipolar voltage ($PPC_{chg,dis}$), unfolding circuit (UF) and virtual DC-link (qDC). The voltage of the battery is approximately twice as low as the amplitude of the grid voltage. Because of that PPC is connected in series with the battery on the DC-link side and in parallel on the battery side. PPC can be constructed as any isolated bipolar bidirectional circuit, including the circuits with resonant tanks; for example, a bidirectional DAB is presented in [98]. This configuration is shown in Figure 3.9.(a)

Another configuration of BESS with the PPC and UF inverter is shown in Figure 3.9.(b). It includes an isolated bidirectional unipolar PPC, a "pulsating" DC-bus (qDC+), and an additional unfolding inverter (UF+). The unipolar PPC with the additional inverter UF+ operates as the bipolar PPC of the previous configuration. This reduces number of the switches operating in the high-frequency mode and, therefore, the corresponding switching losses.

One more improvement in the initial BESS configuration assumes the splitting of the bidirectional PPC into two unidirectional PPCs. One of them operates only in the battery charging mode, while another one operates during battery discharge. This means the absence of bidirectional switches that reduce the number of semiconductor elements in each current loop and the corresponding conduction losses. This BESS's configuration is shown in Figure 3.9.(c)

Finally, the combining of the two above-mentioned improvements, i.e., the splitting of the bidirectional PPC into two unidirectional ones and the use of unipolar PPC with the extra unfolder instead of the bipolar PPC, provides the achievement of their benefits together. In addition, such configuration enables the fine-tuning of the design of these separated parts of the two-stage BESS interface converter. This configuration is shown in Figure 3.9.(d).

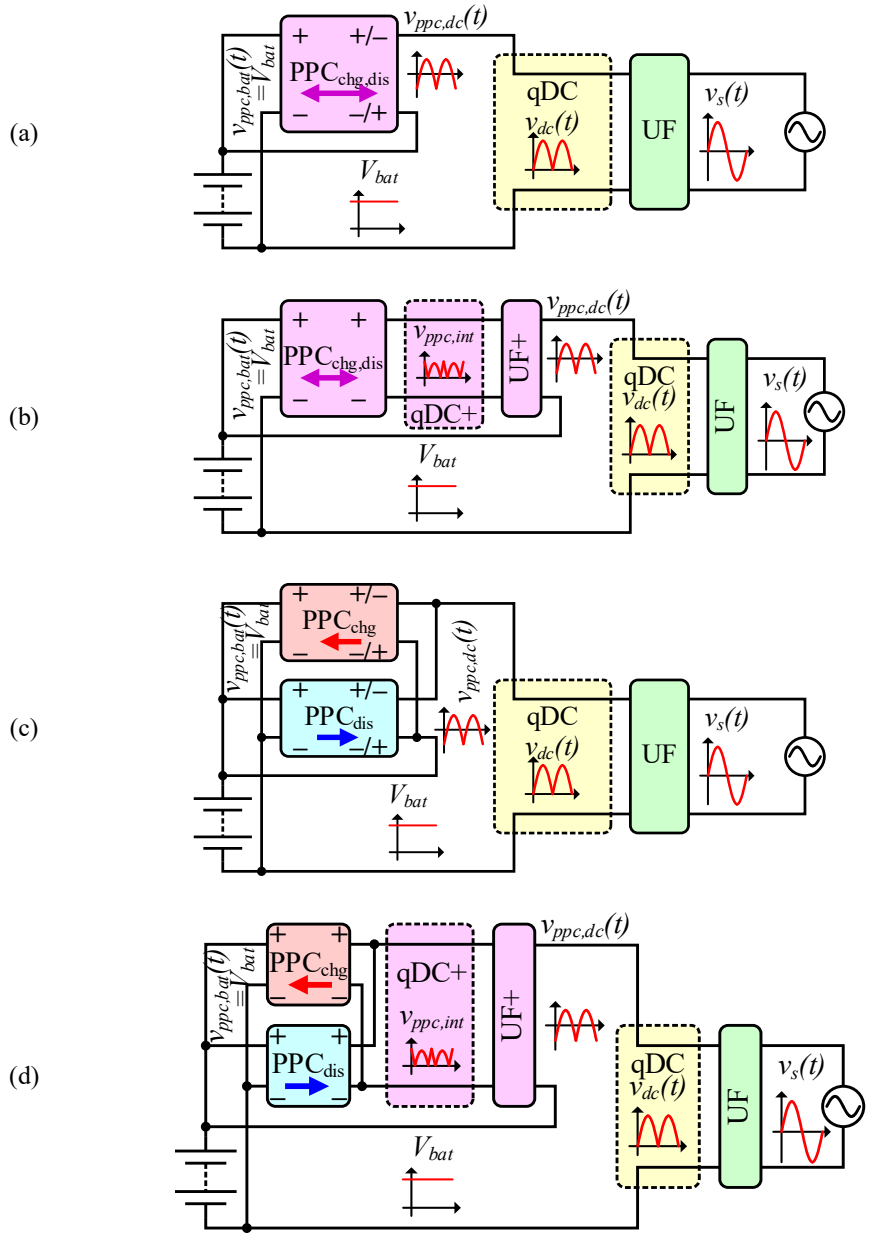

Fig. 3.9. Structural diagrams of two-stage converters utilizing PPC and unfolding grid frontend: (a) basic configuration. (b) configuration with additional unfolder, (c) configuration with two converters dedicated for battery charging and discharging, (d) configuration with additional unfolder and two converters.

4. UNFOLDING MULTILEVEL CONVERTERS WITH INDEPENDENT SOURCES

Author's publications II [2], VIII [99] and the unpublished paper III are related to Chapter 4.

Unfolding frontend can also be combined with multilevel half-sine shapers. Classical configuration of MLC with independent sources without an unfolder assumes that several H-bridge modules, fed from a small group of battery cells, are connected in series, thus creating one phase cascade [100]. The use of MLCs in BESS provides natural balancing of battery cells without an explicit battery management system.

Adding an unfolding circuit at the grid side enables bipolar operation of MLC shaper [99]. It turns the series connected H-bridges into half bridges, because the bipolar operation of these modules is not necessary. Fig. 4.1. shows the configuration of the one phase cascade with and without the unfolding circuit. Therefore, the use of unfolding circuit reduces switch count in current paths and, therefore, simplifies the design.

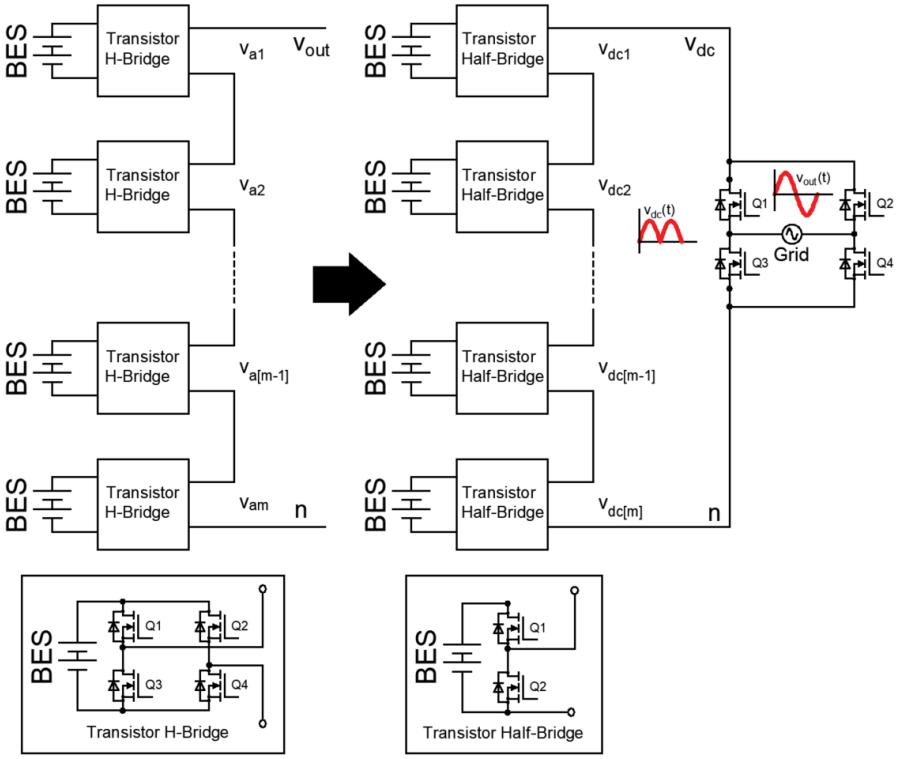

Fig. 4.1. Structure of MLC with and without unfolding frontend.

4.1. Evaluation of operation

To evaluate the performance of MLC with independent sources and an unfolding frontend, a testbench of a 3-level MLC with an unfolder was developed. IRF540 n-channel MOSFETs

have been utilized for the switches' realization due to their relatively low cost and high reliability. HCPL-3120 optocouplers were chosen for driving the MOSFETs with bipolar voltage modulation: +15 V for logical "1" and –15 V for logical "0". In order to operate the MOSFETs with this voltage scheme, each HCPL-3120 is connected to the IR0515S board mount power supply with an input voltage equal to 5 V. The LAUNCHXL-F2837D development board from Texas Instruments has been used to control the operation of the converter. Input voltage was set equal to 8.4 V, which equals the voltage of two fully charged series-connected 18650 battery cells. The developed testbench is shown in Fig. 4.2. An RL load was utilized for the performance evaluation (R = 16 Ω and L = 5 mH).

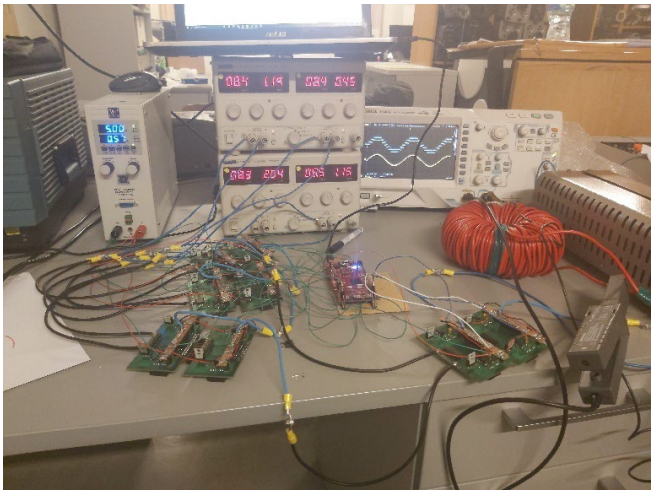

Fig. 4.2. Testbench of MLC with independent sources and unfolding frontend.

Evaluation results are shown at Fig. 4.3.

(a)

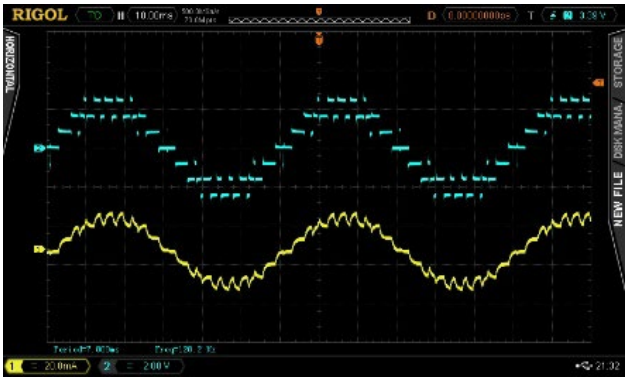

(b)

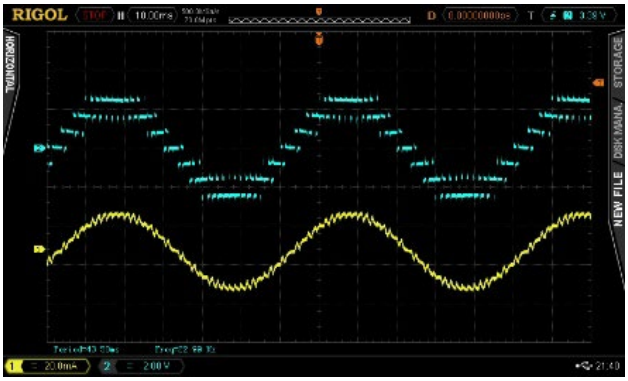

(c)

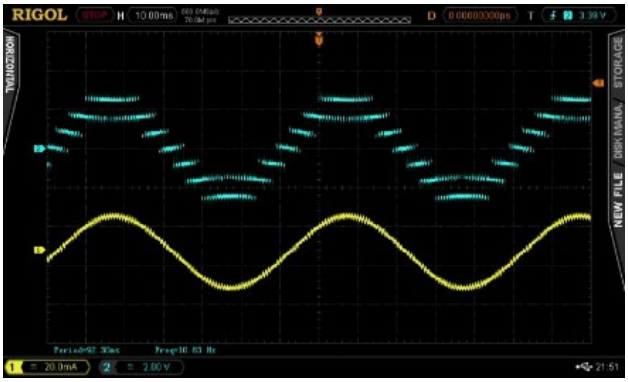

Fig. 4.3. MLC with unfolder evaluation results (blue waveform – voltage, yellow – current): (a) 1 kHz PWM modulation frequency, (b) 2 kHz PWM modulation frequency, (c) 3 kHz PWM modulation frequency.

The experimental results reveal the proper operation of the MLC with independent sources and the unfolding circuit. The impact of the switching frequency of the converter on the distortion of the output current can be observed. In particular, at 1 kHz switching frequency, the pulsations of the output current are significantly larger compared to the corresponding waveform at 4 kHz.

4.2. Evaluation of impact of unfolding frontend on power losses

The influence of combining an unfolding circuit with MLC with independent sources is studied in this section. It is based on the mathematical models of MLC with independent sources, with and without an additional unfolding circuit. In the case of classical MLC with independent sources, the output current of series-connected H-bridge converters is sinusoidal. The output voltage of each H-bridge is equal to $+V_{bat}$, 0 V and $-V_{bat}$ (V_{bat} being source voltage, typically battery in BESS applications), and the output voltage of the cascade is equal to the sum of the output voltages of each transistor H-bridge. When the unfolding circuit is applied, series-connected H-bridges are conducting semi-sine current. As for the commutated voltage, each half-bridge commutates the voltage of the input battery. The cascade of series-connected

transistor half-bridges generates unipolar voltages that are applied to the grid by means of the unfolding circuit with a correct polarity.

Previously, it was mentioned that the combination of an unfolding inverter with MLC gives the ability to reduce the loss of MLC with independent sources. For a simplified analysis of the converter losses, several assumptions should be made:

- Commutated voltages of series-connected sub-modules are equal to the fractions of peak grid voltage equally distributed between sources (i.e., for example, for a 3-level converter source (battery) voltage $V_{bat} = 325/3 \approx 108.33$ V).
- Voltage rise time and voltage fall time of the MOSFET transistor are equal and are proportional to commutated voltage (i.e., they are the same for constant voltage and the same number of levels).
- Current rise time and current fall time are proportional to commutated current.
- Voltage/current change times are equal in the middle of the semi-sine half-wave at maximal current. This parameter is designated Maximal Duration of Switching (MDS) and for simplicity reasons is equal to 200 ns.
- Drain-to-source on resistance for simplicity reasons is taken equal to 0.1 Ω.
- The analysis is provided for the battery discharge mode only.

Figure 4.4. shows the example of voltage waveform forming with the corresponding voltage and current waveforms of 3-level MLC.

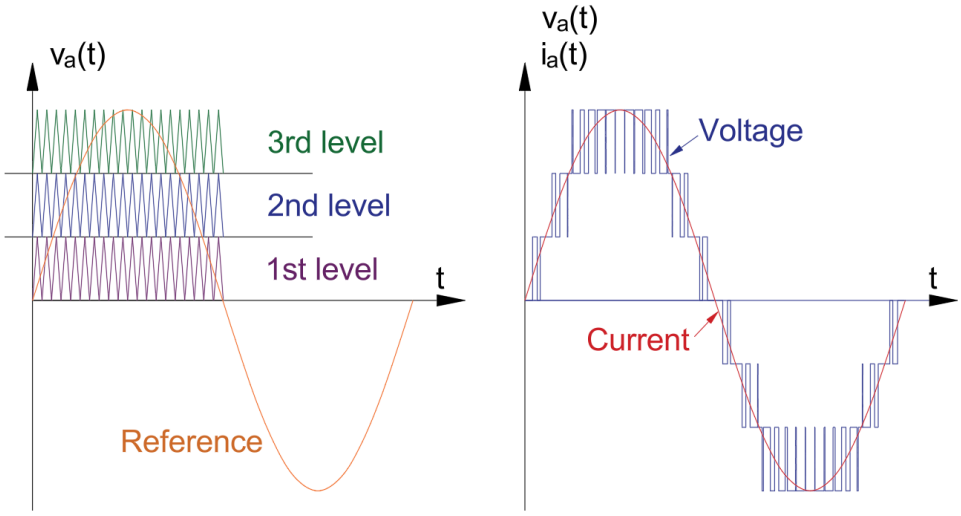

(a) (b)

Fig. 4.4. 3-level MLC voltage waveform synthesis with PWM modulation (a) and the corresponding voltage/current waveforms of 3-level MLC (b).

Conduction losses of classical MLC with independent sources.

For classical MLC with independent sources sub-module consists of full transistor bridge. In continuous current mode 2 switches of each transistor bridge are always conducting semi-sine current. For m-level MLC with independent sources:

$$\Delta P_{FBMLC,c} = m \cdot 2 \cdot \frac{1}{\pi} \int_0^{\pi} \Delta p_c(t) dt = m \cdot 2 \cdot \frac{1}{\pi} \int_0^{\pi} R_{DSon} \cdot (I_{s,m} \cdot \sin\theta)^2 d\theta =$$
$$= m \cdot 2 \cdot \frac{1}{\pi} \cdot R_{DSon} \cdot I_{s,m}^2 \cdot \frac{1}{2} \pi = m \cdot R_{DSon} \cdot I_{s,m}^2 \quad (4.1)$$

where

$\Delta P_{FBMLC,c}$ – conduction losses of classical MLC with independent sources, W;
m – number of levels;
$\Delta p_c(t)$ – instantaneous conduction losses, W;
R_{DSon} – drain-to-source on-state resistance, Ω;
$I_{s,m}$ – peak value of grid current, A.

Switching losses of classical MLC with independent sources.

Speaking about switching losses of MLC with independent sources, it can be said that at each moment of time 1 full transistor bridge is working in PWM mode (i.e. 2 transistors are constantly switching). Switching losses can be calculated by assuming triangular shape of instantaneous power on the switches during the commutation. Maximal energy loss of turn-on and turn-off transitions is achieved at grid phase 90 ° when current is maximal. For full-bridge converter:

$$E_{FB,sw,m} = 2 \cdot 2 \cdot \frac{V_{bat} \cdot I_{s,m} \cdot (t_{i,m} \cdot t_{v,m})}{2} = 2 \cdot V_{bat} \cdot I_{s,m} \cdot (t_{i,m} \cdot t_{v,m}) = 2 \cdot V_{bat} \cdot I_{s,m} \cdot MDS \quad (4.2)$$

where

$E_{FB,sw,m}$ – maximal energy loss for full transistor bridge at 90 ° phase, J;
V_{bat} – battery voltage, V;
$t_{i,m}$ – maximal current rise/fall time, s;
$t_{v,m}$ – maximal voltage rise/fall time, s;
MDS – Maximal Duration of Switching – previously defined parameter, s.

And maximal power losses are equal to:

$$\Delta P_{FB,sw,m} = 2 \cdot V_{bat} \cdot I_{s,m} \cdot \frac{MDS}{T_{sw}} \quad (4.3)$$

where $\Delta P_{FB,sw,m}$ – maximal power loss for full transistor bridge at 90 ° phase, W.

Since the current change times are proportional to current that is semi-sinusoidal for other points, the equivalent switching losses are calculated as:

$$\Delta P_{FB,sw,k} = \frac{1}{T_{sw}} \cdot 2 \cdot 2 \cdot \frac{V_{bat} \cdot I_{sw,k} \cdot (t_{i,k} \cdot t_{v,k})}{2} = \frac{2}{T_{sw}} \cdot V_{bat} \cdot I_{s,m} \sin\theta_k \cdot (t_{i,m} \frac{I_{s,k}}{I_{s,m}} + t_v) =$$

$$= \frac{2}{T_{sw}} \cdot V_{bat} \cdot I_{s,m} \cdot \sin\theta_k \cdot (t_{i,m} \cdot \sin\theta_k + t_v) = \frac{2 \cdot V_{bat} \cdot I_{s,m} \sin^2\theta_k \cdot \frac{1}{2} MDS}{T_{sw}} + \quad (4.4)$$

$$+ \frac{2 \cdot V_{bat} \cdot I_{s,m} \sin\theta_k \cdot \frac{1}{2} MDS}{T_{sw}} = \frac{V_{bat} \cdot I_{s,m} \cdot MDS}{T_{sw}} \cdot (\sin^2\theta_k + \sin\theta_k)$$

where

$\Delta P_{FB,sw,k}$ – equivalent power loss for full transistor bridge, W;

T_{sw} – switching period, s;

$I_{sw,k}$ – equivalent commutated current, A;

$t_{i,k}$ – equivalent current rise/fall time, s;

$t_{v,k}$ – equivalent voltage rise/fall time, s;

$I_{s,k}$ – equivalent grid current, A.

Then the total switching losses of classical MLC with independent sources are equal to:

$$\Delta P_{FBMLC,sw} = \frac{1}{N} \sum_{k=1}^{N} \Delta P_{FB,sw,k} \quad (4.5)$$

where N – number of PWM cycles.

Conduction losses of multilevel structure of MLC with independent sources and unfolding frontend.

Taking into account, that in case of MLC with independent sources and unfolding circuit series connected multilevel structure consists of half-bridges, and in case of half-bridges the number of conducting switches for each sub-module is 1. Therefore, taking into consideration (4.1), conduction losses of series connected half-bridges in MLC with independent sources and unfolder are equal to:

$$\Delta P_{HBMLC,c} = m \cdot 2 \cdot \frac{1}{\pi} \int_0^{\pi} \Delta p_c(t) dt = \frac{m}{2} \cdot R_{DSon} \cdot I_{s,m}^2 \quad (4.6)$$

where $\Delta P_{HBMLC,c}$ – conduction losses of multilevel structure of MLC with independent sources and unfolding frontend, W.

Switching losses of multilevel structure of MLC with independent sources and unfolding frontend.

As it was previously said, for classical MLC with independent sources at each moment of time 1 sub-module is working in PWM mode. The same is true for MLC with independent sources and in the case of half-bridge modules 2 transistors are also constantly switching. Switching losses of multilevel structure of MLC with unfolding frontend will be the same as in (4.4) and (4.5):

$$\Delta P_{HB,sw,k} = \frac{V_{bat} \cdot I_{s,m} \cdot MDS}{T_{sw}} \cdot (\sin^2 \theta_k + \sin \theta_k) \quad (4.7)$$

where $\Delta P_{HB,sw,k}$ – equivalent power loss for transistor half-bridge, W.

$$\Delta P_{HBMLC,sw} = \frac{1}{N} \sum_{k=1}^{N} \Delta P_{HB,sw,k} \quad (4.8)$$

where $\Delta P_{HBMLC,sw}$ – total switching losses of multilevel structure of MLC with independent sources and unfolding frontend, W.

Losses of unfolding frontend.

In case of unfolding frontend, the grid current in each half-period is constantly flowing through the couple of front-end switches. In this case the frontend produces only conduction losses, and since switching takes place only each half-period, switching losses can be neglected. This means, that:

$$\Delta P_{UF,c} = 2 \cdot \frac{1}{\pi} \int_0^{\pi} \Delta p_c(t) dt = 2 \cdot \frac{1}{\pi} \int_0^{\pi} R_{DSon} \cdot (I_{s,m} \cdot \sin \theta)^2 d\theta = R_{DSon} \cdot I_{s,m}^2 \quad (4.9)$$

$$\Delta P_{UF,sw} = 0 \quad (4.10)$$

where $\Delta P_{UF,c}$ – conduction losses of unfolding frontend, W;

$\Delta P_{UF,sw}$ – switching losses of unfolding frontend, W.

The power losses of MLC with independent sources with and without unfolding circuit, as well as with level modulation, but without pulse modulation are calculated in a similar way. In this case, switching occurs only 2 times per half-period. Therefore, the corresponding switching losses can be excluded from the analysis. For m-level MLC:

$$\Delta P_{FBMLC,lm,c} = m \cdot 2 \cdot \frac{1}{\pi} \int_0^{\pi} \Delta p_c(t) dt = m \cdot 2 \cdot \frac{1}{\pi} \int_0^{\pi} R_{DSon} \cdot (I_{s,m} \cdot \sin \theta)^2 d\theta = m \cdot R_{DSon} \cdot I_{s,m}^2 \quad (4.11)$$

$$\Delta P_{HBMLC,lm,c} = m \cdot \frac{1}{\pi} \int_0^{\pi} \Delta p_c(t) dt = m \cdot \frac{1}{\pi} \int_0^{\pi} R_{DSon} \cdot (I_{s,m} \cdot \sin \theta)^2 d\theta = \frac{m}{2} \cdot R_{DSon} \cdot I_{s,m}^2 \quad (4.12)$$

$$\Delta P_{FBMLC,lm,sw} = 0 \quad (4.13)$$

$$\Delta P_{HBMLC,lm,c} = 0 \quad (4.14)$$

where

$\Delta P_{FBMLC,lm,c}$ – conduction losses of multilevel structure of MLC with independent sources with level modulation, W;

$\Delta P_{HBMLC,lm,c}$ – conduction losses of multilevel structure of MLC with independent sources and unfolding frontend with level modulation, W;

$\Delta P_{FBMLC,lm,sw}$ – switching losses of classical multilevel structure of MLC with independent sources with level modulation, W;

$\Delta P_{HBMLC,lm,sw}$ – switching losses of multilevel structure of MLC with independent sources and unfolding frontend with level modulation, W.

Evaluation of losses.

Power losses of classical MLC with independent sources:

$$\Delta P_{FBMLC} = \Delta P_{FBMLC,c} + \Delta P_{FBMLC,sw} \tag{4.15}$$

Power losses of MLC with independent sources and unfolding frontend:

$$\Delta P_{HBMLC} = \Delta P_{HBMLC,c} + \Delta P_{HBMLC,sw} + \Delta P_{UF,c} \tag{4.16}$$

Since the above-described calculation methodology has multiple assumptions, it is irrelevant to demonstrate the actually calculated power losses. However, given that calculation assumptions are the same for all calculation points, for topology comparison, it is reasonable to normalize calculated losses. Calculations were performed for 24 cases – for 3-level, 4-level and 5-level MLC, with unfolding frontend and without it (classical topology). In addition, each topology is combined with 3 + 1 PWM modulation types: with frequencies 2 kHz, 5 kHz and 10 kHz, as well as without PWM modulation (only with level modulation). The resulting losses are normalized with respect to the power losses of a classical 3-level MLC with independent sources. This power loss comparison is shown in Fig. 4.5.

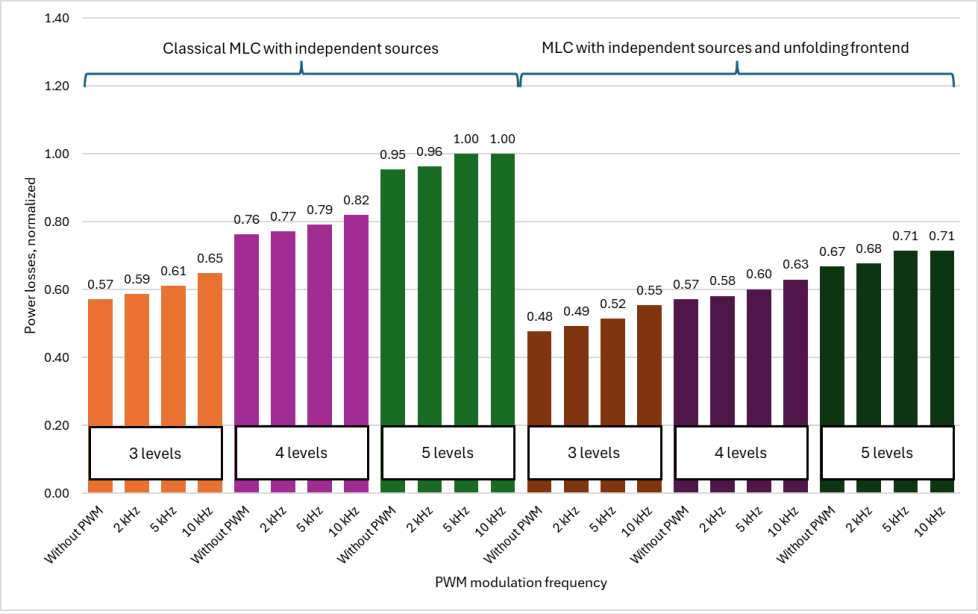

Fig. 4.5. Comparison of power losses of classical MLC with independent sources and MLC with independent sources and unfolding frontend with different level count and different modulation frequencies.

As shown in Fig. 4.5, combining the unfolding frontend with MLC with independent sources gives the ability not only to simplify the topology, but also to reduce overall losses of MLC. With classical MLC with independent sources, when the level count is increased, power losses also noticeably increase. Due to the lower number of transistors in each current path, the change in power losses of MLC with independent sources and unfolder is not so perceivable

with an increase in the level count. For example, the power losses of a 3-level MLC with independent sources and an unfolding frontend without PWM are 1.2 times lower. So, the losses are 1.4 times lower in the case of 5-level MLC, unfolding frontend and 10 kHz PWM. Also, it can be seen that switching frequency has a weak impact on the power losses in both cases. Therefore, the conduction losses are the main contributor to the total losses.

4.3. Generalized comparison of topology with fitness function

First of all, a mathematical model for numerical comparison of topologies (classical MLC with independent sources and unfolding MLC with independent sources) has to be brought forward. There is a set of parameters that can be used for the description of these topologies. Some of these parameters are defined by the topology. However, the majority of them are not only defined by the topology but also by the operation mode and working conditions. So, the suitable model is a fitness function with the following parameters:

- Number of switches - S. Number of switches used has an impact on system complexity and cost. For each active switch there should be a driver circuit, which also affects the overall cost of the converter. The number of switches for m-level single phase classical MLC with independent sources and unfolding MLC with independent sources can be found as:

$$\begin{aligned} S &= 4 \cdot m \ - \text{for classical MLC with independent sources} \\ S &= 2 \cdot m + 4 \ - \text{for unfolding MLC with independent sources} \end{aligned} \tag{4.17}$$

- Redundancy – 1/R. Redundancy can be represented as the number of possible switching states for voltage levels. Considering that, for example, full transistor bridge can have $+V_{bat}$, 0 V and $-V_{bat}$, there are 3 switching states for each level. Redundancy represents control flexibility and in some cases fault tolerant capability of a converter and for m-level converter can be expressed as:

$$R = \frac{3^m}{2m+1} \tag{4.18}$$

- Power losses ΔP. As it was mentioned in 4.2. section, there are two types of losses – conduction losses and switching losses that here are considered together.
- Harmonic distortion. Harmonic distortion can be divided into two parts: low-frequency harmonic distortion (LFHD) and high-frequency harmonic distortion (HFHD). According to Electromagnetic Compatibility (EMC) standards (for example, IEC TR 61000-2-5 [101]), frequencies below 9 kHz are considered low. However, for the comparison, frequencies up to 50th harmonic of the fundamental frequency (2500 Hz for 50 Hz fundamental frequency) will be considered as low-frequency harmonics and frequencies higher than 50th harmonic – high frequencies. High frequency harmonics can easily be filtered. Low frequencies are more difficult to filter without corrupting output waveforms of the converter. With the increase of level count and PWM modulation frequency, THD will decrease. With PWM modulation, modulation frequency is affecting output voltage. Modulation frequency and frequencies divisible

by modulation frequency will have an impact on distortion. For case without PWM, harmonic distribution is reverse proportional to the number of harmonic and the impact on LFHD is significant. Within the comparison, cases without PWM are considered with LFHD=1, when PWM frequency is lower, than 2500 Hz, LFHD is set to 0.5 and for other cases – 0. When PWM is not used – HFHD is going to be set to 0, for PWM frequencies for other cases – it will be set to 1.

Fitness function for topology comparison:

$$F = w_1 \cdot S + w_2 \cdot \frac{1}{R} + w_3 \cdot \Delta P + w_4 \cdot LFHD + w_5 \cdot HFHD \tag{4.19}$$

where w_1, w_2, w_3, w_4, w_5 – are weight coefficients for each function parameter.

Depending on weight coefficients, the priorities for the comparison can be set. Since fitness function mainly is used for optimization, the function is written in such a way, that lower function value means better and more optimized performance of the converter. If the function is used for optimization, function value should be minimized:

$$F \rightarrow \min \tag{4.20}$$

In this case, fitness function is used for topology comparison, therefore, the sum of (?) all weight coefficients are assumed to be equal to 1. Also, for better representation, all parameters were normalized to maximal values of each parameter. Table 4.1. shows the calculated normalized parameters of fitness function for 24 cases – 3-level, 4-level, 5-level MLC with independent sources with unfolding frontend and without it (classical topology). Each case is evaluated with 3 PWM modulation frequencies (2 kHz, 5 kHz and 10 kHz) and without PWM modulation (with level modulation only). Normalized losses were taken from calculations described in section 4.2.

Fitness function values, represented in Table 4.1. and Figure 4.6. show that the overall performance of the MLC with independent sources and unfolding frontend is better than that of the classical MLC with independent sources. Comparing switch count, unfolding MLC with independent sources has 1.2 (for 3-level converter) to 1.43 times (for 5-level converter) lower switch count. The higher level count corresponds to the stronger impact of the unfolding converter. In contrast, the higher level count corresponds to lower redundancy 1/R parameter. As it was previously concluded (section 4.2.), the use of unfolding converter leads to lower losses of the converter. Regarding LFHD and HFHD, it can be said, that PWM frequency should be chosen considering EMC standards and should be higher, than 50^{th} harmonic of the fundamental frequency.

Table 4.1.

Parameters of fitness function.

			S (normalized)	1/R (normalized)	ΔP (normalized)	LFHD	HFHD
Classical MLC	3 levels	No PWM	0.6	1.00	0.57	1	0
		2 kHz	0.6	1.00	0.59	0.5	0.5
		5 kHz	0.6	1.00	0.61	0	1
		10 kHz	0.6	1.00	0.65	0	1
	4 levels	No PWM	0.8	0.43	0.76	1	0
		2 kHz	0.8	0.43	0.77	0.5	0.5
		5 kHz	0.8	0.43	0.79	0	1
		10 kHz	0.8	0.43	0.82	0	1
	5 levels	No PWM	1	0.17	0.95	1	0
		2 kHz	1	0.17	0.96	0.5	0.5
		5 kHz	1	0.17	1.00	0	1
		10 kHz	1	0.17	1.00	0	1
MLC with unfolding frontend	3 levels	No PWM	0.5	1.00	0.48	1	0
		2 kHz	0.5	1.00	0.49	0.5	0.5
		5 kHz	0.5	1.00	0.52	0	1
		10 kHz	0.5	1.00	0.55	0	1
	4 levels	No PWM	0.6	0.43	0.57	1	0
		2 kHz	0.6	0.43	0.58	0.5	0.5
		5 kHz	0.6	0.43	0.60	0	1
		10 kHz	0.6	0.43	0.63	0	1
	5 levels	No PWM	0.7	0.17	0.67	1	0
		2 kHz	0.7	0.17	0.68	0.5	0.5
		5 kHz	0.7	0.17	0.71	0	1
		10 kHz	0.7	0.17	0.71	0	1

Figure 4.6. shows the values of the calculated fitness function values.

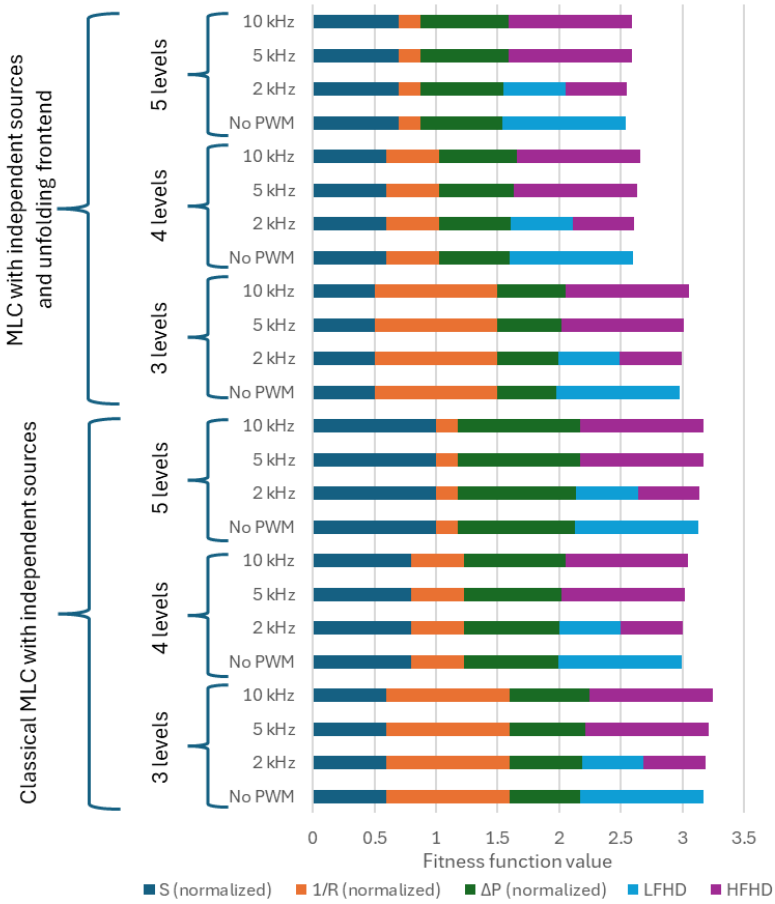

Fig. 4.6. Comparison of classical MLC with independent sources and unfolding MLC with independent sources at different level count and different modulation frequencies by means of fitness function (lower is better).

5. MULTILEVEL CONVERTERS WITH INDEPENDENT SOURCES AND HYBRID MODULTAION

Author's publications X [102] and V [103], patent XIII and unpublished publication IV are related to Chapter 5.

5.1. Multilevel converters with hybrid modulation in DC-DC applications

Separate regulation of the current or light flux of individual LED strings (segmented LED light source, SLLS) is associated with a known problem: the necessity of using a controllable LED driver for each string, which increases the total component count, overall system complexity and costs. Therefore, a special multiple-channel LED driving approach (single-inductor multiple-output (SIMO) current source mode (CSM) LED driver) has been chosen to overcome the shortcomings mentioned above. The same multiple-output driving approach can be useful in many other LED applications such as horticultural lighting, controllable RGB ambient lighting, adjustable correlated color temperature applications, matrix automotive lighting, etc. The approach itself can be considered as a multilevel current and light regulation method with fluent control between levels. The current regulation in the given application is not the primary goal (the primary goal is light regulation) and it is not explicit. However, having an isolating and parallelizing current commutating matrix and combining it with a set of simplified uncontrolled current sources with one controlled current source, it becomes possible to achieve more straightforward and explicit current regulation that widens the range of potential applications. For instance, it enables the use of a similar approach in battery applications—BESSs and chargers for larger or smaller AEV.

To control individual LED strings SIMO CSM driver approach (which by itself can be represented as a multilevel structure) was derived and multilevel structure with constant current source (CCS) and light flux regulator (LR) was proposed (shown at Figure 5.1.(a)). Each LR1 is constructed as a combination (series connection) of single current regulator CR1 and a chosen number of current switches CS1y, which are controllable switches Q31y connected in parallel with light-emitting diodes LED1y1 … LED1yz, where y is the numbering index for current switches, while z is the numbering index for LEDs. Current regulator CR1 consists of capacitor C21 connected in parallel with LED11 … LED1z, they are connected in series with an uncontrolled switch—diode VD21 (which, in general, can also be a controllable switch). Controllable power switch Q21 is connected in parallel with all these components. Q21 is controlled by a PWM signal. The average current value $I_{LED,CR1}$ of the CR1 branch of light diodes LED11 … LED1z depends on the value of the transistor Q21 control signal duty cycle D_{Q21} and the constant current value I_{L1}, and is equal to:

$$I_{LED,CR1} = I_{L1} \cdot (1 - D_{Q21}) \tag{5.1}$$

LR implementation in such configuration allow the control of light flux with the help of hybrid modulation – 1 stage is controlled by PWM signal, other stages are turned on and off

fully. This, in turn, makes this proposed multilevel structure similar to MLC with independent sources, but in this case light flux is being controlled.

To optimize the number of controllable switches in LR, it is possible to choose binary-weighted LED numbers in the CSxy branches, *x* is the numbering index of LRs and CRs (as it is shown at Fig. 5.1.(a)).

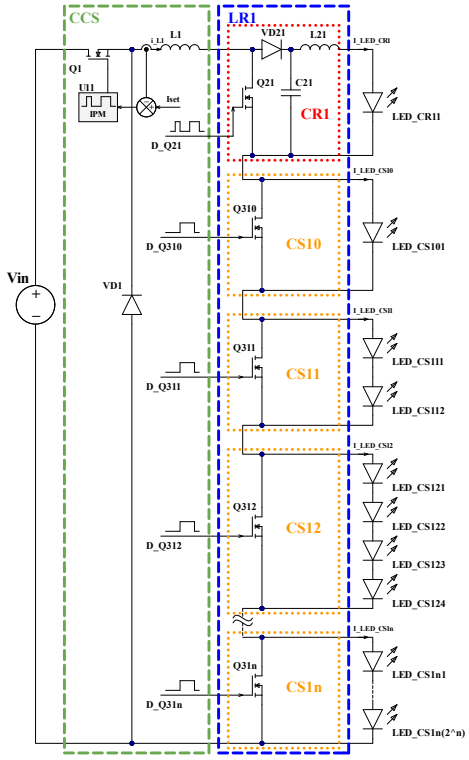

(a)

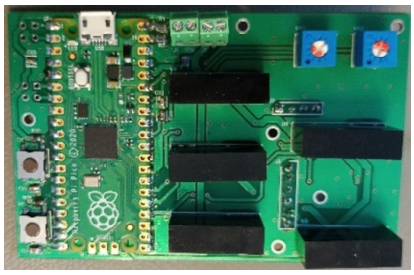

(b)

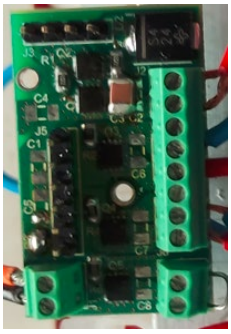

(c)

Fig. 5.1. (a) Implementation of light flux regulator in CSM SIMO LED driver using binary-weighted LEDs, (b) Prototype of control and FET driver board, (c) Prototype of power part

For experimental validation, the prototype of the proposed modified SIMO driver was built by combining CCS based on an MP24833 LED driver IC and one LR stage. The LR for testing purposes was built on two separate stackable PCBs/boards, splitting the power and control parts. The LR stage (power part, which is shown in Fig. 5.1.(c)) of the prototype is configured as the combination of one current regulator CR1 with four current switches, CS0 … CS3. For testing purposes, the most robust FET driving circuit configuration was selected for implementation in the prototype board: isolated gate drivers with an isolated supply for each driver. The control system was implemented using LR RP2040 microcontroller. For testing purposes, two control parameter input methods were implemented: (1) by trimmer and MCU readings of its set value on ADC input and (2) by “increase”/“decrease” push-buttons. A board of the control parts of the prototype is shown in Fig. 5.1.(b). The testing setup for the

experimental validation of the proposed LR is shown in Figure 5.2. Summaries of the initial tests are given in Figures 5.3. and 5.4.

The experimental validation of single LR stage luminous flux regulation is shown in Figure 5.3. The measurements were made with an indirect method using a luxmeter at the central point below the LED module. Correspondence of the control signals to the illuminance at the center point below the LED module at 1.1 m distance is shown there. The tests were conducted with the white, high-power LEDs available in the laboratory: Seoul Semiconductor W724C0 LEDs. The configuration of the module was made as shown in Figure 5.1.(a), except for the number of CS stages (three stages). The placement of LEDs is close to each other, but not perfectly symmetrical. Thus, the deviation of the experimental points across a linear interpolation is seen in Figure 5.3., close to the transition points when switching to the next CS combination state.

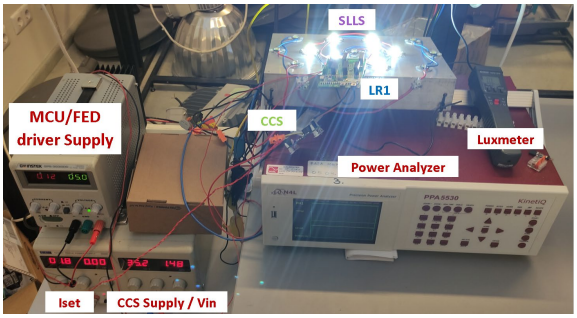

Fig. 5.2. Testing setup for experimental validation.

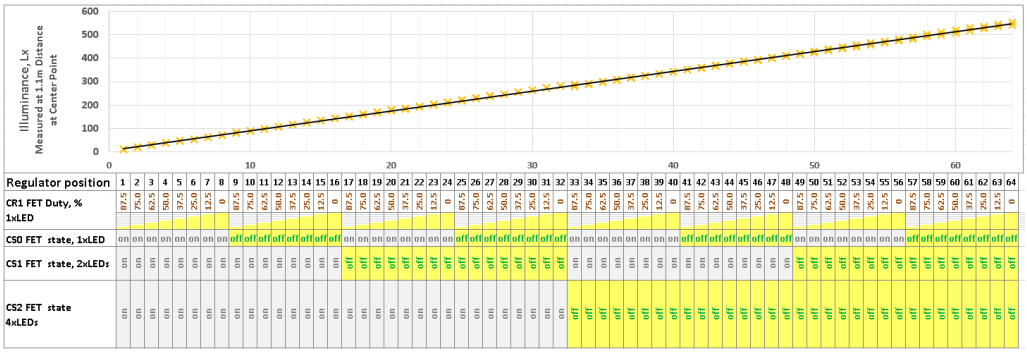

Fig. 5.3. Experimental validation of single LR stage: correspondence of control signals to the illuminance at center point below LED module at 1.1 m distance.

The assessment of the efficiency of the proposed system configuration is given in Figure 5.4. The tests for all dimming options were performed in similar conditions to the LED module mentioned above, with the maximum output power approximately 50 W using eight LEDs in total. Input voltage in all conducted experiments was the same, 35 V. The data obtained using PPA5530 precision power analyzer were used for this experimental efficiency validation. It is seen here that the efficiency of the bare CCS part is noticeably better in comparison with the combination of CCS + current regulator (CR), which is the price for using such a kind of SIMO

driver in high-power applications. However, as can be seen from Figure 5.4., some efficiency improvements can be achieved using the proposed configuration with light regulator stages.

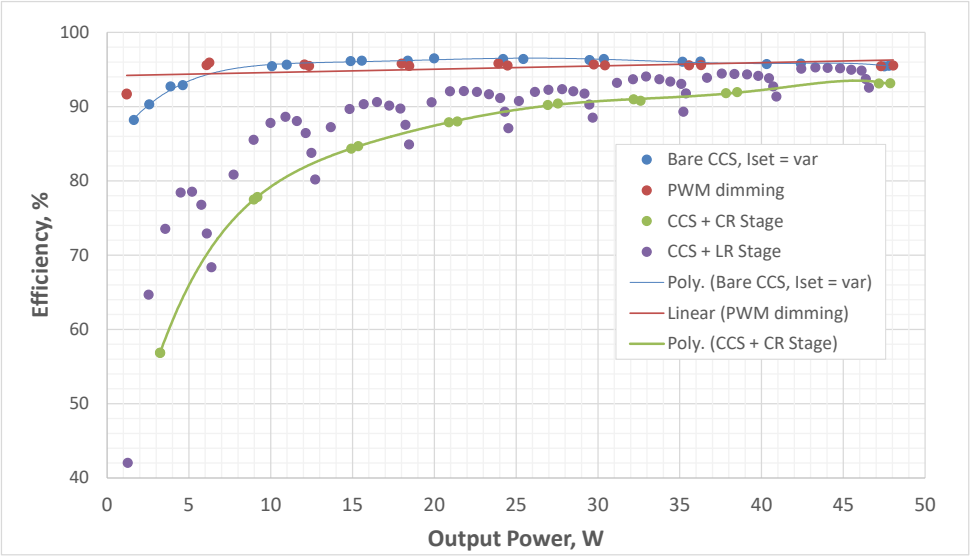

Fig. 5.4. Comparison of the efficiency of different dimmable system configurations by the assessment of experimental data at similar conditions

5.2. Multilevel converters with independent sources and hybrid modulation in DC-AC applications

As it was mentioned in Chapter 4, application of unfolding frontend together with MLC with independent sources allows to reduce switch count without losing the advantages of converter. However, considering applications with batteries and voltage dependence on SOC, as well as the fact that both full transistor bridge and half-bridge are operating only in buck-mode, number of battery cells connected as MLC inputs should be chosen in respect with fully discharged battery cell voltage, which is not always an option. The other option is to ensure voltage pre-regulation with additional conversion stage. Such approach was proposed in [103], where to the structure of MLC with independent sources and unfolding frontend buck-boost stage between the batteries and the half-bridges was added. This allows to regulate the voltage of each module connected in series. Proposed converter structure is shown in Figure 5.5.

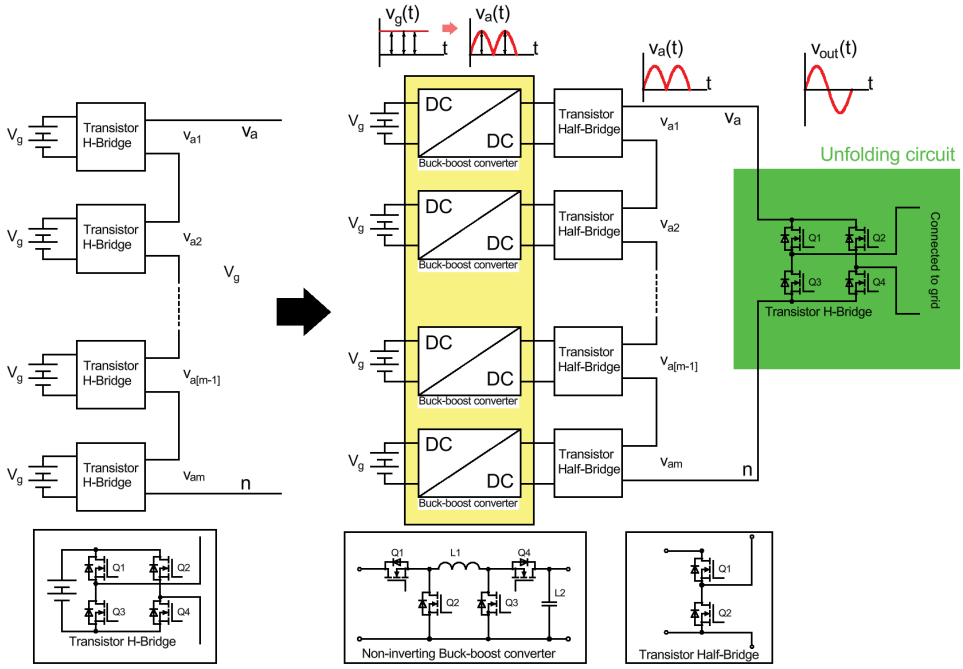

Fig. 5.5. MLC with independent sources, unfolding frontend and pre-regulation stage.

However, considering additional conversion stage for each series connected sub-module and significant increase of switches (which would cause increase of switching losses), this solution is out of practical interest.

But, in different configuration, by combining MLC with unfolder and hybrid modulation, described in subchapter 5.1., it is possible to achieve fluent waveform regulation without losing advantages of MLC with independent sources. New configuration of MLC with unfolding frontend and hybrid modulation is shown in Figure 5.6.

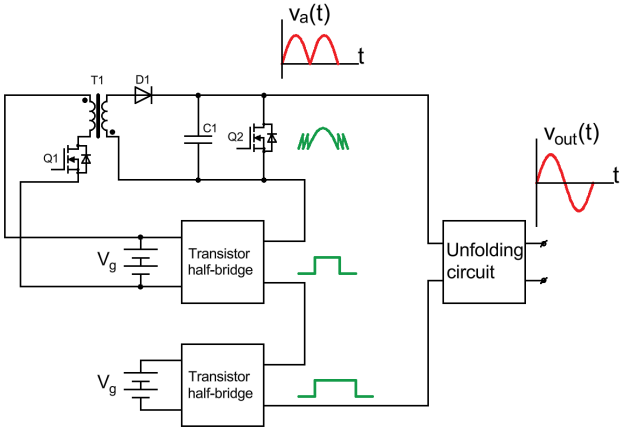

Fig. 5.6. MLC with independent sources, unfolding frontend and hybrid modulation.

As it is shown in Figure 5.6., flyback converter is added to the structure of two-level MLC with unfolder. Flyback converter is capable to operate both in buck and boost modes, and by constantly changing duty cycle according to the reference signal, can regulate output waveforms, while series connected half bridges operate in “on” / “off” mode (without PWM modulation). Operation principles of flyback are derived from [104]. To ensure bidirectional operation, switch Q2 is added to the schematic. Flyback operation modes are shown in Figure 5.7.

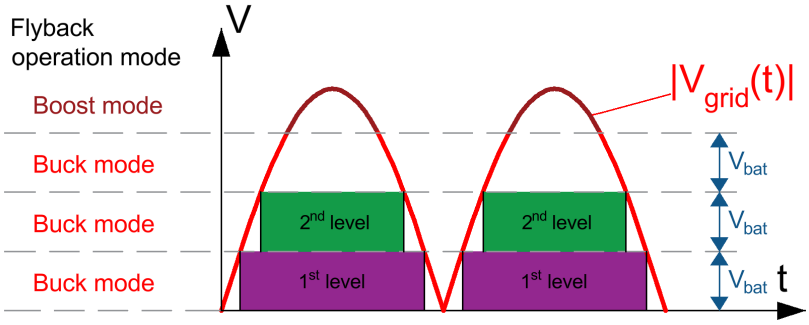

Fig. 5.7. Flyback and half-bridge operation modes.

To evaluate proposed topology Matlab/Simulink model was developed (shown in Figure 5.8.). Primary model parameters are shown in Table 5.1.

Table 5.1.

Simulation model parameters.

Parameter	Value
Input voltage	2 batteries, 100 V each
Output voltage	AC 50 Hz, 325 V peak
Load	R = 20 Ω
Flyback transformer parameters	L1 = L2 = 4 μH, Coupling coefficient = 0.99
Flyback output capacitor	20 μF
Flyback voltage closed loop PI controller parameters	K_P = 0.449; K_I = 0.000398
Flyback switching frequency	100 kHz

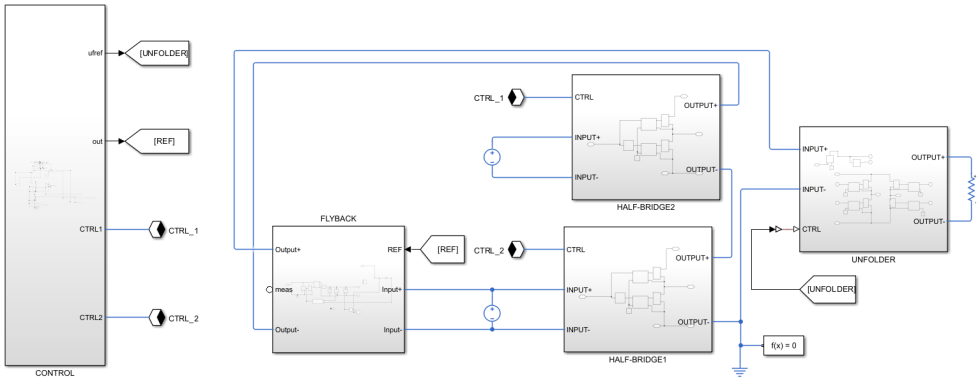

Fig. 5.8. Matlab/Simulink model of proposed MLC configuration.

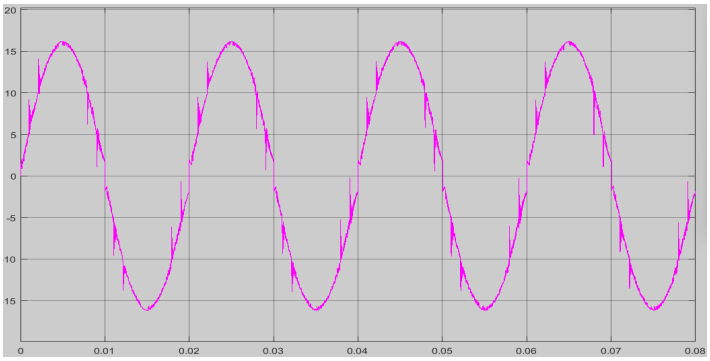

Fig. 5.9. Simulated current waveform of proposed topology.

Shown in Fig. 5.9. simulated current waveform shows working capability of the proposed topology. Current spikes are visible on obtained waveform, which are appearing during half-bridge module commutation. This can be explained by the insufficient reaction time of the control system (voltage closed loop control was implemented in the model).

CONCLUSIONS

The study of classical multilevel converter topologies has led to conclusions about the applications of these topologies with batteries, especially multilevel converters with independent sources being more distinguished for that application. This topology has natural battery balancing capability, which is an advantage in applications with batteries.

A novel source balancing method during one period of output voltage for multilevel converters with independent sources was proposed. The method was validated with the help of a simulation model; the results indicate balanced discharge of a three-phase multilevel converter with independent sources.

Several configurations of multilevel converters with independent sources were proposed to enhance the properties of the classical multilevel converter with independent sources topology without losing all the topology advantages.

The impact of the application of the unfolding circuit on power electronic converters was analyzed. Due to low commutation frequency, the unfolding circuit reduces overall switching losses of a converter compared with the pulse-mode frontend. By integrating an unfolding circuit with a multilevel converter with independent sources, it is possible to simplify the multilevel converter topology and reduce the number of switches in the current path. Comparison of classical MLC with independent sources and unfolding MLC with independent sources has been performed with the help of a mathematical model for loss evaluation and with the help of a fitness function. It can be concluded:

- Use of an unfolding frontend enables the opportunity for switch reduction. The effect is more noticeable if the level count is higher. Switch count of unfolding MLC is 1.2 times lower in the case of 3-level converter and 1.43 times lower in the case of 5 levels (compared with classical MLC).
- Lower switch count results in lower overall converter power losses. Power losses are 1.2 times lower in the case of 3-level unfolding MLC with independent sources and 1.4 times lower in the case of 5-level unfolding MLC.
- Higher PWM frequency results in lower low-frequency distortion and higher high-frequency distortion. High-frequency distortion imposes conditions for the output filter. However, high frequencies can be filtered. Low-frequency distortion is difficult to filter without corrupting output waveforms.

With the switch count decrease, the converter losses are also decreased, thereby confirming the proposed hypothesis.

A hybrid modulation method for multilevel converters was proposed and adapted for LED applications. A multilevel structure was developed, which is not a classical multilevel converter with independent sources. However, the operating principles are the same in relation to light flux. After experimental verification of the systems, it can be concluded that although in terms of efficiency the proposed solution is not superior to current source mode dimming driver (reaching up to 94 % maximal efficiency at higher power, with lower efficiency at lower power – starting from 42 % efficiency), in terms of light flux regulation gives the ability of fluent control of light flux.

The same modulation method can be applied to a multilevel converter with independent sources and an unfolding circuit. By adding a flyback converter to the multilevel structure (and the flyback converter input connecting to one of the half-bridge sources), fluent output waveform regulation can be achieved, saving all the multilevel converter advantages. The proposed solution was evaluated using a simulation model, and the results confirm the functionality of the proposed solution; however, some improvements in the control system are required.

Solutions described in this Doctoral Thesis were implemented in four national and international research projects.

REFERENCES

[1] I. A. Galkin, A. Blinov, M. Vorobyov, A. Bubovich, R. Saltanovs, and D. Peftitsis, "Interface Converters for Residential Battery Energy Storage Systems: Practices, Difficulties and Prospects," *Energies 2021, Vol. 14, Page 3365*, vol. 14, no. 12, p. 3365, Jun. 2021, doi: 10.3390/EN14123365.

[2] A. Bubovich, M. Vorobyov, I. Galkin, A. Blinov, and A. Giannakis, "Overview of Bidirectional Unfolding Converters for Battery Energy Storage Systems," *2022 IEEE 13th International Symposium on Power Electronics for Distributed Generation Systems, PEDG 2022*, 2022, doi: 10.1109/PEDG54999.2022.9923093.

[3] R. Spotnitz, "Introduction to Batteries | IEEE Courses | IEEE Xplore." Accessed: Sep. 24, 2022. [Online]. Available: https://ieeexplore.ieee.org/courses/details/EDP351

[4] X. Hu, C. Zou, C. Zhang, and Y. Li, "Technological Developments in Batteries: A Survey of Principal Roles, Types, and Management Needs," *IEEE Power and Energy Magazine*, vol. 15, no. 5, pp. 20–31, Sep. 2017, doi: 10.1109/MPE.2017.2708812.

[5] "Electricity storage and renewables: Costs and markets to 2030," 2017. Accessed: Sep. 24, 2022. [Online]. Available: https://www.irena.org/publications/2017/oct/electricity-storage-and-renewables-costs-and-markets

[6] J. Cao and A. Emadi, "Batteries need electronics: Battery management systems vary according to chemistry and applications," *IEEE Industrial Electronics Magazine*, vol. 5, no. 1, pp. 27–35, Mar. 2011, doi: 10.1109/MIE.2011.940251.

[7] B. Ferreira, "Batteries, the New Kids on the Block," *IEEE Power Electronics Magazine*, vol. 6, no. 4, pp. 32–34, Dec. 2019, doi: 10.1109/MPEL.2019.2947980.

[8] C. Chen, S. Plunkett, M. Salameh, S. Stoyanov, S. Al-Hallaj, and M. Krishnamurthy, "Enhancing the Fast Charging Capability of High-Energy-Density Lithium-Ion Batteries: A Pack Design Perspective," *IEEE Electrification Magazine*, vol. 8, no. 3, pp. 62–69, Sep. 2020, doi: 10.1109/MELE.2020.3005700.

[9] "Energy." Accessed: Sep. 24, 2022. [Online]. Available: https://energy.ec.europa.eu/index_en

[10] G. Fulli, M. Masera, A. Spisto, and S. Vitiello, "A change is coming: How regulation and innovation are reshaping the european union's electricity markets," *IEEE Power and Energy Magazine*, vol. 17, no. 1, pp. 53–66, Jan. 2019, doi: 10.1109/MPE.2018.2872303.

[11] S. M. Lukic and A. Emadi, "Charging ahead," *IEEE Industrial Electronics Magazine*, vol. 2, no. 4, pp. 2–12, 2008, doi: 10.1109/MIE.2008.930361.

[12] A. Khaligh and Z. Li, "Battery, ultracapacitor, fuel cell, and hybrid energy storage systems for electric, hybrid electric, fuel cell, and plug-in hybrid electric vehicles: State of the art," *IEEE Trans Veh Technol*, vol. 59, no. 6, pp. 2806–2814, Jul. 2010, doi: 10.1109/TVT.2010.2047877.

[13] J. Quirós-Tortós, L. Ochoa, and T. Butler, "How electric vehicles and the grid work together: Lessons learned from one of the largest electric vehicle trials in the world,"

IEEE Power and Energy Magazine, vol. 16, no. 6, pp. 64–76, 2018, doi: 10.1109/MPE.2018.2863060.

[14] N. Chen, J. Ma, M. Li, M. Wang, and X. Shen, "Energy management framework for mobile vehicular electric storage," *IEEE Netw*, vol. 33, no. 6, pp. 148–155, Nov. 2019, doi: 10.1109/MNET.2019.1800546.

[15] S. Chandler, J. Gartner, and D. Jones, "Integrating electric vehicles with energy storage and grids: New technology and specific capabilities spur numerous applications," *IEEE Electrification Magazine*, vol. 6, no. 3, pp. 38–43, Sep. 2018, doi: 10.1109/MELE.2018.2849899.

[16] S. Al-Rubaye, A. Al-Dulaimi, and Q. Ni, "Power Interchange Analysis for Reliable Vehicle-to-Grid Connectivity," *IEEE Communications Magazine*, vol. 57, no. 8, pp. 105–111, Aug. 2019, doi: 10.1109/MCOM.2019.1800657.

[17] P. Arboleya, P. Bidaguren, and U. Armendariz, "Energy is on board: Energy storage and other alternatives in modern light railways," *IEEE Electrification Magazine*, vol. 4, no. 3, pp. 30–41, Sep. 2016, doi: 10.1109/MELE.2016.2584938.

[18] P. Sinhuber, W. Rohlfs, and D. U. Sauer, "Study on power and energy demand for sizing the energy storage systems for electrified local public transport buses," *2012 IEEE Vehicle Power and Propulsion Conference, VPPC 2012*, pp. 315–320, Jan. 2012, doi: 10.1109/VPPC.2012.6422680.

[19] M. Guarnieri, M. Morandin, A. Ferrari, P. Campostrini, and S. Bolognani, "Electrifying water buses," *IEEE Industry Applications Magazine*, vol. 24, no. 1, pp. 71–83, Jan. 2018, doi: 10.1109/MIAS.2017.2739998.

[20] A. J. Sorensen *et al.*, "Toward Safer, Smarter, and Greener Ships: Using Hybrid Marine Power Plants," *IEEE Electrification Magazine*, vol. 5, no. 3, pp. 68–73, Sep. 2017, doi: 10.1109/MELE.2017.2718861.

[21] D. Paul, "A History of Electric Ship Propulsion Systems [History]," *IEEE Industry Applications Magazine*, vol. 26, no. 6, pp. 9–19, Nov. 2020, doi: 10.1109/MIAS.2020.3014837.

[22] A. Vicenzutti, D. Bosich, G. Giadrossi, and G. Sulligoi, "The Role of Voltage Controls in Modern All-Electric Ships: Toward the all electric ship," *IEEE Electrification Magazine*, vol. 3, no. 2, pp. 49–65, Jun. 2015, doi: 10.1109/MELE.2015.2413437.

[23] X. Roboam, B. Sareni, and A. Andrade, "More electricity in the air: Toward optimized electrical networks embedded in more-electrical aircraft," *IEEE Industrial Electronics Magazine*, vol. 6, no. 4, pp. 6–17, 2012, doi: 10.1109/MIE.2012.2221355.

[24] A. Misra, "Energy storage for electrified aircraft: The need for better batteries, fuel cells, and supercapacitors," *IEEE Electrification Magazine*, vol. 6, no. 3, pp. 54–61, Sep. 2018, doi: 10.1109/MELE.2018.2849922.

[25] M. Crittenden, "Ultralight batteries for electric airplanes," *IEEE Spectr*, vol. 57, no. 9, pp. 44–49, Sep. 2020, doi: 10.1109/MSPEC.2020.9173903.

[26] M. Stecca, L. R. Elizondo, T. B. Soeiro, P. Bauer, and P. Palensky, "A comprehensive review of the integration of battery energy storage systems into distribution networks,"

IEEE Open Journal of the Industrial Electronics Society, vol. 1, no. 1, pp. 46–65, 2020, doi: 10.1109/OJIES.2020.2981832.

[27] D. Manz, R. Piwko, and N. Miller, "Look before you leap: The role of energy storage in the grid," *IEEE Power and Energy Magazine*, vol. 10, no. 4, pp. 75–84, 2012, doi: 10.1109/MPE.2012.2196337.

[28] M. Farrokhabadi *et al.*, "Energy Storage in Microgrids: Compensating for Generation and Demand Fluctuations while Providing Ancillary Services," *IEEE Power and Energy Magazine*, vol. 15, no. 5, pp. 81–91, Sep. 2017, doi: 10.1109/MPE.2017.2708863.

[29] A. Cagnano, E. de Tuglie, and P. Mancarella, "Microgrids: Overview and guidelines for practical implementations and operation," *Appl Energy*, vol. 258, p. 114039, Jan. 2020, doi: 10.1016/J.APENERGY.2019.114039.

[30] J. L. Torres-Moreno, A. Gimenez-Fernandez, M. Perez-Garcia, and F. Rodriguez, "Energy Management Strategy for Micro-Grids with PV-Battery Systems and Electric Vehicles," *Energies 2018, Vol. 11, Page 522*, vol. 11, no. 3, p. 522, Feb. 2018, doi: 10.3390/EN11030522.

[31] P. Lezynski, P. Szczesniak, B. Waskowicz, R. Smolenski, and W. Drozdz, "Design and Implementation of a Fully Controllable Cyber-Physical System for Testing Energy Storage Systems," *IEEE Access*, vol. 7, pp. 47259–47272, 2019, doi: 10.1109/ACCESS.2019.2907612.

[32] Z. Ma, A. Pesaran, V. Gevorgian, D. Gwinner, and W. Kramer, "Energy Storage, Renewable Power Generation, and the Grid: NREL Capabilities Help to Develop and Test Energy-Storage Technologies," *IEEE Electrification Magazine*, vol. 3, no. 3, pp. 30–40, Sep. 2015, doi: 10.1109/MELE.2015.2447972.

[33] E. Rodriguez-Diaz, F. Chen, J. C. Vasquez, J. M. Guerrero, R. Burgos, and D. Boroyevich, "Voltage-Level Selection of Future Two-Level LVdc Distribution Grids: A Compromise between Grid Compatibiliy, Safety, and Efficiency," *IEEE Electrification Magazine*, vol. 4, no. 2, pp. 20–28, Jun. 2016, doi: 10.1109/MELE.2016.2543979.

[34] "Tesla Powerwall 3 - Datasheet." Accessed: Feb. 23, 2025. [Online]. Available: https://energylibrary.tesla.com/docs/Public/EnergyStorage/Powerwall/3/Datasheet/en-us/Powerwall-3-Datasheet.pdf

[35] "Tesla Powerwall 2 - Datasheet." Accessed: Feb. 23, 2025. [Online]. Available: https://energylibrary.tesla.com/docs/Public/EnergyStorage/Powerwall/2/Datasheet/en-us/Powerwall-2-Datasheet.pdf

[36] "Tesla Powerwall+ - Datasheet." Accessed: Feb. 23, 2025. [Online]. Available: https://energylibrary.tesla.com/docs/Public/EnergyStorage/Powerwall/+/Datasheet/en-us/Powerwall-+-Datasheet.pdf

[37] "sonnenBatterie 10 | sonnen." Accessed: Feb. 23, 2025. [Online]. Available: https://sonnenbatterie.co.uk/products/sonnenbatterie-10/

[38] "sonnenBatterie Hybrid | sonnen." Accessed: Feb. 23, 2025. [Online]. Available: https://sonnenbatterie.co.uk/products/sonnenbatterie-hybrid/

[39] "Powervault P4 • Powervault." Accessed: Feb. 23, 2025. [Online]. Available: https://www.powervault.co.uk/products/powervault-p4/

[40] “PURESTORAGE-II AC 5/10KWH.” Accessed: Feb. 23, 2025. [Online]. Available: https://www.puredrive-energy.co.uk/wp-content/uploads/2025/01/PSII-AC-All-in-One-V2.pdf

[41] “Dura5 - Stack or Wall-Mount Battery.” Accessed: Feb. 23, 2025. [Online]. Available: https://www.duracellenergy.com/wp-content/uploads/2025/02/Dura5-Datasheet-V5.4-UK-web-PD.pdf

[42] “Dura-i Inverter.” Accessed: Feb. 23, 2025. [Online]. Available: https://www.duracellenergy.com/wp-content/uploads/2024/12/Dura-i-Inverter-Datasheet-V5.4-web-UK.pdf

[43] “Enphase Encharge 3.” Accessed: Feb. 23, 2025. [Online]. Available: https://enphase.com/sites/default/files/2021-04/Encharge-3-DS-EN-US_0.pdf?srsltid=AfmBOookPWleCNX3O2Xbw8Q9nx9W7Bittvhu6zwB_-Eau6aWCnjKRZhK

[44] “Enphase Encharge 10.” Accessed: Feb. 23, 2025. [Online]. Available: https://enphase.com/sites/default/files/2021-04/Encharge-10-DS-EN-US.pdf?srsltid=AfmBOordpQrwujf39eAozvXfF140XKBbTCKvgCXb2etv1rm2dEJUJDgR

[45] “xStorage Home | Energy Storage | Eaton.” Accessed: Feb. 23, 2025. [Online]. Available: https://www.eaton.com/gb/en-gb/catalog/energy-storage/xstorage-home.html

[46] “SAMSUNG SDI - ENERGY STORAGE SYSTEM for Home.” Accessed: Feb. 23, 2025. [Online]. Available: https://samsungsdi.com/upload/ess_brochure/ESS%20for%20Residential.pdf

[47] “VARTA pulse / pulse neo.” Accessed: Feb. 23, 2025. [Online]. Available: https://www.varta-ag.com/fileadmin/varta_storage/downloads/products/energy/varta-pulse/Datasheet_VARTA_pulse_en_17.pdf

[48] “EasySolar-II - Datasheet.” Accessed: Feb. 23, 2025. [Online]. Available: https://www.victronenergy.com/upload/documents/Datasheet-EasySolar-II-24V-48V-3kVA-48V-5kVA-MPPT-250-70-100-GX-EN.pdf

[49] “SolaX X3 HYBRID G4 | 3 phase MPPT hybrid solar inverter.” Accessed: Feb. 23, 2025. [Online]. Available: https://www.solaxpower.com/products/x3-hybrid-g4/

[50] “SolaX T-BAT-SYS-HV-5.8 | LiFePO4 Battery For Solar System.” Accessed: Feb. 23, 2025. [Online]. Available: https://www.solaxpower.com/products/t-bat-sys-hv-5-8/

[51] “Power your home with SolarEdge Home Hub Inverters | SolarEdge.” Accessed: Feb. 23, 2025. [Online]. Available: https://www.solaredge.com/en/products/residential/pv-inverters/solaredge-home-hub-inverters

[52] “Residential Solutions: SolarEdge Home Battery 400V | SolarEdge.” Accessed: Feb. 23, 2025. [Online]. Available: https://www.solaredge.com/en/products/residential/storage-and-backup/solaredge-home-battery-400v

[53] “AlphaESS SMILE-T10-HV 10kW Solar System With Battery Storage For Sale.” Accessed: Feb. 23, 2025. [Online]. Available: https://www.alphaess.com/smile-t10-hv-10kw-residential-energy-storage-system

[54] “High Voltage Lithium Stackable Solar Battery 204.8V - 716.8V.” Accessed: Feb. 23, 2025. [Online]. Available: https://bslbatt.com/hv-battery-home/high-voltage-lithium-stackable-solar-battery/

[55] “High Voltage Inverter Integrated Home LiFePo4 Battery - ETEKWARE Battery.” Accessed: Feb. 23, 2025. [Online]. Available: https://etekware.com/product/high-voltage-inverter-integrated-home-lifepo4-battery/

[56] “Sunny Boy Storage 3.7 / 5.0 / 6.0 | SMA Solar.” Accessed: Feb. 23, 2025. [Online]. Available: https://www.sma.de/en/products/battery-inverters/sunny-boy-storage-37-50-60

[57] “FoxESS Stackable AIO.” Accessed: Feb. 23, 2025. [Online]. Available: https://www.fox-ess.com/wp-content/uploads/2025/02/EN-Stackable-AIO-PQ-datasheet-V1.2-20241227.pdf

[58] A. Bubovich, M. Vorobyov, A. Blinov, and D. Peftitsis, “Peculiarities of Multilevel Power Electronic Converters for Interfacing Battery Energy Storages with AC Loads,” *2020 IEEE 8th Workshop on Advances in Information, Electronic and Electrical Engineering, AIEEE 2020 - Proceedings*, Apr. 2021, doi: 10.1109/AIEEE51419.2021.9435798.

[59] A. Bubovich and I. Galkin, “Evaluation of Optimal Switching of Modular Multilevel Inverter with Independent Voltage Sources,” in *2020 IEEE 61st Annual International Scientific Conference on Power and Electrical Engineering of Riga Technical University, RTUCON 2020 - Proceedings*, Institute of Electrical and Electronics Engineers Inc., Nov. 2020. doi: 10.1109/RTUCON51174.2020.9316581.

[60] I. Colak, E. Kabalci, and R. Bayindir, “Review of multilevel voltage source inverter topologies and control schemes,” *Energy Convers Manag*, vol. 52, no. 2, pp. 1114–1128, Feb. 2011, doi: 10.1016/j.enconman.2010.09.006.

[61] A. Nabae, I. Takahashi, and H. Akagi, “A New Neutral-Point-Clamped PWM Inverter,” *IEEE Trans Ind Appl*, vol. IA-17, no. 5, pp. 518–523, 1981, doi: 10.1109/TIA.1981.4503992.

[62] S. Khomfoi and L. M. Tolbert, “Multilevel Power Converters,” in *Power Electronics Handbook*, 2nd ed., Elsevier Inc., 2006, ch. 17, pp. 451–482. [Online]. Available: http://web.eecs.utk.edu/~tolbert/publications/multilevel_book_chapter.pdf

[63] M. Moradpour, P. Ghani, P. Pirino, and G. Gatto, “A GaN-Based Battery Energy Storage System for Three-Phase Residential Application with Series-Stacked Devices and Three-Level Neutral Point Clamped Topology,” in *SyNERGY MED 2019 - 1st International Conference on Energy Transition in the Mediterranean Area*, Institute of Electrical and Electronics Engineers Inc., May 2019. doi: 10.1109/SyNERGY-MED.2019.8764117.

[64] U. Abronzini *et al.*, “A Dual-Source DHB-NPC Power Converter for Grid Connected Split Battery Energy Storage System,” in *2018 IEEE Energy Conversion Congress and Exposition, ECCE 2018*, Institute of Electrical and Electronics Engineers Inc., Dec. 2018, pp. 2483–2488. doi: 10.1109/ECCE.2018.8557563.

[65] I. Trintis, S. Munk-Nielsen, and R. Teodorescu, “Single stage grid converters for battery energy storage,” in *IET Conference Publications*, 2010. doi: 10.1049/cp.2010.0016.

[66] T. A. Meynard and H. Foch, “Multi-level conversion: High voltage choppers and voltage-source inverters,” in *PESC Record - IEEE Annual Power Electronics Specialists Conference*, Institute of Electrical and Electronics Engineers Inc., 1992, pp. 397–403. doi: 10.1109/PESC.1992.254717.

[67] J. S. Lai and F. Z. Peng, “Multilevel converters - a new breed of power converters,” in *Conference Record - IAS Annual Meeting (IEEE Industry Applications Society)*, IEEE, 1995, pp. 2348–2356. doi: 10.1109/ias.1995.530601.

[68] J. Asakura and H. Akagi, “State-of-Charge (SOC)-Balancing Control of a Battery Energy Storage System Based on a Cascade PWM Converter,” *IEEE Trans Power Electron*, vol. 24, no. 6, pp. 1628–1636, 2009, doi: 10.1109/TPEL.2009.2014868.

[69] I. A. Galkin, R. Saltanovs, A. Bubovich, A. Blinov, and D. Peftitsis, “Considerations on Combining Unfolding Inverters with Partial Power Regulators in Battery–Grid Interface Converters,” *Energies 2024, Vol. 17, Page 893*, vol. 17, no. 4, p. 893, Feb. 2024, doi: 10.3390/EN17040893.

[70] O. Matiushkin, O. Husev, R. Strzelecki, S. Ivanets, and A. Fesenko, “Novel single-stage buck-boost inverter with unfolding circuit,” in *2017 IEEE First Ukraine Conference on Electrical and Computer Engineering (UKRCON)*, IEEE, May 2017, pp. 538–543. doi: 10.1109/UKRCON.2017.8100298.

[71] O. Husev, O. Matiushkin, C. Roncero-Clemente, F. Blaabjerg, and D. Vinnikov, “Novel Family of Single-Stage Buck-Boost Inverters Based on Unfolding Circuit,” *IEEE Trans Power Electron*, vol. 34, no. 8, pp. 7662–7676, 2019, doi: 10.1109/TPEL.2018.2879776.

[72] O. Matiushkin, O. Husev, C. Roncero-Clemente, S. Ivanets, and A. Fesenko, “Component design guidelines for new single-stage buck-boost inverter with unfolding circuit,” *2017 IEEE International Young Scientists Forum on Applied Physics and Engineering, YSF 2017*, vol. 2017-January, pp. 40–45, Dec. 2017, doi: 10.1109/YSF.2017.8126589.

[73] O. Matiushkin, O. Husev, D. Vinnikov, and C. Roncero-Clemente, “Model predictive control for buck-boost inverter based on unfolding circuit,” *2019 IEEE 2nd Ukraine Conference on Electrical and Computer Engineering, UKRCON 2019 - Proceedings*, pp. 431–436, Jul. 2019, doi: 10.1109/UKRCON.2019.8879870.

[74] R. W. Erickson and A. P. Rogers, “A microinverter for building-integrated photovoltaics,” *Conference Proceedings - IEEE Applied Power Electronics Conference and Exposition - APEC*, pp. 911–917, 2009, doi: 10.1109/APEC.2009.4802771.

[75] C. H. Chang and K. H. Ho, “A Transformer-Less High-Gain Inverter with Step-Up/Down and Single Energy-Processing Features,” *IEEE J Emerg Sel Top Power Electron*, vol. 9, no. 4, pp. 4726–4738, Aug. 2021, doi: 10.1109/JESTPE.2020.3023107.

[76] W. Wu, J. Ji, and F. Blaabjerg, “Aalborg inverter - A new type of ‘buck in buck, boost in boost’ grid-tied inverter,” *IEEE Trans Power Electron*, vol. 30, no. 9, pp. 4784–4793, Sep. 2015, doi: 10.1109/TPEL.2014.2363566.

[77] S. Zhang, W. Wu, H. Wang, M. Huang, N. Gao, and F. Blaabjerg, “Single-stage MPPT control realization for Aalborg inverter in photovoltaic system,” *Proceedings IECON*

2017 - 43rd Annual Conference of the IEEE Industrial Electronics Society, vol. 2017-January, pp. 4233–4238, Dec. 2017, doi: 10.1109/IECON.2017.8216726.

[78] W. Wu, Z. Wang, J. Ji, and F. Blaabjerg, "Performance analysis of new type grid-tied inverter-Aalborg Inverter," *2014 16th European Conference on Power Electronics and Applications, EPE-ECCE Europe 2014*, 2014, doi: 10.1109/EPE.2014.6910861.

[79] A. Diab-Marzouk and O. Trescases, "SiC-Based Bidirectional ĆUK Converter With Differential Power Processing and MPPT for a Solar Powered Aircraft," *IEEE Transactions on Transportation Electrification*, vol. 1, no. 4, pp. 369–381, Dec. 2015, doi: 10.1109/TTE.2015.2505302.

[80] D. Bortis, D. Neumayr, and J. W. Kolar, "ηρ-Pareto optimization and comparative evaluation of inverter concepts considered for the GOOGLE Little Box Challenge," *2016 IEEE 17th Workshop on Control and Modeling for Power Electronics, COMPEL 2016*, 2016, doi: 10.1109/COMPEL.2016.7556767.

[81] J. Everts, F. Krismer, J. Van Den Keybus, J. Driesen, and J. W. Kolar, "Optimal zvs modulation of single-phase single-stage bidirectional dab ac-dc converters," *IEEE Trans Power Electron*, vol. 29, no. 8, pp. 3954–3970, 2014, doi: 10.1109/TPEL.2013.2292026.

[82] J. Everts, F. Krismer, J. Van Den Keybus, J. Driesen, and J. W. Kolar, "Comparative evaluation of soft-switching, bidirectional, isolated AC/DC converter topologies," *Conference Proceedings - IEEE Applied Power Electronics Conference and Exposition - APEC*, pp. 1067–1074, 2012, doi: 10.1109/APEC.2012.6165951.

[83] L. Xue, Z. Shen, D. Boroyevich, P. Mattavelli, and D. Diaz, "Dual Active Bridge-Based Battery Charger for Plug-in Hybrid Electric Vehicle with Charging Current Containing Low Frequency Ripple," *IEEE Trans Power Electron*, vol. 30, no. 12, pp. 7299–7307, Dec. 2015, doi: 10.1109/TPEL.2015.2413815.

[84] H. S. Kim, M. H. Ryu, J. W. Baek, and J. H. Jung, "High-efficiency isolated bidirectional AC-DC converter for a DC distribution system," *IEEE Trans Power Electron*, vol. 28, no. 4, pp. 1642–1654, Apr. 2013, doi: 10.1109/TPEL.2012.2213347.

[85] A. Tong, L. Hang, G. Li, X. Jiang, and S. Gao, "Modeling and Analysis of a Dual-Active-Bridge-Isolated Bidirectional DC/DC Converter to Minimize RMS Current with Whole Operating Range," *IEEE Trans Power Electron*, vol. 33, no. 6, pp. 5302–5316, Jun. 2018, doi: 10.1109/TPEL.2017.2692276.

[86] W. Choi, K. M. Rho, and B. H. Cho, "Fundamental Duty Modulation of Dual-Active-Bridge Converter for Wide-Range Operation," *IEEE Trans Power Electron*, vol. 31, no. 6, pp. 4048–4064, Jun. 2016, doi: 10.1109/TPEL.2015.2474135.

[87] J. Hiltunen, V. Vaisanen, R. Juntunen, and P. Silventoinen, "Variable-Frequency Phase Shift Modulation of a Dual Active Bridge Converter," *IEEE Trans Power Electron*, vol. 30, no. 12, pp. 7138–7148, Dec. 2015, doi: 10.1109/TPEL.2015.2390913.

[88] N. Hou and Y. W. Li, "Overview and Comparison of Modulation and Control Strategies for a Nonresonant Single-Phase Dual-Active-Bridge DC-DC Converter," *IEEE Trans Power Electron*, vol. 35, no. 3, pp. 3148–3172, Mar. 2020, doi: 10.1109/TPEL.2019.2927930.

[89] Y. Shen, X. Sun, W. Li, X. Wu, and B. Wang, "A Modified Dual Active Bridge Converter with Hybrid Phase-Shift Control for Wide Input Voltage Range," *IEEE Trans Power Electron*, vol. 31, no. 10, pp. 6884–6900, Oct. 2016, doi: 10.1109/TPEL.2015.2510033.

[90] D. Sha, X. Wang, and D. Chen, "High-Efficiency Current-Fed Dual Active Bridge DC-DC Converter With ZVS Achievement Throughout Full Range of Load Using Optimized Switching Patterns," *IEEE Trans Power Electron*, vol. 33, no. 2, pp. 1347–1357, Feb. 2018, doi: 10.1109/TPEL.2017.2675945.

[91] M. H. Kheraluwala, R. W. Gascoigne, D. M. Divan, and E. D. Baumann, "Performance Characterization of a High-Power Dual Active Bridge dc-to-dc Converter," *IEEE Trans Ind Appl*, vol. 28, no. 6, pp. 1294–1301, 1992, doi: 10.1109/28.175280.

[92] S. A. Q. Mohammed and J. W. Jung, "A State-of-the-Art Review on Soft-Switching Techniques for DC-DC, DC-AC, AC-DC, and AC-AC Power Converters," *IEEE Trans Industr Inform*, vol. 17, no. 10, pp. 6569–6582, Oct. 2021, doi: 10.1109/TII.2021.3058218.

[93] "Design Guide: TIDA-010054 Bidirectional, Dual Active Bridge Reference Design for Level 3 Electric Vehicle Charging Stations," 2021.

[94] A. K. Jain and R. Ayyanar, "PWM control of dual active bridge: Comprehensive analysis and experimental verification," *IEEE Trans Power Electron*, vol. 26, no. 4, pp. 1215–1227, 2011, doi: 10.1109/TPEL.2010.2070519.

[95] D. Wang, W. Zhang, and J. Li, "A PWM plus phase shift control strategy for dual-active-bridge DC-DC converter in electric vehicle charging/discharging system," *IEEE Transportation Electrification Conference and Expo, ITEC Asia-Pacific 2014 - Conference Proceedings*, Oct. 2014, doi: 10.1109/ITEC-AP.2014.6940986.

[96] Z. Pavlović, J. A. Oliver, P. Alou, Ó. Garcia, and J. A. Cobos, "Bidirectional dual active bridge series resonant converter with pulse modulation," *Conference Proceedings - IEEE Applied Power Electronics Conference and Exposition - APEC*, pp. 503–508, 2012, doi: 10.1109/APEC.2012.6165867.

[97] H. Wu, K. Sun, Y. Li, and Y. Xing, "Fixed-Frequency PWM-Controlled Bidirectional Current-Fed Soft-Switching Series-Resonant Converter for Energy Storage Applications," *IEEE Transactions on Industrial Electronics*, vol. 64, no. 8, pp. 6190–6201, Aug. 2017, doi: 10.1109/TIE.2017.2682020.

[98] A. Blinov *et al.*, "High Gain DC-AC High-Frequency Link Inverter With Improved Quasi-Resonant Modulation," *IEEE Transactions on Industrial Electronics*, vol. 69, no. 2, pp. 1465–1476, Feb. 2022, doi: 10.1109/TIE.2021.3060657.

[99] A. Bubovich, M. Vorobyov, and A. Giannakis, "Initial Evaluation of a Multilevel Inverter with Unfolding Stage for BESS Applications," *Proceedings of the 9th IEEE Workshop on Advances in Information, Electronic and Electrical Engineering, AIEEE 2021*, 2021, doi: 10.1109/AIEEE54188.2021.9670386.

[100] H. Akagi, "Classification, terminology, and application of the modular multilevel cascade converter (MMCC)," *IEEE Trans Power Electron*, vol. 26, no. 11, pp. 3119–3130, 2011, doi: 10.1109/TPEL.2011.2143431.

[101] INTERNATIONAL ELECTROTECHNICAL COMMISSION, “IEC TR 61000-2-5 - Electromagnetic compatibility (EMC) – Part 2-5: Environment – Description and classification of electromagnetic environments.”

[102] O. Tetervenoks, I. Galkin, and A. Bubovich, “Considerations on Practical Implementation of Current Source Mode Single-Inductor Multiple-Output LED Driver,” *Electronics 2024, Vol. 13, Page 54*, vol. 13, no. 1, p. 54, Dec. 2023, doi: 10.3390/ELECTRONICS13010054.

[103] A. Bubovich, V. Parinova, I. Galkin, and A. Giannakis, “Initial Evaluation of Multilevel Converter with Unfolding Stage and Voltage Regulators for applications in BESSs,” *Proceedings of the Biennial Baltic Electronics Conference, BEC*, vol. 2022-October, 2022, doi: 10.1109/BEC56180.2022.9935611.

[104] Z. Zhao, J. S. Lai, and Y. Cho, “Dual-mode double-carrier-based sinusoidal pulse width modulation inverter with adaptive smooth transition control between modes,” *IEEE Transactions on Industrial Electronics*, vol. 60, no. 5, pp. 2094–2103, 2013, doi: 10.1109/TIE.2012.2227900.

APPENDICES / PUBLICATIONS

Only the accepted version of my articles, **not the final published version**, may be posted in online version of this Thesis.

Publication I

Galkin, I.A.; Blinov, A.; Vorobyov, M.; **Bubovich, A.**; Saltanovs, R.; Peftitsis, D. Interface Converters for Residential Battery Energy Storage Systems: Practices, Difficulties and Prospects. Energies 2021, 14, 3365. https://doi.org/10.3390/en14123365

energies

IMPACT FACTOR 3.0

CITESCORE 6.2

Article

Interface Converters for Residential Battery Energy Storage Systems: Practices, Difficulties and Prospects

Ilya A. Galkin, Andrei Blinov, Maxim Vorobyov, Alexander Bubovich, Rodions Saltanovs and Dimosthenis Peftitsis

Special Issue

Power Electronics and Energy Management for Battery Storage Systems

Edited by

Dr. Andrei Blinov and Prof. Dr. Sheldon Williamson

MDPI

https://doi.org/10.3390/en14123365

energies

MDPI

Article

Interface Converters for Residential Battery Energy Storage Systems: Practices, Difficulties and Prospects

Ilya A. Galkin [1,*], Andrei Blinov [2], Maxim Vorobyov [1], Alexander Bubovich [1], Rodions Saltanovs [1] and Dimosthenis Peftitsis [3]

[1] Faculty of Electrical and Environmental Engineering, Riga Technical University, LV1048 Riga, Latvia; maksims.vorobjovs@rtu.lv (M.V.); aleksandrs.bubovics@rtu.lv (A.B.); rodions.saltanovs@rtu.lv (R.S.)
[2] Department of Electrical Power Engineering and Mechatronics, Tallinn University of Technology, 19086 Tallinn, Estonia; andrei.blinov@taltech.ee
[3] Department of Electrical Power Engineering, Norwegian University of Science and Technology, NO-7491 Trondheim, Norway; dimosthenis.peftitsis@ntnu.no
* Correspondence: gia@eef.rtu.lv

Abstract: Recent trends in building energy systems such as local renewable energy generation have created a distinct demand for energy storage systems to reduce the influence and dependency on the electric power grid. Under the current market conditions, a range of commercially available residential energy storage systems with batteries has been produced. This paper addresses the area of energy storage systems from multiple directions to provide a broader view on the state-of-the-art developments and trends in the field. Present standards and associated limitations of storage implementation are briefly described, followed by the analysis of parameters and features of commercial battery systems for residential applications. Further, the power electronic converters are reviewed in detail, with the focus on existing and perspective non-isolated solutions. The analysis covers well-known standard topologies, including buck-boost and bridge, as well as emerging solutions based on the unfolding inverter and fractional/partial power converters. Finally, trends and future prospects of the residential battery storage technologies are evaluated.

Keywords: residential energy storage; battery energy storage systems; standards; grid interface converters; intellectual property; bidirectional converters; AC-DC power converters; DC-DC power converters; multilevel converters; partial power converters

Citation: Galkin, I.A.; Blinov, A.; Vorobyov, M.; Bubovich, A.; Saltanovs, R.; Peftitsis, D. Interface Converters for Residential Battery Energy Storage Systems: Practices, Difficulties and Prospects. *Energies* **2021**, *14*, 3365. https://doi.org/10.3390/en14123365

Academic Editor: Teuvo Suntio

Received: 31 March 2021
Accepted: 2 June 2021
Published: 8 June 2021

1. Introduction

Consumption of resources as well as their collection and processing are usually uneven. First of the all, it involves energy resources, traditionally, food and various fissile fuels. Nowadays, the necessity to store energy has gained new forms that are applied to the energy resources, specific for the dedicated technology equipment. This, in particular, regards electrical engineering, the rapid development of which during the last two centuries has formed the demand for storages of electrical energy even at the level of residential applications. During recent years, this tendency has become more topical due to several reasons. Firstly, renewable energy sources are in much wider use. In addition, this use is obliged by some administrative regulations like EU directives [1–3]. In spite of the irregular generation profile, the renewable energy sources are being installed even at the households. Secondly, the range and number of various household devices have expanded. There exist plenty of storages dedicated to electrical energy [4]. For example, it is possible to convert electrical energy into chemical (in the form of pure hydrogen) by means of electrolysis and then back—by means of a fuel cell [5]. However, in spite of the most recent achievements in the field of fuel cells [6,7] and development of converter technologies for fuel cells [8], the most functional, reliable and energy efficient equipment for electrical energy is an electrochemical battery energy storage (BES) system.

The constantly increasing number of papers (Figure 1) devoted to battery energy storage systems (BESSs) proves the importance of these energy storage devices in various applications. These papers address all aspects of their use, but particular attention is paid to the interface converters of BESSs. The numerous review papers devoted to this topic [9–12] describe a generalized state of the art in this field. Typically, they evaluate which converter schemes are more energy efficient, with a reduced component count and lower voltage/current stresses. At the same time, the role and peculiarities of the interface converters in the context of the BESS structure are usually not clear-cut and detailed in these reports.

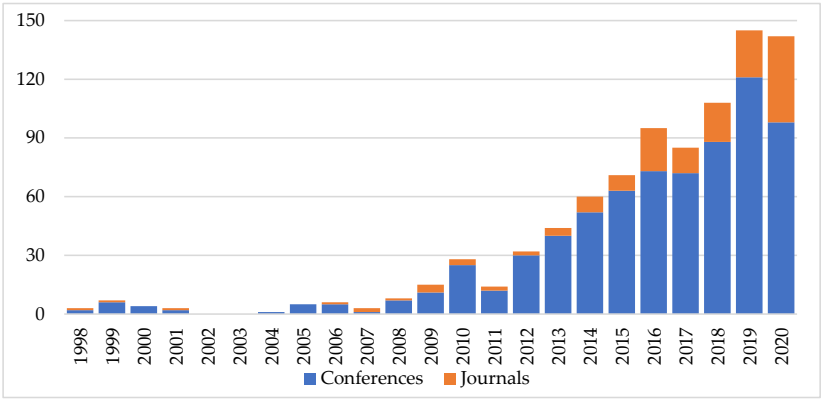

Figure 1. Number of recent IEEE publications about BESS.

BESSs nowadays are also readily commercially available. The analysis of the market of household electrical equipment [13,14] shows that numerous BESSs are already available as a market offering. On the one hand, the variety of their parameters and operation conditions provides wide choices; on the other hand, it makes the choice more complicated for the final users of BESS and complicates the development of the interface converters for different BESSs. In addition, the elaboration and commercialization of BESSs and their interface converters have a strong link to the market of some renewable energy sources and pure electric vehicles, which may not only act as BESSs, but also, after their recycling, provide high voltage (HV) second-life Li-ion batteries for use in BESS [15,16].

The goal of this work is to analyze the majority of interface converters in the context of the corresponding BESSs, their operation conditions (standards, energy tariffs, subsidies and other elements of energy policy), BESS market trends and after this analysis, to formulate prospective development directions of the BESS interface converters. In particular, this regards the converter schemes for HV batteries.

The rest of the paper is organized in five sections. Section 2 reviews the motivating factors of the BESS study: battery technologies, their applications, as well as standards and other regulations that may regard this work. Section 3 briefly analyzes the commercially available BESSs, trying to emphasize their internal structure. Section 4 provides a broad analysis of converter technologies applicable to BESSs. Section 5 discusses the previously analyzed equipment and technologies in the context of BESS development. Finally, the conclusions are given in Section 6.

2. Motivation and Driving Factors for Use of Battery Energy Storage Systems

2.1. Development of Electrochemical Energy Storages

The most intensive development of electrochemical batteries has taken place since the late 20th century and it is still progressing. Due to the constantly growing demand for portable electronics, vehicular technologies and energy systems, the battery technologies of

known electrochemistry have been "polished" and new technologies have been introduced to the market. Presently, the most significant commercially available battery technologies are [17,18]: advanced lead-acid (LA), nickel-oxyhydroxide (NiMH), sodium–sulfur (NaS), various kinds of Li-ion batteries, as well as redox flow batteries (RFBs), in particular, vanadium redox batteries (VRBs) [18]. LA technology, the oldest among them, is still the cheapest as well as quite energy efficient (up to 85%). The drawbacks of LA batteries are rather low specific energy (Figure 1) and low number of charge-discharge cycles (lifetime). Historically, the next successive NiMH technology (replacement for NiCd) is characterized by average specific power, specific energy and lifetime, but undergoes significant self-discharge and is of low charge-discharge efficiency (65%). The NaS batteries are of high specific energy, energy efficiency and lifetime (90% and 4000 cycles, respectively [18]), but their operation temperature is high—they require heating, which makes them impractical in many cases. Today, the most quickly developing battery technology is the Li-Ion. Its high specific energy, specific power (Figure 2), lifetime (up to 10k cycles), energy efficiency (up to 95%) achieved at reasonable price makes the technology very suitable for use in portable electronics, all-electric vehicles, household energy systems, and, even, in energy distribution grids [19]. However, the specific parameters of Li-Ion batteries depend on relevant chemistry and all advantages are typically not concentrated in one device. Finally, RFBs, in particular VRBs, are the batteries that utilize reduction–oxidation reaction between two liquids, which occurs through a membrane. The liquids are pumped to the membrane that makes RFBs similar to fuel cells, where the liquids are chemically restorable. The main advantage of these batteries is their potentially infinite lifetime. Lastly, it must be mentioned that modern batteries are not just a series connection of galvanic cells. They often include electronics for balancing, management and protection as well as chargers in some cases. Therefore, these batteries can be considered as complex complete energy units for immediate use [20–22].

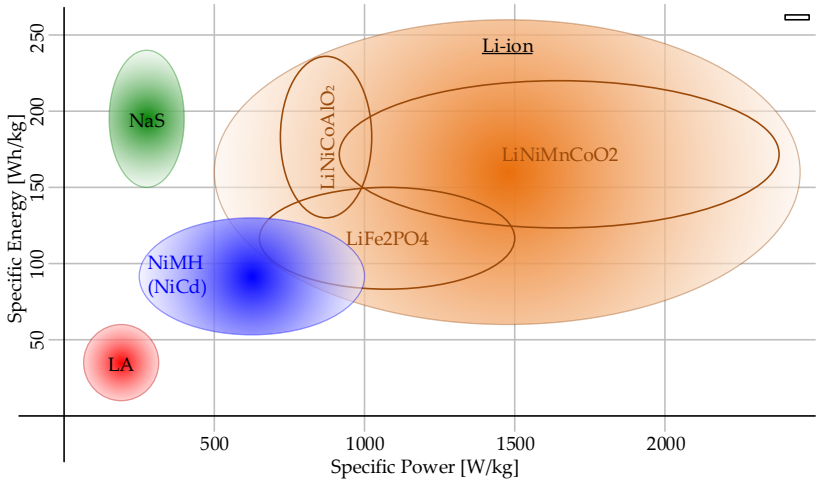

Figure 2. Specific energy and specific power of the commercially available batteries (based on data from [18]).

2.2. Extensive Use of Battery Energy Storages in Transport

One of the recent global societal and legislative tendencies on the national and international levels is the request to reduce the consumption of fossil fuels and to increase the efficiency of energy consumption [3,23]. Among other areas, this involves vehicular technologies as well. Regarding ground vehicles, this initiative means wider use of plug-in electric vehicles (PEVs) or all-electric vehicles (AEVs) and hybrid ones, equally in the public and private sectors. In [24,25], the availability of cost-effective batteries of several

hundred volts for main electrochemical energy storage of PEV is reported. More recent papers [26–29] consider these PEV storage systems valuable enough to be a part of the energy supply grid. Further development of the BESs makes their use possible in larger ground vehicles—first of all, in the public transport [30,31].

Better BESs are also required for water vehicles, first of all, for smaller auxiliary vehicles—boats, yachts, water buses, etc. For example, in [32], the electrification of the water buses in Venice is considered as a successful example of BES use in water transport. At the same time, with regard to bigger ships and vessels, the role of BESs differs with time. While earlier configurations of marine energy systems utilize high voltage batteries for stabilizing the traditional on-board AC grid and power smoothing [33,34], modern systems also take into account the possibility of all-electric propulsion of the ship [34,35].

Finally, the most advanced BESs are applicable in aircraft. The traditional electrical supply of an aircraft combines an AC and DC grid. Better performance of the applied batteries leads to a better quality of the 28 V DC grid [36,37]. At the same time, top BES technologies allow production of extremely light batteries that enable all-electric aircraft [38].

In conclusion, the extensive use of batteries in transport, in particular, the growing number of light PEVs, high capacity of their batteries and huge capacity of these batteries in total, as well as their wide distribution, make these BESs a substantial grid resource for storing energy. These BESs and their interface converters are typically high-voltage devices, but the corresponding solutions of the interface converters can be adopted for residential use.

2.3. Recent Challenges in the Field of Power and Energy Supply

The request to reduce fossil fuel consumption [3,23] regards also power distribution and supply networks. For the power and energy supply systems, this means that the burning of fossil fuels must be substituted with renewable energy generation. In turn, the main properties of renewable energy generation are:

(1) Uneven generation profile—regardless of the kind, the renewable energy sources typically do not provide constant power. In particular, the generation of PV panels depends on solar irradiation and varies with the daytime, cloudiness, season, location of PV and solar activity. The generation of wind turbines depends on the wind strength, which is unique for its location, season and occasional weather fluctuation. The generation of hydro and waves turbines depends on the amount of water that is a long-term function of seasonal and global weather changes.
(2) Variety of power ratings and types of energy sources exist even within the same group. For example, the power of PV depends on the local properties and financial abilities of a particular household.
(3) Variety of allocation of the renewable energy sources—depending on the particular economic conditions and policy of energy operator, these sources may be allocated differently.

Altogether, this makes renewable energy generation less stable and reliable. This, as well as several other problems [9,39–43], can be solved with the help of Battery Energy Storage Systems (BESSs).Figure 3 shows the use of BESSs in energy applications.

When considering a BESS in a small household with different loads and renewable energy sources, it is very important to smoothen renewable energy generation—providing storage for excessive renewable or cheap grid energy [44–46]. The BESS is also capable of performing the function of an uninterruptible power supply. This is the main function in the case of islanded residential grids [47–49]. At very uneven loads, the BESS may also smoothen the real-time loading of supply equipment—transformers and lines.

In the distribution grids, the functions of the dedicated BESS are similar but more specified. Price compensation now can be considered as a complete function of energy trading, smoothening of power generation regards not only renewables, but smoothening of consumed power at this level saves the capacity of distribution equipment. Additionally, BESS in distribution grids may perform grid service functions: grid black restart as well as voltage and frequency regulation [39,50]. The choice of BESS parameters is a subject

of multiple factors [51]: standards, power losses, voltage of majority of available PEVs, compatibility with pure resistive loads.

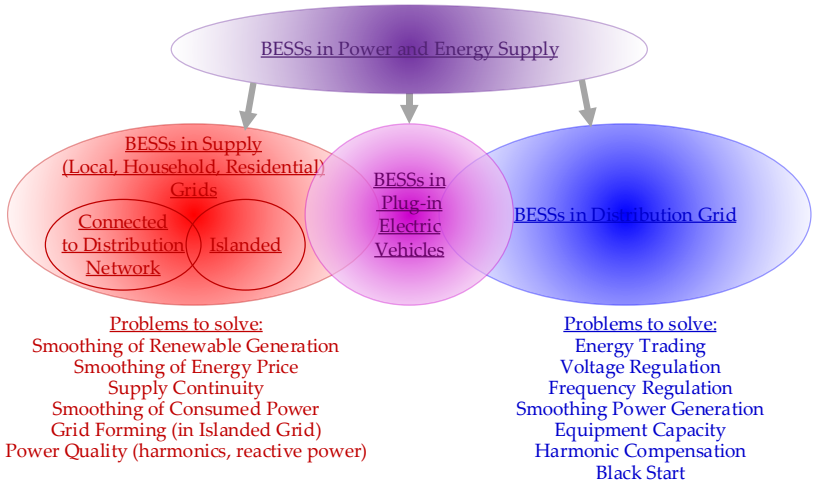

Figure 3. Battery Energy Storage Systems (BESSs) in power and energy supply at a glance.

2.4. Standards and Other Regulations Applicable to Battery Energy Storage Systems

The standards directly related to the electrical energy storage systems of households are still under development. In Europe, this is being done by the IEC 120 committee group [52]. They have developed a roadmap for developing standards, which is planned to be completed by the end of 2023. Until that date, European manufacturers have to use general standards for the production of power converters, in particular, power interfaces for alternative energy sources and uninterruptible power supply (Table 1).

Table 1. Summary of Standards and Regulations applicable to BESS.

Reference	Application Area of the Standard
[53]	USA, Converter housing and selection of components
[54]	IEC, Classification of BESS locations in households
[55]	IEC, Voltage inverters for high voltage DC networks
[56]	IEC, Controlling of converters in microgrids
[57]	IEC, Connection of PV to the grid and requirements for electromagnetic compatibility parameters
[58]	IEC, Bidirectional low voltage (up to 1000 V AC and 1500 V DC) converters connected to the grid and description of the terms used in these networks
[59,60]	IEC, Test methods and acceptable parameters for low voltage uninterruptible power supplies
[61]	IEC, Disposal of converters of uninterruptible power supplies
[62]	USA, Safety regulations within data centers and telecom central offices

In the USA, a universal standard has been developed that describes the operation of electrical energy converters in distributed networks. With regard to BESS, the manufacturers also have to apply general standards for converters. This includes standards for interface converters of energy storage. In addition, in the USA, the parameters of batteries are defined and standardized and based on the standards of telecommunication equipment (Table 1).

3. Commercially Available Residential Storage Systems

In this section, the BESs available on the market are analyzed taking into account the parameters available from the product datasheets or application manuals. Despite the market for such devices still being dynamic, some common properties and features can already be distinguished as common practice in the field.

3.1. Typical Example of Battery Energy Storage Systems Dedicated to Household Applications

The Tesla Powerwall 1 (3.3 kW/6.4 kWh) was one of the first attempts to include BESS into a household energy system and has been available on the market since 2015. It operates with a DC-bus and, in general, has to be installed in conjunction with a grid inverter, which is sold separately.

This precluded its use as a completely independent BESS, reduced market prospects and shortly led to its replacement by the Tesla Powerwall 2 (5 kW/13.2 kWh) [63]. In contrast to the previous model, the Powerwall 2 (Figure 4a) includes an AC inverter and can be connected directly to the AC grid. This enables its use as a residential BESSs, regardless of the renewable generation source (solar panels or a wind generator). Therefore, the functional features of Powerwall 2 have expanded significantly, including the possibility of stand-alone operation without grid connection (islanded mode). For normal operation, it requires an additional commutation unit called "energy gateway" and its full cycle efficiency is 90%.

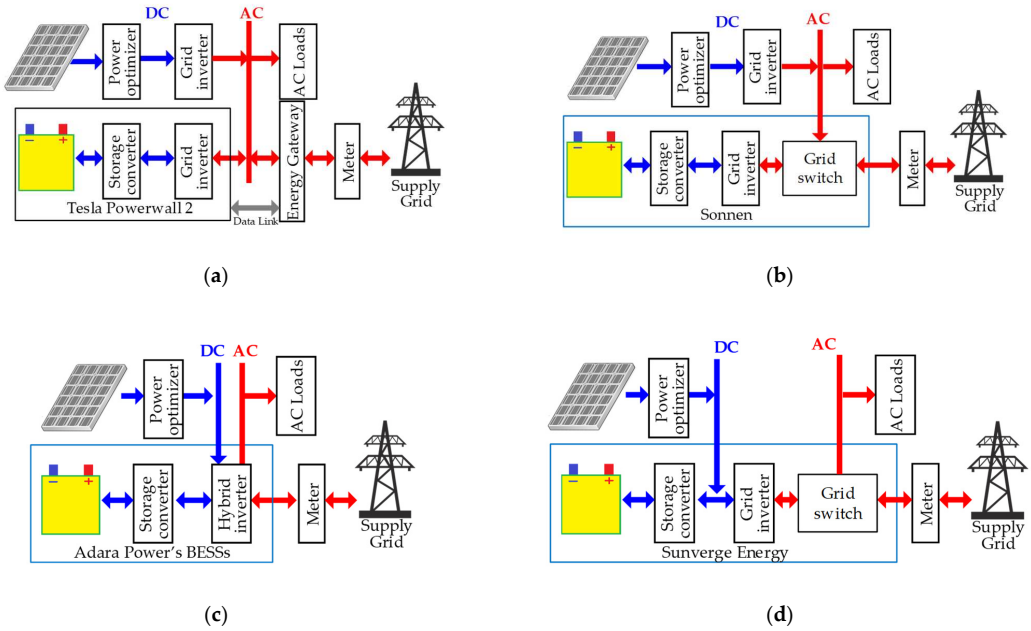

Figure 4. Typical examples of system configurations of different BESs: (**a**) Tesla Powerwall 2, (**b**) SonnenBatterie, (**c**) Adara Power-Residential and (**d**) Sunverge energy.

Sonnen is another early market player that began offering its residential BESSs in December 2015 [64]. These BESSs are designed for households with solar and wind power generators providing energy storage and backup power. They are available in two versions, with a built-in inverter for PVs (hybrid output) and without it (eco output). In Germany, the company launched a coordination network that brings together power producers and storage owners. This service allows the participants resided in the same network to exchange electricity with each other, exporting surplus to the grid. Currently, this service

has over 10,000 users. With $LiFePO_4$ batteries in its system, the manufacturer claims an output power of 2.5–3.3 kW in the "eco output" version and 5.5 kW in the "hybrid output" version. The energy capacity of the base model is 5 kWh with the ability to increase it up to 15 kWh in 2.5 kWh steps. The manufacturer promises a 98% maximum efficiency of the batteries and a 96% efficiency of the converter, which gives a total cycle efficiency of around 88.5%. The internal topology of SonnenBatterie and SonnenFlat is not disclosed, but the structural diagram of their operational environment (Figure 4b) shows that it is connected to the main supply grid as well as to the secondary grid formed by the solar panel inverter through an automatic transfer switch (ATS). This enables a SonnenBatterie to operate in an uninterruptible power supply mode.

Enphase Energy is another company that entered the residential storage market with its "AC Battery" in 2015. It is a very compact (0.27 kW/1.2 kWh) modular system that can be used in conjunction with micro-inverters and the "Envoy-S gateway" [65]. Later, the company's storage portfolio was extended with the Encharge 3 (1.28 kW/3.3 kWh) [66] and Encharge 10 [67], which is composed of three of the former units. According to the datasheet information, the cycle efficiency of a newer Enphase product is 89% at half power. Backup power from the battery can be provided using an additional microgrid interconnection device.

Other notable market players are Victron Energy with a range of products like Easy Solar and MultiPlus [68]; Adara Power's Residential [69,70] coupled with an inverter from Schneider Electric (Figure 4c) [71] and Sunverge Energy (Figure 4d) [72]. Moreover, one of the key market players is the battery manufacturer LG Chem [73], who is offering its low- and high-voltage battery modules for integration with SMA, Fronius, SolarEdge, and Huawei inverters/chargers.

3.2. Summary of Parameters and Features of Commercial Residential BESs

Due to the market dynamics, with both large and small companies are entering and leaving the market continuously, so it is hard to determine a global leader in the area. Moreover, some of the products currently have a limited proposal or are available only in certain regions. The typical price for typical residential BESs is currently in the range of 1–2 kEUR/kWh (Table 2). Technical information on these products is mostly limited—only general specifications are typically available. Still, certain common properties of residential BESSs can already be distinguished. In the majority of cases, the utilized energy storage is a low-voltage (50 V) Li-ion battery, which is associated with relatively high currents. Although the particular topology configurations used in these systems are not revealed by the manufacturers, such voltage level would in general require a rather complex interface converter featuring a transformer for the required voltage step-up. Using RESU10 and RESU10H from LG as a reference, one of the reasons for using a battery with such voltage level is its 14% reduced price, as compared with the higher voltage battery of the same energy capacity. This results in round-trip efficiencies of most residential BESS being around 90%, which seems to be a current technological limit for such configurations.

The current market of BESSs shows a clear trend of their transformation from the auxiliary BESSs, complementing a solar or wind farm with a smoothing energy storage (AC and DC coupling), towards a complete energy system with BES that does not depend on the availability of alternative energy (only AC coupling). While the BESSs of the first type have a DC output and often need a separate grid converter, newer BESSs of the second type are intended for AC operation due to the intrinsic AC interface. From the point of view of their features and functions, the earlier BESSs were focused on local power supply and equalization or shift of peak consumption, but the newer systems have a range of advanced functions, for example, integration on energy system level, i.e., possibility of combining several household grids with BESS into a distributed power plant.

Table 2. Summary of BESS for general use and use with renewable energy sources available on the market.

BESS Manufacturer/Model	Maximal Energy Capacity [kWh]	Charge/Discharge BES Power [kW]	Battery Voltage [V]	Coupling	Reference
Tesla PowerWall	13.5	5	50	AC	[63]
Sonnen Batterie Eco	15	3.3	48	AC	[64]
Adara Power (Residential)	20	12	50	AC/DC	[70]
Sunverge	Modular up to 19.4	6	48	AC/DC	[72]
Solax X-ESS G4 or Hybrid X1/X3 + Triple Power (BES)	Stackable up to 23 (4 modules)	4	300	AC/DC	[74]
SolarEdge + RESU10H	9.8	5	400	AC/DC	[75]
PowerVault 3	20	3.3/5.5	52	AC	[76]
Puredrive Storage II AC 5 kWh	5/10	3	50	AC	[77]
Duracell Energy Bank	3.3	3.3	52	AC	[78]
Enphase Encharge 3	3.5	1.3	67	AC	[79,80]
Enphase Encharge 10	10.5	3.8			
Nissan/Eaton xStorage	4.2 . . . 10	3.6 . . . 6	90	AC/DC	[81]
Samsung SDI All in One	3.6	4.6	60	AC/DC	[82]
Varta Pulse/Pulse Neo 3	3.3	1.6/1.4	50	AC	[83]
Varta Pulse/Pulse Neo 6	6.5	2.5/2.3			
Sunny Boy Storage	External battery	3.7/5/6	360	AC	[84]
Victron Energy EasySolar	External battery	0.9/1.7/3.5	12.8–51.2	DC	[85]

3.3. Isolated Converters of Commercially Available Residential BESSs

As it was shown in Sections 3.1 and 3.2, most of the commercially available BESSs utilize a low voltage battery (see Table 2 for details). The use of such a low-voltage battery while maintaining, at the same time, good control performance, requires that the entire BES interface converter or part of it be a low voltage circuit that, in turn, typically means the use of an isolation transformer. The use of the transformer also allows satisfying the potential safety requirements (see Section 2.4 for details). The transformer may be a network transformer operating at the frequency of the supply grid or a high-frequency transformer. Both solutions have benefits and disadvantages briefly considered below.

3.3.1. Converters with Grid-Frequency Isolating Transformers at AC Side

In general, adding of a transformer at the grid side moves the entire semiconductor circuitry into a low voltage operation, but its topology may be almost of any type, as presented below in Section 4. Therefore, there are two large groups of converters with a network transformer: single stage converters (Figure 5a) and converters with two conversion stages (Figure 5b). The BESS may also be equipped with a transformer at the request of the operator and/or legal regulations, in order to meet the operational requirements. This, however, regards more to BESSs for distribution grids, in particular, ABB with the ESSPro product line [86] and NIDEC with the Silcolstart product line [87]. The transformer installed at the AC side makes the operation of the converter possible at lower voltages, but makes the BESS heavier and bulky.

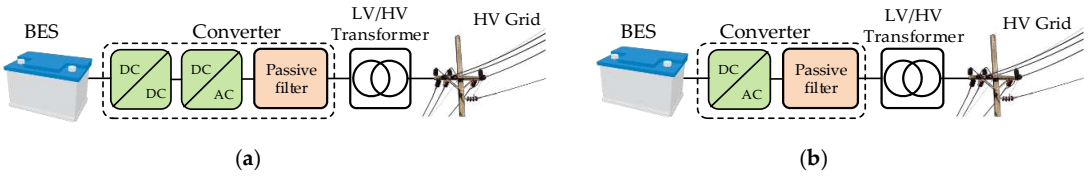

Figure 5. BESS power electronics converters with a transformer: (**a**) single-stage, (**b**) two-stage.

3.3.2. Converters with High-Frequency Isolating Transformers

A high-frequency transformer may be allocated in the DC-link (Figure 6a). The most versatile and straightforward kind of the implementation of this approach is the use the circuitry known as dual active bridge (DAB, Figure 6b). Classical DAB [88] is a hard-switching topology that, compared with non-isolated interface converters, considered

below in Section 4, is less reliable and energy efficient due to the extra components as well as due to its hard-switching nature. However, if combined with a soft-switching technique, for example, applying a resonant network, it may operate with better efficiency [89,90].

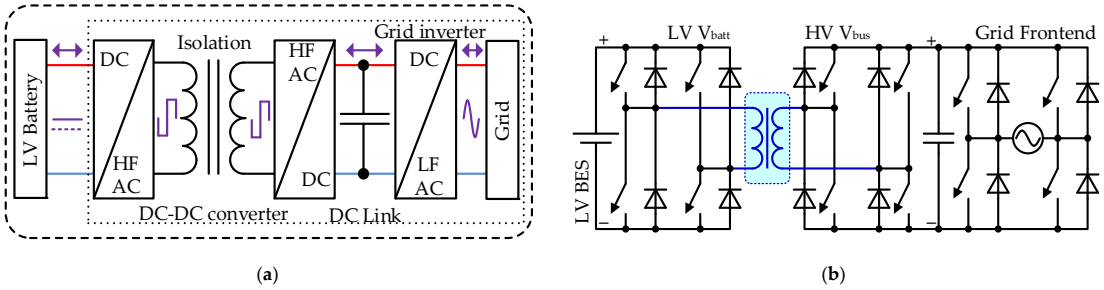

Figure 6. High-frequency transformers in the DC-link of the interface converter of LV BES: (**a**) functional diagram, (**b**) transformer in conjunction with classical DAB.

In a more advanced approach (Figure 7a), the high-frequency transformer is located at the edge of the DC-link and the AC grid [91]. This requires that the AC part of the topology contains bidirectional switches so that it can operate at both polarities of the grid voltage. The performance of this topology can be improved with the help of resonant networks (red elements in Figure 7b) and advanced modulation methods [92]. Similar topologies and their properties are well described in [93].

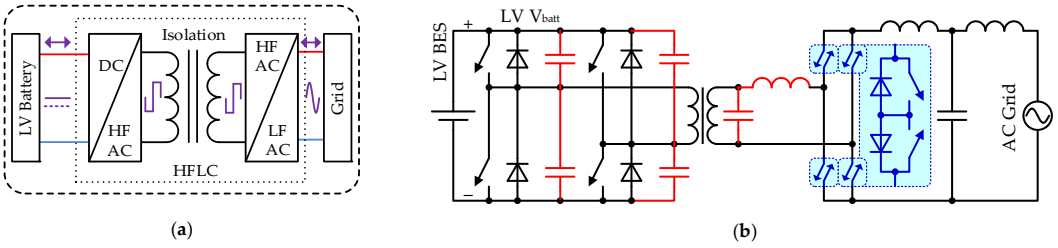

Figure 7. Full-bridge DC-AC converter with a high-frequency transformer: (**a**) functional diagram, (**b**) converter derived from DAB.

The abovementioned DC-DC and DC-AC converters contain an energy-bypassing transformer. Alternatively, the high frequency link may contain also a storage transformer (split coil). In the most explicit form, this storage transformer is seen in a flyback converter. This converter, however, is a DC-DC circuit and its use, therefore, is directly possible only in the DC-link [94] similar to DAB (Figure 6b). At the same time, adopting of the principle to AC networks is possible. For example, the converter presented in [95] contains two flyback converters dedicated to positive and negative half-waves. The inputs of the converters are connected in parallel to a low voltage battery, but their outputs—in series to the grid (Figure 8). The interface converters with a high-frequency storage transformer have the same drawbacks as original flyback converters: rather low power and highly pulsating current on both sides (including battery side) that requires sufficient filtering.

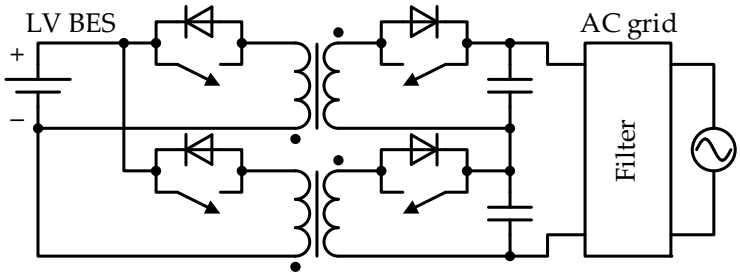

Figure 8. Inverter with a high-frequency transformer derived from a flyback converter.

4. Topologies of Non-Isolated Interface Converters for High-Voltage Battery Energy Storage Systems

One of the ways to overcome some limitations of the existing residential BESS is to utilize a battery with higher voltage (~200–500 V) and enable the use of a simpler and more efficient interface converter. In fact, some companies, like SolaX, SMA and SunnyBoy, are already on this path. Due to massive electrification of transportation where higher voltage batteries are used to reduce charging current and time, the cost for higher voltage batteries should decline further and make the use of high voltage (HV) batteries more feasible for residential BESSs.

This section is devoted to the analysis of existing and perspective non-isolated power electronic interfaces that can be applicable to the residential HV BESs. The main goal is to highlight the benefits and limitations of various configurations and assess their feasibility and performance. In addition to the standard single-, two-stage and multilevel topologies, emerging configurations like impedance-source, partial and fractional power converters are analyzed.

4.1. Functions and Structure of Interface Converters for BES

According to the analysis of commercially available residential BESSs, two main configurations can be distinguished: DC- and AC-coupled. The first group is generally represented by the power electronic systems that are often referred to as "hybrid inverters" (Figure 9a). They allow integration of both PV and battery into a single multiport unit. Such solutions are well-suited for new installations, but the choice of suitable storage configurations could be limited. On the other hand, the AC-coupled storages are often stand-alone systems that are directly connected to the residential AC grid (Figure 9b). In general, such solutions are more flexible, as they can be integrated into any existing installation. However, for such systems, charging of a battery from a PV typically involves more energy conversion stages, with a negative impact on efficiency.

The interface converter of a BES needs to perform two main functions, along with a range of auxiliary application-based functions. The main functions of the BES are sinusoidal shaping of the AC grid current and forming the DC current of the BES in both directions of power flow. The abovementioned functions can be implemented in a single stage bidirectional DC-AC inverter/rectifier; however, such solutions are typically overall less efficient due to battery voltage variation as compared to two-stage systems [96]. Therefore, the BES interface is usually comprised of a bidirectional DC-DC stage that is interfaced with a battery, followed by the DC-AC inverter/rectifier. The state-of-the-art and other potential configurations of power electronic interfaces for HV BES are analyzed in the following sections.

4.2. Single Stage DC-AC Bidirectional Inverters/Rectifiers

This section presents the state-of-the-art and emerging single-stage grid-tie inverter/rectifier topologies. The main goal of these systems is to convert a DC voltage into the sinusoidal AC waveform and vice versa. Most commercial systems require the

DC voltage to be relatively stable, with their value higher than the amplitude of the grid voltage, while some of the emerging topologies potentially offer enhanced flexibility.

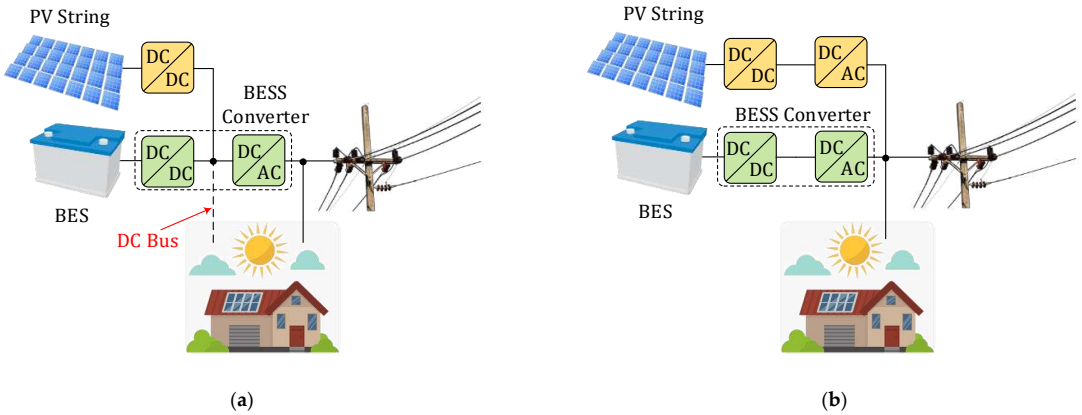

Figure 9. Coupling of units in residential energy systems: (**a**) DC coupling, (**b**) AC coupling.

4.2.1. Bridge Converters

A high voltage battery can be attached to the grid through a single stage bidirectional (four-quadrant) interface converter. The most frequently mentioned converter is a transistor bridge. Such bridge itself is a parallel connection of two (three) transistor legs with two transistors (and anti-parallel diodes) in each (Figure 10). The converter includes also an inductance coil between its AC terminals and the grid implementing an AC current source (Figure 10a). A diagonal couple of transistors and the couple of diodes located in the opposite diagonal form a chopper capable of converting the grid voltage at its particular polarity. In Figure 10a, red elements represent the chopper for the positive half-wave, but blue elements—for the negative. The chopper is bidirectional and can be considered as a buck converter supplied from the DC bus or as a boost converter supplied from the AC grid [97]. One transistor leg can be substituted by a series connected capacitors (capacitor leg), thus forming a transistor-capacitor bridge (Figure 10b), more frequently named "half-bridge" [97]. In this topology, it is also possible to identify two choppers for both half-waves of AC voltage. Finally, it is possible to apply this approach of schematic synthesis to three phase systems (Figure 10c,d). This forms the three-phase transistor bridge and the three-phase transistor bridge with a capacitor leg coupled to the grid via inductor-based AC current source [98].

4.2.2. Topologies without Explicit Bridge

The intrinsic choppers shown in Figure 10 can be deployed without forming an explicit bridge. This scheme is defined as a dual-buck grid converter known since 1997 [99,100]. With this approach, the elements of the "positive" and "negative" choppers are different, which enables them to be further optimized.

Figure 11 shows how the elements of implicit choppers are extracted (red elements—for positive and blue elements—for negative). With this approach, the inductance coil is not shared between "positive" and "negative" branches (Figure 11a). These coils can be magnetically coupled (Figure 11b), providing their lower weight/volume and therefore, lower weight/volume of the converter itself [101], without the reduction of the performance and reliability of the converter. Alternatively, both branches can be combined through a couple of series connected diodes (Figure 11c) [102], keeping the same advantages.

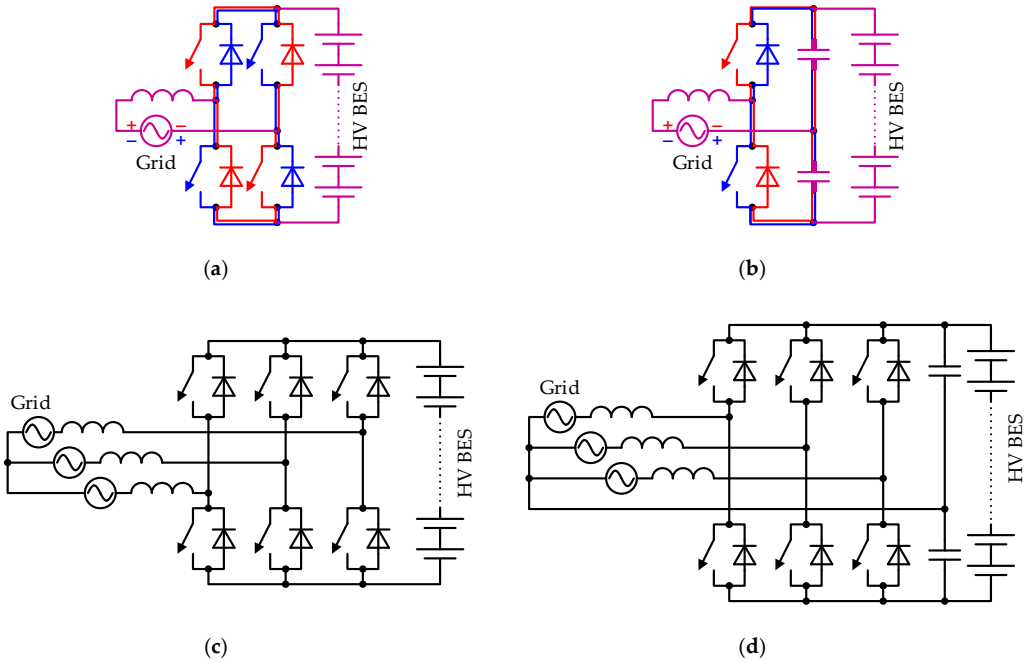

Figure 10. Configurations of single-stage bridge rectifiers-inverters for BESs: (**a**) AC current sourced transistor bridge, (**b**) AC current sourced transistor/capacitor bridge (half-bridge), (**c**,**d**) three-phase schemes.

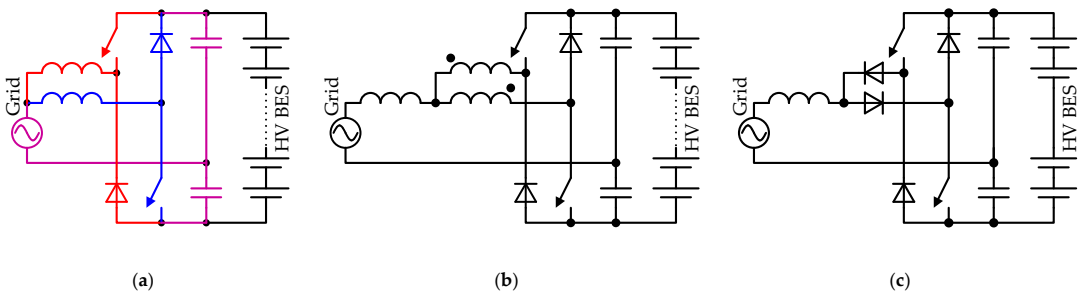

Figure 11. Dual-buck grid converter: (**a**) derived from half-bridge, (**b**) magnetically coupled branches, (**c**) diode coupled.

Extracting of the intrinsic voltage converters at both grid terminals of a full-bridge converter forms another kind of the dual-buck grid converter (Figure 12a) [102]. Another version derived from the full-bridge topology can be synthesized by means of direct combining of two DC sourced buck converters—attached to each terminal of the grid [76]. In this converter, the switches located at the grid side are continuously conducting at the corresponding grid voltage polarity that reduces switching losses. Additionally, such converter may be "tied to positive voltage node" (as shown in Figure 12b) or "ground tied". Finally, adding two diodes at the grid side (Figure 12c) allows operating in "ground tied" and "positive node tied" modes [103,104], making the operation of the switches more symmetrical. The converter shown in Figure 12b can be equipped with magnetically coupled inductance coils or coupling diodes, as shown in Figure 11.

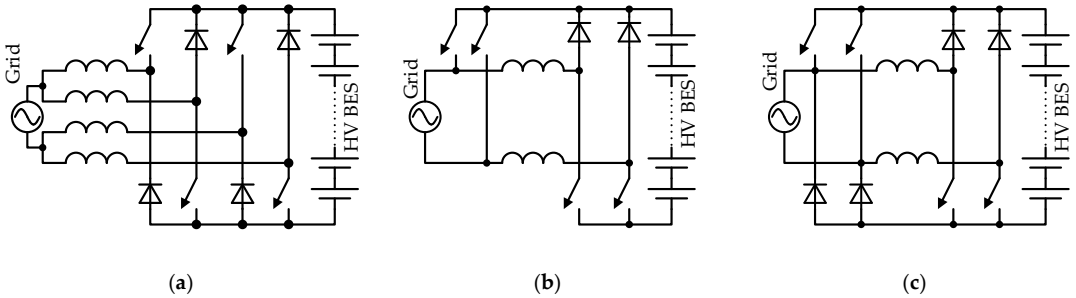

(**a**) (**b**) (**c**)

Figure 12. Dual-buck grid converters: (**a**) derived from full-bridge, (**b**,**c**) synthesized of two combined buck converters.

Due to a low number of elements, the considered single-stage converters operate with best efficiency at their particular operation point. However, when considered in conjunction with the attached battery, their efficiency is not outstanding and drops significantly at other operation points due to the higher losses in the converter and the battery [86]. In addition, these converters operate as an AC grid supplied boost or a BES supplied buck converter that requires minimal battery voltage to be higher than the amplitude of the grid voltage.

4.2.3. Multilevel Converters

Multilevel converters (MLC) can be considered as a specific kind of the single-stage converters, processing energy in separate cells of a BESS battery. In contrast to the above-considered topologies that always deal with the same DC voltage or with the entire battery, the multilevel converters form their output of DC voltage that may have several levels obtained directly from the battery. The advantages of multilevel converters are lower harmonic distortion, switching losses and electromagnetic interference [105]. There are three main topologies of multilevel converters: cascaded H-bridge converters (also known as multilevel converters with independent sources), neutral point clamped multilevel converters (also known as diode clamped multilevel converters), and multilevel converters with flying capacitors.

Cascaded H-Bridge Converter Structures

In the case of cascaded H-bridge multilevel converters, each phase contains several series-connected modules (Figure 13a) composed of dedicated cells and an inverter, together forming an independent source. Within a BESS [106], these sources can be charged and discharged more evenly due to the independent nature of their involvement in the current path and potentially free exchange of the sources [107].

There exist various types of power converters and energy storage building blocks. The most common converter is a single-phase transistor bridge (H-bridges) shown in Figure 14a, which generates AC voltage on its output, thus controlling the charge or discharge process of the connected battery cells. Another typical configuration given in Figure 14b includes an AC generating H-bridge in conjunction with a synchronous buck converter that compensates voltage changes in the cell(s).

Lastly, a successful commercial implementation of BESS with a multilevel converter was offered by SolarEdge [108]. It is based on a multilevel DC converter with multiple DC modules connected in series (Figure 13b). Allocation of the multilevel structure in the DC bus enables significant simplification of the cell converters (Figure 14c). The DC/DC converters can operate in the following modes: balancing circuit, charger and battery discharger. In turn, if the DC bus is formed by an MLC, the grid frontend can be a simple commutation matrix or an efficient pulse mode inverter or a short-circuit proof converter with an impedance network. A similar topology developed by ABB for distribution networks [109] includes an array of complex cells containing two transistors and a battery

with switches and capacitors. A cell may work as a boost or buck converter and is capable of shunting the cell if needed.

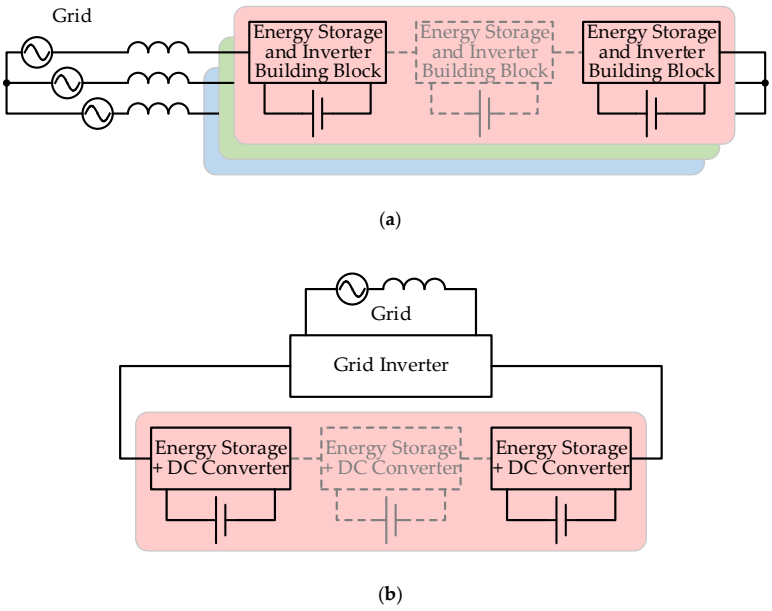

Figure 13. Functional diagrams of cascaded H-Bridge multilevel converters: (**a**) traditional configuration of AC MLC, (**b**) configuration DC MLC with unipolar cell converters and grid frontend.

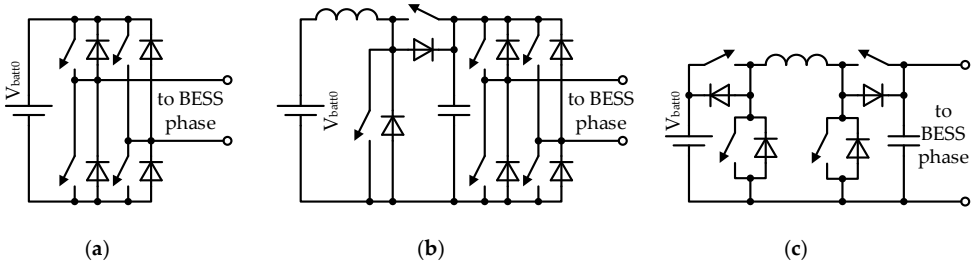

Figure 14. Power converters for multilevel converter building blocks: (**a**) full bridge or H-bridge, (**b**) H-bridge with correcting synchronous buck converter, (**c**) unipolar bidirectional converter [108].

Neutral Point Clamped Multilevel Converters

The simplest kind of the neutral point clamped multilevel converters is known as the diode clamped topology (Figure 15a). It has quite high efficiency compared to other topologies. However, there are some disadvantages: the number of power diodes is quadratic related to the level count, which makes this topology quite difficult to use when a large number of levels is needed. Another disadvantage of the topology is that charge balancing in the capacitors is needed. Another type of the neutral point clamped multilevel converter is an active clamped multilevel converter shown in Figure 15b. Additional switches enable the distribution of power losses more evenly between the switches. Besides, it is possible to synthesize 0 V level differently, providing different charge/discharge paths.

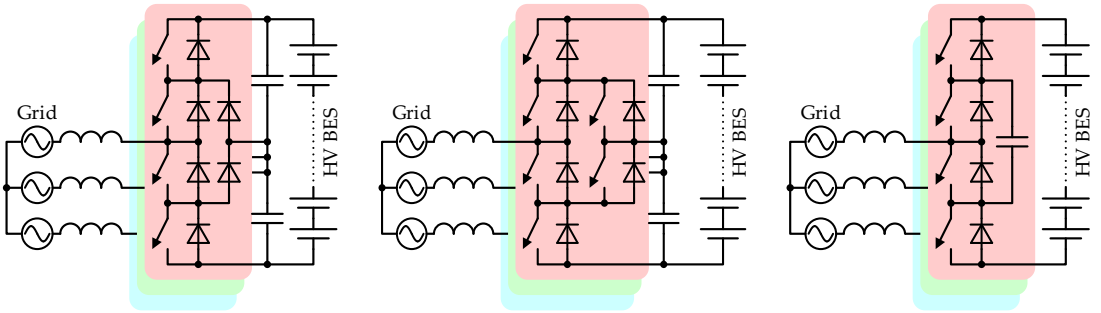

(**a**) (**b**) (**c**)

Figure 15. Multilevel converters with solid HV battery: (**a**) diode clamped, (**b**) active clamped, (**c**) flying capacitor.

The use of neutral point clamped converters in the BESS system is described in [110,111]. Reference [112] demonstrates the use of neutral point clamped and active neutral point clamped converters in BESSs. In [113], an overview of modular converters (including active neutral point clamped converters) in BESS systems is given. Diode clamped and independent source multilevel converters in BESS applications, indicating also larger operating range of the diode clamped converters, are compared in [114].

Multilevel Inverter with Flying Capacitors

The main difference between multilevel converters with neutral point clamped and multilevel converters with flying capacitors (Figure 15c) is that instead of clamping diodes, capacitors are used. Similar to the diode-clamped topology, the main disadvantage of the multilevel inverter with flying capacitors is the large number of used capacitors, which makes the practical implementation of this solution larger in terms of packaging. In spite of this drawback, some recent papers report that the topology itself can be successfully applied in BESS based on GaN switches: [115] presents a BESS with a 13-level converter, but [116]—a 9-level converter for aircraft. In addition, the BESS interface converter offered by SolarEdge in [108] utilizes the MLC with flying capacitors as a grid inverter.

4.3. Impedance-Source Bidirectional Inverters/Rectifiers

The problems of conventional topologies related to the battery voltage variation can be mitigated with the family of impedance source (IS) converters. These topologies incorporate a special network, which allows step-up of the input voltage using a shoot-through state in the inverter bridge, which is a prohibited condition in conventional inverters. As a result, IS converters can be less prone to short-circuit faults. There is a variety of impedance source networks proposed in the literature for a range of applications with different properties and features (Figure 16), including three-phase and multilevel configurations [117]. The majority of basic impedance source topologies were initially unidirectional; however, some studies address the bidirectional versions potentially suitable for residential BES [118,119].

4.4. Bidirectional Two-Stage DC-AC Converters

This section presents the state-of-the-art and emerging power electronic interfaces for BES, featuring two explicit stages. In a general case, the first stage is a bidirectional DC-DC converter, which processes varying battery voltage and controls the charge/discharge current. It operates in conjunction with the DC-AC inverter/rectifier addressed in the previous section, which provides interface with the grid.

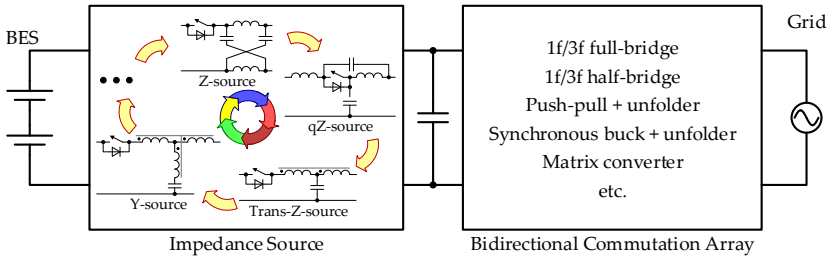

Figure 16. Generalized configuration of the BES interface converter with an impedance source.

In the most obvious operation mode, this DC-DC converter provides the stabilized voltage in the DC-link at all operation points of the battery (Figure 17a) while the rectifier-inverter modulates the voltage at the grid end according to the phase of the network voltage and required grid current. It was demonstrated that two-stage configurations are overall superior to the single DC-AC inverter/rectifier in terms of efficiency throughout the battery voltage range [86]. Moreover, the stable DC-link voltage allows integration of other DC sources and loads; therefore, such solutions can be suited for both DC- and AC-coupled BESS.

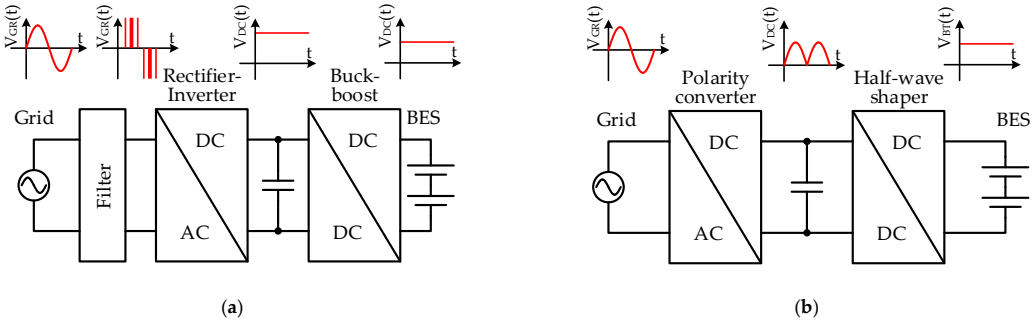

Figure 17. Operation and configuration of BES interface converters with two stages: (**a**) common DC-link, (**b**) unfolding topology.

However, one more operation mode and configuration is possible. In this mode, the DC-DC converter forms unipolar sine half-waves in the DC-link, but the rectifier-inverter applies the formed half-waves to the grid with the correct polarity (Figure 17b). In the second case, the rectifier-inverter does not operate in a real switch-mode—it just commutates the half-waves at the grid frequency. Therefore, in this operation mode, the switching losses of the rectifier-inverter are negligible, while the grid filter can be omitted or reduced due to the continuous profile of the voltage at the grid port of the rectifier-inverter [120]. In the single-phase configuration, the AC-DC converter is a bridge or half-bridge circuit, close to that shown in Figure 16 without the inductance coil. Depending on the required power and input connection, it can be a single-phase [120–122] or a three-phase [122,123] circuit.

4.4.1. Two-Stage Converters with Stabilized DC-Link

The typical configuration of a two-stage converter assumes voltage stabilization at an intermediate DC-link to compensate battery voltage variation and provide optimal operating conditions for the DC-AC inverter/rectifier. Such configuration can be suited for both DC- and AC-coupled BES. The standard DC-DC stage topologies include buck, boost, buck-boost, etc. The common disadvantage of these standard configurations is that both stages have to be rated for the full power of the system. This results in increased cost and

negative impact on the efficiency. One of the recent trends in the power electronic studies is the use of advanced topologies of the DC-DC stage like differential, partial and fractional power converters that allow operation with lower voltages/currents and minimization of power losses. The use of these topologies in BES interface is considered below.

Standard Topologies of DC-DC Converters

The choice of the secondary (DC-DC) converter or the converter at the battery end depends on several factors. First of the all, this converter has to be bidirectional. Besides, this reduction of the losses requires that the number of switches is minimal, which enables only simple choppers. Finally, the configuration/mode of the two-stage interface converter (stabilizing or unfolding) as well as the voltage of the battery are important. Below, the latter issue is addressed in detail.

In the case of the two-stage converter with a stabilized DC-link, its grid unit may operate correctly if the voltage of the DC-link is higher than the amplitude of the grid voltage. On the other hand, keeping this voltage level on the battery is not reasonable because it would reduce the advantages of the two-stage configuration. Taking into account the realistic voltage gains of the circuits with the boost function of 2–3 and voltage difference of the fully discharged and fully charged Li-Ion batteries of 60–100%, the voltage of the fully charged battery could be at least twice lower than the amplitude of the grid voltage or about 200 V. In the given paper, this level is considered as a medium level, but such batteries abbreviated as MV BES. The case of the unfolding configuration/mode additionally requires that the DC-DC chopper is capable of converting the BES voltage down to zero level. Together, as a result, the following buck-boost converters are suitable for both configurations/modes: classical (Figure 18a) and non-inverting (Figure 18b) bidirectional buck-boost converter, Zeta-SEPIC circuitry that is linked through its primary inductor to the battery or the grid (Figure 18c), as well as the bidirectional Čuk converter (Figure 18d). In addition, a synchronous buck converter (Figure 18) is applicable in the case of the stabilizing configuration/mode only.

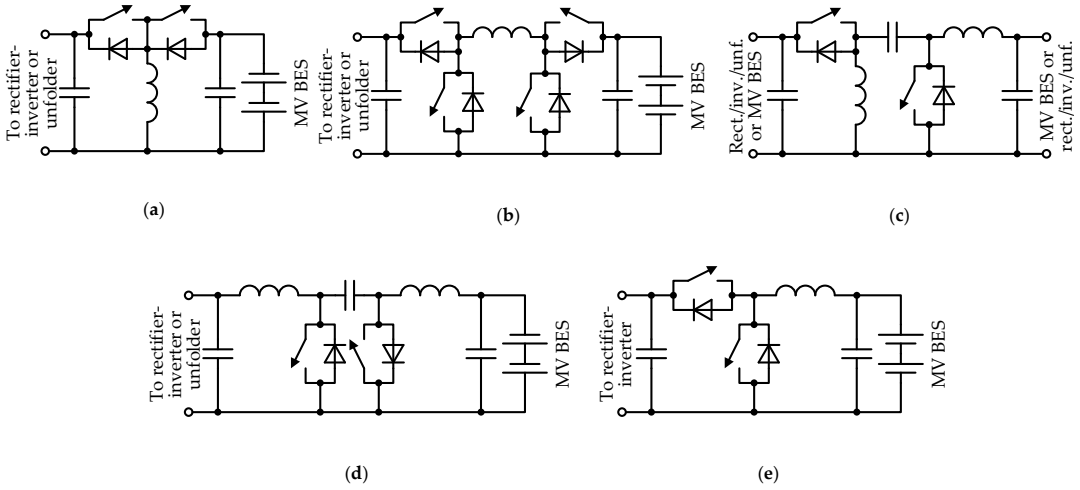

Figure 18. DC-DC stage of BES interface converters with two stages: (**a**) inverting bidirectional buck-boost, (**b**) bidirectional non-inverting buck-boost, (**c**) bidirectional zeta-SEPIC, (**d**) bidirectional Čuk, (**e**) synchronous buck.

Zeta-SEPIC-Čuk topologies, however, are usually not considered as powerful converters, which disables them for applications like BESS. On the other hand, the remaining (non)inverting buck-boost and synchronous buck topologies can be equipped with additional elements for reducing losses, smoothing current ripple and better control per-

formance (more accurate regulation for the same range of duty cycle): add-on circuits for zero-current/resonant switching, tapped (coupled) inductors or qZ links [120].

Differential Power Converters

Differential power converters (DPCs) are a kind of partial power processor (PPP). In turn, PPPs are a quite recent group of converters that are typically used in conjunction with renewable energy sources and storages. As it follows from their title, the main feature refers to dealing only with a part of the total system power. PPPs can be systematized in a number of ways, such as considering their topology or application. However, most commonly, PPPs can be divided into different groups [124] according to their power flow. From this point of view, three groups could be differentiated: differential power converters that internally link elements of the systems, partial power converters connecting system input and output, fractional power converters dealing with a fraction of entire set of power sources/storages, as well as mixed topologies. Finally, it must be noted that the difference between differential, partial and fractional power converters is sometimes quite fuzzy. For example, in [125,126], identical topologies are entitled as partial and differential. In a similar way, most of the topologies considered in [127] as partial power converters, in fact, operate as fractional power converters.

DPCs are mainly used in various balancing systems [128,129]. There are two types of such converters. The first one transfers the energy between two typically adjacent elements and is known as element-to-element (E2E) converter; alternatively, in another option, the energy circulates through a common bus (B2E). The DPC normally operates with batteries, but according to some reports, this converter technology is applied to photovoltaics [128].

The E2E architecture is used in systems with the same type of cells, for example, for balancing batteries (Figure 19a). The main advantage of this architecture is that each converter operates at significantly lower voltage and current values than the entire system. The disadvantages of this architecture are the interconnectedness of the converters and the impossibility of their operation separately.

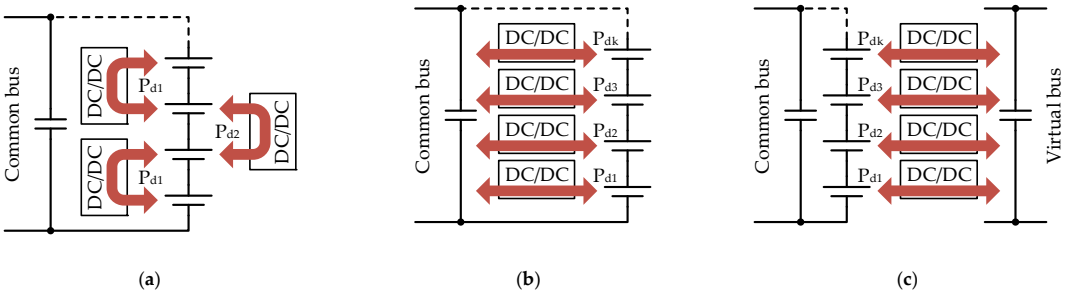

Figure 19. Differential power converters: (**a**) Element-to-Element, (**b**) Element-to-common-bus, (**c**) Element-to-virtual-bus.

The B2E architecture works with a common bus connected to the output (Figure 19b) or with the independent "virtual" bus dedicated to the energy transfer (Figure 19c). Each element is connected to the bus via own converter. Compared to the E2E architecture, this approach is more flexible, but neighboring cells are independent of each other. However, an isolating converter suitable for the full bus voltage is required.

All kinds of DPCs fit well the cell balancing function needed also in BESSs. At the same time, the use of B2E DPCs as BES and grid interface converters is complicated due to the following: (1) DC output requires an inverter or unfolder and (2) because the total power of converters, in fact, is not reduced, but just split into several parts. Lastly, the E2E DPCs are not applicable as BES and grid interface converters due to the absence of the common link.

Partial Power Converters

Another group of PPP links the input and the output of the system. While one part of the energy from the source to the load goes directly, the converter transfers only the necessary reminder. As can be seen from Figure 20, in the classical converter type (Figure 20a), all the output power passes through the converter, which leads to a higher efficiency and significant losses. In the case of a PPC, a significant part of the total energy enters the load without conversion and does not produce losses. Only the energy going through the converter, adjusted by the converter to control the energy flow, produces losses (Figure 20b). Thus, compared to a classic converter, PPCs have potentially better efficiency and smaller dimensions for the same power. The PPCs may operate with reduced voltage (Figure 20c), current or both.

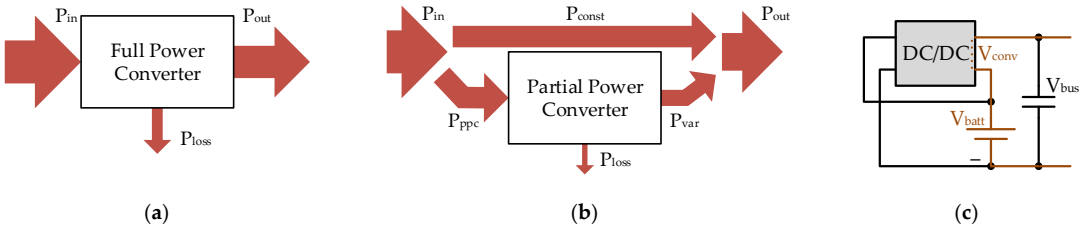

Figure 20. Full power operation vs. partial power operation: (**a**) power distribution in full power converter, (**b**) power distribution in partial power converter, (**c**) diagram showing operation with reduced voltage.

It is possible to distinguish two groups of PPCs: with an isolated and with a non-isolated converter. The isolated converter can be applied in a quite free form. That is why such PPCs can be of two types: parallel input—serial output, as well as serial input—parallel output (Figure 21). In the first case (Figure 21a), the input source and the input of the converter are connected in parallel, while the output of the converter and the input source are connected in series (S-PPC). The configuration is suitable to increase the voltage. In respect to the battery, the parallel input converters can be considered as partial current converters because only part of their battery current is transferred to the output (bus) through the converter. On the other hand, in respect to the output, operation occurs with reduced voltage because only part of output voltage is applied to the converter (see also Figure 20c).

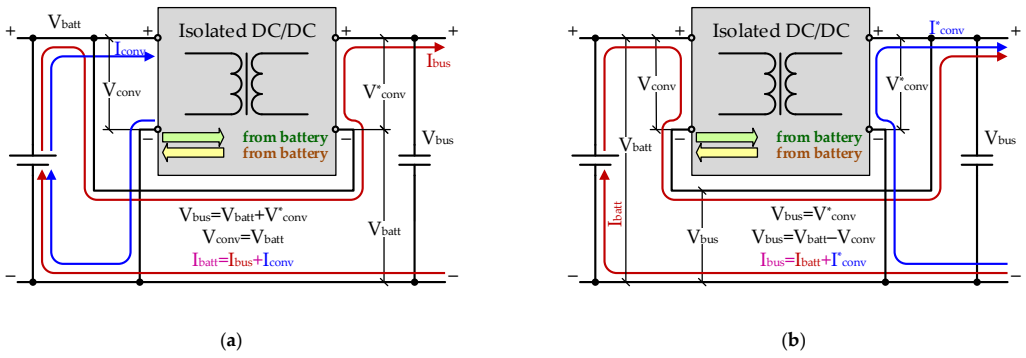

Figure 21. Structures of partial power converters: (**a**) parallel input—series output, (**b**) parallel output—series input.

In the second case (Figure 21b), the input source is connected in series with the input of the converter, but its output and the source are connected in parallel (P-PPC). The configuration is suitable to obtain higher output current. In respect to the battery, the series

input converters can be considered as partial voltage converters because only part of their battery voltage is converted and passed to the output.

It is obvious that both topologies are symmetrical and counter-reversible. In respect to the output (bus), the first configuration is a partial voltage converter, but the second one—a partial current converter. To some extent, these PPCs are similar to an autotransformer and can be described by similar mathematical expressions extracted from Kirchhoff's voltage and current laws.

The PPC topology provides benefits when the difference between the input and the output voltage is relatively small and only a small amount of energy is being converted by PPC. Due to a more complex design and a larger number of active elements, the larger difference between the input and the output voltages produces lower efficiency. Moreover, at 100% of the difference, the efficiency will be less than that of a classical converter.

Practical PPC implementation depends on the particular application. Normally, reports consider PPC with a DAB converter at each end of an isolating transformer that produces a fully bidirectional PPC (Figure 22a). In many applications, the bidirectionality can be omitted, but PPC—reasonably simplified. For example, in [130,131], which address PV systems, the simplification finally produces full-bridge + buck configuration, in [131,132]—full-bridge + push-pull, but in [130,132]—a kind of classical flyback. The latest converter can be easily turned to a bidirectional one (Figure 22b).

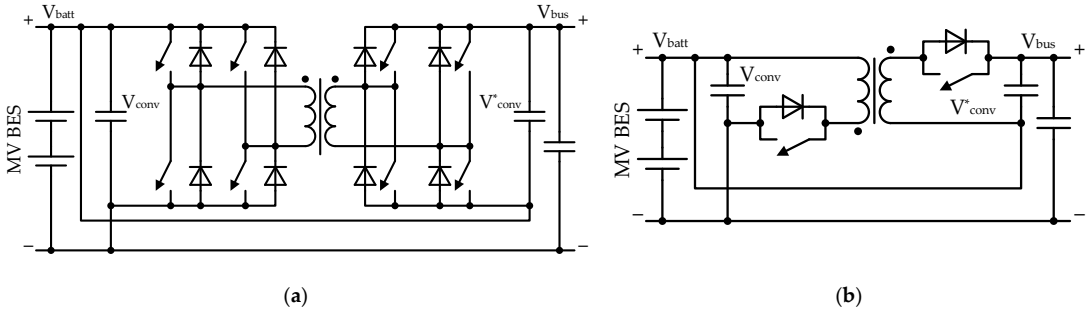

Figure 22. Examples of PPCs: (**a**) parallel input—series output PPC with DAB, (**b**) parallel input—series output PPC with flyback converter.

A PPC topology with a non-isolating converter could be potentially simpler, contain fewer components, and have higher efficiency. Attempts have been made to implement such non-isolating schemes. For example, refs. [133–135] report the voltage buck-boost topology based implementation applied for battery or bus voltage magnification. It is pointed out that the extra feedback capacitor installed in these schematics is required for direct power feedforwarding. However, it is possible to show that the obtained converters are, in fact, ordinary boost or buck converters—see [136] for details.

Fractional Power Converters

Fractional Power Converters (FPCs) deal with an explicit part of the entire power supply, for example, with several cells of BES [137,138]. In contrast to PPCs, where the reduced operating voltage of the converter is obtained as a difference on the entire input/output, FPCs process already reduced voltage—a section of the entire power supply (similar consideration could be applied to current conversion).

The fractional power processing may utilize an isolated (Figure 23b) or a non-isolated (Figure 23c) scheme. Successful examples of non-isolated converter use have been demonstrated in conjunction with a battery of PEVs [137] or grid BESS [138]. The mentioned reports explore several DC-DC choppers functioning as FPC (Figure 24 shows discharging configurations in black, but charging—in gray). In this case, the non-isolated converter obviously deals with reduced voltage, thus providing true partial power processing. On

the other hand, the fraction of the power supply associated with the converter operates differently from the rest of BES. It has different average charge/discharge current. Moreover, depending on the applied chopper, it may conduct pulse-mode current. This may lead to shorter operation cycles, limited state of charge and, finally, may lead to a worse state of health for the "processed" cells.

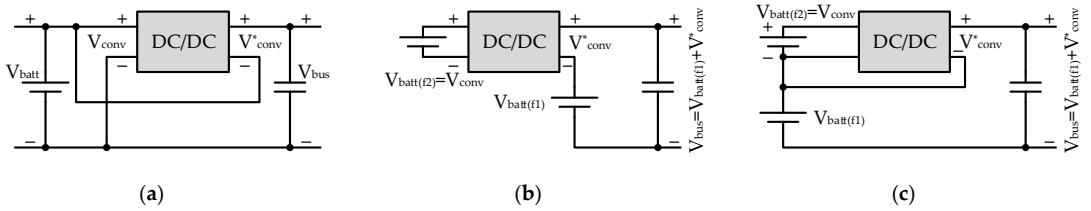

Figure 23. Partial power converters (**a**) vs. fractional power converters: (**b**) isolated, (**c**) non-isolated.

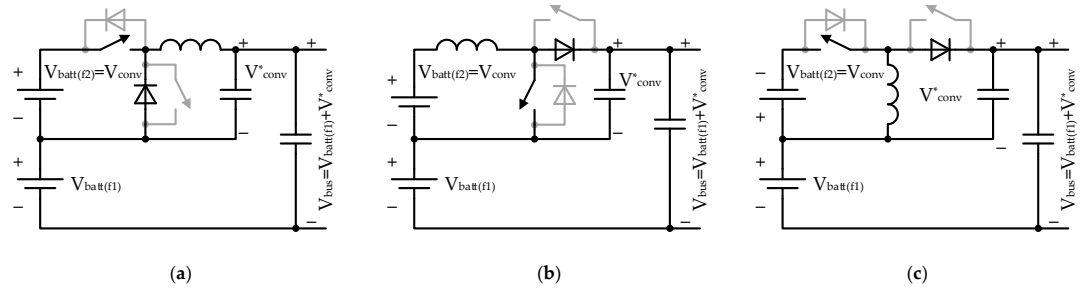

Figure 24. Examples of non-isolated fractional power converters (in discharge mode): (**a**) buck, (**b**) boost, (**c**) buck-boost.

The FPC shown in Figure 24c is also quite impractical because the polarities of the input/output voltage are different, which splits the battery or narrows the regulation range. On the other hand, the use of non-inverting buck-boost topology would double the static and dynamic losses of the switches.

Finally, the considerations on the non-isolated PPC with a feedback capacitor (given in the previous section) may also produce, in fact, an FPC if the feedback capacitor is substituted with an energy source or storage (battery, supercapacitor, PV cells etc.) capable of keeping its voltage at a constant level. Then the part of the current is actually bypassed, but the other—processed in the converter (Figure 25a). Practical importance of this converter is questionable because one fraction of the battery is loaded with increased current and charged/discharged more intensively.

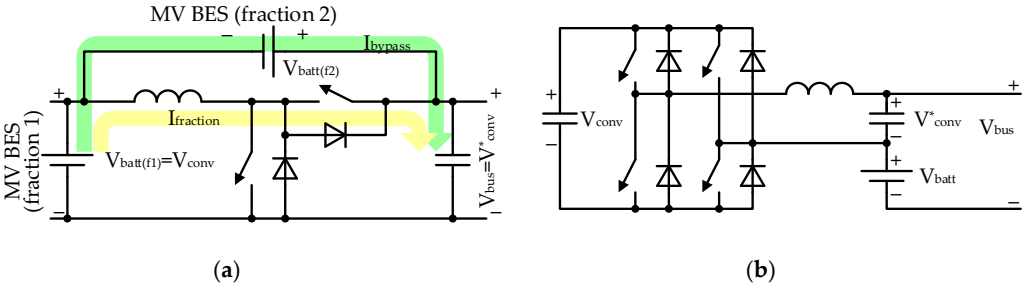

Figure 25. Specific kinds of FPC: (**a**) FPC synthesized from "non-isolated" synchronous buck PPC, (**b**) fractional power conversion with "virtual fraction" [139].

Another example of the implementation of non-isolated partial power conversion is given in [139]. This example, however, may also be considered as a fractional power converter with "virtual" fraction formed of a DAB and an ordinary capacitor. Here, the DAB processes low voltage of the capacitor while the battery is attached in series without processing (Figure 25b). Although, in [139], with the focus on the DC-AC systems, partial conversion of power occurs in the DC-link. Due to the limited energy capacity, the configuration is suitable for compensation of regular short term voltage fluctuation or current compensation that happens, for example, within the cycle of the supply grid (20 ms).

4.4.2. Two-Stage Converters with Pulsating DC-Link

In order to reduce the overall switching losses of the two-stage system, a configuration with inverting unfolder can be used. In this case, the DC-DC converter forms unipolar sine half-waves in the pulsating DC-link, but the interface inverter applies it to the grid with the proper polarity.

The Li-ion battery can handle the current ripple without significant effect on their lifetime, thus the use of pulsating current can be justified [140,141].

1-ph Unfolders

As it was stated previously, an unfolding circuit provides grid-frequency commutation of the unipolar voltage formed by a high-frequency switch mode DC-DC converter to provide sinewave matching to the grid polarity. Paper [142] proposes a combination of a buck/boost non-inverting converter and an unfolding H-bridge (Figure 26a). This configuration directly corresponds to Figure 17b and can be considered as a standard double stage converter with a pulsating DC-link. In [143], the operation and the experimental verification of a buck-boost inverter/converter based on tapped inductor are addressed. The inductor magnetically couples four windings with equal turn-ratio (Figure 26b). In the converter presented in [143], in contrast to [142], explicit parts cannot be identified.

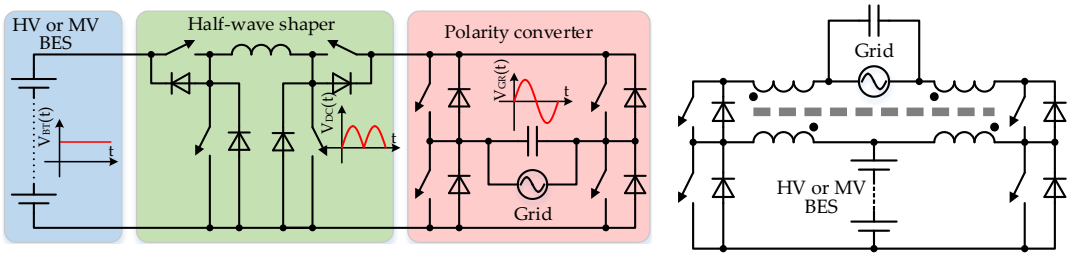

(**a**) (**b**)

Figure 26. Examples of single-phase unfolders: (**a**) buck-boost converter with unfolding H-bridge, (**b**) tapped inductor buck-boost converter.

3-ph Unfolders

Three-phase converters with low frequency unfolding stage utilize principles similar to those of single-phase unfolders. However, the presence of three phases requires that at least two voltages/currents be formed actively by the dedicated voltage/current source (shaper), but the third one is obtained as a sum/difference of the other two. Within a period of the grid, the principles how the actively shaped voltages/currents are applied to the grid change six times (Figure 27a,b).

Working principles of unfolder topologies are provided in [144]; however, the converters described there are unidirectional and do not fit the requirements of bidirectional operation. An example of such converter from [144] is a topology derived from a three-phase two-level voltage source inverter. In this case, amplitude modulated high-frequency

output of a phase modulated high-frequency inverter (H-bridge was taken as an example) is rectified and filtered. Then the output of a filter is unfolded by a three-phase inverter, thus forming three-phase alternating current. For the bidirectional operation, one or multiple DC-DC converters should be used as current sources. For example, refs. [145,146] show a three-phase inverter, where two DC-DC converters were taken as current sources and are connected in parallel to the BES. DC-DC converter outputs are connected in series, thus forming three voltage levels—high, low and neutral. Then the modulated voltage waveforms are unfolded by a three-level inverter, which is derived from a diode clamped multilevel converter [146] or Vienna rectifier [145] (Figure 27c). The study in [147] provides experimental verification of the topology in [146].

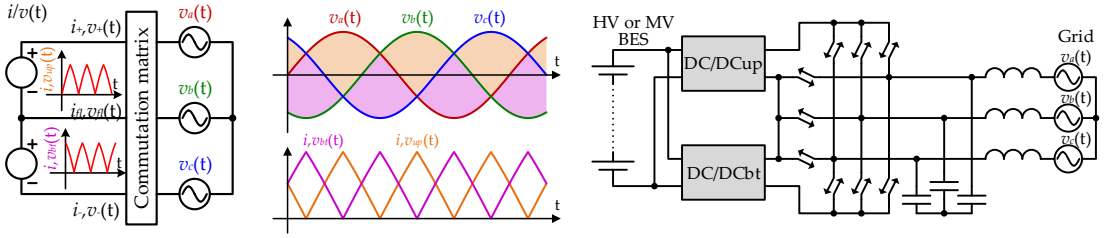

Figure 27. Three-phase unfolders: (**a**) general principle, (**b**) operation diagram, (**c**) example of implementation.

5. Generalizations and Discussion

One of the main trends in the area of residential BESSs is a shift from stand-alone systems for a particular task, like the increasing local renewable energy self-consumption using basic algorithms, to a complex integrated system, aiming to achieve multiple different goals. Some commercial BESSs can provide a supply during a power cut, effectively acting as uninterruptable power supplies. The use of advanced energy management algorithms enables smart scheduling and energy trading, further improving the functionality of these systems. The integration on a system level allows provision of ancillary grid services and enables forming of a microgrid with extended levels of flexibility. Nevertheless, currently there are still a number of technological and legal barriers that limit a ubiquitous application of the residential BESS. However, the new regulations, subsidies and initiatives offered and developed by governmental structures in many countries are aimed to stimulate the installation of these systems and make full use of their potential [148].

Our review of the commercially available BESS and the corresponding intellectual property right items shows that despite a whole range of available solutions, the market of residential BESSs is still advancing. Presently, it is strongly influenced by a forecasted price reduction of the Li-ion battery cells and further improvements in the battery chemistry. Technical information about available products is rather limited. Most of the BESSs utilize a low-voltage (around 50 V) Li-ion battery, which results in high current and requires the use of a transformer. Most likely, two-stage converters with galvanic isolation are used, limiting the overall efficiency of the system. The typical BESSs have the efficiency below 90%, whereas power electronic converters could be responsible for around half of power losses in the system. On the other hand, the low voltage batteries require simpler battery management and protection systems, making them less expensive and more feasible commercially. Because of these compromises, the current BESSs have strict limitations on the efficiency due to the use of low voltage batteries that are associated with high currents and more complex converter topologies. On the other hand, the batteries with increased voltages would enable the use of non-isolated topologies with potentially higher efficiencies. Several companies have already introduced such products to the market.

The typical power electronic interface of a battery with the grid is based on a two-stage configuration, comprised of a bidirectional DC-DC converter and a DC-AC inverter/rectifier connected via an intermediate DC-link. Modern Li-ion batteries can sustain current ripples associated with the grid frequency very well, even in single-phase systems. It is therefore possible to connect a battery of sufficiently high voltage to an inverter directly. Still, due to variation of battery voltage depending on its state of charge, the efficiency and power quality of such system is compromised. As a result, the intermediate DC-DC stage is still necessary to stabilize the DC voltage and obtain better performance.

With the possibility of using non-isolated converters to interface HV batteries, the standard approach would assume application of well-known DC-DC topologies, like buck, boost and buck-boost together with the grid inverter stage. This makes both of the two conversion stages process full power and exhibit high switching frequency, which still compromises the efficiency. One of the approaches that is widely addressed in recent studies is to use emerging solutions, like PPCs and FPCs at the DC-DC stage, which, as it is already reported, have been achieved extremely high efficiency values. However, the practical aspects, including transient operating modes, protection and cost, need to be evaluated further to justify this technology.

A range of alternative concepts utilizes a pulsating DC-link instead of the stabilized one. This brings the converter system closer to the single-stage converter, where only DC-DC stage operates with high frequency, while the grid-side inverter just unfolds the unipolar pulses into the sine wave and exhibits conduction losses only. A similar approach can be applicable to both single- and three-phase systems [145]. In addition, mixed concepts with fluctuating DC-link were also proposed, aiming to distribute losses more evenly between the stages [149]. On the other hand, it would be much more difficult to integrate other sources into such DC-link and therefore such solutions are generally suitable for AC-coupled BESS only.

Impedance source inverters are another group of topologies that allow voltage pre-regulation at a "virtual DC-link" before it is inverted into a sinusoidal waveform. Single-phase, three-phase and three-level configurations of these inverters were proposed in [150]. They can be more short-circuit-proof, as the shoot-through state is one of the inherent operating modes of such topologies. However, some studies show that the voltage stress on semiconductors and volume of components can be larger than for the standard two-stage configurations [151]. Moreover, only few studies address bidirectional operation of impedance-source converters [152,153].

In conclusion, there is a range of solutions for HV BESSs that are potential alternatives to standard buck-boost plus inverter configuration. The most optimal choice would evidently depend on the parameters of the system and its configuration. For the systems that incorporate a DC bus for integration of renewables and loads, a PPC/FPC with a bridge-type bidirectional inverter/rectifier seems to be a very promising solution. On the other hand, for an AC-coupled BES, the use of pulsating/fluctuating DC-link and unfolding inverter can bring an advantage in terms of switching loss and absence of a bulky capacitor. Still, the behavior of such configurations in practical applications, including transient modes and fault ride-through capabilities, needs to be addressed in more detail.

The configurations that include multilevel inverter topologies also seem quite promising for residential BESs. Despite generally being used in high-power applications, there are successful commercialization examples of this technology in residential applications. Recent works aim to bring such inverters on a new level, particularly taking advantage of developments in WBG semiconductors [115,116]. The systems with multilevel topologies potentially enable the use of battery stacks with lower voltage levels as compared to standard two-level inverters. This could result in a more optimal storage configuration. On the other hand, presently, the cost of WBG devices is still relatively high to make such multilevel inverters feasible in commercial BESSs.

The comparative analysis of evaluated power electronic interfaces is presented in Tables 3 and 4. The considerations above show that the most promising units of composite

BESS grid interface converters have somehow completing features (see Table 3 for details). For example, unfolding circuits provide neither DC regulation at the corresponding port nor AC half wave forming. This functionality, however, can be performed by a DC-DC converter. Multilevel converters without pulse mode control do not provide pulse mode regulation between levels, but partial power converters—provide regulation within a narrow range. Besides, the multilevel converters and unfolding units have no switching losses, but have significant conduction losses (Table 3). At the same time, the partial power converters can reduce both. A logical conclusion from the above is to combine the units with the adjacent features (Table 4).

Table 3. Losses of converters and energy conversion principles in BESS grid interface.

Stage	Main Function	Peculiarities
Full Power Switch-Mode Rectifiers/Inverter (origin for comparison)	Forming AC	+ Established technology, − High voltage input, high switching frequency, bulky filter
Full Power Switch-Mode DC/DC Converters	Forming DC	+ Established technology, wide regulation range, − Full power operation, high switching frequency
Partial Power Converters	Forming DC	+ Operation with part of rated power − Developing technology, limited regulation range
Multilevel Converters	Forming AC or DC	+ Established technology, small grid filter − Control and hardware complexity
Unfolding Circuits	Commutation	+ No switching losses − Developing technology, no regulation

Table 4. Promising combination of converters to form BESS grid interface.

Configuration	Advantages	Disadvantages
Single stage DC-AC Bidirectional Inverters/Rectifiers	Max. efficiency at a particular operation point	Lower efficiency at most of the operation points, Minimal battery voltage > amplitude of grid voltage
Impedance-Source Bidirectional Inverters/Rectifiers	Battery voltage pre-regulation Short-Circuit Proof	Voltage stress on semiconductors and volume of components is larger Complicated bidirectional operation Developing technology
Bidirectional inverter/ rectifier + Full Power DC-DC	Higher efficiency at the most of operation points, Wide battery voltage range, Allows integration of renewables into DC-link	Lower maximal efficiency, Both stages operate at full power and high switching frequency
Bidirectional inverter/ rectifier + PPC DC-DC	Higher efficiency at the most of operation points, Allows integration of renewables into DC-link, DC-DC operates with part of rated power	Narrow battery voltage range, Developing technology
Multilevel DC-DC and DC-AC	Low grid filter size and volume, Utilization of low voltage semiconductors, Modular design	High component count Complex control
Unfolder + Full Power DC-DC	Higher efficiency at the most of operation points, Wide battery voltage range, No switching losses in grid stage, No DC-link capacitor	No integration of renewables into DC-link

6. Conclusions and Future Trends

This paper gives an insight into the field of storage systems for residential applications together with associated technologies and developments. To provide a broader view, the

current state of these systems is addressed from multiple directions, including battery technologies, their market, standards, and grid interface converters.

Instigated by the on-going paradigm shift from centralized to distributed power generation, the storage technologies will become one of the key components of the future electrical grids that enable more optimal use of the conventional and local renewable energy sources and ensure the power supply security. However, a range of technological and regulatory barriers still stand in the way of these systems, limiting their benefits and potential.

Today's market for dedicated residential storage systems is still in the process of being established. It is currently very dynamic, and several manufacturers have already introduced and commercialized their solutions, with more companies and products being announced and trying to enter the market every year. Still, the price for residential solutions is relatively high for a private client, while the return of investment is not evident in many cases.

The developments and price reduction of Li-ion battery technologies are mainly driven by massive transportation electrification and this trend will continue in the following years. Despite the distinct potential of vehicle to grid (V2G) solutions, they are unlikely to be able to replace stationary battery systems and their functions due to economic reasons, mainly related to lifetime and cycle-cost. Nevertheless, the use of second-life Li-ion batteries for stationary storage has certain potential.

Batteries based on the Li-ion technology are currently dominating the market, however, at a certain point, the price and performance of other battery technologies, like flow batteries, is likely to make them a more expedient choice for larger-scale stationary solutions.

According to our analysis, the majority of commercial residential storages are currently using low voltage batteries with voltages of around 50 V, mainly due to the cheaper price per kWh. These batteries are typically interfaced with the grid by means of a power electronic converter with a transformer to provide required voltage matching and galvanic isolation. However, the mass production of HV EV batteries along with their second-life use is likely to make the HV stationary storage solutions more popular in the residential sector. This would make the use of non-isolated interface converter topologies attractive due to their typically lower component count and higher efficiency. In addition to standard and typically used topologies, like buck-boost or bridge, which are rated for full power of the system, the recent research interest is also focused on partial- (fractional-, differential-) power converters. Such topologies have the potential to offer even further improvement of efficiency in various operating conditions.

Presently, many countries are introducing initiatives that are either directly (by subsidies) or indirectly (via marginal feed-in tariffs) encouraging the use of local energy storage. Moreover, a range of standards is being developed to regulate the use of such systems and facilitate unleashing of their full potential. In addition to basic renewable energy self-consumption increase, battery-based storage systems can provide uninterruptable power supply functionality, offer ancillary grid service support, enable peer-to-peer energy trading etc. Together with the large-scale global investments in the battery technologies it is highly likely that in the following decades, the residential battery systems will follow the route of photovoltaics and become an essential and inherent part of the future power grid.

Author Contributions: Conceptualization, I.A.G. and A.B. (Andrei Blinov); investigation of BESS market solutions, R.S.; investigation of IP right items and BESS market state for distribution grids, M.V.; topological analysis of single stage pulse mode converters, I.A.G.; topological analysis of multilevel converters, A.B. (Alexander Bubovich); topological analysis of partial power processors, I.A.G. and R.S.; supervision, I.A.G.; Validation, I.A.G.; writing—original draft, all; Supervision and editing—A.B. (Andrei Blinov) and D.P. All authors have read and agreed to the published version of the manuscript.

Funding: This work was supported in part by the European Economic Area (EEA) and Norway Financial Mechanism 2014–2021 under Grant EMP474 and in part by the Estonian Research Council grant (PRG1086).

Institutional Review Board Statement: Not applicable.

Informed Consent Statement: Not applicable.

Data Availability Statement: Data is contained within the article.

Conflicts of Interest: The authors declare no conflict of interest.

References

1. The European Parliament and Council of the European Union. Directive 2009/28/EC on the promotion of the use of energy from renewable sources. *Off. J. Eur. Union* **2009**, *L140*, 16–62.
2. The European Parliament and Council of the European Union. Directive (EU) 2018/2001 on the promotion of the use of energy from renewable sources. *Off. J. Eur. Union* **2018**, *L328*, 82–209.
3. European Commission. Energy Strategy. Available online: https://ec.europa.eu/energy/topics/energy-strategy-and-energy-union_en (accessed on 13 November 2020).
4. Andrijanovits, A.; Hoimoja, H.; Vinnikov, D. Comparative Review of Long-Term Energy Storage Technologies for Renewable Energy Systems. *Elektron. Elektrotechnika* **2012**, *118*, 21–26. [CrossRef]
5. Vinnikov, D.; Hoimoja, H.; Andrijanovits, A.; Roasto, I.; Lehtla, T.; Klytta, M. An improved interface converter for a medium-power wind-hydrogen system. In Proceedings of the 2009 International Conference on Clean Electrical Power, Capri, Italy, 9–11 June 2009; Institute of Electrical and Electronics Engineers (IEEE): New York, NY, USA, 2009; pp. 426–432. [CrossRef]
6. Liang, M.; Liu, Y.; Xiao, B.; Yang, S.; Wang, Z.; Han, H. An analytical model for the transverse permeability of gas diffusion layer with electrical double layer effects in proton exchange membrane fuel cells. *Int. J. Hydrog. Energy* **2018**, *43*, 17880–17888. [CrossRef]
7. Liang, M.; Fu, C.; Xiao, B.; Luo, L.; Wang, Z. A fractal study for the effective electrolyte diffusion through charged porous media. *Int. J. Heat Mass Transf.* **2019**, *137*, 365–371. [CrossRef]
8. Vinnikov, D.; Andrijanovits, A.; Roasto, I.; Jalakas, T. Experimental study of new integrated DC/DC converter for hydrogen-based energy storage. In Proceedings of the 2011 10th International Conference on Environment and Electrical Engineering, Rome, Italy, 8–11 May 2011; Institute of Electrical and Electronics Engineers (IEEE): New York, NY, USA, 2011; pp. 1–4.
9. Stecca, M.; Elizondo, L.R.; Soeiro, T.; Bauer, P.; Palensky, P. A Comprehensive Review of the Integration of Battery Energy Storage Systems into Distribution Networks. *IEEE Open J. Ind. Electron. Soc.* **2020**, *1*, 46–65. [CrossRef]
10. Wang, G.; Konstantinou, G.; Townsend, C.D.; Pou, J.; Vazquez, S.; Demetriades, G.D.; Agelidis, V.G. A Review of Power Electronics for Grid Connection of Utility-Scale Battery Energy Storage Systems. *IEEE Trans. Sustain. Energy* **2016**, *7*, 1778–1790. [CrossRef]
11. Pires, V.F.; Romero-Cadaval, E.; Vinnikov, D.; Roasto, I.; Martins, J. Power converter interfaces for electrochemical energy storage systems–A review. *Energy Convers. Manag.* **2014**, *86*, 453–475. [CrossRef]
12. Yao, Z. Review of Dual-Buck Type Single-Phase Grid-Connected Inverters. *IEEE J. Emerg. Sel. Top. Power Electron.* **2020**, *1*. [CrossRef]
13. Available online: https://nakedsolar.co.uk/storage/ (accessed on 7 June 2021).
14. Available online: https://www.which.co.uk/reviews/solar-panels/article/solar-panels/solar-panel-battery-storage-a2AfJ0s5tCyT (accessed on 7 June 2021).
15. Saez-De-Ibarra, A.; Laserna, E.M.; Stroe, D.-I.; Swierczynski, M.J.; Rodriguez, P. Sizing Study of Second Life Li-ion Batteries for Enhancing Renewable Energy Grid Integration. *IEEE Trans. Ind. Appl.* **2016**, *52*, 4999–5008. [CrossRef]
16. Rezania, R.; Prüggler, W. Business models for the integration of electric vehicles into the Austrian energy system. In *2012 9th International Conference on the European Energy Market*; Institute of Electrical and Electronics Engineers (IEEE): New York, NY, USA, 2012; pp. 1–8.
17. Robert, S. *Introduction to Batteries—An IEEE Course*; IEEE: New York, NY, USA, 2013.
18. Hu, X.; Zou, C.; Zhang, C.; Li, Y. Technological Developments in Batteries: A Survey of Principal Roles, Types, and Management Needs. *IEEE Power Energy Mag.* **2017**, *15*, 20–31. [CrossRef]
19. *Electricity Storage and Renewables: Costs and Markets to 2030*; The International Renewable Energy Agency (IRENA): Abu Dhabi, United Arab Emirates, 2017; pp. 36–49.
20. Cao, J.; Emadi, A. Batteries Need Electronics. *IEEE Ind. Electron. Mag.* **2011**, *5*, 27–35. [CrossRef]
21. Ferreira, B. Batteries, the New Kids on the Block. *IEEE Power Electron. Mag.* **2019**, *6*, 32–34. [CrossRef]
22. Chen, C.; Plunkett, S.; Salameh, M.; Stoyanov, S.; Al-Hallaj, S.; Krishnamurthy, M. Enhancing the Fast Charging Capability of High-Energy-Density Lithium-Ion Batteries: A Pack Design Perspective. *IEEE Electrif. Mag.* **2020**, *8*, 62–69. [CrossRef]
23. Fulli, G.; Masera, M.; Spisto, A.; Vitiello, S. A Change is Coming: How Regulation and Innovation Are Reshaping the European Union's Electricity Markets. *IEEE Power Energy Mag.* **2019**, *17*, 53–66. [CrossRef]
24. Lukic, S.; Emadi, A. Charging ahead. *IEEE Ind. Electron. Mag.* **2008**, *2*, 22–31. [CrossRef]
25. Khaligh, A.; Li, Z. Battery, Ultracapacitor, Fuel Cell, and Hybrid Energy Storage Systems for Electric, Hybrid Electric, Fuel Cell, and Plug-In Hybrid Electric Vehicles: State of the Art. *IEEE Trans. Veh. Technol.* **2010**, *59*, 2806–2814. [CrossRef]
26. Quiros-Tortos, J.; Ochoa, L.; Butler, T. How Electric Vehicles and the Grid Work Together: Lessons Learned from One of the Largest Electric Vehicle Trials in the World. *IEEE Power Energy Mag.* **2018**, *16*, 64–76. [CrossRef]

27. Chen, N.; Ma, J.; Li, M.; Wang, M.; Shen, X.S. Energy Management Framework for Mobile Vehicular Electric Storage. *IEEE Netw.* **2019**, *33*, 148–155. [CrossRef]
28. Chandler, S.; Gartner, J.; Jones, D. Integrating Electric Vehicles with Energy Storage and Grids: New Technology and Specific Capabilities Spur Numerous Applications. *IEEE Electrif. Mag.* **2018**, *6*, 38–43. [CrossRef]
29. Al-Rubaye, S.; Al-Dulaimi, A.; Ni, Q. Power Interchange Analysis for Reliable Vehicle-to-Grid Connectivity. *IEEE Commun. Mag.* **2019**, *57*, 105–111. [CrossRef]
30. Arboleya, P.; Bidaguren, P.; Armendariz, U. Energy Is on Board: Energy Storage and Other Alternatives in Modern Light Railways. *IEEE Electrif. Mag.* **2016**, *4*, 30–41. [CrossRef]
31. Sinhuber, P.; Rohlfs, W.; Sauer, D.U. Study on power and energy demand for sizing the energy storage systems for electrified local public transport buses. In *2012 IEEE Vehicle Power and Propulsion Conference*; Institute of Electrical and Electronics Engineers (IEEE): New York, NY, USA, 2012; pp. 315–320. [CrossRef]
32. Guarnieri, M.; Morandin, M.; Ferrari, A.; Campostrini, P.; Bolognani, S. Electrifying Water Buses: A Case Study on Diesel-to-Electric Conversion in Venice. *IEEE Ind. Appl. Mag.* **2017**, *24*, 71–83. [CrossRef]
33. Sorensen, A.J.; Skjetne, R.; Bo, T.; Miyazaki, M.R.; Johansen, T.A.; Utne, I.B.; Pedersen, E. Toward Safer, Smarter, and Greener Ships: Using Hybrid Marine Power Plants. *IEEE Electrif. Mag.* **2017**, *5*, 68–73. [CrossRef]
34. Paul, D. A History of Electric Ship Propulsion Systems [History]. *IEEE Ind. Appl. Mag.* **2020**, *26*, 9–19. [CrossRef]
35. Vicenzutti, A.; Bosich, D.; Giadrossi, G.; Sulligoi, G. The Role of Voltage Controls in Modern All-Electric Ships: Toward the all electric ship. *IEEE Electrif. Mag.* **2015**, *3*, 49–65. [CrossRef]
36. Roboam, X.; Sareni, B.; De Andrade, A. More Electricity in the Air: Toward Optimized Electrical Networks Embedded in More-Electrical Aircraft. *IEEE Ind. Electron. Mag.* **2012**, *6*, 6–17. [CrossRef]
37. Misra, A. Energy Storage for Electrified Aircraft: The Need for Better Batteries, Fuel Cells, and Supercapacitors. *IEEE Electrif. Mag.* **2018**, *6*, 54–61. [CrossRef]
38. Crittenden, M. Ultralight batteries for electric airplanes. *IEEE Spectr.* **2020**, *57*, 44–49. [CrossRef]
39. Manz, D.; Piwko, R.; Miller, N. Look before You Leap: The Role of Energy Storage in the Grid. *IEEE Power Energy Mag.* **2012**, *10*, 75–84. [CrossRef]
40. Farrokhabadi, M.; Solanki, B.V.; Canizares, C.A.; Bhattacharya, K.; Koenig, S.; Sauter, P.S.; Leibfried, T.; Hohmann, S. Energy Storage in Microgrids: Compensating for Generation and Demand Fluctuations While Providing Ancillary Services. *IEEE Power Energy Mag.* **2017**, *15*, 81–91. [CrossRef]
41. Cagnano, A.; De Tuglie, E.; Mancarella, P. Microgrids: Overview and guidelines for practicalimplementations and operation. *Appl. Energy* **2020**, *258*, 114039. [CrossRef]
42. Torres-Moreno, J.L.; Gimenez-Fernandez, A.; Perez-Garcia, M.; Rodriguez, F. EnergyManagement Strategy for Micro-Grids with PV-Battery Systems and Electric Vehicles. *Energies* **2018**, *11*, 522. [CrossRef]
43. Lezynski, P.; Szczesniak, P.; Waskowicz, B.; Smolenski, R.; Drozdz, W. Design andimplementation of a fully controllable cyber-physical system for testing energy storage systems. *IEEE Access* **2019**, *7*, 47259–47272. [CrossRef]
44. Restrepo, C.; Salazar, A.; Schweizer, H.; Ginart, A. Residential Battery Storage: Is the Timing Right? *IEEE Electrif. Mag.* **2015**, *3*, 14–21. [CrossRef]
45. González, I.; Calderón, A.J.; Portalo, J.M. Innovative Multi-Layered Architecture forHeterogeneous Automation and Moni-toring Systems: Application Case of a Photovoltaic SmartMicrogrid. *Sustainability* **2021**, *13*, 2234. [CrossRef]
46. James, G.; Peng, W.; Deng, K. Managing Household Wind-Energy Generation. *IEEE Intell. Syst.* **2008**, *23*, 9–12. [CrossRef]
47. Duryea, S.; Islam, S.; Lawrance, W. A battery management system for stand-alone photovoltaic energy systems. *IEEE Ind. Appl. Mag.* **2001**, *7*, 67–72. [CrossRef]
48. Lu, X.; Wang, J. A Game Changer: Electrifying Remote Communities by Using Isolated Microgrids. *IEEE Electrif. Mag.* **2017**, *5*, 56–63. [CrossRef]
49. Zhong, Q.-C.; Wang, Y.; Ren, B. Connecting the Home Grid to the Public Grid: Field Demonstration of Virtual Synchronous Machines. *IEEE Power Electron. Mag.* **2019**, *6*, 41–49. [CrossRef]
50. Ma, Z.; Pesaran, A.; Gevorgian, V.; Gwinner, D.; Kramer, W. Energy Storage, Renewable Power Generation, and the Grid: NREL Capabilities Help to Develop and Test Energy-Storage Technologies. *IEEE Electrif. Mag.* **2015**, *3*, 30–40. [CrossRef]
51. Rodriguez-Diaz, E.; Chen, F.; Vasquez, J.C.; Guerrero, J.M.; Burgos, R.; Boroyevich, D. Voltage-Level Selection of Future Two-Level LVdc Distribution Grids: A Compromise Between Grid Compatibiliy, Safety, and Efficiency. *IEEE Electrif. Mag.* **2016**, *4*, 20–28. [CrossRef]
52. IEC TC 120 Group BESS Systems Standardization Plan. Available online: https://assets.iec.ch/public/miscfiles/sbp/120.pdf (accessed on 28 February 2021).
53. *UL STD 1741. Inverters Converters and Controllers for Use in Independent Power Systems*; IEEE: New York, NY, USA, 2018.
54. *IEC TS 62933-5-1. Electrical Energy Storage (EES) Systems-Part 5-1: Safety Considerations for Grid-Integrated EES Systems-General Specification*; IEEE: New York, NY, USA; ISO/IEC: Geneva, Switzerland, 2017.
55. *IEC T R 62543. High-Voltage Direct Current (HVDC) Power Transmission Using Voltage Sourced Converters (VSC)*; ISO/IEC: Geneva, Switzerland, 2017.
56. *Standard IEC TR 61850-90-7. Communication Networks and Systems for Power Utility Automation-Part 90-7: Object Models for Power Converters in Distributed Energy Resources (DER) Systems*; ISO/IEC: Geneva, Switzerland, 2013.

57. *Standard IEC 62920. Photovoltaic Power Generating Systems-EMC Requirements and Test Methods for Power Conversion Equipment*; ISO/IEC: Geneva, Switzerland, 2017.
58. *Standard IEC 62909-1. Bi-Directional Grid Connected Power Converters-Part 1: General Requirements*; ISO/IEC: Geneva, Switzerland, 2017.
59. *Standard IEC 62040-5-3. Uninterruptible Power Systems (UPS)-Part 5-3: DC Output UPS-Performance and Test Requirements*; ISO/IEC: Geneva, Switzerland, 2016.
60. *Standard IEC 62040-4. Uninterruptible Power Systems (UPS)-Part 4: Environmental Aspects-Requirements and Reporting*; ISO/IEC: Geneva, Switzerland, 2013.
61. *Standard IEC62040-3. Uninterruptible Power Systems (UPS)-Part 3: Method of Specifying the Performance and Test Requirements*; ISO/IEC: Geneva, Switzerland, 2011.
62. The EMerge Alliance Data/Telecom Center Standard Creates an Integrated, Open Platform for Power, Infrastructure, Peripheral Device and Control Applications to Facilitate the Hybrid Use of AC and DC Power within Data Centers and Telecom Central Offices. Available online: https://www.emergealliance.org/standards/data-telecom/standard-faqs/ (accessed on 28 February 2021).
63. Tesla Powerwall Review. Available online: https://www.cleanenergyreviews.info/blog/tesla-powerwall-2-solar-battery-review (accessed on 25 April 2021).
64. Sonnen Documentation. Available online: http://www.sonnensupportaustralia.com.au/documentation.html (accessed on 25 April 2021).
65. Available online: https://store.enphase.com/storefront/en-us/pub/media/productattach/e/n/envoys-ds-en-us.pdf (accessed on 7 June 2021).
66. Available online: https://store.enphase.com/storefront/en-us/pub/media/productattach/e/n/enphase_encharge_3_datasheet.pdf (accessed on 7 June 2021).
67. Available online: https://store.enphase.com/storefront/en-us/pub/media/productattach/e/n/encharge_10_datasheet.pdf (accessed on 7 June 2021).
68. Victron Energy Blue Power. Available online: https://www.victronenergy.com/upload/documents/Brochure-Energy-Storage-EN_web.pdf (accessed on 25 February 2021).
69. ADARA Power Commercial Energy Storage System. Available online: http://www.adarapower.com/home/commercial-energy-storage-system/ (accessed on 25 February 2021).
70. Adara Power Introduces 20-kWh Residential Energy Storage Solution. Available online: https://www.solarpowerworldonline.com/2017/04/adara-power-introduces-20-kwh-residential-energy-storage-solution/ (accessed on 25 February 2021).
71. Schnoder Electric Hybrid Inverter/Charger XW+. Available online: https://solar.schneider-electric.com/wp-content/uploads/2020/08/DS20200812_XW-120-240-V.pdf (accessed on 25 February 2021).
72. Sunverge Energy AC-Coupled Solar Integration System (SIS). Available online: https://cdn2.hubspot.net/hubfs/2472485/WebsiteContent/Sunverge_ACSIS_NA_12092016.pdf?t=1485218396447 (accessed on 25 February 2021).
73. LG Home Battery RESU. Available online: https://www.lgessbattery.com/eu/main/main.lg (accessed on 25 April 2021).
74. Solax Triple Power Battery–LFP. Available online: https://www.solaxpower.com/triple-power-battery/ (accessed on 25 April 2021).
75. StorEdge™ On-Grid Solution. Available online: https://www.solaredge.com/solutions/self-consumption#/ (accessed on 25 April 2021).
76. 4 kWh Powervault Lead-Acid Solar Energy Storage Systems. Available online: https://www.ecopowersupplies.com/4kwh-powervault-lead-acid-solar-energy-storage-systems (accessed on 25 February 2021).
77. Purestorage, I.I. Available online: https://www.puredrive-energy.co.uk/ (accessed on 25 April 2021).
78. Duracell Energy Bank. Available online: https://www.duracellenergybank.com/ (accessed on 25 April 2021).
79. Enphase Encharge 3. Available online: https://store.enphase.com/storefront/en-us/enphase_encharge_3 (accessed on 25 April 2021).
80. Enphase Encharge 10. Available online: https://store.enphase.com/storefront/en-us/enphase_encharge_10 (accessed on 25 April 2021).
81. Available online: https://www.eaton.com/content/eaton/gb/en-gb/catalog/energy-storage/xstorage-home.html/ (accessed on 25 April 2021).
82. xStorage Home. Available online: https://www.samsungsdi.com/ess/index.html (accessed on 25 April 2021).
83. VARTA Pulse Neo. Available online: https://www.varta-ag.com/en/consumer/product-categories/energy-storage-systems/varta-pulse-neo (accessed on 25 April 2021).
84. Sunny Boy Storage 2.5. Available online: https://www.sma.de/en/products/battery-inverters/sunny-boy-storage-25.html (accessed on 25 April 2021).
85. EasySolar. Available online: https://www.victronenergy.ru/inverters-chargers/easysolar (accessed on 25 April 2021).
86. EssProTM-Battery Energy Storage. The Power to Control Energy. Available online: https://new.abb.com/docs/librariesprovider78/eventos/jjtts-2017/presentaciones-peru/(dario-cicio)-bess---battery-energy-storage-system.pdf?sfvrsn=2 (accessed on 28 February 2021).
87. Battery Energy Storage Solutions for Stable Power Supply. Available online: https://www.nidec-industrial.com/markets/renewable-energy/battery-energy-storage-solutions/ (accessed on 28 February 2021).

88. Kheraluwala, M.; Gascoigne, R.; Divan, D.; Baumann, E. Performance characterization of a high-power dual active bridge DC-to-DC converter. *IEEE Trans. Ind. Appl.* **1992**, *28*, 1294–1301. [CrossRef]
89. Stynski, S.; Luo, W.; Chub, A.; Franquelo, L.G.; Malinowski, M.; Vinnikov, D. Utility-Scale Energy Storage Systems: Converters and Control. *IEEE Ind. Electron. Mag.* **2020**, *14*, 32–52. [CrossRef]
90. Inoue, S.; Akagi, H. A Bidirectional DC–DC Converter for an Energy Storage System with Galvanic Isolation. *IEEE Trans. Power Electron.* **2007**, *22*, 2299–2306. [CrossRef]
91. Manias, S.; Ziogas, P.; Olivier, G. Bilateral DC to AC convertor using a high frequency link. *IEE Proc. B Electr. Power Appl.* **1987**, *134*, 15. [CrossRef]
92. Blinov, A.; Korkh, O.; Chub, A.; Vinnikov, D.; Peftitsis, D.; Norrga, S.; Galkin, I. High Gain DC-AC High-Frequency Link Inverter with Improved Quasi-Resonant Modulation. *IEEE Trans. Ind. Electron.* **2021**. [CrossRef]
93. Korkh, O.; Blinov, A.; Vinnikov, D.; Chub, A. Review of Isolated Matrix Inverters: Topologies, Modulation Methods and Applications. *Energies* **2020**, *13*, 2394. [CrossRef]
94. Chung, H.; Cheung, W.-L.; Tang, K. A ZCS Bidirectional Flyback DC/DC Converter. *IEEE Trans. Power Electron.* **2004**, *19*, 1426–1434. [CrossRef]
95. Lessing, M.H.; Agostini, E.; Barbi, I. An improved modulation strategy for the high-frequency-isolated DC-AC flyback converter with differential output connection. In Proceedings of the 2016 12th IEEE International Conference on Industry Applications (INDUSCON), Curitiba, Brazil, 20–23 November 2016; Institute of Electrical and Electronics Engineers (IEEE): New York, NY, USA, 2017; pp. 1–7.
96. Ponnaluri, S.; Linhofer, G.; Steinke, J.; Steimer, P.K. Comparison of single and two stage topologies for interface of BESS or fuel cell system using the ABB standard power electronics building blocks. In Proceedings of the 2005 European Conference on Power Electronics and Applications, Dresden, Germany, 11–14 September 2005; Institute of Electrical and Electronics Engineers (IEEE): New York, NY, USA, 2005.
97. Srinivasan, R.; Oruganti, R. A unity power factor converter using half-bridge boost topology. *IEEE Trans. Power Electron.* **1998**, *13*, 487–500. [CrossRef]
98. Vazquez, S.; Lukic, S.M.; Galvan, E.; Franquelo, L.G.; Carrasco, J.M. Energy Storage Systems for Transport and Grid Applications. *IEEE Trans. Ind. Electron.* **2010**, *57*, 3881–3895. [CrossRef]
99. Stanley, G.; Bradshaw, K. Precision DC-to-AC power conversion by optimization of the output current waveform-the half bridge revisited. *IEEE Trans. Power Electron.* **1999**, *14*, 372–380. [CrossRef]
100. Zhang, L.; Zhu, T.; Chen, L.; Sun, K. A systematic topology generation method for dual-buck inverters. In *2016 IEEE Energy Conversion Congress and Exposition (ECCE)*; Institute of Electrical and Electronics Engineers (IEEE): New York, NY, USA, 2017; pp. 1–6.
101. Xie, J.; Zhang, F.; Ren, R.; Wang, X.; Wang, J. A novel high power density dual-buck inverter with coupled filter inductors. In *IECON 2014-40th Annual Conference of the IEEE Industrial Electronics Society*; Institute of Electrical and Electronics Engineers (IEEE): New York, NY, USA, 2014; pp. 1111–1117.
102. Zhou, L.; Gao, F. Dual buck inverter with series connected diodes and single inductor. In *2016 IEEE Applied Power Electronics Conference and Exposition (APEC)*; Institute of Electrical and Electronics Engineers (IEEE): New York, NY, USA, 2016; pp. 2259–2263.
103. Araujo, S.V.; Zacharias, P.; Mallwitz, R. Highly Efficient Single-Phase Transformerless Inverters for Grid-Connected Photovoltaic Systems. *IEEE Trans. Ind. Electron.* **2010**, *57*, 3118–3128. [CrossRef]
104. Gu, B.; Dominic, J.; Lai, J.-S.; Chen, C.-L.; Labella, T.; Chen, B. High Reliability and Efficiency Single-Phase Transformerless Inverter for Grid-Connected Photovoltaic Systems. *IEEE Trans. Power Electron.* **2012**, *28*, 2235–2245. [CrossRef]
105. Colak, I.; Kabalci, E.; Bayindir, R. Review of multilevel voltage source inverter topologies and control schemes. *Energy Convers. Manag.* **2011**, *52*, 1114–1128. [CrossRef]
106. Liu, C.; Cai, X.; Chen, Q. Self-Adaptation Control of Second-Life Battery Energy Storage System Based on Cascaded H-Bridge Converter. *IEEE J. Emerg. Sel. Top. Power Electron.* **2018**, *8*, 1428–1441. [CrossRef]
107. Ling, Z.; Zhang, Z.; Li, Z.; Li, Y. State-of-charge balancing control of battery energy storage system based on cascaded H-bridge multilevel inverter. In Proceedings of the 2016 IEEE 8th International Power Electronics and Motion Control Conference (IPEMC-ECCE Asia); Institute of Electrical and Electronics Engineers (IEEE): New York, NY, USA, 2016; pp. 2310–2314.
108. Yoscovich, I.; Glovinsky, T.; Sella, G.; Galin, Y. SolarEdge Patent for HD-Wave Inverters-Distributed Power System Using Direct Current Power Sources. U.S. Patent 9368964B2, 14 June 2016.
109. Demetriades, G.D. Modular Multilevel Converter with Cell-Connected Battery Storages. European Patent EP2695273B1, 25 November 2015.
110. Moradpour, M.; Ghani, P.; Pirino, P.; Gatto, G. A GaN-Based Battery Energy Storage System for Three-Phase Residential Application with Series-Stacked Devices and Three-Level Neutral Point Clamped Topology. In *2019 1st International Conference on Energy Transition in the Mediterranean Area (SyNERGY MED)*; Institute of Electrical and Electronics Engineers (IEEE): New York, NY, USA, 2019; pp. 1–6.
111. Abronzini, U.; Attaianese, C.; Di Monaco, M.; Tomasso, G.; Damiano, A.; Porru, M.; Serpi, A. A Dual-Source DHB-NPC Power Converter for Grid Connected Split Battery Energy Storage System. In *2018 IEEE Energy Conversion Congress and Exposition (ECCE)*; Institute of Electrical and Electronics Engineers (IEEE): New York, NY, USA, 2018; pp. 2483–2488.

112. Trintis, I.; Teodorescu, R.; Munk-Nielsen, S. Single stage grid converters for battery energy storage. In Proceedings of the 5th IET International Conference on Power Electronics, Machines and Drives (PEMD 2010), Brighton, UK, 19–21 April 2010; Institution of Engineering and Technology (IET): London, UK, 2010; p. 234.
113. Bragard, M.; Soltau, N.; Thomas, S.; De Doncker, R.W. The Balance of Renewable Sources and User Demands in Grids: Power Electronics for Modular Battery Energy Storage Systems. *IEEE Trans. Power Electron.* **2010**, *25*, 3049–3056. [CrossRef]
114. Cheng, Y.; Qian, C.; Crow, M.L.; Pekarek, S.; Atcitty, S. A Comparison of Diode-Clamped and Cascaded Multilevel Converters for a STATCOM with Energy Storage. *IEEE Trans. Ind. Electron.* **2006**, *53*, 1512–1521. [CrossRef]
115. Barth, C.B.; Assem, P.; Foulkes, T.; Chung, W.H.; Modeer, T.; Lei, Y.; Pilawa-Podgurski, R.C.N. Design and Control of a GaN-Based, 13-Level, Flying Capacitor Multilevel Inverter. *IEEE J. Emerg. Sel. Top. Power Electron.* **2019**, *8*, 2179–2191. [CrossRef]
116. Modeer, T.; Pallo, N.; Foulkes, T.; Barth, C.B.; Pilawa-Podgurski, R.C.N. Design of a GaN-Based Interleaved Nine-Level Flying Capacitor Multilevel Inverter for Electric Aircraft Applications. *IEEE Trans. Power Electron.* **2020**, *35*, 12153–12165. [CrossRef]
117. Siwakoti, Y.P.; Peng, F.Z.; Blaabjerg, F.; Loh, P.C.; Town, G.E. Impedance-Source Networks for Electric Power Conversion Part I: A Topological Review. *IEEE Trans. Power Electron.* **2015**, *30*, 699–716. [CrossRef]
118. Mande, D.; Trovão, J.P.; Ta, M.C. Comprehensive Review on Main Topologies of Impedance Source Inverter Used in Electric Vehicle Applications. *World Electr. Veh. J.* **2020**, *11*, 37. [CrossRef]
119. You, K.; Rahman, M.F. A Matrix–Z-Source Converter with AC–DC Bidirectional Power Flow for an Integrated Starter Alternator System. *IEEE Trans. Ind. Appl.* **2009**, *45*, 239–248. [CrossRef]
120. Matiushkin, O.; Husev, O.; Strzelecki, R.; Ivanets, S.; Fesenko, A. Novel single-stage buck-boost inverter with unfolding circuit. In Proceedings of the 2017 IEEE First Ukraine Conference on Electrical and Computer Engineering (UKRCON), Kyiv, Ukraine, 29 May–2 June 2017; Institute of Electrical and Electronics Engineers (IEEE): New York, NY, USA, 2017; pp. 538–543.
121. Han, B.; Lai, J.-S.; Kim, M. Bridgeless Cuk-Derived Single Power Conversion Inverter with Reactive-Power Capability. *IEEE Trans. Power Electron.* **2019**, *35*, 2629–2645. [CrossRef]
122. Pal, A.; Basu, K. A Single-Stage Soft-Switched Isolated Three-Phase DC–AC Converter with Three-Phase Unfolder. *IEEE Trans. Power Electron.* **2019**, *35*, 3601–3615. [CrossRef]
123. Tytelmaier, K.; Husev, O.; Veligorskyi, O.; Yershov, R. A review of non-isolated bidirectional dc-dc converters for energy storage systems. In *2016 II International Young Scientists Forum on Applied Physics and Engineering (YSF)*; Institute of Electrical and Electronics Engineers (IEEE): New York, NY, USA, 2016; pp. 22–28.
124. Anzola, J.; Aizpuru, I.; Romero, A.A.; Loiti, A.A.; Lopez-Erauskin, R.; Sevil, J.S.A.; Bernal, C. Review of Architectures Based on Partial Power Processing for DC-DC Applications. *IEEE Access* **2020**, *8*, 103405–103418. [CrossRef]
125. Pape, M.; Kazerani, M. An Offshore Wind Farm with DC Collection System Featuring Differential Power Processing. *IEEE Trans. Energy Convers.* **2019**, *35*, 222–236. [CrossRef]
126. Pape, M.; Kazerani, M. Turbine Startup and Shutdown in Wind Farms Featuring Partial Power Processing Converters. *IEEE Open Access J. Power Energy* **2020**, *7*, 254–264. [CrossRef]
127. Iyer, V.M.; Gulur, S.; Gohil, G.; Bhattacharya, S. An Approach towards Extreme Fast Charging Station Power Delivery for Electric Vehicles with Partial Power Processing. *IEEE Trans. Ind. Electron.* **2020**, *67*, 8076–8087. [CrossRef]
128. Schaef, C.; Stauth, J.T. Multilevel Power Point Tracking for Partial Power Processing Photovoltaic Converters. *IEEE J. Emerg. Sel. Top. Power Electron.* **2014**, *2*, 859–869. [CrossRef]
129. Shenoy, P.S. Improving Performance, Efficiency, and Reliability of DC/DC Conversion Systems by Differential Power Processing. Ph.D. Thesis, Graduate College of the University of Illinois at Urbana-Champaign, Champaign, IL, USA, 2012.
130. Zientarski, J.R.R.; Martins, M.L.D.S.; Pinheiro, J.R.; Hey, H.L. Evaluation of Power Processing in Series-Connected Partial-Power Converters. *IEEE J. Emerg. Sel. Top. Power Electron.* **2019**, *7*, 343–352. [CrossRef]
131. Zientarski, J.R.R.; Martins, M.L.D.S.; Pinheiro, J.R.; Hey, H.L. Series-Connected Partial-Power Converters Applied to PV Systems: A Design Approach Based on Step-Up/Down Voltage Regulation Range. *IEEE Trans. Power Electron.* **2018**, *33*, 7622–7633. [CrossRef]
132. Zapata, J.W.; Kouro, S.; Carrasco, G.; Renaudineau, H.; Meynard, T.A. Analysis of Partial Power DC–DC Converters for Two-Stage Photovoltaic Systems. *IEEE J. Emerg. Sel. Top. Power Electron.* **2019**, *7*, 591–603. [CrossRef]
133. Agamy, M.S.; Harfman-Todorovic, M.; Elasser, A.; Chi, S.; Steigerwald, R.L.; Sabate, J.A.; McCann, A.J.; Zhang, L.; Mueller, F.J. An Efficient Partial Power Processing DC/DC Converter for Distributed PV Architectures. *IEEE Trans. Power Electron.* **2014**, *29*, 674–686. [CrossRef]
134. Marti-Arbona, E.; Mandal, D.; Bakkaloglu, B.; Kiaei, S. PV panel power optimization using sub-panel MPPT. In Proceedings of the 2015 IEEE Applied Power Electronics Conference and Exposition (APEC), Charlotte, NC, USA, 15–19 March 2015; Institute of Electrical and Electronics Engineers (IEEE): New York, NY, USA, 2015; pp. 235–238.
135. Loera-Palomo, R.; Morales-Saldaña, J.A.; Palacios-Hernández, E. Quadratic step-down dc–dc converters based on reduced redundant power processing approach. *IET Power Electron.* **2013**, *6*, 136–145. [CrossRef]
136. Spiazzi, G. Reduced redundant power processing concept: A reexamination. In Proceedings of the 2016 IEEE 17th Workshop on Control and Modeling for Power Electronics (COMPEL), Trondheim, Norway, 27–30 June 2016; pp. 1–8. [CrossRef]
137. Xue, F.; Yu, R.; Huang, A. Fractional converter for high efficiency high power battery energy storage system. In Proceedings of the 2017 IEEE Energy Conversion Congress and Exposition (ECCE), Cincinnati, OH, USA, 1–5 October 2017; Institute of Electrical and Electronics Engineers (IEEE): New York, NY, USA, 2017; pp. 5144–5150.

138. Xue, F.; Yu, R.; Huang, A. A Family of Ultrahigh Efficiency Fractional dc–dc Topologies for High Power Energy Storage Device. *IEEE J. Emerg. Sel. Top. Power Electron.* **2021**, *9*, 1420–1427. [CrossRef]
139. Neumayr, D.; Knabben, G.C.; Varescon, E.; Bortis, D.; Kolar, J.W. Comparative Evaluation of a Full- and Partial-Power Processing Active Power Buffer for Ultracompact Single-Phase DC/AC Converter Systems. *IEEE J. Emerg. Sel. Top. Power Electron.* **2021**, *9*, 1994–2013. [CrossRef]
140. Bala, S.; Tengner, T.; Rosenfeld, P.; Delince, F. The effect of low frequency current ripple on the performance of a Lithium Iron Phosphate (LFP) battery energy storage system. In *2012 IEEE Energy Conversion Congress and Exposition (ECCE)*; Institute of Electrical and Electronics Engineers (IEEE): New York, NY, USA, 2012; pp. 3485–3492.
141. Brand, M.J.; Hofmann, M.H.; Schuster, S.S.; Keil, P.; Jossen, A. The Influence of Current Ripples on the Lifetime of Lithium-Ion Batteries. *IEEE Trans. Veh. Technol.* **2018**, *67*, 10438–10445. [CrossRef]
142. Husev, O.; Matiushkin, O.; Roncero-Clemente, C.; Blaabjerg, F.; Vinnikov, D. Novel Family of Single-Stage Buck–Boost Inverters Based on Unfolding Circuit. *IEEE Trans. Power Electron.* **2018**, *34*, 7662–7676. [CrossRef]
143. Zhao, B.; Abramovitz, A.; Liu, C.; Yang, Y.; Huangfu, Y. A Family of Single-Stage, Buck-Boost Inverters for Photovoltaic Applications. *Energies* **2020**, *13*, 1675. [CrossRef]
144. Oguchi, K.; Ikawa, E.; Tsukiori, Y. A three-phase sine wave inverter system using multiple phase-shifted single-phase resonant inverters. *IEEE Trans. Ind. Appl.* **1993**, *29*, 1076–1083. [CrossRef]
145. Rabkowski, J.; Blinov, A.; Zinchenko, D.; Wrona, G.; Zdanowski, M. Grid-frequency Vienna rectifier and isolated current-source DC-DC converters for efficient off-board charging of electric vehicles. In Proceedings of the 2020 22nd European Conference on Power Electronics and Applications (EPE'20 ECCE Europe), Piscataway, NJ, USA, 7–11 September 2020; IEEE: New York, NY, USA, 2020.
146. Jacobson, B.S.; Holmansky, E.N. Methods and Apparatus for Three-Phase Inverter with Reduced Energy Storage. U.S. Patent 7839023B2, 23 November 2010.
147. Chen, W.W.; Zane, R.; Corradini, L. Isolated Bidirectional Grid-Tied Three-Phase AC–DC Power Conversion Using Series-Resonant Converter Modules and a Three-Phase Unfolder. *IEEE Trans. Power Electron.* **2017**, *32*, 9001–9012. [CrossRef]
148. Van Soest, H. Peer-to-peer electricity trading: A review of the legal context. *Compet. Regul. Netw. Ind.* **2018**, *19*, 180–199. [CrossRef]
149. Zhang, D.; Guacci, M.; Kolar, J.W.; Everts, J. Synergetic Control of a 3-Φ Buck-Boost Current DC-Link EV Charger Considering Wide Output Range and Irregular Mains Conditions. In Proceedings of the 2020 IEEE 9th International Power Electronics and Motion Control Conference (IPEMC2020-ECCE Asia), Nanjing, China, 31 May–3 June 2020; pp. 1688–1695.
150. Husev, O.; Roncero-Clemente, C.; Romero-Cadaval, E.; Vinnikov, D.; Stepenko, S. Single phase three-level neutral-point-clamped quasi-Z-source inverter. *IET Power Electron.* **2015**, *8*, 1–10. [CrossRef]
151. Panfilov, D.; Husev, O.; Blaabjerg, F.; Zakis, J.; Khandakji, K. Comparison of three-phase three-level voltage source inverter with intermediate dc–dc boost converter and quasi-Z-source inverter. *IET Power Electron.* **2016**, *9*, 1238–1248. [CrossRef]
152. Baier, T.; Piepenbreier, B. Bidirectional magnetically coupled T-Source Inverter for extra low voltage application. In Proceedings of the 2016 IEEE Applied Power Electronics Conference and Exposition (APEC), Long Beach, CA, USA, 20–24 March 2016; pp. 2897–2904.
153. Hu, S.; Liang, Z.; He, X. Ultracapacitor-Battery Hybrid Energy Storage System Based on the Asymmetric Bidirectional Z -Source Topology for EV. *IEEE Trans. Power Electron.* **2016**, *31*, 7489–7498. [CrossRef]

Publication II

A. Bubovich, M. Vorobyov, I. Galkin, A. Blinov and A. Giannakis, "Overview of Bidirectional Unfolding Converters for Battery Energy Storage Systems," 2022 IEEE 13th International Symposium on Power Electronics for Distributed Generation Systems (PEDG), Kiel, Germany, 2022, pp. 1-7, doi: 10.1109/PEDG54999.2022.9923093.

Overview of Bidirectional Unfolding Converters for Battery Energy Storage Systems

Alexander Bubovich[1], Maxim Vorobyov[2], Ilya Galkin[3], Andrei Blinov[4], Andreas Giannakis[5]
[1,2,3]*Institute of Industrial Electronics and Electrical Engineering, Riga Technical University, Riga, LV1048, Latvia*
[4]*Department of Electrical Power Engineering and Mechatronics, Tallinn University of Technology, Tallinn, 19086, Estonia*
[5]*Department of Electrical Power Engineering, Norwegian University of Science and Technology, Trondheim, NO-7491, Norway*
[1]aleksandrs.bubovics@rtu.lv, [2]maksims.vorobjovs@rtu.lv, [3]gia@eef.rtu.lv, [4]andrei.blinov@taltech.ee, [5]andreas.giannakis@ntnu.no

***Abstract*— In order to support wider use of distributed renewable sources and mitigate the negative effects of their intermittent behavior, nowadays they are often installed together with energy storages, located on-site or nearby. Battery energy storage systems (BESS) allow not only to match consumption and generation profiles more closely, but also they provide various ancillary grid-supporting services. The enabling technology for these emerging opportunities is related to power electronic interfaces between the DC battery and the AC grid. Generally, a two-stage power conversion approach is used, where the battery-side DC-DC stage is responsible for controlling the battery current and grid-side DC-AC stage controls the current taken or injected to the grid. These two stages are connected through a bulky DC-link capacitor with stabilized voltage. Such an approach has however reached its limits in terms of efficiency, power density and cost. Therefore, a lot of research is currently focused on alternative topologies, enabling higher performances than the well-developed two stages approach. One of the promising configurations of such alternative topology includes a DC-DC converter, that forms sine voltage half-waves and an unfolding circuit, which provides the commutation of these half-waves to the grid. This paper presents a review of unfolding converters in the context of BESS. Configurations of unfolding circuits with DC-DC choppers, dual active bridge converters and multilevel converters, as well as the partial power converters are analyzed.**

Keywords*— Converters, DC-AC converters, Energy storage, Renewable energy sources, DC-AC power converters, DC-DC power converters, multilevel converters

I. Introduction

Recently, a clear trend of increasingly use of renewable energy sources has been seen. First of all, various national and international regulations limit the exhaust of greenhouse gases and the use of fossil fuels [1], [2]. At the same time, recent technological advances in the field of renewable generation, power electronic converters and energy storages made the application of renewable energy sources more efficient, reliable, convenient and affordable [3], [4]. Nowadays generation of renewable energy is applied down to the level of households [5], [6]. Considering the intermittent nature of renewable electrical energy generation, it is reasonable to combine the corresponding energy sources with energy storages (for example, with Battery Energy Storage Systems – BESSs) to compensate the difference between production and consumption patterns [7]. In addition to increase of on-site renewable energy consumption, the BESS could participate in energy arbitrage or provide ancillary services to the power grid. Moreover, the BESS can be used as an uninterruptible power supply, which is critical for households, located in remote locations, where the electrical grid is less stable.

Various residential BESSs have already been commercialized and they can be found in the corresponding market. For example, Tesla Powerwall+ has energy capacity of 13.5 kWh with 5 kW output power and can be connected directly to the grid via inverter [8]. SonnenBatterie is another product, offered by Sonnen Gmbh. The capacity of these BESS can be chosen within the range from 5kWh up to 15 kWh with maximal output power reaching 5.5 kW [9]. Also there are the products from SolarEdge [10], Enphase Energy [11], Adara Power [12] etc. The majority of these products is designed for small households. However, they focus not only on the local power supply and energy storage, but also on the further integration of these BESSs into energy system and combination of several households into a distributed BESS plant [7].

A typical BESS consists of a battery and bidirectional AC-DC power converters, which control the charge and discharge of the battery. Various isolated and non-isolated topologies of such converters can be used. The isolated ones can be used for low voltage batteries that require voltage step-up to match the grid level or if the application requires galvanic isolation for safety reasons. The non-isolated solutions are typically simpler and can be applied if the voltage levels of grid and the battery are close to each other.

A two-stage energy conversion approach has currently been a well-established configuration for the grid interconnection of BESSs. In such configuration, the battery-side DC-DC stage is interfaced with grid side inverter through a stabilized bulky DC link. At the same time, alternative solutions like single- [13], [14] and quasi-single stage topologies [15], [16] can potentially offer advantages in terms of efficiency, power density and reliability, as they do not incorporate and require these bulky DC-link capacitors. Particularly, the converters with unfolding circuit feature pulsating DC-link that is made of a small capacitor, while its inverter semiconductors operate at the grid frequency with negligible switching losses.

This paper presents an overview of various topologies with unfolding inverter applicable to BESS. The main goal is to demonstrate the flexibility of such an approach and highlight its potential possibilities and advantages in battery applications, as well as to select the prospective UC configurations for further experimental research.

II. General Description of BESS Technologies

Traditionally, lead-acid was the most developed battery technology. Although such batteries are cheap, they have such drawbacks as low specific energy and short lifetime. Another battery technology, Nickel-Metal Hydride (NiMH), provides better specific power and lifetime, yet having higher self-discharge and lower efficiency. Finally, the most recent and rapidly developing battery technology is Li-ion. These batteries combine high energy density with longer lifecycle and high efficiency. While the price of these batteries is still rather high, due to the large investments in the manufacturing facilities the cost is estimated to steadily decrease in the near future [17].

The batteries as DC power sources, are interfaced with the AC grid through a dedicated bidirectional AC/DC converter. The traditional two-stage converter structure generally assumes that the DC-DC part is responsible for stabilizing the battery voltage at the DC link or manage the battery state of charge, while the DC-AC stage is responsible for sinusoidal grid current wave-shaping [18]. The batteries, particularly the lead-acid ones, are generally sensitive to the quality of the charging/discharging current. Therefore, in single-phase BESS the DC-link is made quite bulky to decouple the double line frequency ripple. At the same time, the Li-ion batteries were found to be practically not susceptible to performance degradation when operating with current having large low frequency component [19]. This opens the possibility to implement alternative converter configurations that do not filter out the current ripple associated with the grid frequency. In battery charger applications this property is often referred to as "sinusoidal charging". The generalized comparison between the traditional two-stage solution and the one without bulky DC-link is listed in Table I. In the latter solution the DC-DC stage is responsible for shaping the unipolar (rectified) sine half-waves that appear in the small (pulsating) DC link [20], [21], while the DC-AC grid side part is a low frequency commutator that unfolds these sine half-waves into sinewave.

The right part of Table 1 expresses UCs with explicit unfolding circuit and halfwave shaper (Fig. 1-a). However, these two parts can be integrated into a solid unit (Fig, 1-b) – see [22]–[24] for details. Unfolding circuits can also be divided into single-phase and three-phase circuits. A full transistor bridge (H-bridge) is typically used as a single-phase unfolder [25]. Three phase unfolding circuits are more complicated, combine a three-phase bridge with bi-directional switches, and commutate 120^0 pieces of a sine [26], [27].

TABLE I. Two-Stage Topologies of Converters for BESS [7].

	Pulse Mode Inverter	**Unfolding Inverter**
Standard pre-regulator	Wide range higher efficiency Wide battery voltage range, DC coupling is possible Lower maximal efficiency High switching frequency Higher EMI	Wide range higher efficiency Wide battery voltage range No switching losses in grid stage No (or small) DC-link capacitor DC coupling with renewable energy sources is complicated
Partial power pre-regulator	Wide range higher efficiency DC coupling is possible DC-DC operates with reduced power Narrow battery voltage range Developing technology	Questionable due to limited range of operation
Multi-level pre-regulator	Questionable due to repeated functionality	Low grid filter size and volume Low voltage semiconductors Modular design Intrinsic balancing High component count Complex control

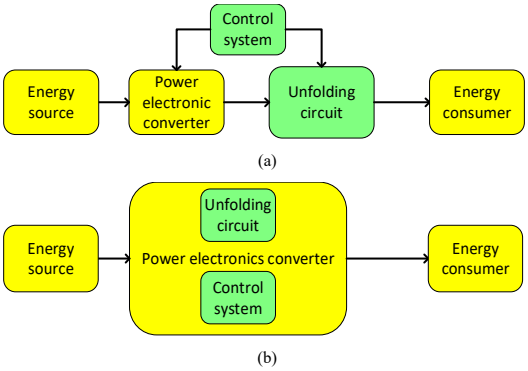

Fig. 1. Structure of unfolding converter: (a) with separated unfolding circuit, (b) with integrated unfolding circuit.

III. Non-Isolated Topologies for Unfolding Converters

A. Methods of synthesis of voltage sine half-waves

Battery-side stage of a UC – a DC-DC unit should form semi-sine half-waves with value from zero to amplitude of the grid voltage. At the same time, it must be capable of operating at different state of the charge (SOC) of the battery and cope fluctuations of the grid voltage. Therefore, in the general case, the battery stage of UC should be a buck-boost chopper; for example, non-inverting buck-boost converter, Ćuk, SEPIC, Zeta etc. [28].

The hard-switching Pulse Width Modulation (PWM) is one of the most common approaches used for the modulation (forming) of the half-waves at the output of these buck-boost DC-DC converters [29]–[31]. With this approach the output voltage of the DC-DC stage is split into two parts. Depending on the instantaneous voltage in the grid, the DC-DC part will switch between buck and boost operation modes (Fig. 2). If the

battery voltage is higher than the absolute value of the grid voltage, then the DC-DC stage of UC is working in a buck mode. In contrast, if the absolute value of the grid voltage is higher than the battery voltage, then DC-DC stage is working in a boost mode. Practically, it is often implemented by using two carrier signals for PWM synthesis – separately for buck and boost mode. It is also possible to modify different parameters of the carrier waveforms: offsets (Fig. 3), phase shifts (if parallel branches are used, see Fig 3-b), or frequencies (Fig 3-c) [30].

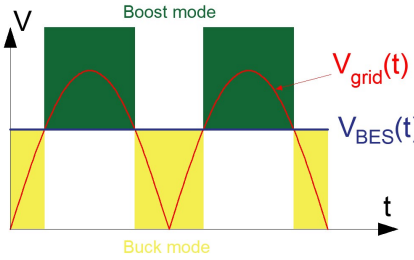

Fig. 2. Operation principle of half-wave generation by DC-DC stage of UC.

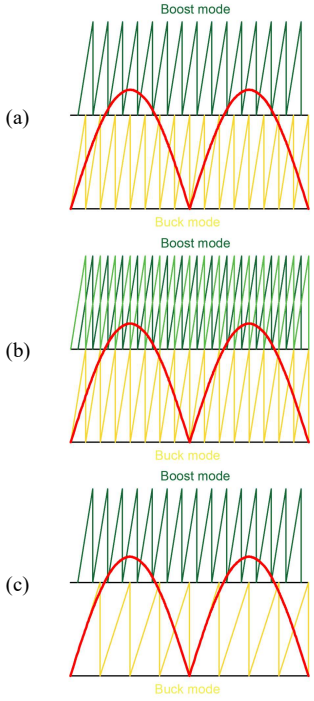

Fig. 3. PWM modulation principles of DC-DC stage of UC: (a) – carriers for buck and boost operation are with offset; (b) – PWM modulation with double carrier in boost; (c) – PWM modulation with decreased buck carrier frequency.

B. DC-DC topologies for Unfolding Converters

A number of DC-DC choppers for two-stage converters with unfolding circuit exist. The major part deals with unidirectional applications like photovoltaic (PV) systems. However, the review of these systems is important for further understanding of the operation of bi-directional choppers.

Papers [32]–[34] propose buck-boost choppers in grid-connected PV systems. The combination of buck and boost operation modes combined with unfolding circuit gives the ability of voltage regulation to match the value of grid voltage.

Paper [35] shows the simulation of model predictive control of buck-boost converter with unfolding circuit (Fig. 4-a). Papers [36], [37] also describe the application of UCs in PV systems. In [36] the combination of buck converter and unfolding circuit is implemented in the form of low-profile microinverter. Paper [37] focuses on the high-gain operation of boost converter, tied with full-bridge unfolding circuit. In addition, this unfolding circuit is working in partial sine-form PWM when voltage has to be stepped down.

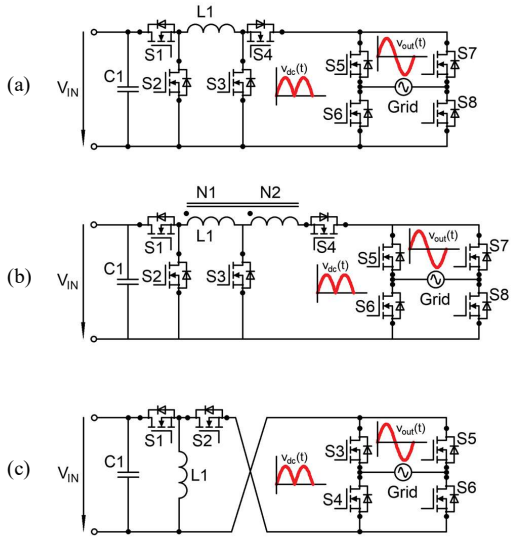

Fig. 4. Topologies of UCs: (a) single inductor buck-boost converter with unfolding circuit, (b) tapped inductor buck-boost converter with unfolding circuit, (c) single inductor twisted buck boost converter with unfolding circuit

An example of buck-boost topology with integrated unfolding circuit (Aalborg Inverter) is described in [23], [24], [38]. Reference [39] describes the implementation of isolated Ćuk converter with unfolding circuit as differential power processor for aircraft application. In this case the unfolding circuit gives the ability of four-quadrant operation of converter and reduces the worst-case processed power. Paper [40] describes the evaluation of inverter topology based on a buck converter and unfolding circuit within Google's "Little Box

Challenge". The major advantage of the topology is the reduction of volume and complexity of the system.

Since the unfolding circuit is commutating half-waves at the grid frequency, the major losses of the power semiconductors in the unfolding circuit are the conduction losses. Therefore, the switches having low on-state resistance allow significant reduction of these losses and improve the overall efficiency.

IV. Isolated Topologies for Unfolding Converters

A particular UC configuration is based on dual active bridge (DAB). Typically, the DAB is connected with power factor correction (PFC) rectifier through intermediate DC link. DAB gives the ability of bidirectional energy flow, which perfectly fits the requirements of BESS [41], [42].

Most commonly, DAB contains two full bridges, a series inductor and a high frequency (HF) isolation transformer (Fig. 5) [41]–[49]. The main advantage of the DAB topology is easy implementable zero-voltage switching (ZVS), which decreases power losses of the converter.

There are two main types of DAB converters: current-fed and voltage-fed. The voltage-fed DAB converters are implemented in various applications, where bidirectional power flow is needed. One of the simplest control methods of the voltage-fed DAB converters is phase shift control [50]–[52]. With phase shift control, both H-bridges of DAB operate with the same duty cycle. In this case power is controlled by phase shift between the sides of DAB converter [53]. Combining the phase shift with PWM enables minimizing the losses of the converter and also extends the operation range, when ZVS can be provided [54], [55].

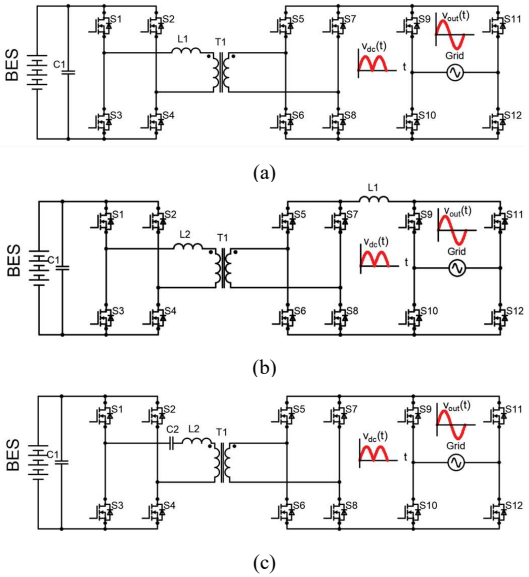

Fig. 5. DAB converter with unfolding circuit: (a) voltage-fed DAB; (b) current-fed DAB (c) series resonant DAB

A current-fed DAB is implemented by adding an inductor to the input port (Fig. 5-b). The current-fed DAB converters have some advantages over the voltage-fed DAB converters, such as lower current ripple, lower circulating current, direct current control and voltage boosting capability [56]. This makes the current-fed DAB converter more suitable for the BESS applications.

Paper [57] proposed bidirectional microinverter for residential power system application, including BESS and vehicle-to-grid (V2G). This bidirectional microinverter is implemented in the form of DAB converter with unfolding circuit. On the primary side of the DAB there is a full transistor bridge, on the secondary side – transistor half bridge. Half-bridge on the secondary side of the DAB converter can allow reduction of turns ratio of the high-frequency transformer [58], [59].

Papers [60], [61] describe series resonant DAB converter (shown at Fig. 5-c). LC circuit is added at the primary side of the transformer to provide series-resonance. By adding series resonant circuit to the topology, it is possible to achieve ZCS (zero current switching) operation of the DAB converter.

Papers [62], [63] propose the configuration of two DABs with series connected outputs and three phase unfolder. In [62] a three-phase unfolder is derived from a three-level neutral point clamped converter (NPC) operating at grid frequency. Here, the use of unfolder circuit reduces the capacitance of DC-link and switching losses, as well as improves the parameters of grid filter.

V. Emerging Concepts of Unfolding Converters

A. Multilevel topologies with unfolding circuits

The unfolders can also be combined with multilevel half-sine shapers. Classical configuration without unfolder, known as Modular Multilevel Converters (MMCs) with independent sources (also cascaded H-bridge converters), assumes that several H-bridge modules, fed from a small group of battery cells, are connected in series, thus creating one phase cascade [56], [57], [58]. The use of MMCs in BESS provides natural balancing of battery cells without explicit battery management system.

Adding an unfolding circuit at the grid side enables bipolar operation of MMC shaper [59]. It turns the series connected H-bridges into half bridges, because the bipolar operation of these modules is not necessary. Fig.6 shows the configuration of the one phase cascade with and without unfolding circuit. Therefore, the use of unfolding circuit reduces switch count in current paths and, therefore, simplifying the design. In addition, the control of the converter is becoming simpler.

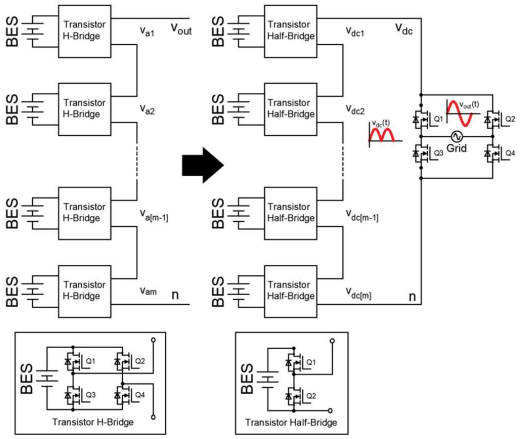

Fig. 6. Structure of MMC with and without unfolding circuit

B. *Application of partial power converters with unfolding circuits*

Recent trend in the field of power interface converters for renewable energy sources is the use of Partial Power Converters (PPCs) that have large potential of effective power conversion [60], [61]. In PPCs, part of the energy goes to the load directly and PPC is processing only a remaining amount of energy. There are two basic PPC types that are reversible: parallel input – serial output and serial input – parallel output [7]. Application of PPCs may have some advantages comparing with conventional converter topologies – reduction of size, reduction of losses and PPCs can also operate with reduced voltage, current or both.

It would be beneficial to implement PPCs as a part of the UC. At the same time, their direct implementation seems not realistic, as the PPCs do not operate within a full DC voltage/current range and cannot provide voltage/currents close to zero. Therefore, the implementation of PPCs in UCs requires more sophisticated schematic solutions with extra components and units for range extension. This, however, sounds contradictive with the principle of partial power conversion.

VI. Discussion and Conclusions

This paper presented an overview of various UCs for Li-ion based BESSs, which opens up new possibilities in the design of such systems. The elimination of bulk DC link potentially allows achieving higher power density, lower cost and improved reliability. Moreover, since the switches in unfolding circuit operate at grid frequency, the major losses of these switches are conduction losses. Choosing the switches with low on-state resistance allows the minimization of overall losses of the converter.

The use of particular DC/DC voltage shaper may provide some additional advantages. Table II shows the comparison of observed converters in terms of BESS application. The use of buck-boost chopper enables easy voltage regulation (constant duty cycles in discontinuous conduction mode) to match grid voltage. The use of current-fed DAB in addition to galvanic isolation and voltage matching, provides lower current ripple and simple current control, while the use of unipolar MMCs gives the ability of natural battery balancing, which is a significant advantage in BESS application. However, all three observed UC types vary in maximal voltage and power, therefore in BESS applications the choice of the topology depends on the particular scenario – either BESS is placed in household, or it is BESS integrated into the energy system of larger area.

TABLE II. Application of UCs in terms of BESS.

UC Type		Characteristics of BES	Peculiarities
Non-isolated topologies	Non-inverting buck-boost converter	Low voltage Low to medium power	Easier voltage regulation. Higher maximal efficiency, however, small range of higher efficiency.
	Ćuk, SEPIC, Zeta	Low voltage Low power	
Isolated topologies	DAB converter	Low to medium voltage Low to medium power	Soft switching capability Galvanic isolation
Multilevel topologies	MMC with independent sources	Low to high voltage Low to high power	Natural battery balancing capability. Sophisticated control.

Regarding the PPCs, further research is required to find a solution to their range extension, keeping their partiality principle. In this way, the design and the operation of a PPC based half-sine shaper for use with unfolding inverters becomes possible. Finally, the completion of this evaluation of the unfolding inverters for BESS would require the comparison of all considered topologies at least at the level of mathematical or physical model providing the comparable environment for all analyzed cases. This is planned as a future work.

Acknowledgement

This work was supported by the European Economic Area (EEA) and Norway Financial Mechanism 2014–2021 under Grant EMP474 “Optimised Residential Battery Energy Storage Systems (ORBES)”.

References

[1] “Regulation (EU) 2018/1999 of the European Parliament and of the Council of 11 December 2018 on the Governance of the Energy Union and Climate Action.” https://eur-lex.europa.eu/legal-content/EN/TXT/?uri=uriserv:OJ.L_.2018.328.01.0001.01.ENG&toc=OJ:L:2018:328:TOC (accessed Feb. 21, 2022).

[2] “National energy and climate plans (NECPs).” https://energy.ec.europa.eu/topics/energy-strategy/national-energy-and-climate-plans-necps_en (accessed Feb. 21, 2022).

[3] G. Wang *et al.*, “A review of power electronics for grid connection of utility-scale battery energy storage systems,” *IEEE Transactions on Sustainable Energy*, vol. 7, no. 4, pp. 1778–1790, Oct. 2016, doi: 10.1109/TSTE.2016.2586941.

[4] A. Chub, D. Vinnikov, R. Kosenko, E. Liivik, and I. Galkin, “Bidirectional DC-DC Converter for Modular Residential Battery Energy Storage Systems,” *IEEE Transactions on Industrial Electronics*, vol. 67, no. 3, pp. 1944–1955, Mar. 2020, doi: 10.1109/TIE.2019.2902828.

[5] “Solar Roof | Tesla.” https://www.tesla.com/solarroof (accessed Mar. 22, 2022).

[6] “Solar Roof - Roofit.solar.” https://roofit.solar/ (accessed Mar. 22, 2022).

[7] I. A. Galkin, A. Blinov, M. Vorobyov, A. Bubovich, R. Saltanovs, and D. Peftitsis, "Interface Converters for Residential Battery Energy Storage Systems: Practices, Difficulties and Prospects," *Energies 2021, Vol. 14, Page 3365*, vol. 14, no. 12, p. 3365, Jun. 2021, doi: 10.3390/EN14123365.

[8] "Powerwall | Tesla." https://www.tesla.com/powerwall (accessed Mar. 22, 2022).

[9] "Energieversorgung der Zukunft. Heute. | sonnen." https://sonnen.de/ (accessed Mar. 22, 2022).

[10] "SolarEdge Energy Bank Battery. Increase Power, Performance, and Safety." https://www.solaredge.com/products/solaredge-energy-bank#/ (accessed Mar. 22, 2022).

[11] "Storage | Enphase." https://enphase.com/store/storage (accessed Mar. 22, 2022).

[12] "Adara Commercial Energy Storage System." http://www.adarapower.com/home/commercial-energy-storage-system/ (accessed Mar. 22, 2022).

[13] O. Korkh, A. Blinov, D. Vinnikov, and A. Chub, "Review of Isolated Matrix Inverters: Topologies, Modulation Methods and Applications," *Energies 2020, Vol. 13, Page 2394*, vol. 13, no. 9, p. 2394, May 2020, doi: 10.3390/EN13092394.

[14] A. Blinov, D. Vinnikov, E. Romero-Cadaval, J. Martins, and D. Peftitsis, "Isolated High-Frequency Link PFC Rectifier with High Step-Down Factor and Reduced Energy Circulation," *IEEE Journal of Emerging and Selected Topics in Industrial Electronics*, pp. 1–1, Nov. 2021, doi: 10.1109/JESTIE.2021.3126226.

[15] D. Zinchenko, A. Blinov, A. Chub, D. Vinnikov, I. Verbytskyi, and S. Bayhan, "High-efficiency single-stage on-board charger for electrical vehicles," *IEEE Trans Veh Technol*, vol. 70, no. 12, pp. 12581–12592, Dec. 2021, doi: 10.1109/TVT.2021.3118392.

[16] C. Li, Y. Zhang, Z. Cao, and D. Xu, "Single-Phase Single-Stage Isolated ZCS Current-Fed Full-Bridge Converter for High-Power AC/DC Applications," *IEEE Trans Power Electron*, vol. 32, no. 9, pp. 6800–6812, Sep. 2017, doi: 10.1109/TPEL.2016.2623771.

[17] X. Hu, C. Zou, C. Zhang, and Y. Li, "Technological Developments in Batteries: A Survey of Principal Roles, Types, and Management Needs," *IEEE Power and Energy Magazine*, vol. 15, no. 5, pp. 20–31, Sep. 2017, doi: 10.1109/MPE.2017.2708812.

[18] V. Fernão Pires, E. Romero-Cadaval, D. Vinnikov, I. Roasto, and J. F. Martins, "Power converter interfaces for electrochemical energy storage systems – A review," *Energy Conversion and Management*, vol. 86, pp. 453–475, Oct. 2014, doi: 10.1016/J.ENCONMAN.2014.05.003.

[19] M. J. Brand, M. H. Hofmann, S. S. Schuster, P. Keil, and A. Jossen, "The Influence of Current Ripples on the Lifetime of Lithium-Ion Batteries," *IEEE Trans Veh Technol*, vol. 67, no. 11, pp. 10438–10445, Nov. 2018, doi: 10.1109/TVT.2018.2869982.

[20] K. Wang, F. C. Lee, and W. Dong, "New soft-switched quasi-single-stage (QSS) bi-directional inverter/charger," *Conference Record - IAS Annual Meeting (IEEE Industry Applications Society)*, vol. 3, pp. 2031–2038, 1999, doi: 10.1109/IAS.1999.806016.

[21] Z. Wang, Y. Zhang, S. You, H. Xiao, and M. Cheng, "An Integrated Power Conversion System for Electric Traction and V2G Operation in Electric Vehicles with a Small Film Capacitor," *IEEE Trans Power Electron*, vol. 35, no. 5, pp. 5066–5077, May 2020, doi: 10.1109/TPEL.2019.2944276.

[22] W. Wu, Z. Wang, J. Ji, and F. Blaabjerg, "Performance analysis of new type grid-tied inverter-Aalborg Inverter," *2014 16th European Conference on Power Electronics and Applications, EPE-ECCE Europe 2014*, Sep. 2014, doi: 10.1109/EPE.2014.6910861.

[23] W. Wu, J. Ji, and F. Blaabjerg, "Aalborg inverter - A new type of 'buck in buck, boost in boost' grid-tied inverter," *IEEE Trans Power Electron*, vol. 30, no. 9, pp. 4784–4793, Sep. 2015, doi: 10.1109/TPEL.2014.2363566.

[24] S. Zhang, W. Wu, H. Wang, M. Huang, N. Gao, and F. Blaabjerg, "Single-stage MPPT control realization for Aalborg inverter in photovoltaic system," *Proceedings IECON 2017 - 43rd Annual Conference of the IEEE Industrial Electronics Society*, vol. 2017-January, pp. 4233–4238, Dec. 2017, doi: 10.1109/IECON.2017.8216726.

[25] Q. Mo, M. Chen, Z. Zhang, M. Gao, and Z. Qian, "Research on a non-complementary active clamp flyback converter with unfolding DC-AC inverter for decentralized grid-connected PV systems," *IEEE Energy Conversion Congress and Exposition: Energy Conversion Innovation for a Clean Energy Future, ECCE 2011, Proceedings*, pp. 2481–2487, 2011, doi: 10.1109/ECCE.2011.6064098.

[26] N. H. Pham, T. Mannen, and K. Wada, "Power Factor Operation of a Boost Integrated Three-Phase Solar Inverter using Current Unfolding and Active Damping Methods," *2018 IEEE Energy Conversion Congress and Exposition, ECCE 2018*, pp. 2896–2903, Dec. 2018, doi: 10.1109/ECCE.2018.8558360.

[27] A. Blinov, D. Zinchenko, J. Rabkowski, G. Wrona, and D. Vinnikov, "Quasi Single-Stage Three-Phase Filterless Converter for EV Charging Applications," *IEEE Open Journal of Power Electronics*, vol. 3, pp. 51–60, Dec. 2021, doi: 10.1109/OJPEL.2021.3134460.

[28] E. Makovenko *et al.*, "Novel quasi-Z-source derived inverter with unfolding circuit and battery storage," *Proceedings - 2018 IEEE 12th International Conference on Compatibility, Power Electronics and Power Engineering, CPE-POWERENG 2018*, pp. 1–6, Jun. 2018, doi: 10.1109/CPE.2018.8372557.

[29] Z. Zhao, M. Xu, Q. Chen, J.-S. Lai, and Y. Cho, "Derivation, Analysis, and Implementation of a Boost–Buck Converter-Based High-Efficiency PV Inverter," *IEEE Trans Power Electron*, vol. 27, no. 3, pp. 1304–1313, Mar. 2012, doi: 10.1109/TPEL.2011.2163805.

[30] Z. Zhao, J. S. Lai, and Y. Cho, "Dual-mode double-carrier-based sinusoidal pulse width modulation inverter with adaptive smooth transition control between modes," *IEEE Transactions on Industrial Electronics*, vol. 60, no. 5, pp. 2094–2103, 2013, doi: 10.1109/TIE.2012.2227900.

[31] O. Husev, J. Belikov, O. Matiushkin, D. Vinnikov, R. Ahmadiahangar, and N. Vosoughi Kurdkandi, "Optimal Tuning of Resonant and Repetitive Based Controller for Single-Phase Buck-Boost Inverter with Unfolding Circuit," *IEEE Journal of Emerging and Selected Topics in Industrial Electronics*, pp. 1–1, Oct. 2021, doi: 10.1109/JESTIE.2021.3121190.

[32] O. Matiushkin, O. Husev, R. Strzelecki, S. Ivanets, and A. Fesenko, "Novel single-stage buck-boost inverter with unfolding circuit," in *2017 IEEE First Ukraine Conference on Electrical and Computer Engineering (UKRCON)*, May 2017, pp. 538–543. doi: 10.1109/UKRCON.2017.8100298.

[33] O. Husev, O. Matiushkin, C. Roncero-Clemente, F. Blaabjerg, and D. Vinnikov, "Novel Family of Single-Stage Buck-Boost Inverters Based on Unfolding Circuit," *IEEE Trans Power Electron*, vol. 34, no. 8, pp. 7662–7676, 2019, doi: 10.1109/TPEL.2018.2879776.

[34] O. Matiushkin, O. Husev, C. Roncero-Clemente, S. Ivanets, and A. Fesenko, "Component design guidelines for new single-stage buck-boost inverter with unfolding circuit," *2017 IEEE International Young Scientists Forum on Applied Physics and Engineering, YSF 2017*, vol. 2017-January, pp. 40–45, Dec. 2017, doi: 10.1109/YSF.2017.8126589.

[35] O. Matiushkin, O. Husev, D. Vinnikov, and C. Roncero-Clemente, "Model predictive control for buck-boost inverter based on unfolding circuit," *2019 IEEE 2nd Ukraine Conference on Electrical and Computer Engineering, UKRCON 2019 - Proceedings*, pp. 431–436, Jul. 2019, doi: 10.1109/UKRCON.2019.8879870.

[36] R. W. Erickson and A. P. Rogers, "A microinverter for building-integrated photovoltaics," *Conference Proceedings - IEEE Applied Power Electronics Conference and Exposition - APEC*, pp. 911–917, 2009, doi: 10.1109/APEC.2009.4802771.

[37] C. H. Chang and K. H. Ho, "A Transformer-Less High-Gain Inverter with Step-Up/Down and Single Energy-Processing Features," *IEEE J Emerg Sel Top Power Electron*, vol. 9, no. 4, pp. 4726–4738, Aug. 2021, doi: 10.1109/JESTPE.2020.3023107.

[38] W. Wu, Z. Wang, J. Ji, and F. Blaabjerg, "Performance analysis of new type grid-tied inverter-Aalborg Inverter," *2014 16th European Conference on Power Electronics and Applications, EPE-ECCE Europe 2014*, 2014, doi: 10.1109/EPE.2014.6910861.

[39] A. Diab-Marzouk and O. Trescases, "SiC-Based Bidirectional ĆUK Converter With Differential Power Processing and MPPT for a Solar Powered Aircraft," *IEEE Transactions on Transportation Electrification*, vol. 1, no. 4, pp. 369–381, Dec. 2015, doi: 10.1109/TTE.2015.2505302.

[40] D. Bortis, D. Neumayr, and J. W. Kolar, "ηρ-Pareto optimization and comparative evaluation of inverter concepts considered for the

GOOGLE Little Box Challenge," *2016 IEEE 17th Workshop on Control and Modeling for Power Electronics, COMPEL 2016*, 2016, doi: 10.1109/COMPEL.2016.7556767.

[41] J. Everts, F. Krismer, J. Van Den Keybus, J. Driesen, and J. W. Kolar, "Optimal zvs modulation of single-phase single-stage bidirectional dab ac-dc converters," *IEEE Trans Power Electron*, vol. 29, no. 8, pp. 3954–3970, 2014, doi: 10.1109/TPEL.2013.2292026.

[42] J. Everts, F. Krismer, J. Van Den Keybus, J. Driesen, and J. W. Kolar, "Comparative evaluation of soft-switching, bidirectional, isolated AC/DC converter topologies," *Conference Proceedings - IEEE Applied Power Electronics Conference and Exposition - APEC*, pp. 1067–1074, 2012, doi: 10.1109/APEC.2012.6165951.

[43] L. Xue, Z. Shen, D. Boroyevich, P. Mattavelli, and D. Diaz, "Dual Active Bridge-Based Battery Charger for Plug-in Hybrid Electric Vehicle with Charging Current Containing Low Frequency Ripple," *IEEE Trans Power Electron*, vol. 30, no. 12, pp. 7299–7307, Dec. 2015, doi: 10.1109/TPEL.2015.2413815.

[44] H. S. Kim, M. H. Ryu, J. W. Baek, and J. H. Jung, "High-efficiency isolated bidirectional AC-DC converter for a DC distribution system," *IEEE Trans Power Electron*, vol. 28, no. 4, pp. 1642–1654, Apr. 2013, doi: 10.1109/TPEL.2012.2213347.

[45] A. Tong, L. Hang, G. Li, X. Jiang, and S. Gao, "Modeling and Analysis of a Dual-Active-Bridge-Isolated Bidirectional DC/DC Converter to Minimize RMS Current with Whole Operating Range," *IEEE Trans Power Electron*, vol. 33, no. 6, pp. 5302–5316, Jun. 2018, doi: 10.1109/TPEL.2017.2692276.

[46] W. Choi, K. M. Rho, and B. H. Cho, "Fundamental Duty Modulation of Dual-Active-Bridge Converter for Wide-Range Operation," *IEEE Trans Power Electron*, vol. 31, no. 6, pp. 4048–4064, Jun. 2016, doi: 10.1109/TPEL.2015.2474135.

[47] J. Hiltunen, V. Vaisanen, R. Juntunen, and P. Silventoinen, "Variable-Frequency Phase Shift Modulation of a Dual Active Bridge Converter," *IEEE Trans Power Electron*, vol. 30, no. 12, pp. 7138–7148, Dec. 2015, doi: 10.1109/TPEL.2015.2390913.

[48] N. Hou and Y. W. Li, "Overview and Comparison of Modulation and Control Strategies for a Nonresonant Single-Phase Dual-Active-Bridge DC-DC Converter," *IEEE Trans Power Electron*, vol. 35, no. 3, pp. 3148–3172, Mar. 2020, doi: 10.1109/TPEL.2019.2927930.

[49] Y. Shen, X. Sun, W. Li, X. Wu, and B. Wang, "A Modified Dual Active Bridge Converter with Hybrid Phase-Shift Control for Wide Input Voltage Range," *IEEE Trans Power Electron*, vol. 31, no. 10, pp. 6884–6900, Oct. 2016, doi: 10.1109/TPEL.2015.2510033.

[50] D. Sha, X. Wang, and D. Chen, "High-Efficiency Current-Fed Dual Active Bridge DC-DC Converter With ZVS Achievement Throughout Full Range of Load Using Optimized Switching Patterns," *IEEE Trans Power Electron*, vol. 33, no. 2, pp. 1347–1357, Feb. 2018, doi: 10.1109/TPEL.2017.2675945.

[51] M. H. Kheraluwala, R. W. Gascoigne, D. M. Divan, and E. D. Baumann, "Performance Characterization of a High-Power Dual Active Bridge dc-to-dc Converter," *IEEE Trans Ind Appl*, vol. 28, no. 6, pp. 1294–1301, 1992, doi: 10.1109/28.175280.

[52] S. A. Q. Mohammed and J. W. Jung, "A State-of-the-Art Review on Soft-Switching Techniques for DC-DC, DC-AC, AC-DC, and AC-AC Power Converters," *IEEE Trans Industr Inform*, vol. 17, no. 10, pp. 6569–6582, Oct. 2021, doi: 10.1109/TII.2021.3058218.

[53] "Design Guide: TIDA-010054 Bidirectional, Dual Active Bridge Reference Design for Level 3 Electric Vehicle Charging Stations," 2021.

[54] A. K. Jain and R. Ayyanar, "PWM control of dual active bridge: Comprehensive analysis and experimental verification," *IEEE Trans Power Electron*, vol. 26, no. 4, pp. 1215–1227, 2011, doi: 10.1109/TPEL.2010.2070519.

[55] D. Wang, W. Zhang, and J. Li, "A PWM plus phase shift control strategy for dual-active-bridge DC-DC converter in electric vehicle charging/discharging system," *IEEE Transportation Electrification Conference and Expo, ITEC Asia-Pacific 2014 - Conference Proceedings*, Oct. 2014, doi: 10.1109/ITEC-AP.2014.6940986.

[56] H. Akagi, "Classification, terminology, and application of the modular multilevel cascade converter (MMCC)," *IEEE Trans Power Electron*, vol. 26, no. 11, pp. 3119–3130, 2011, doi: 10.1109/TPEL.2011.2143431.

[57] S. Khomfoi and L. M. Tolbert, "Multilevel Power Converters," in *Power Electronics Handbook*, 2nd ed., Elsevier Inc., 2006, pp. 451–482.

[58] A. Bubovich, "Use of Multilevel Converters in Light Vehicles of Orthopedic Rehabilitation," *2021 IEEE 62nd International Scientific Conference on Power and Electrical Engineering of Riga Technical University (RTUCON)*, pp. 1–4, Nov. 2021, doi: 10.1109/RTUCON53541.2021.9711728.

[59] A. Bubovich, M. Vorobyov, and A. Giannakis, "Initial Evaluation of a Multilevel Inverter with Unfolding Stage for BESS Applications," pp. 1–4, Jan. 2022, doi: 10.1109/AIEEE54188.2021.9670386.

[60] N. G. F. Dos Santos, J. R. R. Zientarski, and M. L. da S. Martins, "A Review of Series-Connected Partial Power Converters for DC-DC Applications," *IEEE Journal of Emerging and Selected Topics in Power Electronics*, 2021, doi: 10.1109/JESTPE.2021.3082869.

[61] J. R. R. Zientarski, M. L. Da Silva Martins, J. R. Pinheiro, and H. L. Hey, "Evaluation of Power Processing in Series-Connected Partial-Power Converters," *IEEE Journal of Emerging and Selected Topics in Power Electronics*, vol. 7, no. 1, pp. 343–352, Mar. 2019, doi: 10.1109/JESTPE.2018.2869370.

Publication V

A. Bubovich, V. Parinova, I. Galkin and A. Giannakis, "Initial Evaluation of Multilevel Converter with Unfolding Stage and Voltage Regulators for applications in BESSs," 2022 18th Biennial Baltic Electronics Conference (BEC), Tallinn, Estonia, 2022, pp. 1-5, doi: 10.1109/BEC56180.2022.9935611.

Initial Evaluation of Multilevel Converter with Unfolding Stage and Voltage Regulators for Applications in BESSs

Alexander Bubovich[1], Veronika Parinova[2], Ilya Galkin[3], Andreas Giannakis[4]
[1,2,3]Institute of Industrial Electronics and Electrical Engineering, Riga Technical University, Riga, Latvia
[4]Norwegian University of Science and Technology, Department of Electric Power Engineering, Trondheim, Norway
[1]aleksandrs.bubovics@rtu.lv, [2]nika.parinova@gmail.com, [3]gia@eef.rtu.lv, [4]andreas.giannakis@ntnu.no

***Abstract*— Redundant and backup energy source is crucial in both household and industry. Energy storage systems are already used extensively to provide solutions to various issues such as grid frequency stabilization and electrification of remote areas. In addition to that, they can cover potential excessive energy demand when required. One of the most important parts of battery energy storage systems is power electronic converter that is used for the power transmission from the batteries to the grid and vice-versa. A typical power electronic converter topology is the multilevel converter with independent sources. This topology has several advantages compared to other topologies utilized in battery energy storage systems, such as, lower harmonic distortion of the output waveforms and battery balancing which can be obtained in natural way. This paper investigated and presents a modified multilevel converter with independent sources – multilevel converter with unfolding stage and voltage regulators.**

Keywords*— *Modular multilevel converters, DC-AC power converters, Energy storage, batteries.

I. Introduction

Environmental concerns, as well as increasing energy consumption have resulted in significant increase of usage of renewable energy sources and decrease of usage of fossil fuels. Nowadays there are various national and international regulations that are limiting the usage of fossil fuels for energy production [1]. This inspired the increase of demand for use of renewable energy sources. New technological advances in the field of power electronics made the application of renewable energy systems more reliable and efficient, which increased the demand of installing such systems. Nowadays it is even possible to generate energy from renewable energy sources in households by installing solar panels on roofs of houses, or by installing small wind generators [2].

However, there is one disadvantage of renewable energy sources – the energy is generated intermittently and energy production pattern does not match energy consumption pattern. Considering this drawback, it is reasonable to use Battery Energy Storage Systems (BESSs) which allow to compensate the difference between production and consumption, and also increases the stability of the electrical grid since BESSs can also be used as uninterruptible power supplies.

Taking into account increasing demand of storing the energy, and also the fact, that small renewable energy sources are available even for residual sector [3], [4], on the market there are various solutions for residual sector as well, for example, Tesla Powerwall [5], sonnenBatterie 10 from Sonnen [6] etc. Paper [2] describes usage of different types of interface converters in residential battery energy storage systems.

A typical BESS consists of Battery Energy Storage (BES) and bidirectional charger/discharger connected to the AC grid. There are various types of BESs: lead-acid technology (these BESs are cheaper, but with short lifetime and low specific energy), Nickel-Metal Hydride (good specific power and lifetime, but higher self-discharge and low efficiency) and most recent BES technology – Li-ion (high energy density, high efficiency, long lifecycle and low price) [7].

II. Power electronic converter for BESSs

BESs are connected to the grid with the help of AC/DC converter. There is wide range of AC/DC converter topologies. Generally, they can be divided into single-stage, two-stage and multilevel converters.

The first option is to make two separated converters – one for charging of the battery, the second one – for discharging. The second option is to use bidirectional AC/DC converters. In case of bidirectional converters, two cases can be described – single stage AC/DC converters (for example, full transistor bridge for single phase application [8] and three-phase full transistor bridge [9], dual buck half bridge in single and three-phase implementation) and two-stage AC/DC converters. Two-stage AC/DC converters consists of DC/DC converter and AC/DC inverter [10] or low frequency unfolding inverter [11]–[13].

In addition to single level AC/DC converters, multilevel converters (MLCs) can also be used in BESSs [14]. MLCs are used in medium and high power applications, and they have such advantages as lower switch power losses, lower harmonic contents and low electromagnetic interference [15]. There are three main MLC topologies: diode clamped multilevel converters (also known as neutral point clamped multilevel converters), which has one subtype – active neutral point clamped multilevel converter, multilevel converters with flying capacitors and modular multilevel converters with independent voltage sources. Paper [16] describes the design of MLC with flying capacitors, used for aircraft applications. In [16] also experimental verification of the designed converter is provided. Paper [17] provides an example of 13 level flying capacitor multilevel converter, based on GaN

978-1-6654-6295-2/22/$31.00 ©2022 IEEE

switches. The use of neutral point clamped multilevel converter in BESSs is described in [18], paper [19] describes the use of multilevel converters in BESSs, including active neutral point clamped multilevel converters. In case of MLCs, output voltage is formed by several levels of DC voltage. MLCs can be used either as bidirectional DC/AC converter or as part of two-stage implementation as DC/AC inverter or low-frequency unfolder. MLCs with independent sources have one main advantage comparing with other MLC types, which is valuable in BESS applications. Battery balancing in MLCs with independent sources is achieved in natural way [20], [21], as the sources are connected to the output independently and can be swapped, which is great advantage of this topology in application with BESSs, and this topology was chosen for further investigation.

III. Multilevel converters with independent sources

In classical implementation, one phase cascade of multilevel converter with independent voltage sources (also known as cascaded H-bridge converter with separate DC sources) consists several single-phase full bridge converters connected in series [22], [23]. Inputs of single-phase full bridge converters are connected to separate (or, independent) DC sources, which, in case of implementation of multilevel converters in BESSs, are batteries. Fig. 1 shows the structural schematics of multilevel converter with independent sources.

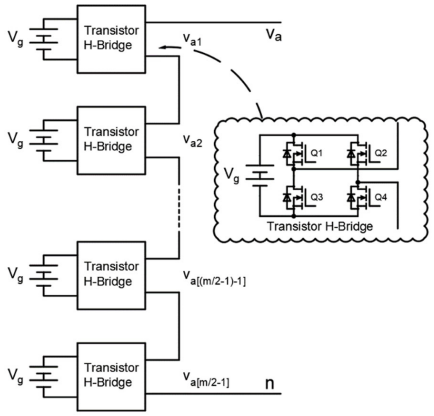

Fig. 1. One phase cascade for m-level modular multilevel converters with independent sources

Adding an unfolding circuit at the grid side enables bipolar operation of MLC shaper [24]. It turns the series connected H-bridges into half bridges, because the bipolar operation of these modules is not necessary. Fig. 2 shows the structural schematics and difference between two observed cases.

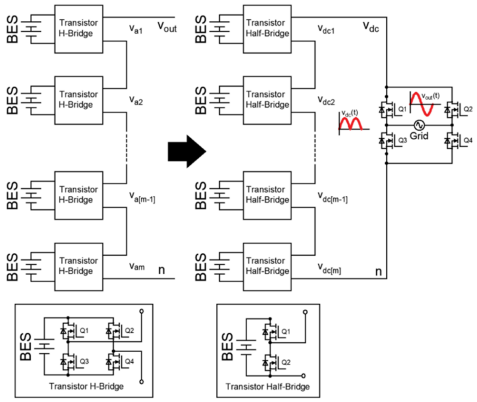

Fig. 2. Classical MLC with independent sources and MLC with independent sources and unfolding circuit.

Unfolding circuit used with MLC with independent sources gives the ability of lowering high-frequency switch count, as the switches in unfolding circuit are operating at grid frequency. That gives the ability of decreasing commutation losses of the whole converter.

However, half-bridges are capable to operate in buck-mode – that means, that the output voltage of the converter can only be stepped down from the nominal voltage of the battery. However, taking into account the fact, that voltage of the battery is dependent on State Of Charge (SOC) of the battery and is not linear, there are scenarios, when the output voltage should be higher than the input voltage. Therefore, it is reasonable to make additional modification of the proposed topology – by adding additional conversion stage, buck-boost stage, between the batteries and the half-bridges it now will be possible to regulate the voltage of each module connected in series. Fig. 3. shows the structure of the proposed topology.

Synchronous buck-boost converters were chosen as source voltage regulators, because of ability of bidirectional operation of these the buck-boost converters. This gives the ability not only to discharge stored energy from batteries, but also to charge the batteries when it is needed.

By adding regulation of sources it is possible to regulate the output voltage of each connected in series module, which decreases the requirements of the batteries connected as sources to each module. It even makes possible to take as sources batteries with different chemistries – for example, for one module Li-ion battery pack is taken, for other – NiMH battery and for the third one – Lead-acid battery etc. Also, it can increase the reliability of the system – if one module fails, output voltage can be tuned and failed module will be disconnected from the others.

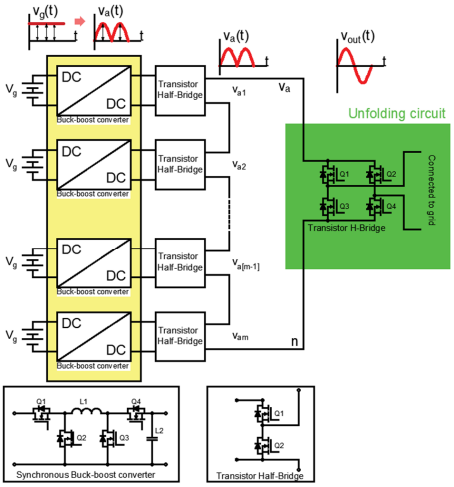

Fig. 3. MLC with independent sources and voltage regulators

IV. Evaluation of Performance

In order to evaluate the performance of the MLC with independent sources and voltage regulators, MATLAB-Simulink model of three-level MLC with independent sources and voltage regulators was created. The main subject of the evaluation is the verification of working capability of introduced idea. Models of synchronous buck-boost converters and half-bridges as well as model of unfolding circuit were created quite ideal (with ideal switches), however accurate models of batteries were created using Li-ion Samsung 30Q 18650 3000mAh 15A Battery INR18650-30Q batteries. Amplitude of output voltage was taken equal to 36V, output frequency is 50Hz. In order to show the ability of correcting voltage, input voltages of each buck-boost converter were taken different – for the first one input voltage was taken equal to 16.8V (i.e. 4 fully charged INR18650-30Q battery cells connected in series), for the second one – input voltage was taken equal to 8.4V (2 fully charged battery cells connected in series) and for the third one input voltage was taken equal to 25.2V (six fully charged battery cells connected in series). That means, that first and third buck-boost converters are operating in buck mode, and second is operating in boost mode. Fig. 4 shows the overall structure of model.

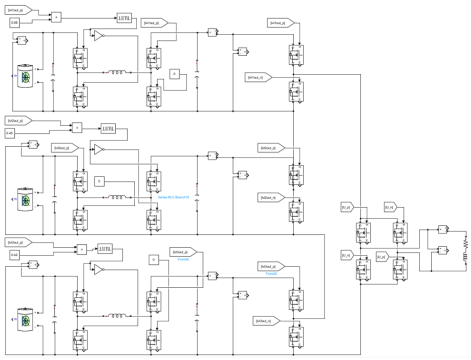

Fig. 4. MATLAB-Simulink model of MLC with independent sources and volatge regulators

V. Results and Discussion

Output voltage waveform of the simulation is shown at Fig. 5. Figures 6-8 show input and output voltages of buck-boost converters.

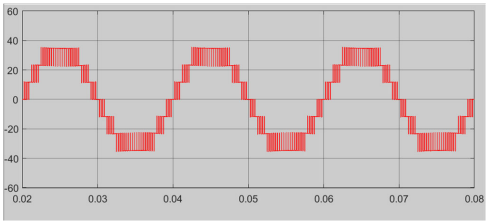

Fig. 5. Simulation results of output waveforms of the MLC with independent sources and volatge regulators.

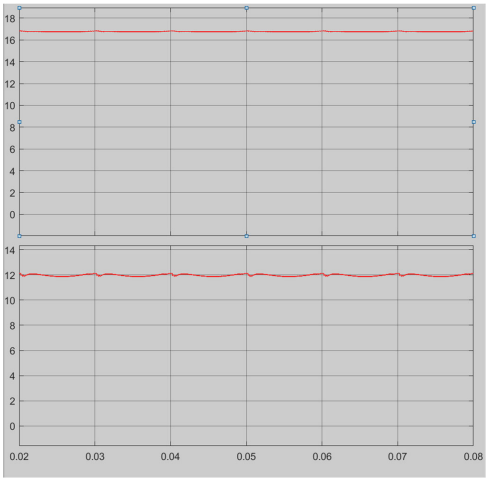

Fig. 6. Simulation results of input (upper waveform) and output (lower waveform) voltages of buck-boost converter, operating in buck mode (with 4 battery cells connected in series as voltage source)

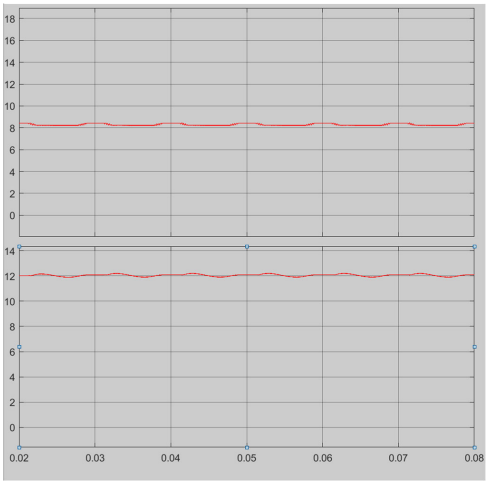

Fig. 7. Simulation results of input (upper waveform) and output (lower waveform) voltages of buck-boost converter, operating in boost mode (with 2 battery cells connected in series as voltage source)

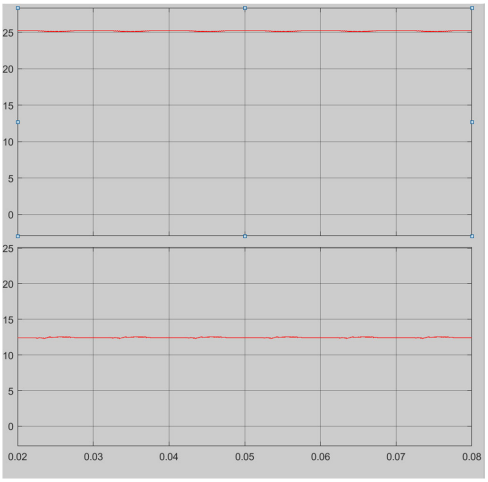

Fig. 8. Simulation results of input (upper waveform) and output (lower waveform) voltages of buck-boost converter, operating in buck mode (with 6 battery cells connected in series as voltage source)

Simulation results demonstrate the working capability of the idea. However, it is necessary to implement closed loop system to reduce the output voltage fluctuations.

VI. Conclusions

Multilevel converter with independent voltage sources, unfolding circuit and voltage regulators is presented in this paper. Initial simulation results demonstrate working capability of the idea of using synchronous buck-boost converters to regulate voltage of the sources in MLC. However, it is reasonable to use closed loop system to reduce voltage fluctuations of the output voltages of buck-boost choppers.

Acknowledgment

This publication was supported from Baltic Research Program funded by the European Economic Area and Norway 2014-2021 financial mechanisms within the contract EMP474 “Optimised Residential Battery Energy Storage Systems (ORBES)” of the first (Estonian) call of this program and was supported by Riga Technical University's Doctoral Grant programme.

References

[1] “National energy and climate plans (NECPs).” https://energy.ec.europa.eu/topics/energy-strategy/national-energy-and-climate-plans-necps_en (accessed Feb. 21, 2022).

[2] I. A. Galkin, A. Blinov, M. Vorobyov, A. Bubovich, R. Saltanovs, and D. Peftitsis, “Interface Converters for Residential Battery Energy Storage Systems: Practices, Difficulties and Prospects,” *Energies 2021, Vol. 14, Page 3365*, vol. 14, no. 12, p. 3365, Jun. 2021, doi: 10.3390/EN14123365.

[3] “SolarEdge | A World Leader in Smart Energy Solutions.” https://www.solaredge.com/ (accessed May 17, 2021).

[4] “Best Home Wind Turbines Updated: 2021.” https://www.10powerup.com/best-home-wind-turbine/ (accessed May 17, 2021).

[5] “Powerwall | Tesla.” https://www.tesla.com/powerwall?redirect=no (accessed May 17, 2021).

[6] “Energy supply of the future. Today. | to sunbathe.” https://sonnen.de/ (accessed May 17, 2021).

[7] X. Hu, C. Zou, C. Zhang, and Y. Li, “Technological Developments in Batteries: A Survey of Principal Roles, Types, and Management Needs,” *IEEE Power Energy Mag.*, vol. 15, no. 5, pp. 20–31, Sep. 2017, doi: 10.1109/MPE.2017.2708812.

[8] S. J. Chiang, C. M. Liaw, W. C. Chang, and W. Y. Chang, “Multi-module parallel small battery energy storage system,” *IEEE Trans. Energy Convers.*, vol. 11, no. 1, pp. 146–154, 1996, doi: 10.1109/60.486589.

[9] H. Yamamoto, C. Y. Inaba, E. Hiraki, T. Horiuchi, Y. Sugawara, and M. Nakaoka, “Three-phase voltage source soft-switching inverter for battery and super capacitor energy storage plants,” in *TELESCON 2000 - 3rd International Telecommunications Energy Special Conference, Proceedings*, 2000, pp. 271–275. doi: 10.1109/TELESC.2000.918451.

[10] S. Ponnaluri, G. O. Linhofer, J. K. Steinke, and P. K. Steimer, “Comparison of single and two stage topologies for interface of BESS or Fuel Cell system using the ABB standard Power Electronics Building Blocks,” in *2005 European Conference on Power Electronics and Applications*, 2005, vol. 2005. doi: 10.1109/epe.2005.219502.

[11] B. Zhao, A. Abramovitz, C. Liu, Y. Yang, and Y. Huangfu, “A family of single-stage, buck-boost inverters for photovoltaic applications,” *Energies*, vol. 13, no. 7, p. 1675, Apr. 2020, doi: 10.3390/en13071675.

[12] O. Husev, O. Matiushkin, C. Roncero-Clemente, F. Blaabjerg, and D. Vinnikov, “Novel Family of Single-Stage Buck-Boost Inverters Based on Unfolding Circuit,” *IEEE Trans. Power Electron.*, vol. 34, no. 8, pp. 7662–7676, Aug. 2019, doi: 10.1109/TPEL.2018.2879776.

[13] B. S. Jacobson and E. N. Holmansky, “Methods and apparatus for three-phase inverter with reduced energy storage, US7839023B2,” 2010

[14] J. S. Lai and F. Z. Peng, “Multilevel converters - a new breed of power converters,” in *Conference Record - IAS Annual Meeting (IEEE Industry Applications Society)*, 1995, vol. 3, pp. 2348–2356. doi: 10.1109/ias.1995.530601.

[15] I. Colak, E. Kabalci, and R. Bayindir, “Review of multilevel voltage source inverter topologies and control schemes,” *Energy Convers. Manag.*, vol. 52, no. 2, pp. 1114–1128, Feb. 2011, doi: 10.1016/j.enconman.2010.09.006.

[16] T. Modeer, N. Pallo, T. Foulkes, C. B. Barth, and R. C. N. Pilawa-Podgurski, “Design of a GaN-Based Interleaved Nine-Level Flying Capacitor Multilevel Inverter for Electric Aircraft Applications,” *IEEE Trans. Power Electron.*, vol. 35, no. 11, pp. 12153–12165, Nov. 2020, doi: 10.1109/TPEL.2020.2989329.

[17] C. B. Barth *et al.*, “Design and control of a GaN-based, 13-level, flying capacitor multilevel inverter,” Aug. 2016. doi: 10.1109/COMPEL.2016.7556770.

[18] U. Abronzini *et al.*, “A Dual-Source DHB-NPC Power Converter for Grid Connected Split Battery Energy Storage System,” in *2018 IEEE Energy Conversion Congress and Exposition, ECCE 2018*, Dec. 2018, pp. 2483–2488. doi: 10.1109/ECCE.2018.8557563.

[19] M. Bragard, N. Soltau, S. Thomas, and R. W. De Doncker, “The balance of renewable sources and user demands in grids: Power electronics for modular battery energy storage systems,” *IEEE Trans. Power Electron.*, vol. 25, no. 12, pp. 3049–3056, 2010, doi: 10.1109/TPEL.2010.2085455.

[20] A. Bubovich, “Evaluation of Opportunities of Balanced Discharge of Batteries in Cost Effective Assisting Powered Wheelchair,” in *2019 IEEE 60th International Scientific Conference on Power and Electrical Engineering of Riga Technical University (RTUCON)*, 2019, pp. 1.-4.

[21] A. Bubovich, M. Vorobyov, A. Blinov, and D. Peftitsis, “Peculiarities of Multilevel Power Electronic Converters for Interfacing Battery Energy Storages with AC Loads,” in *2020 IEEE 8th Workshop on Advances in Information, Electronic and Electrical Engineering (AIEEE)*, Apr. 2021, pp. 1–4. doi: 10.1109/AIEEE51419.2021.9435798.

[22] L. M. Tolbert, F. Z. Peng, and T. G. Habetler, “Multilevel converters for large electric drives,” *IEEE Trans. Ind. Appl.*, vol. 35, no. 1, pp. 36–44, 1999, doi: 10.1109/28.740843.

[23] S. Khomfoi and L. M. Tolbert, “Multilevel Power Converters,” in *Power Electronics Handbook*, 2nd ed., Elsevier Inc., 2006, pp. 451–482. [Online]. Available: http://web.eecs.utk.edu/~tolbert/publications/multilevel_book_chapter.pdf

[24] A. Bubovich, M. Vorobyov, and A. Giannakis, “Initial Evaluation of a Multilevel Inverter with Unfolding Stage for BESS Applications,” *Proc. 9th IEEE Work. Adv. Information, Electron. Electr. Eng. AIEEE 2021*, 2021, doi: 10.1109/AIEEE54188.2021.9670386.

Publication VI

A. Bubovich, M. Vorobyov, I. Galkin and T. Dovudon, "Quality Evaluation of Jointly Used Modular Multilevel Converters and Battery Energy Storages," 2021 International Conference on Electrical Drives & Power Electronics (EDPE), 2021, pp. 144-151, doi: 10.1109/EDPE53134.2021.9604102

Quality Evaluation of Jointly Used Modular Multilevel Converters and Battery Energy Storages

Alexander Bubovich[1], Maxim Vorobyov[2], Ilya Galkin[3], Tenuun Dovudon[4]
Riga Technical University, Institute of Industrial Electronics and Electrical Engineering, Riga, Latvia
[1]aleksandrs.bubovics@rtu.lv, [2]maksims.vorobjovs@rtu.lv, [3]gia@eef.rtu.lv

***Abstract*—Battery energy storages nowadays are utilized in various applications. The similarity of these applications and multilevel nature of the batteries logically encourages building of the interface converters based on a multilevel scheme. This paper is devoted to the choice of the configuration of this scheme and its operation mode. Tentative quality evaluation is made based on the root-mean declination of output voltage from its reference (THD). MATLAB-Simulink simulation is chosen as a reasonable data collection method. The results of the simulation show that a trade-off configuration may include 3-4 levels with minor inter-level pulse width modulation. In the same time further investigation must be done in order to study the influence of other technical (losses) and economical parameters.**

Keywords— Modular multilevel converters, DC-AC power converters, Energy storage, batteries, circuit simulation

I. INTRODUCTION.

Nowadays electrochemical Battery Energy Storages (BES or just batteries) are considered as the most available, reliable and practical storage of electrical energy for broad range of applications. There exist several BES types at different level of development of their electrochemistry/ technology [1], [2] Traditionally, one of the oldest and most "polished" technologies is Lead-Acid BES technology, which in spite of its drawbacks (lower specific energy and shorter lifetime) is still attractive due to its low cost and high efficiency. Another quite advanced BES technology – Nickel-Metal Hydride – provides good specific power, energy and lifetime, but has higher self-discharge and efficiency. The most recent and still developing group of BES technologies is based on Li-Ion chemistry. The corresponding batteries, depending on the particular chemical process show good specific energy (LiNiCoAlO2), specific power (LiNiMnCoO2), lifetime (LiFe2PO4), efficiency and their combinations providing these parameters at reasonable price.

The above-mentioned high-level parameters of the modern BES enables them for use in practically all fields of electrical engineering. In particular, the use of Li-Ion batteries revolutionized the technical and market parameters of portable electronics. Similarly, the use of these batteries accelerated development of plug-in electric vehicles (PEVs) or all-electric vehicles (AEVs). In addition, the increased specific energy of modern BES makes them applicable in energy supply systems. Recent engineering practices of the authors of this report, concentrated in the field of energy systems [3] and small electric vehicles [4], shows certain similarities in BES use that, first of the all, regards their charging/discharging electronics, considered in this paper. This topic is essential for the evaluation of the power losses in the mentioned applications and understanding of their thermal behavior.

At the moment, numerous national and international regulations in the energy sector limit the use of fossil fuels for energy production and push on the use of renewable energy sources [5]. However, collecting of energy from renewable energy sources is uneven and production pattern of renewable energy sources does not always match the corresponding consumption demand. This mismatch can be compensated by Battery Energy Storage Systems (BESSs), appearing on the market [6]–[9]. The electronic interface of these BESS is a bidirectional charger/discharger tied to AC grid [3].

Another example of BES application, investigated by the authors, is electrical drive of small electric vehicle for needs of orthopedic rehabilitation. According to information, provided by World Health Organization's World report of disability [10], approximately 15% of world population is suffering from some sort of disability of whom 200 million have mobility difficulties. Wider integration of these disabled persons into social and economic life, assumes the use of modern technological equipment, for example, Power Assist Wheelchairs (PAWs). One of possible concepts of such wheelchairs is described in [4]. Its electrical drive is based on a low-speed permanent magnet electrical machine (AC) with segmented stator [11]–[14] and power electronic converter. The charging part of this converter is a rectifier, supplied from AC grid. In turn, its discharging part is an inverter, which supply specific AC load with potential demand of energy return that requires bidirectionality. The electric drive of the considered PAW operates in the closed compartment. Therefore, the accuracy of BES converter operation and its losses are interdependent factors that define the thermal mode of the drive.

As it can be seen, a bidirectional DC-AC inverter is essential part of the interface converter of the battery in both considered applications. This inverter may be built as a single-level pulse-mode circuit that forms pulse width or frequency modulated (PWM/FM) voltage. Alternatively, the inverter may generate level modulated (LM) voltage that requires the use of a multilevel topology. This topology is particularly suitable in both considered applications because they both contains a battery that consists of several cells providing the necessary voltage levels. The objective of this study is to find better configuration of the BES interface inverter considering the quality of the generated voltage. The criteria for the choice is the root-mean declination of the generated voltage from its reference curve. If the reference is sinusoidal, this declination is known as the Total Harmonic Distortion (THD) – in the case of BESS low THD is a real grid requirement. The tasks of the work, therefore, are to evaluate THD for different kinds of modulation (PWM vs. LM vs. mixed) and different number of levels, compare the results and provide conclusions on the better choice, in the same time keeping in mind that these

978-1-6654-3235-1/21/$31.00 ©2021 IEEE

matters affect also the losses and thermal mode of BES converters.

II. Review of Multilevel Converters Utilised Jointly with Batteries.

As it has already been mentioned BESs consist of several galvanic cells, forming a natural set of voltage levels. These levels can be processed by a multilevel converter (MLC). There are three main MLC topologies and each of them utilizes BES cells in a different way. Below a review of some MLC for BES is given.

The first MLC type, semiconductor clamped converters also known as neutral point clamped converters, provides commutation of internal BES levels to the output. There are two kinds of such MLC: diode clamped and active clamped [15]. Since MLC of this type deals with internal levels BES configuration is standard – series connection of several galvanic cells. This simplifies the use of BES at system level. On the other hand, the loading of separate cells is uneven that requires some extra Battery Management System (BMS). The use of neutral point clamped multilevel converter in BESSs is described in [16].

The next MLC type is known as converters with flying capacitors. Here voltage levels are taken from the voltage sources, which both terminals are commuted by converter switches. Typically, these sources are capacitors, but in the case of BES, they may be replaced by cell groups. Paper [17] describes and experimentally verifies the design of multilevel converter with flying capacitors for aircraft applications. Paper [18] provides an example of 13-level flying capacitor multilevel converter, based on GaN switches. If the voltage levels provided from the BES cell groups the entire battery is split into several uneven parts that complicates the use of this topology.

Finally, the third type of MLC utilizes independent voltage sources and is also known as cascaded H-bridge converter with separate DC sources. These MLC consist of several single-phase full bridge converters connected in series [19], [20]. Inputs of single-phase full bridge converters are connected to separate or independent DC sources, which, in case of implementation of multilevel converters in BESs, are battery cells or their groups. The output waveform is generated from such sources through full bridges designated in Figure 1(a) as “Power converter and energy storage building block”. These blocks connect series of sources to the output. A unipolar version of this MLC includes also a common polarity inverter that allows simplification of cell converters – Figure 1(b).

Different configurations of the building blocks can be found in literature [21], [22]. Some alternatives are shown in Figure 2. The most commonly used and simple cell is a single-phase full transistor bridge (H-bridge), shown at Figure 2(a). It is possible to get three voltage levels on the output of the H-bridge: $+V_g$ (battery voltage), $-V_g$ and 0V. Thus, the H-bridge is generating AC voltage and it is possible to control charging and discharging process of the connected battery. The second type of cell has a two-stage configuration – Figure 2(b). The part, forming output voltage – H-bridge – remains without changes. The second converter, added between H-bridge and the battery, is a pre-regulator that controls charging or discharging energy flow from the battery If the MLC forms unipolar voltage the cell converter is simpler, for example, it may be a DC/DC chopper or even a couple of switches.

There are also structures, where transformer is used in order to electrically isolate battery from the converter [21]. However, by using transformers it is possible to increase or decrease voltage, and, therefore, the advantages of cascaded H-bridge converter are being negotiated.

References [23]-[34] provide examples of usage of modular MLCs with independent sources in BESSs. In [23] self-adaptation control of second-life batteries (batteries that were previously used in transportation, the use of second-life batteries makes the BESS more affordable, as the batteries are the most expensive part of the BESS) is provided. This control strategy is based on online capacity estimation of the batteries, thus preventing them from overcharging and over-discharging. In [24] a unified control scheme of the multilevel converter with independent source based BESS is provided, which simplifies the control of state of charge (SOC) balancing and fault tolerant control of the system.

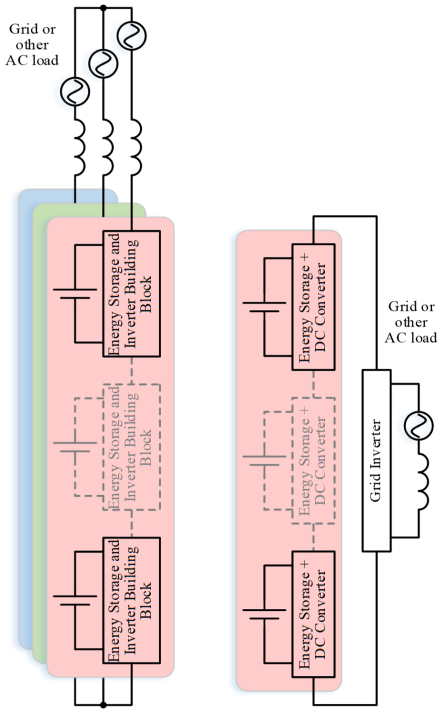

Fig. 1. Structure of multilevel converter with independent sources: (a) typical, (b) unipolar with a frontend (single phase).

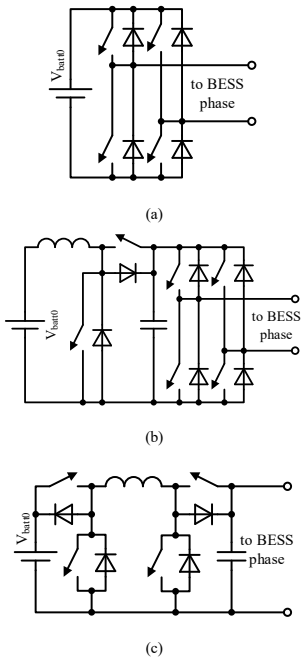

Fig. 2. Types of power electronic converters used in cascaded H-bridge multilevel converters: (a) H-bridge; (b) two-stage converter; (c) cell converter (buck-boost) for unipolar topologies.

Papers [25]–[29] also provide SOC balancing control of the multilevel converter with independent sources. In [30] the design of battery management system (BMS) for multilevel converter with independent source-based BESS is provided. In paper [31] the comparative analysis of SiC and Si switches is given, prototype of multilevel converter with independent sources is presented for the experimental verification. Reference [32] describes a 6.6 kV multilevel converter with independent sources with pulse width modulation (PWM) based BESS, experimental verification of downscaled prototype is also provided. Paper [33] provides analysis of usage modular multilevel converter with independent sources in static synchronous compensator combined with battery energy storage system – STATCOM/BESS for wind farm application. In [34] an example of modular multilevel converter with independent sources, where quasi-Z-source inverter is used as power electronic converter and energy storage building block, with photovoltaic (PV) panels connected to each converter, thus creating combined system of generation of energy from PV panels, and storage of generated energy.

Modular multilevel converters with independent sources provide the ability of active battery balancing, by "swapping" modules that are being turned on more frequently with the ones, that are being turned on less frequently, therefore, providing more even discharge of the cells in the battery pack, and, also more even degradation of the battery cells.

III. Operation of Modular Multilevel Converters with Independent Sources.

There are two types of operation of multilevel converters – with or without the PWM technique. If the PWM technique is used, then commutation losses are higher, considering that the main source of losses of transistors are during the commutations. If the PWM voltage forming technique is not used, then output waveforms are stepped, however, with sufficient level count, it is possible to have output waveforms closer to the sinewave [35]. If the PWM technique is not used, it is possible to reduce commutation losses of switches to minimum, as the commutation of the transistors will be less frequent. There will be higher conduction losses, but, taking into account, that switching losses are much lower, in some cases these can be even neglected.

IV. Evaluation.

In order to evaluate the performance of the multilevel converter with independent sources, MATLAB-Simulink models of different modular multilevel converters with independent sources, with H-bridges as power electronic converters connecting battery to the phase, were created. The main subject of the modulation is the estimation of necessity of using PWM in modular multilevel converters with independent sources. Models of H-bridges were created quite ideal (with ideal switches), however accurate models of batteries were created using Li-ion Samsung 30Q 18650 3000mAh 15A Battery INR18650-30Q batteries, at each H-bridge input batteries were connected in such way, that the amplitude of output voltage is equal to approximately 24V that is equal to operating voltage of the PAW, described in [4]. Output frequency is 50 Hz. Three cases were modulated: without PWM technique, With PWM technique, with different modulation frequencies: 2 kHz and 5 kHz. On Figure 3 example of single level voltage source inverter (VSI) is shown. Figure 4 shows the sub-model of H-bridge that is used to form phase cascades. Figure 5 shows the sub-model of control block.

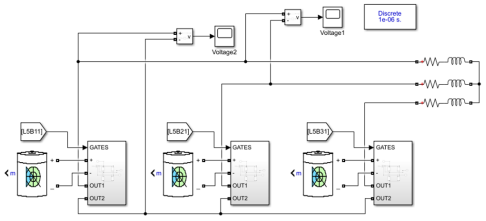

Fig. 3. Model of single level VSI

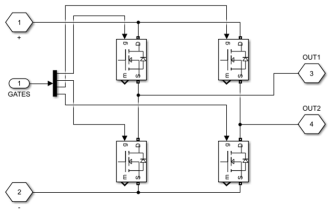

Fig. 4. Model of full bridge cell

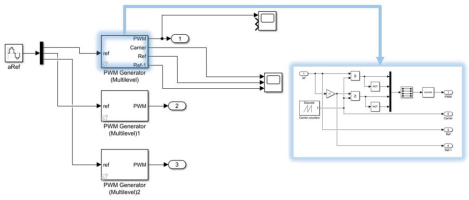

Fig. 5. Model of control block of single level modular multilevel converter with independent sources

Models of two, three and six-level modular multilevel converters with independent sources are made similarly, by increasing number of series connected H-bridges in phase cascades. Figure 6 shows the example of 6 level MLC with independent sources.

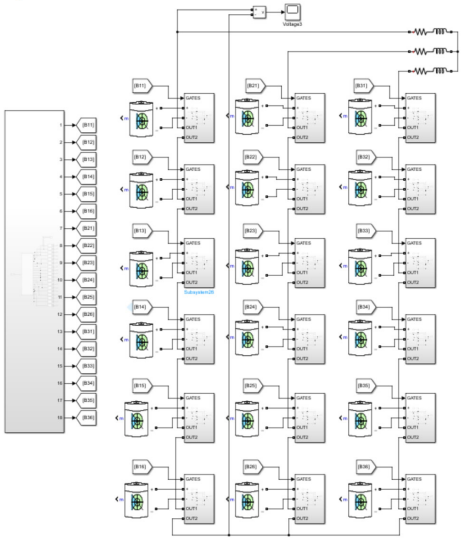

Fig. 6. Model of single level modular multilevel converter with independent sources

V. Results and Discussion.

Output voltages of multilevel converters with independent sources were received in two ways – with and without PWM technique. The results for single level VSI (one H-bridge in each phase cascade), two, three and six level modular multilevel converters with independent sources are given.

Figure 7 shows output phase voltage of single level VSI with PWM modulation frequency equal to 5 kHz, Figure 8 shows output phase voltage single level VSI without PWM modulation.

Figure 9 shows the harmonics of phase voltage for single level modular multilevel converter with modulation frequency equal to 5 kHz, Figure 10 shows harmonics of output phase voltage with modulation frequency 2 kHz and Figure 11 shows harmonics for output phase voltage without PWM.

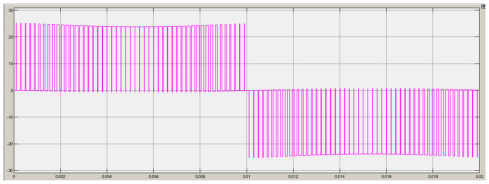

Fig. 7. Output phase voltage of single level VSI with PWM modulation frequency equal to 5 kHz

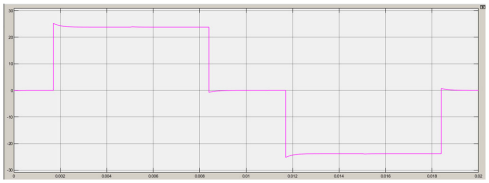

Fig. 8. Output phase voltage of single level VSI without PWM modulation.

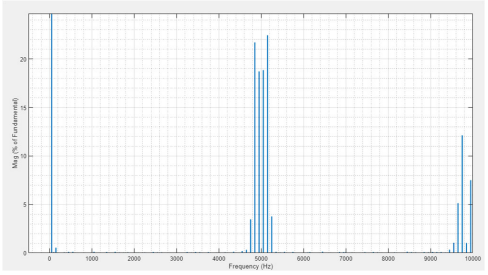

Fig. 9. Harmonics of phase voltage for single level VSI with modulation frequency equal to 5 kHz

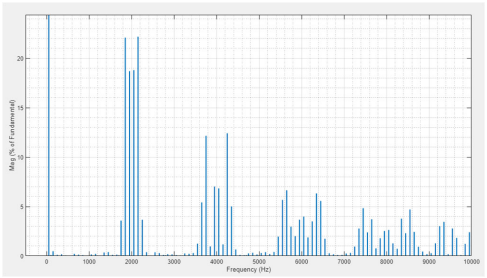

Fig. 10. Harmonics of phase voltage for single level VSI with modulation frequency equal to 2 kHz

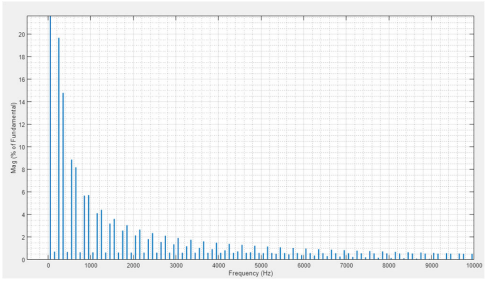

Fig. 11. Harmonics of phase voltage for single level VSI without PWM.

From Figures 9-11 it can be seen, that the modulation frequency is affecting the purity of the output waveform and the total harmonic distortion (THD). For 5 kHz modulation frequency the greatest impact gives exactly harmonics close to switching frequency and harmonics that are the multiplications of the modulation frequency. The same is in cases with 2 kHz modulation frequency. In case when PWM is not used, it is seen that harmonic decomposition is proportional.

The same analysis can be provided also for multilevel converters with more levels – for two, three and six-level MLCs with independent sources.

Figure 12 shows the output voltage of 3-level MLC with modulation frequency equal to 2kHz, Figure 13 shows the output voltage of 6-level MLC without PWM modulation.

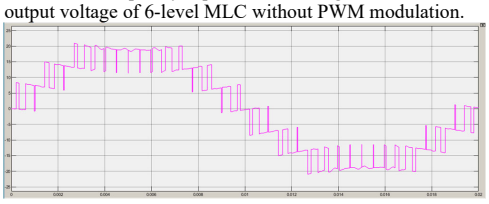

Fig. 12. Output phase voltage of 3-level MLC with independent sources with PWM modulation frequency equal to 2 kHz.

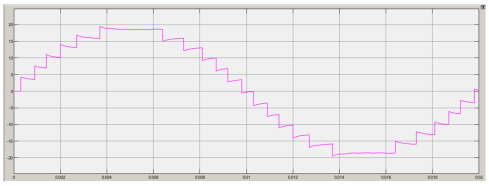

Fig. 13. Output phase voltage of 6-level MLC with independent sources without PWM modulation.

The results are shown at Figures 14-16 for two-level MLC, Figures 17-19 for three-level MLC, and Figure 20-22 – for six-level MLC.

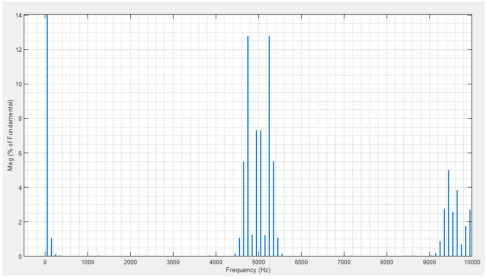

Fig. 14. Harmonics of phase voltage for 2-level MLC with modulation frequency equal to 5 kHz.

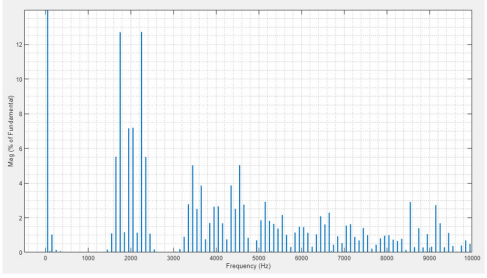

Fig. 15. Harmonics of phase voltage for 2-level MLC with modulation frequency equal to 2 kHz.

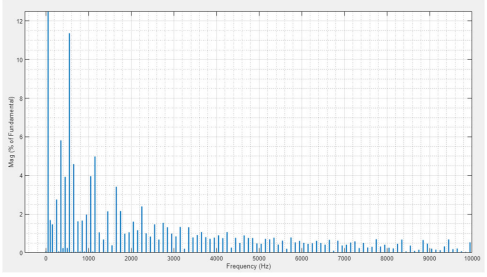

Fig. 16. Harmonics of phase voltage for 2-level MLC without PWM modulation.

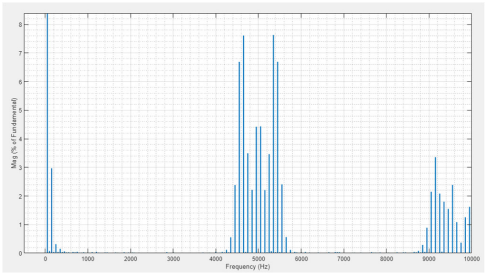

Fig. 17. Harmonics of phase voltage for 3-level MLC with modulation frequency equal to 5 kHz.

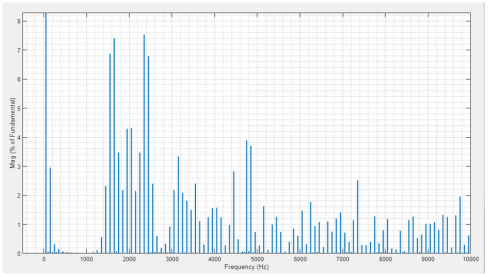

Fig. 18. Harmonics of phase voltage for 3-level MLC with modulation frequency equal to 2 kHz.

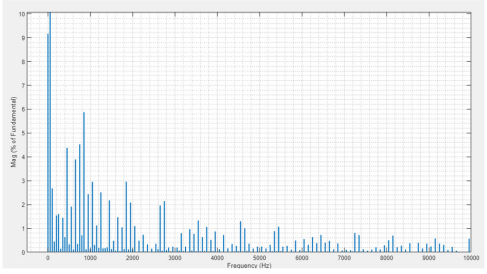

Fig. 19. Harmonics of phase voltage for 3-level MLC without PWM modulation.

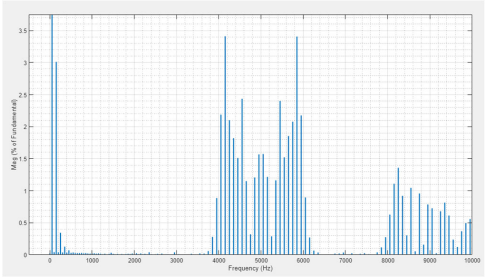

Fig. 20. Harmonics of phase voltage for 6-level MLC with modulation frequency equal to 5 kHz.

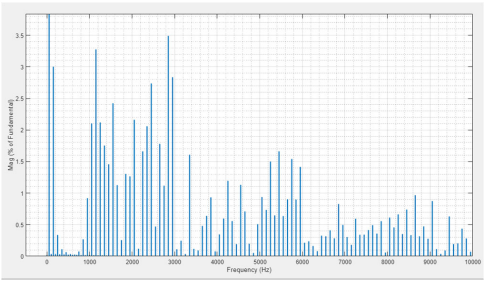

Fig. 21. Harmonics of phase voltage for 6-level MLC with modulation frequency equal to 2 kHz.

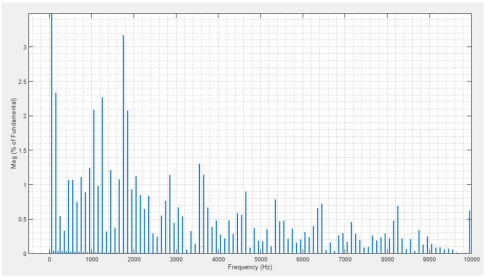

Fig. 22. Harmonics of phase voltage for 6-level MLC without PWM modulation.

In all cases with PWM modulation it can be seen, that modulation frequency is affecting the output voltage. Especially this effect is seen at Figures 10, 14, 17 and 20, when modulation frequency is chosen to be 5 kHz. For output voltage frequency 50 Hz (50 Hz is fundamental frequency), it can be seen, that the 5 kHz and harmonics that are multiples of 5 kHz have great effect. This effect is less noticeable for 2 kHz modulation frequency, however, this effect can also be seen. In case, when PWM is not used, it is seen (Figures 11, 16, 19 and 22) that the harmonic distribution is more proportional.

Table I shows the THD of output voltages for all modulated cases. It can be seen, that THD of output voltage waveforms when PWM is not used is lower, than in all cases, when PWM is used. However, it can be said, that exactly the modulation frequency of PWM is increasing distortion, making THD larger in cases when PWM is used to form output voltage. In the Table I for cases, when PWM is used THD is divided to Low Frequency Harmonic Distortion (LFHD) – Harmonic Distortion, that appears for frequencies $f = (0, \frac{1}{2} f_{\text{mod}}]$ and High Frequency Harmonic Distortion, that appears for frequencies $f > \frac{1}{2} f_{\text{mod}}$ (where f_{mod} - modulation frequency).

TABLE I. THD OF OUTPUT PHASE VOLTAGES OF MULTILEVEL CONVERTERS WITH INDEPENDENT SOURCES

	Modulation frequency 2 kHz			Modulation frequency 5 kHz			THD without PWM
	THD	LFHD	HFHD	THD	LFHD	HFHD	
Single-level VSI	54.46%	0.60%	53.86%	54.35%	0.66%	53.69%	31.44%
2-level MLC	28.67%	1.05%	27.62%	29.16%	1.06%	28.10%	18.50%
3-level MLC	22.17%	2.97%	19.20%	22.43%	3.00%	19.43%	13.78%
6-level MLC	11.59%	3.17%	8.42%	11.73%	3.04%	8.69%	7.97%

From Table I it can be seen, that in spite of the fact, that THD of output voltage waveforms is larger when PWM is used, it can also be said, that exactly higher harmonics (larger, than the half of modulation frequency) are giving that impact to THD. It means, that output voltages can be filtered in order to reduce this negative impact. In cases, when PWM is not used, harmonic distribution is proportional, which means, that even with output filter THD of output voltage will not decrease so significantly, then in case of when PWM is used.

By increasing level count of the MLC it is possible to decrease THD, however, it means, that converter will have higher conduction losses – larger switch count will be opened more time, than in case of lower level count. By implementing PWM + filtering output voltages it is also possible to reduce THD significantly, however, PWM implementation will result in increase of switching losses. One of the optimal solutions of implementation of MLC can be 3 - 4 levels with low frequency inter-level PWM.

VI. CONCLUSIONS AND FUTURE WORKS.

The above given study of the BES interface converters allows synthesis of their best configuration based on MLC topologies. The provided brief review of MLC shows that all three MLC types are compatible with BES. However, the neutral point clamped MLC may deal with simpler battery, but require BMS. On the other hand, modular MLCs with independent sources provides intrinsic management of the battery cell groups, but the battery itself is divided into as many parts as there are levels.

In the same time, the obtained results of the MATLAB-Simulink simulation show that good quality of the generated output voltage, which criteria is the root-mean declination of the voltage from its reference (in the case of sinusoidal reference known as THD), can be achieved in many ways. One way – increasing the number of MLC levels providing pure LM – leads to the higher conduction losses, but the other – the use single-level VSI and PWM – leads to the higher switching losses. Both solutions in pure form leads to thermal complications. However, a trade-off can be found. The optimal configuration may include 3 - 4 levels with minor inter-level pulse width modulation.

Finally, it become obvious, that the evaluation of the actual link between the quality of the output voltage of an MLC and its losses, as well as its thermal mode, requires further dedicated research.

ACKNOWLEDGMENT

This research work is funded by the Latvian Council of Science, project "Enhanced Thermal Management of Electric Drives in Orthopedic Rehabilitation Vehicles for their Better Reliability and Functionality", project No. lzp-2020/2-0390 and Riga Technical University's Doctoral Grant program.

REFERENCES

[1] S. Robert, *Introduction to Batteries—An IEEE Course*. NY, USA: IEEE: New York, 2013.

[2] X. Hu, C. Zou, C. Zhang, and Y. Li, "Technological Developments in Batteries: A Survey of Principal Roles, Types, and Management Needs," *IEEE Power Energy Mag.*, vol. 15, no. 5, pp. 20–31, Sep. 2017, doi: 10.1109/MPE.2017.2708812.

[3] I. A. Galkin, A. Blinov, M. Vorobyov, A. Bubovich, R. Saltanovs, and D. Peftitsis, "Interface Converters for Residential Battery Energy Storage Systems: Practices, Difficulties and Prospects," *Energies 2021, Vol. 14, Page 3365*, vol. 14, no. 12, p. 3365, Jun. 2021, doi: 10.3390/EN14123365.

[4] I. Galkin, A. Podgornovs, A. Blinov, K. Vitols, M. Vorobyov, and R. Kosenko, "Consideretions on Cost effective power assisted wheelchair subsystems," *Electr. Control Commun. Eng.*, vol. 14, no. 1, pp. 71–80, 2018, doi: 10.2478/ecce-2018-0008.

[5] "Energy strategy | Energy." https://ec.europa.eu/energy/topics/energy-strategy-and-energy-union_en (accessed May 10, 2021).

[6] "SolarEdge | A World Leader in Smart Energy Solutions." https://www.solaredge.com/ (accessed May 17, 2021).

[7] "Best Home Wind Turbines Updated: 2021." https://www.10powerup.com/best-home-wind-turbine/ (accessed May 17, 2021).

[8] "Powerwall | Tesla." https://www.tesla.com/powerwall?redirect=no (accessed May 17, 2021).

[9] "Energy supply of the future. Today. | to sunbathe." https://sonnen.de/ (accessed May 17, 2021).

[10] "W.H.O., World Report on Disability, 1st edition. World Health Organization, 2011, p. 350."

[11] R. Geidarovs, A. Podgornovs, and I. Galkin, "Simulation and Initial Evaluation of Modular Motor-Generator for Cost-Effective Power-Assist Wheelchair," in *2018 IEEE 59th International Scientific Conference on Power and Electrical Engineering of Riga Technical University (RTUCON)*, Nov. 2018, pp. 1–5, doi: 10.1109/RTUCON.2018.8659877.

[12] A. Podgornovs and I. Galkin, "Evaluation of Configurations of Modular Motor for Power-Assist Wheelchair," in *2019 26th International Workshop on Electric Drives: Improvement in Efficiency of Electric Drives (IWED)*, Jan. 2019, pp. 1–4, doi: 10.1109/IWED.2019.8664279.

[13] A. Podgornovs, R. Geidarovs, and I. Galkin, "Considerations on Selection of Modular Electric Drive for Power-Assist Wheelchair," Oct. 2019, doi: 10.1109/RTUCON48111.2019.8982291.

[14] I. Galkin, A. Podgornovs, and R. Geidarovs, "Data Evaluation of Novel Modular Wheelchair Motor," Jan. 2020, doi: 10.1109/IWED48848.2020.9069507.

[15] M. Bragard, N. Soltau, S. Thomas, and R. W. De Doncker, "The balance of renewable sources and user demands in grids: Power electronics for modular battery energy storage systems," *IEEE Trans. Power Electron.*, vol. 25, no. 12, pp. 3049–3056, 2010, doi: 10.1109/TPEL.2010.2085455.

[16] U. Abronzini *et al.*, "A Dual-Source DHB-NPC Power Converter for Grid Connected Split Battery Energy Storage System," in *2018 IEEE Energy Conversion Congress and Exposition, ECCE 2018*, Dec. 2018, pp. 2483–2488, doi: 10.1109/ECCE.2018.8557563.

[17] T. Modeer, N. Pallo, T. Foulkes, C. B. Barth, and R. C. N. Pilawa-Podgurski, "Design of a GaN-Based Interleaved Nine-Level Flying Capacitor Multilevel Inverter for Electric Aircraft Applications," *IEEE Trans. Power Electron.*, vol. 35, no. 11, pp. 12153–12165, Nov. 2020, doi: 10.1109/TPEL.2020.2989329.

[18] C. B. Barth *et al.*, "Design and control of a GaN-based, 13-level, flying capacitor multilevel inverter," Aug. 2016, doi:

10.1109/COMPEL.2016.7556770.

[19] L. M. Tolbert, F. Z. Peng, and T. G. Habetler, "Multilevel converters for large electric drives," *IEEE Trans. Ind. Appl.*, vol. 35, no. 1, pp. 36–44, 1999, doi: 10.1109/28.740843.

[20] S. Khomfoi and L. M. Tolbert, "Multilevel Power Converters," in *Power Electronics Handbook*, 2nd ed., Elsevier Inc., 2006, pp. 451–482.

[21] V. Fernão Pires, E. Romero-Cadaval, D. Vinnikov, I. Roasto, and J. F. Martins, "Power converter interfaces for electrochemical energy storage systems - A review," *Energy Convers. Manag.*, vol. 86, pp. 453–475, Oct. 2014, doi: 10.1016/j.enconman.2014.05.003.

[22] M. Adest, L. Handelsman, Y. Galin, A. Fishelov, G. Sella, and Y. Binder, "SolarEdge patent for HD-Wave Inverters - Distributed power system using direct current power sources, US9368964B2," 2016.

[23] C. Liu, X. Cai, and Q. Chen, "Self-Adaptation Control of Second-Life Battery Energy Storage System Based on Cascaded H-Bridge Converter," *IEEE J. Emerg. Sel. Top. Power Electron.*, vol. 8, no. 2, pp. 1428–1441, Jun. 2020, doi: 10.1109/JESTPE.2018.2886965.

[24] Q. Chen, N. Gao, R. Li, X. Cai, and Z. Lu, "A unified control scheme of battery energy storage system based on cascaded H-bridge converter," in *2014 IEEE Energy Conversion Congress and Exposition, ECCE 2014*, Nov. 2014, pp. 2561–2566, doi: 10.1109/ECCE.2014.6953743.

[25] Z. Ling, Z. Zhang, Z. Li, and Y. Li, "State-of-charge balancing control of battery energy storage system based on cascaded H-bridge multilevel inverter," in *2016 IEEE 8th International Power Electronics and Motion Control Conference, IPEMC-ECCE Asia 2016*, Jul. 2016, pp. 2310–2314, doi: 10.1109/IPEMC.2016.7512657.

[26] A. S. Gadalla, X. Yan, and H. Hasabelrasul, "Active power analysis for the battery energy storage systems based on a modern cascaded multilevel converter," in *Proceedings - 2nd IEEE International Conference on Energy Internet, ICEI 2018*, Jul. 2018, pp. 111–116, doi: 10.1109/ICEI.2018.00028.

[27] A. S. Gadalla, X. Yan, and H. Hasabelrasul, "State-of-charge balancing control strategy for battery energy storage systems based on a modern cascaded multilevel PWM converter," in *Proceedings - 2018 IEEE 12th International Conference on Compatibility, Power Electronics and Power Engineering, CPE-POWERENG 2018*, Jun. 2018, pp. 1–6, doi: 10.1109/CPE.2018.8372534.

[28] K. Kandasamy, D. M. Vilathgamuwa, and G. Foo, "Inter-module SoC balancing control for CHB based BESS using multi-dimensional modulation," in *Proceedings of the IEEE International Conference on Industrial Technology*, 2013, pp. 1630–1635, doi: 10.1109/ICIT.2013.6505917.

[29] J. Asakura and H. Akagi, "State-of-Charge (SOC)-Balancing Control of a Battery Energy Storage System Based on a Cascade PWM Converter," *IEEE Trans. Power Electron.*, vol. 24, no. 6, pp. 1628–1636, 2009, doi: 10.1109/TPEL.2009.2014868.

[30] M. Chen, B. Zhang, Y. Li, G. Qi, and J. Liu, "Design of a multi-level battery management system for a Cascade H-bridge energy storage system," in *Asia-Pacific Power and Energy Engineering Conference, APPEEC*, Mar. 2014, vol. 2015-March, no. March, doi: 10.1109/APPEEC.2014.7066076.

[31] K. Mordi, H. Mhiesan, J. Umuhoza, M. M. Hossain, C. Farnell, and H. A. Mantooth, "Comparative Analysis of Silicon Carbide and Silicon Switching Devices for Multilevel Cascaded H-Bridge Inverter Application with Battery Energy storage," Aug. 2018, doi: 10.1109/PEDG.2018.8447775.

[32] L. Maharjan, S. Inoue, and H. Akagi, "A transformerless energy storage system based on a cascade multilevel PWM converter with star configuration," *IEEE Trans. Ind. Appl.*, vol. 44, no. 5, pp. 1621–1630, 2008, doi: 10.1109/TIA.2008.2002180.

[33] L. Zhang, Y. Wang, H. Li, and P. Sun, "Hybrid power control of cascaded STATCOM/BESS for wind farm integration," in *IECON Proceedings (Industrial Electronics Conference)*, 2013, pp. 5288–5293, doi: 10.1109/IECON.2013.6699995.

[34] B. Ge, Y. Liu, H. Abu-Rub, and F. Z. Peng, "State-of-Charge Balancing Control for a Battery-Energy-Stored Quasi-Z-Source Cascaded-Multilevel-Inverter-Based Photovoltaic Power System," *IEEE Trans. Ind. Electron.*, vol. 65, no. 3, pp. 2268–2279, Mar. 2018, doi: 10.1109/TIE.2017.2745406.

[35] A. Bubovich and I. Galkin, "Evaluation of Optimal Switching of Modular Multilevel Inverter with Independent Voltage Sources," Nov. 2020, doi: 10.1109/RTUCON51174.2020.9316581.

Publication VII

A. Bubovich, M. Vorobyov, A. Blinov and D. Peftitsis, "Peculiarities of Multilevel Power Electronic Converters for Interfacing Battery Energy Storages with AC Loads," 2020 IEEE 8th Workshop on Advances in Information, Electronic and Electrical Engineering (AIEEE), 2021, pp. 1-4, doi: 10.1109/AIEEE51419.2021.9435798

Peculiarities of Multilevel Power Electronic Converters for Interfacing Battery Energy Storages with AC Loads

Alexander Bubovich[1], Maxim Vorobyov[2], Andrei Blinov[3], Dimosthenis Peftitsis[4]
[1,2]Riga Technical University, Institute of Industrial Electronics and Electrical Engineering, Riga, Latvia
[3]Tallinn University of Technology, Department of Electrical Power Engineering and Mechatronics, Tallinn, Estonia
[4]Norwegian University of Science and Technology, Department of Electrical Power Engineering, Trondheim, Norway
[1]aleksandrs.bubovics@rtu.lv, [2]maksims.vorobjovs@rtu.lv, [3]andrei.blinov@taltech.ee, [4]dimosthenis.peftitsis@ntnu.no

***Abstract*—This paper deals with the problem of battery balancing in modular multilevel converters with independent voltage sources. Battery balancing algorithm is proposed. Mathematical background of definition of the rules of algorithm are presented. Algorithm is evaluated using MATLAB Simulink 7-level modular multilevel converter with independent sources. Obtained results show, that the algorithm is working properly, the comparison of two different cases with and without implementation of the algorithm is provided.**

Keywords— Modular multilevel converters, DC-AC power converters, circuit simulation

I. Introduction

The demand of efficient conversion of electrical energy from one form to another has been rising drastically as the use of electrical and electronic equipment has been rising through last several years and is awaited to rise. Converters of electrical energy are widely used in various applications, for example, interface converters for renewable energy sources (such as photovoltaics [1], [2]), lightning applications [3], power supply of different electrical equipment, battery energy storage systems, electrical drives and automotive applications [4], etc.

One example of the use of power electronic converters are grid connected battery energy storage systems (BESS). The use of BESS is increasing nowadays, as the use of renewable energy sources is increasing because of the tendencies to decrease the use of fossil fuels for energy production, that is stated on national levels of various countries and internationally [5]. Taking into account the fact, that the consumption profile of energy use is not matching the production profile of renewable energy sources, the idea of using BESS pays its way. Main components of BESS are battery (lead acid, nicked-oxyhydroxide, sodium-sulfur, Redox Flow or lithium-ion battery pack or bank), AC/DC converter (unidirectional – separated to charger and discharger or bidirectional), AC/DC converter can also be single stage or two-stage, and consist of DC/DC converter and DC/AC inverter or unfolder [6]–[8]. Converters can be divided into two level topologies and multilevel topologies. Multilevel converters can be divided into multilevel converter with independent voltage sources, diode clamped (also known as neutral point clamped) multilevel converter and multilevel converter with flying capacitors and topologies that are derived from these three main topologies. In case of BESS system, multilevel converters can be used as bidirectional AC/DC converters or they can be part of two stage implementation and play role of AC/DC inverter or unfolder.

Another example of use of power electronic converters can be battery and electrical machine interface converters of electrical drives and automotive application. As a specific example of automotive application can be medical equipment and rehabilitation assisting powered vehicles.

According to World Health Organization World report of disability, approximately 15% of the world population is suffering from some sort of disability and 200 million people have serious difficulties in functioning [9] and these numbers are awaited to rise in time. In order to provide the integration of disabled people into social and economic life, new innovative technical devices can be used. As an example of such device can be smart wheelchair or assisting verticalizer. The concept of such wheelchair is described in [10]–[12]. The concept of the smart verticalizer is briefly discussed in [13].

Speaking about smart wheelchair, one of the most important parts of the smart wheelchair is electrical drive, as electrical drive is the main energy consumer of such system and is providing the main function of smart wheelchair – movement. Electrical drive subsystem consists of low-speed motor and battery and motor interface converter. In order to provide the recuperation and thus increase efficiency of the wheelchair, direct drive must be used. The design of low speed permanent magnet synchronous machine with segmented stator is described in [14]–[17]. Segmented stator gives the ability of increasing or decreasing of maximal power of the motor by increasing or decreasing the number of segments, which makes it easier to implement assessment function and to change the level of assessment of such wheelchair.

In order to control the electrical machine, power electronic driver should be used. Power electronic driver can be either DC or AC, and in case of DC motor the most commonly used driver topology is the transistor full bridge, and in case of AC motor most commonly used topology is three-phase transistor bridge. Three-phase transistor bridge is the cheaper solution to control AC motor, comparing it with multilevel topologies, as this topology have lower switch count.

However, the main disadvantage of three-phase transistor bridge are power losses of switches, as pulse width modulation (PWM) technique, and main losses of transistors are during commutation. If a converter, that uses PWM is placed in closed space where it is not possible to provide proper ventilation, the problem of power losses of the transistors can decrease the reliability and lower the life time of the device because of the heat that will be affecting every component in closed space.

978-1-6654-2538-4/21/$31.00 ©2021 European Union

One of the solutions of the problem is usage of multilevel converters without PWM technique implemented. In this case, output waveforms are stepped, however, with the sufficient amount of levels this problem can be neglected as with sufficient level count output waveforms will be closer to sinewave. If PWM technique is not used, the only significant source of the power losses is conducting losses and commutation losses can be neglected, as the commutation of the transistors in this case is appearing less frequently (comparing with the case, when PWM is used).

This paper is the continuation of research of modular multilevel converters with independent sources provided in [18], [19] and is focusing on definition of balanced discharge of batteries algorithm for modular multilevel converter with independent voltage sources.

II. Modular Multilevel Converter with Independent Voltage Sources

Modular multilevel converter with independent voltage sources consists of full-transistor bridge converters (H-bridge converters), connected in series [20], [21]. Figure 1 shows one phase cascade for m-level modular multilevel converter (MMC) with independent sources.

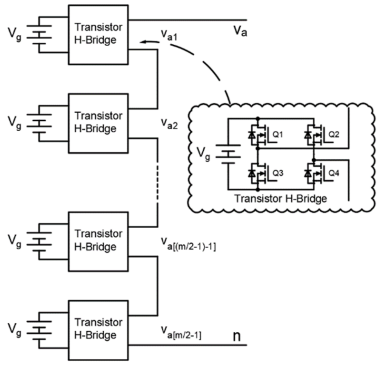

Fig. 1. One phase cascade for m-level modular multilevel converters with independent sources

The output waveform is generated by switching transistors in H-bridges and therefore by connecting voltage sources to the output – the output waveform is formed from the sum of voltages of sources that are connected to the output. Each transistor H-bridge can generate three output voltages: $+V_g$ (switches Q1 and Q4 are turned on), 0V (pair of switches Q1 and Q2 or Q3 and Q4 are turned on) and $-V_g$ (switches Q2 and Q3 are turned on).

III. Balancing of Batteries in MMC with Independent Sources

The state of charge (SOC) of battery can be expressed as percentage of remaining capacity of the battery (the available or "real" capacity) of the maximal (initial) capacity of the battery [22]:

$$SOC = \frac{\text{Real capacity}}{\text{Initial capacity}} \qquad (1)$$

If sinewave with phase angle φ equal to 0 radians, amplitude equal to 1A and frequency equal to 1Hz is examined as reference, then, if no battery balancing algorithm is used, the current waveforms of 7-level MMC with independent sources will look like it is shown at Figure 2.

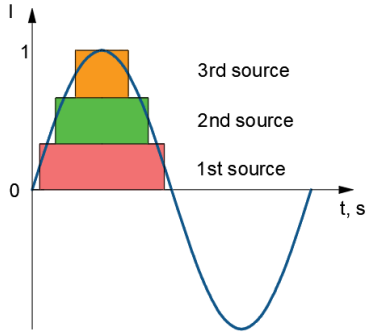

Fig. 2. Current waveform formation of MMC with independent sources

As it is shown at Figure 2, the first source is "turned on" the larger amount of time, to the first source will discharge more, then the others, the second – more, than the third and the third – less, than the others, so, all cells are discharging unevenly.

Let the SOC_a, SOC_b and SOC_c be the mean value of state of charge of all batteries connected as sources to H-bridges of one phase cascade (a,b and c phase respectively). For m-level MMC with independent sources these can be defined as:

$$SOC_a = \frac{1}{(m-1)/2} \sum_{i=1}^{(m-1)/2} SOC_{a\,i}$$
$$SOC_b = \frac{1}{(m-1)/2} \sum_{i=1}^{(m-1)/2} SOC_{b\,i} \qquad (2)$$
$$SOC_c = \frac{1}{(m-1)/2} \sum_{i=1}^{(m-1)/2} SOC_{c\,i}$$

If the time is divided by periods of time Δt, then for each Δt consumed amount of charge can be calculated for each battery can be calculated by multiplying the current with the Δt, and, therefore, the matrix with real state of charge of the batteries can be calculated. The example of 7-level MMC with independent sources will look like that:

$$SOC = \begin{pmatrix} SOC_{a1} & SOC_{b1} & SOC_{c1} \\ SOC_{a2} & SOC_{b2} & SOC_{c2} \\ SOC_{a3} & SOC_{b3} & SOC_{c3} \end{pmatrix} \qquad (3)$$

If in one period for each Δt SOC of all batteries are calculated, then turned on batteries can be swapped in such manner, that "on" are turned only batteries, that have larger SOC. The example of such implementation is shown at Figure 3.

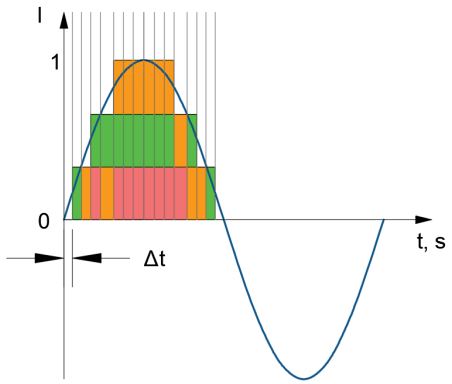

Fig. 3. Swapping of batteries during of one period for 7-level MMC with independent sources.

During each period of time Δt matrix of differences between real values of SOC and mean values of SOC for each phase ΔSOC should be calculated:

$$\Delta SOC = \begin{pmatrix} SOC_a - SOC_{a1} & SOC_b - SOC_{b1} & SOC_c - SOC_{c1} \\ SOC_a - SOC_{a2} & SOC_b - SOC_{b2} & SOC_c - SOC_{c2} \\ SOC_a - SOC_{a3} & SOC_b - SOC_{b3} & SOC_c - SOC_{c3} \end{pmatrix} \quad (4)$$

In order for algorithm to work, ΔSOC should be minimal as possible:

$$\Delta SOC \rightarrow \min \quad (5)$$

IV. Evaluation of Battery Balancing Algorithm

The initial evaluation was made with the help of MATLAB-Simulink model. Since the content of this evaluation is the investigation, whether the battery balancing algorithm is working or not, models of H-bridges were created quite ideal, however accurate models of batteries were created using Li-ion Samsung 30Q 18650 3000mAh 15A Battery INR18650-30Q batteries. Output waveforms were generated without PWM technique. In order to simplify the simulations, the load was chosen in such way, that the output current is 3A. The output frequency was chosen to be 50 Hz.

Two cases were simulated – in first case battery balancing is not implemented, in the second case – battery balancing is implemented.

Figure 4 shows the created model of 7-level MMC with independent sources.

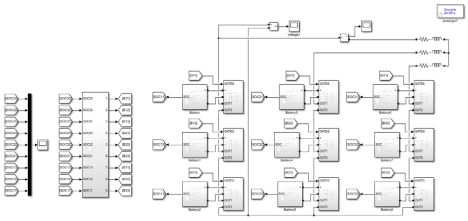

Fig. 4. Simulink model of 7-level MMC with independent sources

V. Results and Discussion

Both cases are compared by one parameter – SOC of all batteries. Figure 5 shows the results when battery balancing algorithm is not implemented, Figure 6 shows the results when battery balancing algorithm is implemented.

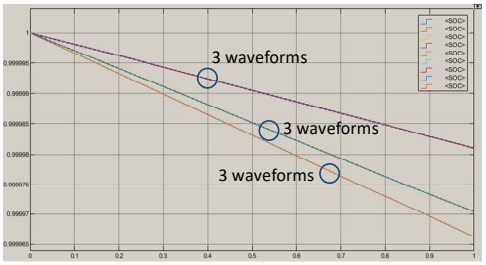

Fig. 5. SOC of batteries of 7-level MMC without battery balancing

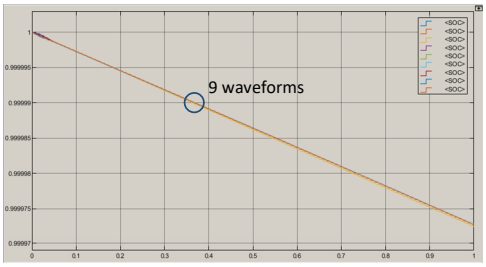

Fig. 6. SOC of batteries of 7-level MMC without battery balancing

As it is seen from Figure 5, for all 3 phases batteries are discharged unevenly, SOC waveforms 3 different lines (each line consists of 3 SOC waveforms, as three phases are examined). In Figure 6 it is shown, that all 9 SOC waveforms form one straight line, that means, that they are being discharged evenly.

VI. Conclusions

The obtained results show, that proposed battery balancing algorithm for three phase MMC with independent sources is working and with implemented algorithm batteries are discharged evenly, comparing with the case, when battery balancing algorithm is not implemented.

Further works include real-life prototype design and testing of the proposed algorithm on prototype, as well as comparison of the results with results obtained with models.

Also, more sophisticated analysis of MMCs with independent sources in order to estimate sufficient level count of MMCs when operating with and without PWM technique in BESS applications.

ACKNOWLEDGMENT

This publication was supported from Baltic Research Program funded by the European Economic Area and Norway 2014-2021 financial mechanisms within the contract EMP474 "Optimised Residential Battery Energy Storage Systems (ORBES)" of the first (Estonian) call of this program, Cross-Platform Research Program 2020 of Riga Technical University within the contract ZI-2020/2 "Development of Orthopedic Rehabilitation Power-Assist Vehicles and Research of their Cyber-Physical Models" and Riga Technical University's Doctoral Grant programme.

REFERENCES

[1] A. Sangwongwanich *et al.*, "Design for Accelerated Testing of DC-Link Capacitors in Photovoltaic Inverters Based on Mission Profiles," *IEEE Trans. Ind. Appl.*, vol. 57, no. 1, pp. 741–753, Jan. 2021, doi: 10.1109/TIA.2020.3030568.

[2] A. Bubovich, "Evaluation of interface converters for natural energy transfer between small sources, storages and low-voltage DC grid: Simulation case," 2017, doi: 10.1109/AIEEE.2016.7821830.

[3] I. Galkin, O. Tetervjonok, and I. Milashevski, "Comparative study of steady-state performance of voltage and current fed dimmable LED drivers," in *International Conference-Workshop Compatibility in Power Electronics , CPE*, 2013, pp. 292–297, doi: 10.1109/CPE.2013.6601172.

[4] A. Bogdanovs, O. Krievs, L. Ribickis, and J. Pforr, "Fuzzy Logic Current Balancing Controller Implementation in an Automotive Multi-Phase DC Converter with Coupled Inductors," Nov. 2020, doi: 10.1109/RTUCON51174.2020.9316473.

[5] "Energy strategy | Energy." https://ec.europa.eu/energy/topics/energy-strategy-and-energy-union_en (accessed May 10, 2021).

[6] M. Stecca, L. Ramirez Elizondo, T. Batista Soeiro, P. Bauer, and P. Palensky, "A Comprehensive Review of the Integration of Battery Energy Storage Systems into Distribution Networks," *IEEE Open J. Ind. Electron. Soc.*, pp. 1–1, Mar. 2020, doi: 10.1109/ojies.2020.2981832.

[7] V. Fernão Pires, E. Romero-Cadaval, D. Vinnikov, I. Roasto, and J. F. Martins, "Power converter interfaces for electrochemical energy storage systems - A review," *Energy Convers. Manag.*, vol. 86, pp. 453–475, Oct. 2014, doi: 10.1016/j.enconman.2014.05.003.

[8] A. Chub, D. Vinnikov, R. Kosenko, E. Liivik, and I. Galkin, "Bidirectional DC-DC Converter for Modular Residential Battery Energy Storage Systems," *IEEE Trans. Ind. Electron.*, vol. 67, no. 3, pp. 1944–1955, Mar. 2020, doi: 10.1109/TIE.2019.2902828.

[9] "W.H.O., World Report on Disability, 1st edition. World Health Organization, 2011, p. 350."

[10] M. Vorobyov and I. Galkin, "Concept of cost-effective power-assisted wheelchair: Human-in-the-loop subsystem," in *Proceedings of the 5th IEEE Workshop on Advances in Information, Electronic and Electrical Engineering, AIEEE 2017*, Jul. 2017, vol. 2018-January, pp. 1–5, doi: 10.1109/AIEEE.2017.8270559.

[11] K. Vitols and A. Podgornovs, "Concept of cost-effective power-assist wheelchair's electrical subsystem," in *Proceedings of the 5th IEEE Workshop on Advances in Information, Electronic and Electrical Engineering, AIEEE 2017*, Jul. 2017, vol. 2018-January, pp. 1–4, doi: 10.1109/AIEEE.2017.8270563.

[12] I. Galkin, A. Podgornovs, A. Blinov, K. Vitols, M. Vorobyov, and R. Kosenko, "Consideretions on Cost effective power assisted wheelchair subsystems," *Electr. Control Commun. Eng.*, vol. 14, no. 1, pp. 71–80, 2018, doi: 10.2478/ecce-2018-0008.

[13] A. Bubovich, I. Galkin, and M. Vorobyov, "Further Improvement of Customized Vibration Generator for Machine–Human Feedbacks with the Help of Resonant Networks," *Electronics*, vol. 10, no. 8, p. 962, Apr. 2021, doi: 10.3390/electronics10080962.

[14] R. Geidarovs, A. Podgornovs, and I. Galkin, "Simulation and Initial Evaluation of Modular Motor-Generator for Cost-Effective Power-Assist Wheelchair," in *2018 IEEE 59th International Scientific Conference on Power and Electrical Engineering of Riga Technical University (RTUCON)*, Nov. 2018, pp. 1–5, doi: 10.1109/RTUCON.2018.8659877.

[15] A. Podgornovs and I. Galkin, "Evaluation of Configurations of Modular Motor for Power-Assist Wheelchair," in *2019 26th International Workshop on Electric Drives: Improvement in Efficiency of Electric Drives (IWED)*, Jan. 2019, pp. 1–4, doi: 10.1109/IWED.2019.8664279.

[16] A. Podgornovs, R. Geidarovs, and I. Galkin, "Considerations on Selection of Modular Electric Drive for Power-Assist Wheelchair," Oct. 2019, doi: 10.1109/RTUCON48111.2019.8982291.

[17] I. Galkin, A. Podgornovs, and R. Geidarovs, "Data Evaluation of Novel Modular Wheelchair Motor," Jan. 2020, doi: 10.1109/IWED48848.2020.9069507.

[18] A. Bubovich, "Evaluation of Opportunities of Balanced Discharge of Batteries in Cost Effective Assisting Powered Wheelchair," in *2019 IEEE 60th International Scientific Conference on Power and Electrical Engineering of Riga Technical University (RTUCON)*, 2019, pp. 1.-4.

[19] A. Bubovich and I. Galkin, "Evaluation of Optimal Switching of Modular Multilevel Inverter with Independent Voltage Sources," 2020, doi: 10.1109/RTUCON51174.2020.9316581.

[20] L. M. Tolbert, F. Z. Peng, and T. G. Habetler, "Multilevel converters for large electric drives," *IEEE Trans. Ind. Appl.*, vol. 35, no. 1, pp. 36–44, 1999, doi: 10.1109/28.740843.

[21] S. Khomfoi and L. M. Tolbert, "Multilevel Power Converters," in *Power Electronics Handbook*, 2nd ed., Elsevier Inc., 2006, pp. 451–482.

[22] J. Asakura and H. Akagi, "State-of-Charge (SOC)-Balancing Control of a Battery Energy Storage System Based on a Cascade PWM Converter," *IEEE Trans. Power Electron.*, vol. 24, no. 6, pp. 1628–1636, 2009, doi: 10.1109/TPEL.2009.2014868.

Publication VIII

A. Bubovich, M. Vorobyov and A. Giannakis, "Initial Evaluation of a Multilevel Inverter with Unfolding Stage for BESS Applications," 2021 IEEE 9th Workshop on Advances in Information, Electronic and Electrical Engineering (AIEEE), 2021, pp. 1-4, doi: 10.1109/AIEEE54188.2021.9670386.

Initial Evaluation of a Multilevel Inverter with Unfolding Stage for BESS Applications

Alexander Bubovich[1], Maxim Vorobyov[2], Andreas Giannakis[3]
[1,2]Riga Technical University, Institute of Industrial Electronics and Electrical Engineering, Riga, Latvia
[3]Norwegian University of Science and Technology, Department of Electric Power Engineering, Trondheim, Norway
[1]aleksandrs.bubovics@rtu.lv, [2]maksims.vorobjovs@rtu.lv, [3] andreas.giannakis@ntnu.no

***Abstract*—Today, the integration of renewable energy sources into power grids has increased significantly. This necessitates the development of more battery energy storage systems. A crucial component in such systems is the power electronic converters, which ensure the proper connection of the batteries to the grid. These bidirectional converters should be able not only to discharge batteries to the grid, but also to charge the batteries when it is needed. Various power converters can be identified for these systems. In particular, multilevel topologies offer several advantages, such as lower harmonic distortion of the output waveforms and lower switching losses. Among all multilevel converter topologies, the multilevel converter with independent sources provides one more benefit – battery balancing is achieved naturally by swapping the module switching order. This paper evaluates the performance of a modular multilevel converter with independent sources and unfolding stage.**

Keywords—batteries, energy storage, DC-AC converters, multilevel converters, performance evaluation

I. Introduction

Nowadays numerous national and international regulations related to the energy market limit the use of fossil fuels for the production of energy [1]. This limitation has led towards the integration of more renewable energy sources into the existed power grids. .It is expected that these tendencies will not change and despite the fact, that fossil fuels continue to play significant role in global energy systems, the proportion of renewable energy is increasing each year [2], [3]. However, renewable energy sources such as solar energy or wind energy have one main drawback due to the intermittent nature of these sources. This means that the energy production pattern of such sources does not match the energy consumption pattern. This discrepancy can be compensated by using Battery Energy Storage Systems (BESSs). A typical BESS consists of Battery Energy Storage (BES) and power electronic converter which connects the BES to an either AC or a DC grid [4].

There are various BES types. Among others, the most typical BES technology is based on Lead-Acid [5], [6]. This type of BES has several drawbacks, such as comparative short lifetime and low specific energy. However, the Lead-Acid BES is still quite popular mostly due to the low price. On the other hand, Nickel-Metal Hydride BES technology [7] has significantly higher specific energy and longer lifetime compared to the Lead-Acid counterparts. However, this battery technology faces a few drawbacks, such as high self-discharge and low efficiency. The last BES technology uses Li-Ion for the chemical process. These batteries have high specific energy, as well as high efficiency and long lifetime (these parameters differ depending on the chemical process) for affordable prices [8], [9]. Additionally, the use of supercapacitors as BES in DC grid can be considered to provide faster charging of the BES and easier service [10], [11].

The power electronic converters used in BESSs should be bidirectional, i.e. they need to be able to discharge the battery, as well as to charge it when required. An option, when charging [12] and discharging of the BES is implemented was initially considered, however, single stage operation of the converters provide maximal efficiency only at one particular operation point [4]. This converter can be built either as single-level voltage source converter or as multilevel converter [4], [13].

Power electronic converters can generate either pulse width of frequency modulated (PWM/FM) output voltage or, in case of using multilevel topology, output voltage can be also level modulated (LM) [14].

In case of BESSs, multilevel converter topologies have several advantages. In those topologies, the output voltage is formed from several voltage levels leading to lower harmonic distortion, lower switching losses and electromagnetic interference compared to two-level counterparts. There are three main types of multilevel converters (MLCs): diode clamped MLC, MLC with flying capacitors and MLC with independent voltage sources. MLC with independent voltage sources offers one main advantage compared to the others MLC types. In particular, the battery balancing in this type of MLCs is achieved naturally, as the batteries that are connected to the output can be easily swapped, leading to a more even discharge rate of the batteries [15].

This paper shows the development of the testbench, as well as it evaluates experimentally the performance of an MLC with independent sources and unfolding stage.

II. Multilevel converters with independent sources

MLC with independent voltage sources (also known as cascaded H-bridge converter) in simplest implementation consists of several series-connected H-bridge converters [16], [17]. Figure 1 shows the schematic diagram of an m-level

978-1-6654-6712-4/21/$31.00 ©2021 IEEE

MLC with independent sources with full transistor bridges used as voltage building block.

Instead of H-bridge converter, there might be different converter structures as well. The main purpose of these converters is to provide compensation of the output voltage of the series-connected converters. For this purpose, for example, synchronous buck converter can be used, that is then connected to the H-bridge that generates AC voltage at the output of the block [4].

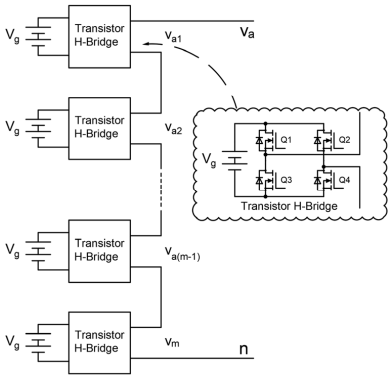

Fig. 1. m-level MLC with independent voltage sources

MLC with independent sources can be implemented in a bit different way. A simplified MLC can be designed by adding unfolding circuit at the output of the converter. In addition to that,transistor half-bridges can be used instead of full transistor bridges, since there is no need to provide alternating output voltage.

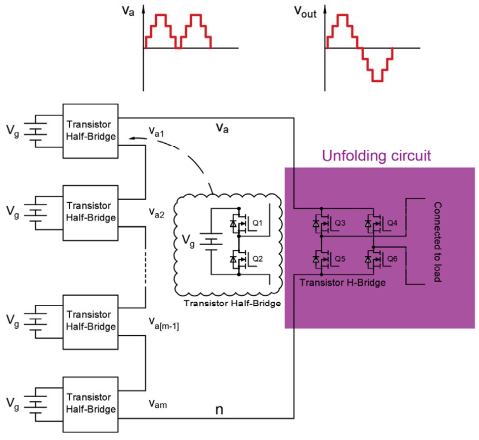

Fig. 2. m-level MLC with independent voltage sources with unfolding circuit connected at the output of the converter

In this case, the MLC forms unipolar voltage half-waves while the unfolding circuit is used to provide the required polarity of the output voltage, and As unfolding circuit full transistor bridge is used. Figure 2 shows the schematic diagram of an MLC with independent sources and unfolding circuit.

The investigated MLC topology circuit has some advantages comparing with classic MLC with independent sources The main reason is the lower number of the required switches. This leads to higher overall efficiency of the converter as well as to easier control of the converter. Besides that, all benefits of the classic MLC with independent sources remain the same, and thus, it is possible to swap modules to provide battery balancing. It should also be mentioned that the transistors of the unfolding circuit are commutated at grid frequency, leading to minimized switching losses.

III. Testbench Development

A down-scaled prototype of a three-level MMC with independent sources and unfolding circuit has been designed and tested.

IRF540 n-channel MOSFETs have been utilized for the switches realization due to theirrelatively low cost and high reliability. HCPL-3120 optocouplers were chosen for driving the MOSFETs with bipolar voltage modulation: +15V for logical “1” and -15V for logical “0”. In order to operate the MOSFETs with this voltage scheme, each HCPL-3120 is connected to the IR0515S board mount power supply with input voltage equal to 5V. LAUNCHXL-F2837D development board from Texas Instruments has been used to control the operation of the converter.

Input voltage for each MOSFET in the half-bridge was chosen to be 8.4V – which equals the voltage of two fully charged series-connected 18650 battery cells. The input voltage was obtained using two power supply units, TTi EX752M, of 5V each one. The power supply of the MOSFETs drivers was obtained using EA-PS 8032-10 T power supply unit. The output voltage, as well as the current are measured with a digital oscilloscope, RIGOL DS4012.

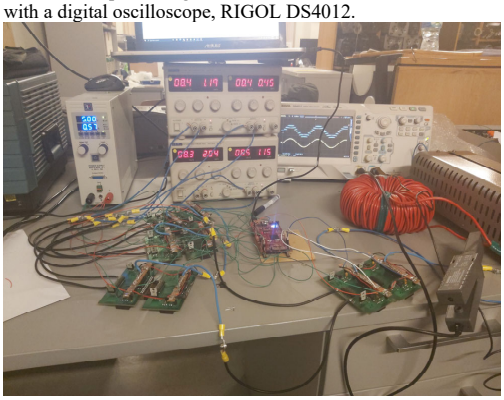

Fig. 3. Setup for experimental verification of the 3-level MLC with independent sources and unfolding circuit.

An RL load has been utilized for the performance evaluation of the considered MLC topology. In particular, a16 Ω and 5mH connected in series were used. The setup of the down-scaled prototype, and the test circuit are shown in Fig. 3.

IV. Results and Discussion

A three-level MLC with independent sources and unfolder circuit was initially tested at low voltages connected to the input of the converter and comparatively small low currents. The output voltage was generated using PWM technique, and the converter was tested with three PWM modulation frequencies, i.e. 1 kHz, 2 kHz and 4 kHz. Output waveforms are shown in Figures 4-6. The blue lines illustrate the output voltage and the yellow lines show the output current in all three oscillograms.

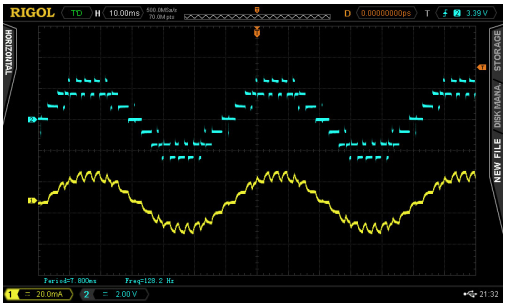

Fig. 4. Output waveforms of 3-level MLC with independent sources and unfolding circuit with 1kHz PWM modulation frequency.

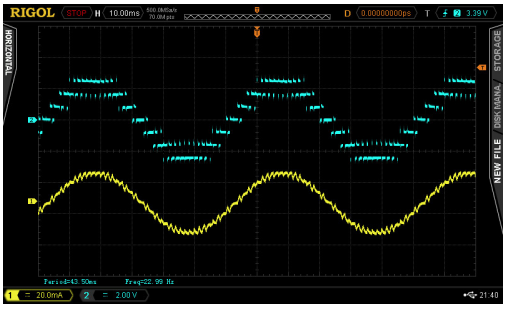

Fig. 5. Output waveforms of 3-level MLC with independent sources and unfolding circuit with 2kHz PWM modulation frequency.

The experimental results reveal the proper operation of the investigated MLC topology. The impact of the switching frequency of the converter on the distortion of the output current can be observed. In particular, at 1 kHz switching frequency, the pulsations of the output current (yellow line in Figure 4) are significantly larger compared to the corresponding waveform at 4 kHz shown in Figure 6.

Additionally, the thermal performance of the MOSFETs has also been investigated by using the thermal camera Fluke Ti450. It can be seen that the devices of the unfolding circuit were not affected by the switching frequency at room temperature. The thermal images of the MOSFETs for all three frequencies are shown in Figures 7-9. On the left side of these Figures, there are thermal images of the MOSFETs with the lowest temperature, while on the right side there are thermal images of the MOSFETs with the highest temperature among all MOSFETs in all half-bridge converters.

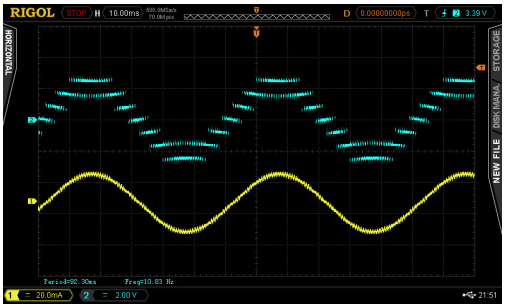

Fig. 6. Output waveforms of 3-level MLC with independent sources and unfolding circuit with 4kHz PWM modulation frequency.

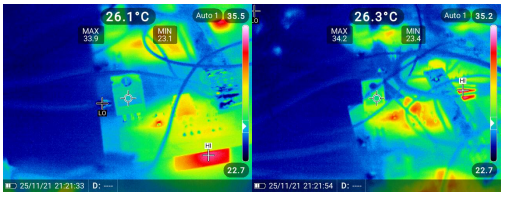

Fig. 7. Thermal images of the MOSFETs in a 3-level MLC with 1 kHz PWM modulation frequency.

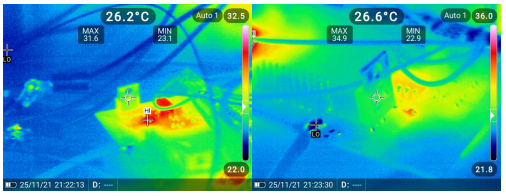

Fig. 8. Thermal images of the MOSFETs in a 3-level MLC with 2 kHz PWM modulation frequency.

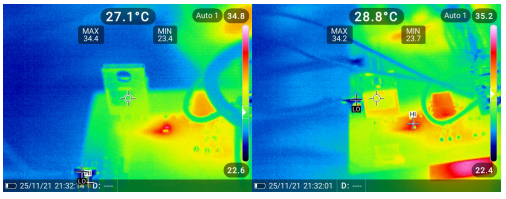

Fig. 9. Thermal images of the MOSFETs in a 3-level MLC with 4 kHz PWM modulation frequency.

The thermal images of the MOSFETs shown in Figures 7-9 reveal that the impact of the switching frequency when it increases from 1 kHz to kHz, on the temperature of the devices is almost negligible. However, at 4 kHz switching frequency, a temperature increase of the MOSFETs case is observed. This result is in accordance with the initial statement, that the increase of the switching frequency leads to higher commutation losses associated with the semiconductor devices.

V. Conclusions and Future Works

A down-scaled prototype of a single-phase MLC with independent sources and unfolding converter was designed and tested. The proposed MLC topology utilizes series-connected half-bridge converters. This reduces the number of the required switches, as well as it simplifies the control of the converter. The experimental results verified the feasibility of the proposed topology. The converter was tested at low voltages and at low currents.

Using thermal camera, the thermal performance of the switches was also studied. It was observed that by increasing the switching frequency, the temperature of the switches was increased. This means, that with higher switching frequencies, the commutation losses associated with the semiconductor devices used in a converter become higher, leading to lower efficiency of the converter. On the other hand, it was shown that the current waveform becomes less distorted with the increase of the switching frequency. It can be concluded that the choice of the switching frequency of the converter is a trade-off between the distortion of the output waveforms and the efficiency of the converter. Additionally, it should be mentioned that with increased losses in the switches, more complex thermal management systems should be designed in order the converter to be able to dissipate the heat more efficiently.

The future work includes more sophisticated and dedicated research of MLC with independent sources in terms of control, and pre-regulation of the voltage from the source. Moreover, the design of a full-scale prototype of the MLC and its experimental validation in bidirectional operation will also be included in the future work.

Acknowledgment

This publication was supported from Baltic Research Program funded by the European Economic Area and Norway 2014-2021 financial mechanisms within the contract EMP474 “Optimised Residential Battery Energy Storage Systems (ORBES)” of the first (Estonian) call of this program

References

[1] “Energy strategy | Energy.” https://ec.europa.eu/energy/topics/energy-strategy-and-energy-union_en (accessed May 10, 2021).

[2] “Energy - Our World in Data.” https://ourworldindata.org/energy (accessed Apr. 06, 2020).

[3] “Renewable Energy Sources: Energy Trends Shaping the Future.” https://justenergy.com/blog/renewable-energy-sources-energy-trends-future/ (accessed Dec. 14, 2021).

[4] I. A. Galkin, A. Blinov, M. Vorobyov, A. Bubovich, R. Saltanovs, and D. Peftitsis, “Interface Converters for Residential Battery Energy Storage Systems: Practices, Difficulties and Prospects,” *Energies*, vol. 14, no. 12, p. 3365, Jun. 2021, doi: 10.3390/en14123365.

[5] “Energy Storage Technology Descriptions-EASE-European Associaton for Storage of Energy lead-aCid battery eleCtroCHemiCal energy Storage.” https://ease-storage.eu/wp-content/uploads/2016/07/EASE_TD_Electrochemical_LeadAcid.pdf (accessed Dec. 16, 2021).

[6] W. Jie, L. Hua, C. Peijie, Q. Deyu, and L. Shan, “Design of Energy Storage System using Retired Valve Regulated Lead Acid (VRLA) Batteries in Substations,” *CENCON 2019 - 2019 IEEE Conf. Energy Convers.*, vol. 2019-January, pp. 132–136, Oct. 2019, doi: 10.1109/CENCON47160.2019.8974821.

[7] J. M. German, “Hybrid Electric Vehicles,” *Encycl. Energy*, pp. 197–213, Jan. 2004, doi: 10.1016/B0-12-176480-X/00180-7.

[8] S. Robert, *Introduction to Batteries—An IEEE Course*. NY, USA: IEEE: New York, 2013.

[9] X. Hu, C. Zou, C. Zhang, and Y. Li, “Technological Developments in Batteries: A Survey of Principal Roles, Types, and Management Needs,” *IEEE Power and Energy Magazine*, vol. 15, no. 5. Institute of Electrical and Electronics Engineers Inc., pp. 20–31, Sep. 01, 2017, doi: 10.1109/MPE.2017.2708812.

[10] I. Galkin, A. Stepanov, and J. Laugis, “Outlook of usage of supercapacitors in uninterruptible power supplies,” *BEC 2006 - 2006 Int. Balt. Electron. Conf. Proc. 10th Bienn. Balt. Electron. Conf.*, pp. 237–240, 2006, doi: 10.1109/BEC.2006.311107.

[11] A. Stepanov, I. Galkin, and L. Bisenieks, “Implementation of supercapacitors in uninterruptible power supplies,” *2007 Eur. Conf. Power Electron. Appl. EPE*, 2007, doi: 10.1109/EPE.2007.4417559.

[12] I. Galkin, A. Blinov, I. Verbytskyi, and D. Zinchenko, “Modular Self-Balancing Battery Charger Concept for Cost-Effective Power-Assist Wheelchairs,” *Energies 2019, Vol. 12, Page 1526*, vol. 12, no. 8, p. 1526, Apr. 2019, doi: 10.3390/EN12081526.

[13] V. Fernão Pires, E. Romero-Cadaval, D. Vinnikov, I. Roasto, and J. F. Martins, “Power converter interfaces for electrochemical energy storage systems - A review,” *Energy Convers. Manag.*, vol. 86, pp. 453–475, Oct. 2014, doi: 10.1016/j.enconman.2014.05.003.

[14] A. Bubovich, M. Vorobyov, I. Galkin, and T. Dovudon, “Quality Evaluation of Jointly Used Modular Multilevel Converters and Battery Energy Storages,” pp. 144–151, Nov. 2021, doi: 10.1109/EDPE53134.2021.9604102.

[15] A. Bubovich, M. Vorobyov, A. Blinov, and D. Peftitsis, “Peculiarities of Multilevel Power Electronic Converters for Interfacing Battery Energy Storages with AC Loads,” in *2020 IEEE 8th Workshop on Advances in Information, Electronic and Electrical Engineering (AIEEE)*, Apr. 2021, pp. 1–4, doi: 10.1109/AIEEE51419.2021.9435798.

[16] S. Khomfoi and L. M. Tolbert, “Multilevel Power Converters,” in *Power Electronics Handbook*, 2nd ed., Elsevier Inc., 2006, pp. 451–482.

[17] L. M. Tolbert, F. Z. Peng, and T. G. Habetler, “Multilevel converters for large electric drives,” *IEEE Trans. Ind. Appl.*, vol. 35, no. 1, pp. 36–44, 1999, doi: 10.1109/28.740843.

Publication IX

A. Bubovich, I. Galkin «Evaluation of Optimal Switching of Modular Multilevel Inverter with Independent Voltage Sources». In: 2020 IEEE 61st International Scientific Conference on Power and Electrical Engineering of Riga Technical University (RTUCON 2020): Conference Proceedings, Latvia, Riga, 5-7 November, 2020. Piscataway: IEEE, 2020, pp.1-4.

Evaluation of Optimal Switching of Modular Multilevel Inverter with Independent Voltage Sources

Alexander Bubovich[1], Ilya Galkin[2]
Institute of Industrial Electronics and Electrical Engineering
Riga Technical University
Riga, Latvia
[1]aleksandrs.bubovics@rtu.lv, [2]gia@eef.rtu.lv

***Abstract* — This paper deals with the problem of the defining optimal switching times in modular multilevel converters (MMC) with independent voltage sources, if no pulse width modulation (PWM) technique is used. By using MATLAB Simulink modulation several schematics were analyzed (starting from 3 level MMC till 15 level MMC) with different module switching patterns. Different switching patterns of modules of MMC are compared by one parameter – total harmonic distortion (THD) of the output voltage waveform. Mathematical background of calculation of optimal switching times is also presented.**

Keywords—Modular multilevel converters, DC-AC power converters, circuit simulation, total harmonic distortion

I. Introduction

With the development of electrical technologies, the need of efficient converting of electrical energy from one form to another (for example, converting between AC and DC, changing frequency, voltage etc.) has risen and is awaited to rise in time. Converters of electrical energy are widely used in different applications, such as interface converters for renewable energy systems, lighting applications, power supply of different electrical equipment, battery energy storage systems, electrical drives etc.

One example of use of power electronic converters are grid connected battery energy storage systems (BESS). The main components of BESS are battery (lead acid or lithium-ion battery pack/bank), AC/DC converter that charges and discharges battery when it is needed/convenient, AC part and DC part filters [1], [2]. AC/DC converter can be either bidirectional or can be separated on battery charger/discharger, as well as AC/DC part can be replaced with two-stage interface converter: DC/DC conversion stage and DC/AC conversion stage (inverter stage). Also, there are division between "standard topologies" i.e. single level topologies (e.g. three phase bridge, dual-buck half-bridge AC/DC converter in single and three phase configuration, and speaking about DC/DC converters: bidirectional Cúk converter, step up DC/DC converters – bidirectional half-bridge, double bidirectional half bridge etc.), and multilevel topologies: multilevel converter with independent voltage sources, diode clamped (also known as neutral point clamped) multilevel converter and multilevel converter with flying capacitors. It can be said, that multilevel converters in this implementation can have applications – multilevel converters can be either as bidirectional converter for charging and discharging battery, or can also be AC/DC part if it is two-stage implementation.

Another example of use of power electronic converters can be the use of electrical drives in medical equipment. According to World Health Organization World report of disability approximately 15% of world population live with some sort of disability of whom approximately 200 million suffer from significant difficulties in functioning [3]. Taking into account the ageing of population and increasing number of chronic diseases it is awaited, that these numbers will increase in the course of time. One of the most important questions is integration of disabled people into social and economic life. It can be done in a variety of ways, for example, by providing disabled people with new technologically advanced and innovative devices. As an example of such device can be smart wheelchairs. The concept of such wheelchair is described in [4]–[6].

Speaking about smart wheelchairs, one of the most important parts of the smart wheelchair is electrical drive, as electrical drive system is one of the main electrical energy consumers The electrical drive of such wheelchair consists of low-speed motor and battery and electrical motor interface converter. The use of high-speed electrical machine is not effective as it is needed to use mechanical gearbox to reduce speed. If gearbox is used, then it is impossible to implement recuperation of energy when wheelchair is slowing down during movement. The design of low-speed permanent magnet synchronous machine with segmented stator is described in [7]–[10]. Low-speed direct drive gives the ability to implement the recuperation, which increases the efficiency of the drive. Segmented stator gives the ability to increase or decrease number of stator segments, thus increasing or decreasing the power of electrical machine. Taking into account, that one of the functions of the designed wheelchair is assessment function, by increasing or decreasing the number of stator segments changes the level of assessment of powered wheelchair.

In order to control electrical machine power electronic driver should be used. Speaking about available in the market powered wheelchairs, they mostly have either DC electrical machine with gearbox and as power electronic driver they have transistor H-bridge, or they have synchronous or asynchronous electrical machine, in most cases also with gearbox and as power electronic driver they have three phase single level voltage source inverter (three phase transistor bridge). Three phase single level voltage source inverter is cheaper solution to

control three phase electrical machine, because of lower switch count.

However, there are also some disadvantages of three phase single level voltage fed inverter. The main disadvantage of this topology are power losses of transistors, as it is needed to use PWM method to control switches. It is known, that main losses of MOSFET or IGBT transistor are during commutation (i.e. during turning on or turning off the transistor). This can be critical, when converter is placed in closed space where there is not possible to provide proper ventilation or cooling of converter or if space, where converter should be placed is so tiny, that there is not possible to use heatsinks to reduce temperature of cases of transistors.

One of the solutions of this problem is usage of the multilevel converters without PWM technique. In this case, output voltage is stepped waveform, however with increase of level count output voltage is closer to sinewave. When PWM is not used to form output voltage, total power losses of switches of the converter are less, as switching losses are minimal and main source of losses are conduction losses.

Current paper focuses on defining optimal switching times of levels of modular multilevel converter with independent voltage sources and evaluation calculated switching times using MATLAB Simulink models.

II. Modular Multilevel Inverter with Independent Voltage Sources

Modular multilevel inverter with independent voltage sources (also known as cascaded H-bridges converter with separate DC sources) consists of series of transistor H-bridge converters [11]. Output waveform is generated from independent voltage sources, that are connected to H-bridges as input voltage sources by switching different combinations of switches in H-bridges. On Figure 1 one phase cascade for m-level MMC with independent voltage sources is shown. Each transistor H-bridge can generate three output voltages: $+V_g$ (switches Q1 and Q4 are turned on), 0V (switches Q1 and Q2 or Q3 and Q4 are turned on) and $-V_g$ (switches Q2 and Q3 are turned on). In case of using PWM technique, it is possible to receive smoother mean voltage values, however, there will be higher commutation losses of switches. If PWM is not used, output voltage of modular multilevel inverter is "squarer", however, the main source of losses are conduction losses. The number of voltage levels in modular multilevel inverter with independent voltage sources with m levels is defined as m=2s+1 (s positive voltage levels + s negative voltage levels and 0V).

The output phase voltage waveform for such cascade (by implementing Fourier transform) with s steps can be described as [11], [12]:

$$V(\omega t) = \frac{4V_g}{\pi} \sum_n \left[\cos(n\theta_1) + \cos(n\theta_2) + \ldots + \cos(n\theta_s)\right] \cdot \cdot \frac{\sin(n\omega t)}{n}, \text{ where } n = 1, 3, 5, 7, \ldots \quad (1)$$

θ_1, θ_2, …, θ_s in (1) are conducting angles, that can be chosen in such way, that total harmonic distortion (THD) of the voltage waveform is minimal.

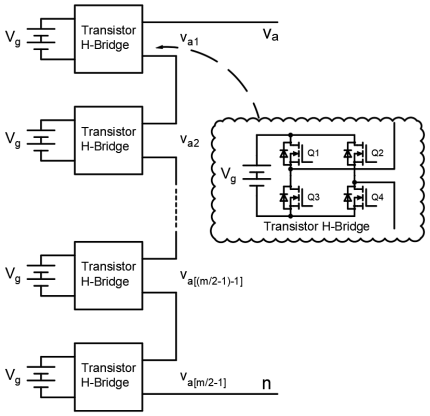

Fig. 1. One phase cascade for m-level MMC with independent voltage sources

III. Calculation of Level Conduction Times

As it follows from above mentioned, conducting angles (or conducting times) can be chosen in such a way that THD of the output waveform is as small, as possible. If sinewave with phase angle φ equal to 0 radians, amplitude is equal to 1V and frequency $f=1Hz$ is examined as reference signal for three level modular multilevel inverter, and instead of radians on x-axis of a plot time in seconds is taken (shown at Figure 2), then instead of conducting angle θ there is conducting time t_{sw}. Taking into account, that sinewave is symmetrical, then only one quarter part of the sinewave should be examined.

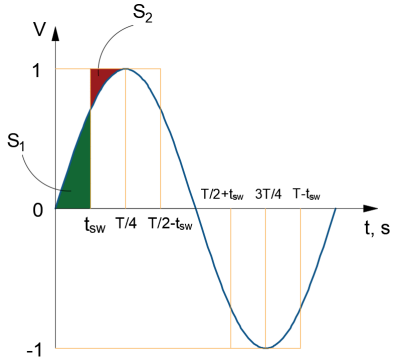

Fig. 2. Reference sinewave for 3-level modular multilevel inverter

As it is shown at Figure 2, during time period from 0 to T/4 there is one commutation time (or level switching time), in Figure 2 it is denominated as t_{sw}. If a line $t=t_{sw}$ is drawn, then there are two areas: S_1 and S_2, that show the displacement of generated output voltage by 3-level multilevel inverter with independent sources from reference sinewave. Areas S_1 and S_2 can be calculated by equations (2) and (3):

$$S_1 = \iint_{S_1} dtdV = \int_0^{t_x} dt \int_0^{\sin(\omega t)} dV \quad (2)$$

$$S_2 = \iint_{S_2} dtdV = \int_{t_x}^{T/4} dt \int_{\sin(\omega t)}^{1} dV \quad (3)$$

Borders of the area S_1 are $V = 0$ and $V = \sin(\omega t)$ by y-axis, and $t = 0$ and $t = T/4$ by x-axis. The borders of the area S_2 are $V = \sin(\omega t)$ and $V = 1$ by y-axis and $t = t_x$ and $t = 1$ by x-axis. In order to simplify calculations in this case $V = \sin(\omega t)$ can be replaced by $V = \sin(6.28t)$, because frequency of the sinewave is *1Hz* and therefore angular frequency ω is roughly equal to 6.28.

In order to have minimal THD, the sum of areas $S_1 + S_2$ should be minimal, and the only parameter, that can be changed in this case to make changes in S_1 and S_2 is the switching time.

The same principles of calculation are applicable when the level count is different (5, 7, 9, 11 etc.), the only thing that changes – the borders of y-axis. It is convenient to use reference sinewave with amplitude 2 for 5 level MMC, with amplitude 3 for 7 level MMC etc. At Figure 3 the reference signal for 5-level modular multilevel inverter is shown.

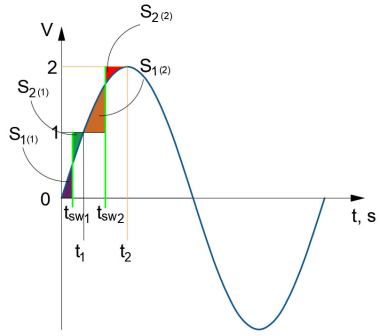

Fig. 3. Reference sinewave for 5-level modular multilevel inverter

IV. Evaluation

The initial evaluation was made with the help of MATLAB-Simulink models. 7 different cases were studied, so 7 models were created. Since the content of this evaluation is the investigation, whether it is needed to calculate optimal switching times or not, the models were created quite ideal, the load was chosen in such way, that the output current is 3A.

Two cases were studied: in the first one levels of modular multilevel converters were switched on and off using proposed calculation algorithm, in the second one, switching times are chosen simply by dividing the period of time when switching time has to be found by 2 (like the middle point between t_n and t_{n+1}).

For all converter models the comparison was made only by one parameter – total harmonic distortion (THD) of the one phase voltage.

At Figures 4-6 three examples of created models are shown (3-level MMC, 7-level MMC and 11-level MMC).

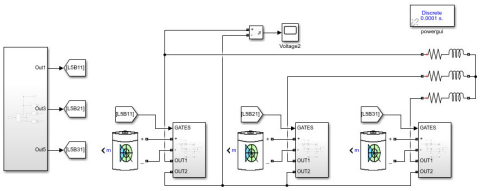

Fig. 4. Simulink model for 3-level modular multilevel converter

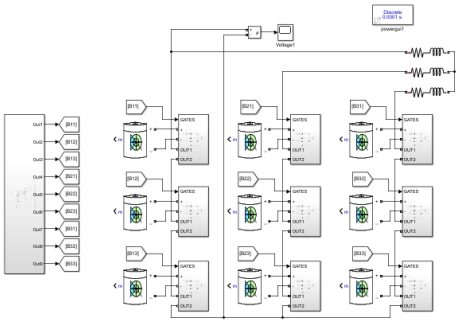

Fig. 5. Simulink model for 7-level modular multilevel converter

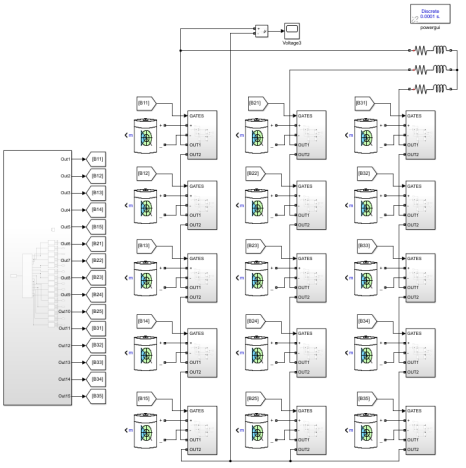

Fig. 6. Simulink model for 11-level modular multilevel converter

V. Results and Discussion

All 7 models were simulated for only one cycle, and only one parameter was taken for comparison – THD of the phase voltage of one phase. After simulation of both evaluated cases, THD of output signals was calculated. The results are shown at Table 1.

TABLE I. Comparison between optimal switching times and case when switching times were taken in the middle of the boserved period.

	$S_1+S_2\rightarrow$min, THD, %	Midpoint between t_n and t_{n+1}, THD, %	ΔTHD, %
3 levels	31.11	49.17	18.06
5 levels	17.61	23.65	6.04
7 levels	12.29	14.74	2.45
9 levels	9.76	11.02	1.26
11 levels	7.84	9.47	1.63
13 levels	7.02	8.27	1.25
15 levels	6.59	7.28	0.69

As it is shown from Table 1, it is needed to calculate optimal switching times, as in this case the THD of output voltage is smaller in all cases. It is also shown, that the smaller the level count is, the larger is the difference of THD between observed two cases.

VI. Conclusions

The obtained results show, that the less levels are in converter, the larger is difference between two level conducting time calculation approaches.

Case, when time when minimal sum of S1 and S2 is searched gives better results – so, for better performance of the modular multilevel converter with independent voltage sources it is needed to make more sophisticated calculations.

Further works include more sophisticated research of modular multilevel inverter with independent sources in terms of battery balancing and creation of control algorithm when battery balancing is implemented.

Acknowledgment

This publication was supported from Baltic Research Program funded by the European Economic Area and Norway 2014-2021 financial mechanisms within the contract EMP474 “Optimised Residential Battery Energy Storage Systems (ORBES)” of the first (Estonian) call of this program and was supported by Riga Technical University's Doctoral Grant programme.

References

[1] M. Stecca, L. Ramirez Elizondo, T. Batista Soeiro, P. Bauer, and P. Palensky, “A Comprehensive Review of the Integration of Battery Energy Storage Systems into Distribution Networks,” *IEEE Open J. Ind. Electron. Soc.*, pp. 1–1, Mar. 2020.

[2] V. Fernão Pires, E. Romero-Cadaval, D. Vinnikov, I. Roasto, and J. F. Martins, “Power converter interfaces for electrochemical energy storage systems - A review,” *Energy Convers. Manag.*, vol. 86, pp. 453–475, Oct. 2014.

[3] “W.H.O., World Report on Disability, 1st edition. World Health Organization, 2011, p. 350.”

[4] M. Vorobyov and I. Galkin, “Concept of cost-effective power-assisted wheelchair: Human-in-the-loop subsystem,” in *Proceedings of the 5th IEEE Workshop on Advances in Information, Electronic and Electrical Engineering, AIEEE 2017*, 2017, vol. 2018-January, pp. 1–5.

[5] K. Vitols and A. Podgornovs, “Concept of cost-effective power-assist wheelchair’s electrical subsystem,” in *Proceedings of the 5th IEEE Workshop on Advances in Information, Electronic and Electrical Engineering, AIEEE 2017*, 2017, vol. 2018-January, pp. 1–4.

[6] I. Galkin, A. Podgornovs, A. Blinov, K. Vitols, M. Vorobyov, and R. Kosenko, “Consideretions on Cost effective power assisted wheelchair subsystems,” *Electr. Control Commun. Eng.*, vol. 14, no. 1, pp. 71–80, 2018.

[7] R. Geidarovs, A. Podgornovs, and I. Galkin, “Simulation and Initial Evaluation of Modular Motor-Generator for Cost-Effective Power-Assist Wheelchair,” in *2018 IEEE 59th International Scientific Conference on Power and Electrical Engineering of Riga Technical University (RTUCON)*, 2018, pp. 1–5.

[8] A. Podgornovs and I. Galkin, “Evaluation of Configurations of Modular Motor for Power-Assist Wheelchair,” in *2019 26th International Workshop on Electric Drives: Improvement in Efficiency of Electric Drives, IWED 2019 - Proceedings*, 2019.

[9] A. Podgornovs, R. Geidarovs, and I. Galkin, “Considerations on Selection of Modular Electric Drive for Power-Assist Wheelchair,” in *2019 IEEE 60th Annual International Scientific Conference on Power and Electrical Engineering of Riga Technical University, RTUCON 2019 - Proceedings*, 2019.

[10] I. Galkin, A. Podgornovs, and R. Geidarovs, “Data Evaluation of Novel Modular Wheelchair Motor,” in *2020 27th International Workshop on Electric Drives: MPEI Department of Electric Drives 90th Anniversary, IWED 2020 - Proceedings*, 2020.

[11] L. M. Tolbert, F. Z. Peng, and T. G. Habetler, “Multilevel converters for large electric drives,” *IEEE Trans. Ind. Appl.*, vol. 35, no. 1, pp. 36–44, 1999.

[12] S. Khomfoi and L. M. Tolbert, “Multilevel Power Converters,” in *Power Electronics Handbook*, 2nd ed., Elsevier Inc., 2006, pp. 451–482.

Publication X

Tetervenoks, O.; Galkin, I.; **Bubovich, A.** Considerations on Practical Implementation of Current Source Mode Single-Inductor Multiple-Output LED Driver. Electronics 2024, 13, 54. https://doi.org/10.3390/electronics13010054.

electronics

IMPACT FACTOR 2.6

CITESCORE 5.3

Article

Considerations on Practical Implementation of Current Source Mode Single-Inductor Multiple-Output LED Driver

Olegs Tetervenoks, Ilya Galkin and Alexander Bubovich

Special Issue

Power Electronics Innovations for New Lighting Power Quality Challenges

Edited by

Prof. Dr. Antonio Moreno-Munoz, Dr. Aurora Gil-de-Castro, Dr. Paula Lamo and Dr. F. Javier Diaz

MDPI

https://doi.org/10.3390/electronics13010054

electronics

MDPI

Article

Considerations on Practical Implementation of Current Source Mode Single-Inductor Multiple-Output LED Driver

Olegs Tetervenoks *, Ilya Galkin and Alexander Bubovich

Institute of Industrial Electronics and Electrical Engineering, Riga Technical University, LV-1048 Riga, Latvia; gia@eef.rtu.lv (I.G.); aleksandrs.bubovics@rtu.lv (A.B.)
* Correspondence: olegs.tetervenoks@rtu.lv

Abstract: There are many possible LED lighting applications where separate regulation of the LED current (luminous flux) of individual LED strings would be desirable—specialized variable correlated color temperature lights for ambient lighting, decorative lighting, surgical lights, horticultural lights, etc. Separate regulation of the current or light flux of individual LED strings is associated with a known problem: the necessity of using a controllable LED driver for each string, which increases the total component count, overall system complexity and costs. One of the possible solutions—a current source mode single-inductor multiple-output LED driver—was discussed in previous different papers. However, the practical implementation of this solution was not discussed in detail. This article aims to correct this omission.

Keywords: current control; current supplies; LED drivers; LED module configurations; segmented LED light sources

Citation: Tetervenoks, O.; Galkin, I.; Bubovich, A. Considerations on Practical Implementation of Current Source Mode Single-Inductor Multiple-Output LED Driver. *Electronics* **2024**, *13*, 54. https://doi.org/10.3390/electronics13010054

Academic Editors: Aurora Gil-de-Castro, Antonio Moreno-Munoz, Paula Lamo and F. Javier Diaz

Received: 23 November 2023
Revised: 15 December 2023
Accepted: 19 December 2023
Published: 21 December 2023

1. Introduction

The idea of a segmented LED light source (SLLS) and an appropriate LED driver for the color/tone regulated LED lamp considered in the scope of this work is an adaptable light source delivering necessary illuminance to the desired area of the illuminated surface. This LED module is formed of an SLLS with independently dimmable/switchable high-power LEDs on its separate branches. Independent driving of this amount of high-power LEDs is expensive and complicated. Therefore, a special multiple-channel LED driving approach (single-inductor multiple-output (SIMO) current source mode (CSM) LED driver) has been chosen to overcome the shortcomings mentioned above. The same multiple-output driving approach can be useful in many other LED applications such as horticultural lighting, controllable RGB ambient lighting, adjustable correlated color temperature (CCT) applications, matrix automotive lighting, etc. The approach itself can be considered as a multilevel current and light regulation method with fluent control between levels. The current regulation in the given application is not the primary goal (the primary goal is light regulation) and it is not explicit. However, having an isolating and parallelizing current commutating matrix and combining it with a set of simplified uncontrolled current sources with one controlled current source, it becomes possible to achieve more straightforward and explicit current regulation that widens the range of potential applications. For instance, it enables the use of a similar approach in battery applications—battery energy storage systems and chargers for larger or smaller all-electric vehicles, for example, personal mobility vehicles like wheelchairs.

The main idea of an LED driver for the SLLS considered in the scope of this paper is derived from the SIMO CSM driver which has been described most accurately in [1]. The authors of [1] describe the SIMO CSM driver as a multiple-output converter with current delivery functions suitable for current consumers such as LEDs and as an approach to simplify independent output controls in comparison with traditional voltage-source-mode

(VSM) converters. These statements are validated by experimental results of the CSM single-inductor dual-output (SIDO) converter example. They also mention the necessity of using a current generator (constant current source) stage at the input of SIMO CSM as a drawback, as the most commonly used power supplies are voltage sources.

A similar idea of current source mode regulators has also been studied by the authors of articles [2–5] several years ago, as well as by other authors quite recently in [6–10]. In [1], as an advantage of the SIMO CSM driver, the simultaneous voltage step-up and step-down functions for multiple-output applications are mentioned. However, the simulations in [2] show that the conditions for energy transfer exist only if the sum of the voltages across all energy transferring (output) capacitors (C21 and C2k in Figure 1) does not exceed the input voltage when using CSM buck topology as an output stage for a SIMO converter.

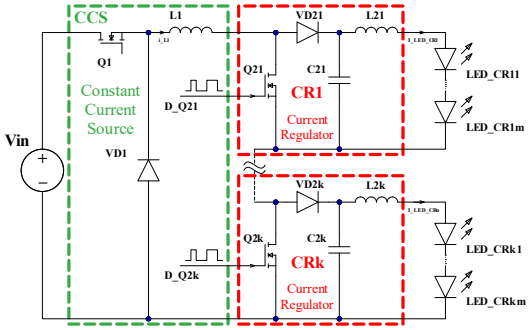

Figure 1. SIMO CSM driver idea [2].

In [3,4], the steady-state performance of three conventional VSM converters (buck, boost and buck–boost) in conjunction with LEDs has been compared with the performance of their corresponding CSM converters by several criteria (maximal dynamic gain, non-linearity and span of usable duty cycle); in addition, static losses were estimated for CSM converters, and it was found that CSM converters are suitable for LED driving when taking into account all this criteria.

In [5], a non-inverting buck–boost converter is considered as a combination of the constant current source (CSS) stage with the single current regulator (CR) stage, which in fact, is the initial configuration of SIMO CSM converters discussed above.

The essence of the idea stated by all these articles is that the current in each channel (individual LED or LED string) can be regulated in a simple way without the need for implementation of closed-loop regulation when using current regulators (CR). The single inductor L1 is used for constant current forming as a constant current source (CSS) for whole circuits, as shown in Figure 1. Only this part of the circuit (single-inductor-based constant current source) needs to be equipped with closed loop regulation (current feedback). The alternative method for independent current regulation is using independent LED drivers (constant current sources equipped with closed-loop regulation) for each channel, which complicates the control system and increases the number of components and the cost of a circuit.

Additionally, in [6,7], a different combinations of CSM buck and boost topology output stages in an SIDO converter are derived, analyzed and summarized by the article authors. In [8,9], the complete set of 16 possible configurations of SIMO CSM converters with multiple outputs is summarized.

In [10], an example of the practical usage of a three-output SIMO converter as an off-line converter is analyzed.

Usually, a configuration of multiple output converters with colored LEDs is considered for applications where precise color control during dimming is required and relatively low-power LEDs are used (in applications such as display backlighting) [10–15].

We are highlighting that our proposed driver configurations are the most appropriate for use with high-power and high-current LEDs in applications where absolutely precise color representation is not critical, but the most critical factor is a fluent transition between different color combinations. The applications where such a driver would be the most appropriate are white light with adjustable CCT (two colored LEDs) and horticultural lighting (two to four different color LEDs).

In contrast with the common inductorless representation of CR stages, we use inductors L21 ... L2k to show the inherent current source nature of the current regulator, as shown in (Figure 1).

SIMO CSM efficiency-related issues have been considered in several articles. Efficiency improvement using the adaptive current bus approach is proposed in [16], and restriction with low-frequency pulse width modulation (PWM) dimming is described (however, this restriction could be under discussion).

Another article on SIMO CSM efficiency issues is [17], with a proposal of soft switching. However, the analysis and discussion of the efficiency results are not presented in the paper.

The question is the impact on the efficiency of the whole driver of the presence of a series diode in the circuit of each individual channel of the driver, especially the in case of using high-power LEDs with high current rates (in the rate of several amperes). The proposed improvement of this issue is discussed further in one of the sections of the paper.

Also, there is lack of discussion on driving circuit implementation for SIMO CSM drivers in existing papers. As the number of controllable switches not referenced to the ground (negative node) or positive node is equal to $n - 1$, where n is the number of independent driver channels, isolated gate driving circuits or other special driving approaches may be required for proper MOSFET transistor driving. Thus, particular attention in this paper has been paid to this issue.

Another topic for discussion is CCS as the input for independent channel current regulators. For the initial investigation, a prototype with an MP24833 integrated circuit (IC)-based CCS was made, which is discussed in the following section. However, the different inductor current limiting/forming control strategies can be implemented using other ICs or control methods, which is another direction for further research.

So, the purpose of this paper is the practical validation of multiple output LED drivers with the simple control method described in the papers mentioned above. The prototype of the modified SIMO LED driver discussed in further sections of this paper has been prepared for the validation of the issues listed above. A detailed discussion is given in the following sections.

2. Implementation of Constant Current Source Based on Common Existing Solution

There are many possible LED driver implementation options. However, existing LED drivers mostly are based on switch mode power converters (SMPC) with closed current regulation circuits due to several advantages. The most valuable among them is high efficiency. Buck SMPC is the most commonly used candidate for these purposes. A common simplified buck SMPC-based constant current LED driver is shown in Figure 2. An LED driver can be considered as a matching element between a voltage source and an electrical current consumer.

Current feedback is formed by the current sensor I_CS, which measures the actual current *i_L* flowing through choke L1, adder SUM, which gives an error signal (the difference between the actual *i_L1* and set current *I_set*), and the control unit U11, which consists of a regulator and a pulse width modulator (PWM). According to the received error signal, it forms a control signal for transistor Q1. Since the current source without load theoretically can generate an infinitely high voltage on its nodes, the protection of the converter output is applied: an output voltage limiter based on comparator U12, which compares the voltage from the divider R1, R2 with the maximal set value.

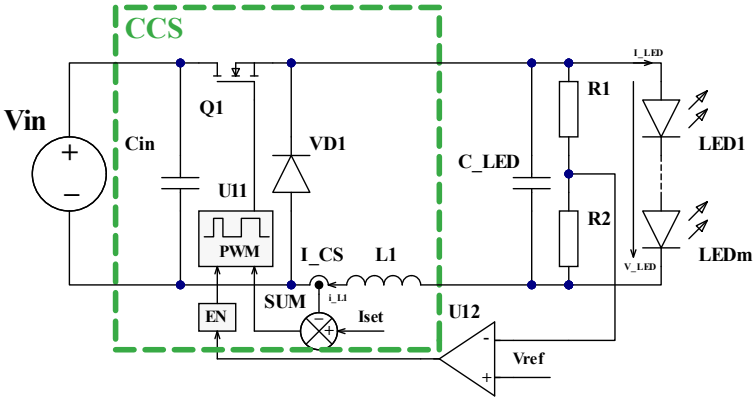

Figure 2. One of the considered options with non-isolated driving of independent channel CRs for practical validation.

Such a typical LED driver with minor modifications can serve a CSM source function. These minor modifications include the removal of the output capacitor C_LED and the output voltage limiter, which is formed by R1, R2 and U12 in Figure 2, or increasing the value of the voltage limiter to the required level, which must be equal to the voltage drop value across all series-connected LEDs in all channels with a small margin.

For experimental validation, a modified EV24833-A-N-00A buck/boost configurable development kit based on MPS MP24833 LED driver IC [18] was used in the scope of this work, as shown in Figure 3. On this development board, the changes mentioned above have been made, thus achieving the desired behavior of the CCS: the removal of capacitor C5 and adjustment of the voltage divider R8, R9.

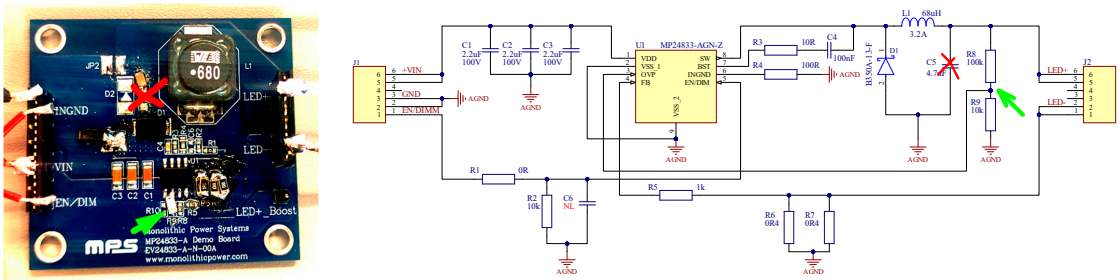

(**a**) (**b**)

Figure 3. EV24833-A-N-00A buck/boost configurable development board based on MPS MP24833 LED driver IC with modifications to perform in CCS mode: (**a**) picture with changes on the board; (**b**) electrical circuit schematic of evaluation kit board [18] with necessary changes; red cross—removed capacitor; green arrow—parts of voltage divider to be modified.

The approach considered in the scope of this paper (the modification of an existing LED driver to CCS and using it in combination with additional modified CRs stages) can be used for upgrading existing no-controllable LED lighting systems to adjustable light output systems with simplified control.

3. Discussion on the Efficiency of CSM SIMO LED Driver

It is evidently seen from the circuit shown in Figure 1 that the overall efficiency of the SIMO CSM driver is noticeably lower in comparison with the bare buck converter in

CCS mode as an additional CR conversion stage(s) is in use with its own controllable and uncontrollable switches and their power loss. The CCS stage current always flows through CR stages. To simplify the control system of the CR stage and the whole system (which is one of the main advantages of this configuration), uncontrolled diodes VD1 . . . VDk are used as top switches in CR stages. When the CR stage gives 100% light/current output, the whole current flows through this uncontrolled diode, causing high power loss, especially if there is a small number of connected LEDs in the regulated string.

There are ways for efficiency improvement, which are considered in the scope of this paper. One of them is the replacement of a high-side uncontrolled diode by a controllable transistor switch, which complicates the driving circuit. Another way is using CR stages in combination with parallel controlled switches, thus bypassing CR's diode. This approach also complicates control; however, it allows for the elimination of diode-associated power losses over part of the regulation range with higher output power and will be discussed in the following sections of this paper.

4. Implementation of Light Flux Regulators

To distinguish the previous discussed CR concept from the new modified CR stage with parallel controlled switches, we introduce the name "light flux regulator" (LR) for this whole combination as well as "current switch" (CS) for parallel controlled switches inside this regulator. The implementation of light flux regulators LR1 for each regulated channel is shown in Figure 4a.

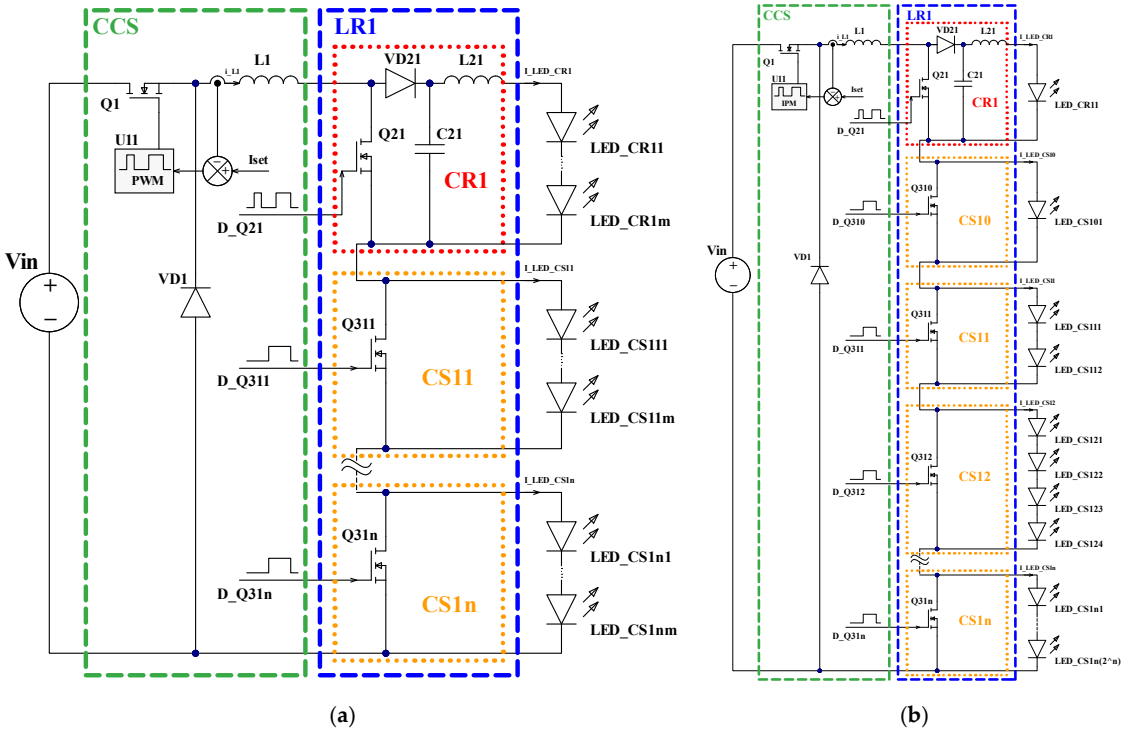

Figure 4. Implementation of light flux regulator LR in CSM SIMO LED driver: (**a**) using the same LED numbers in light flux regulator LRx and current switch CSxy branches; (**b**) using binary-weighted LED numbers in light flux regulator LRx and current switch CSxy branches.

Each LR1 is constructed as a combination (series connection) of single current regulator CR1 and a chosen number of current switches CS1y, which are controllable switches Q31y connected in parallel with light-emitting diodes LED1y1 . . . LED1yz, where y is the numbering index for current switches, while z is the numbering index for LEDs. Current regulator CR1 consists of capacitor C21 connected in parallel with LED11 . . . LED1z, they are connected in series with an uncontrolled switch—diode VD21 (which in general, can also be a controllable switch). As mentioned previously, in comparison with the original CR circuit from [1], we use inductors L21 . . . L2k to show the inherent current source nature of the current regulator as shown in Figure 1 and in [2]. Controllable power switch Q21 is connected in parallel with all these components. Q21 is controlled by a pulse width modulation PWM signal. The average current value *I_LED_CR1* of the CR1 branch of light diodes LED11 . . . LED1z depends on the value of the transistor Q21 control signal duty cycle *D_Q21* and the constant current value *I_L1*, and is equal to [3]:

$$I\_LED\_CR1 = I\_L1 \cdot (1 - D\_Q21), \quad (1)$$

but the current value *I_LED_CS1y* of the CS1y branch of LED1y1 . . . LED1yz is either 0 or *I_L1*, depending on the specified value of the control parameter and the corresponding transistor Q31y control signal duty cycle *D_Q31y*.

As discussed above, the main aim for CR's modification is efficiency improvement by modifying hardware parts as well as a light flux regulation control algorithm to bypass CR's high-side diode over part of the regulation range with higher output power.

A simplified calculation for CR stage diode power loss and the efficiency curves were built for the bare CR stage and for the LR stage. The comparison is shown in Figure 5.

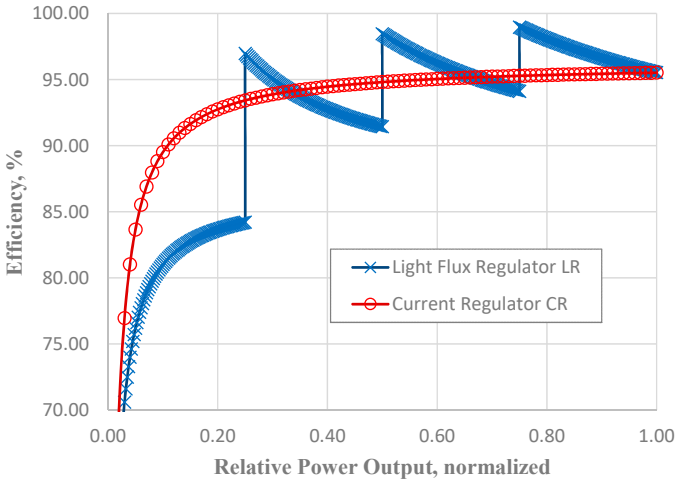

Figure 5. Theoretical estimation of efficiency of bare CR stage and LR stage when driving the same number of LEDs.

It is seen from these graphs that there is better efficiency of the LR stage at a higher output power and worse results in a low power range in comparison with the bare CR stage because only the CR part operates in LR at low light outputs. To achieve better efficiency of the lamp, the light output control strategy for LR can be constructed in such a way that the CR part is involved only in fluent transitions between different brightness states.

5. Binary-Weighted LED Number in Separate LED Light Source Branches

To optimize the number of controllable switches in LR, it is possible to choose binary-weighted LED numbers in the CSxy branches according to the principle:

$$m_{xy} = 2^y, \tag{2}$$

where x is the numbering index of LRs and CRs, y is the numbering index for CSs as mentioned previously, but m is the number of LEDs in the corresponding branch. Then, the last LED index in the CSxy branch is LED_CSxnm or LED_CSxn(2^n) (Figure 4b).

The light flux regulation algorithm as well as control signals of LR's controllable switches for LR with four CSs and binary-weighted numbers of LEDs in these branches are shown in Figure 6.

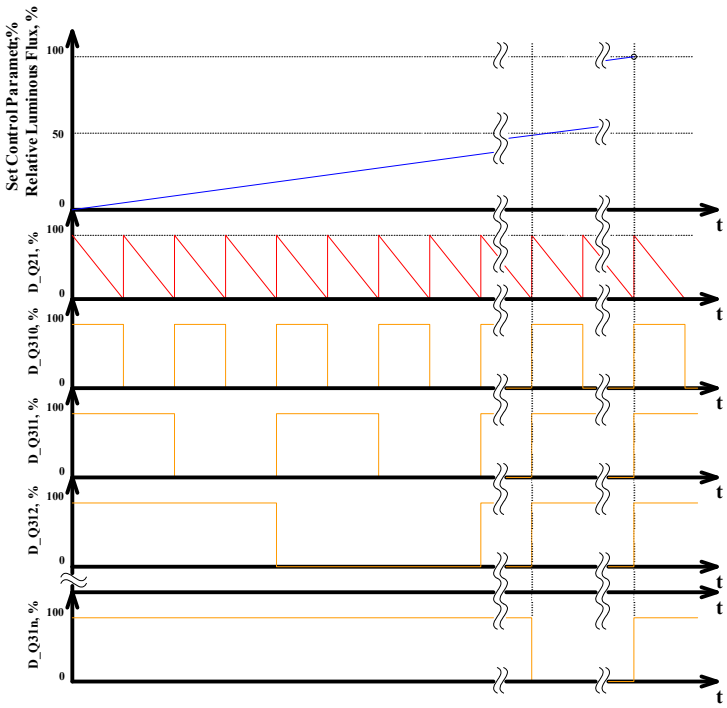

Figure 6. Control strategy of light flux regulator LRx with binary-weighted number of LEDs in CSxy branches. Colors are consistent with Figure 4a: blue—relative luminous flux of whole LRx; red—duty cycle of control signal for CRx stage transistor; orange—control signals for CSxy.

The total luminous flux produced by LEDs is approximately proportional to the given control parameter. Control signals of power switches Q21, Q310 . . . Q31n are formed in accordance with the specified value of the control parameter. CR's power switch Q21 is driven by the signal *D_Q21*, the duty cycle of this signal varies within the range of 0 to 100%. The duty cycle of control signals *D_Q310* . . . *DQ31n* for power switches Q310 . . . Q31n are either 0% or 100%.

Configuration of the proposed SIMO driver for the general case is given in Figure 7. It consists of multiple LRx blocs for multi-channel regulation.

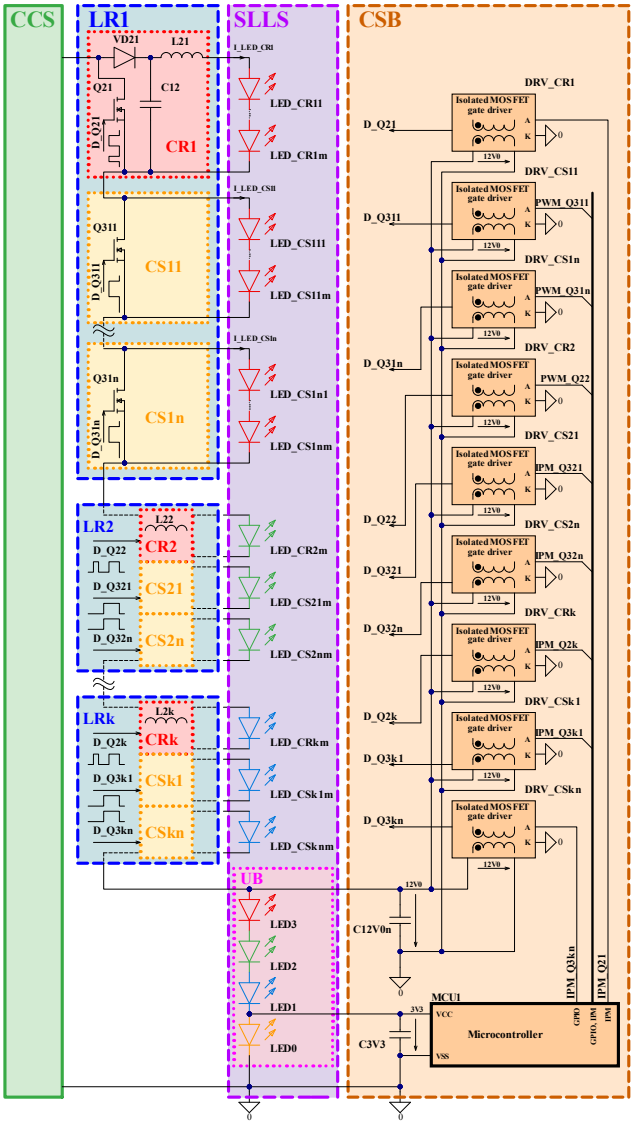

Figure 7. General case configuration of proposed SIMO driver and SLLS with the uncontrolled branch for voltage extraction for CSB.

6. Considerations on Control Circuit Implementation

The main topic of this article is the discussion of the practical implementation of the SIMO LED driver and possible solutions for existing non-controllable LED lamps, upgrading them to regulated light color lamps using this driver.

As discussed above, the standard LED driver with minor modifications can be reconfigured to CCS suitable for use as part of the SIMO driver. In this way, part of the existing non-controllable LED lamp can be used. The problem with the power supplies of existing non-controllable LED systems is an absence of low-voltage output suitable for the supply of control circuits of the proposed SIMO driver: single current source output is

available. One or several LEDs in a separate unregulated branch (UB) of the segmented LED light source (SLLS) can be used for the extraction of suitable voltage for the control system block (CSB) of the proposed SIMO driver from this current source (LED driver). The discussed principle is shown in Figure 7. Of course, this method leads to noticeable disadvantages: such a lamp will always produce a minimum luminous flux of a certain color light, specified by LEDs from the introduced UB of SLLS. However, the described approach of voltage extraction for the supply of control parts can be used in LED lighting applications, where this minimum output light drawback does not matter. This allows for the simplification of the lamp's overall structure and for cost optimization.

LEDs in the unregulated LED branch LED0 . . . LED3 of SLLS function as a voltage stabilizer for both the microcontroller MCU1 at 3V0 and the isolated MOSFET drivers DRV_CR1 . . . DRV_CRk, DRV_CS11 . . . DRV_CSkn of power switches Q21 . . . Q2k, Q311 . . . Q3kn at 12V0. For the optimization of transistor driving circuits, the UB of a segmented LED light source can be split and located at the CCS' both negative and positive nodes as well, and both type N-FET and type P-FET transistors can be used in this case.

7. Considerations on LED Physical Placement for Segmented Light Sources

It is intended that with this type of driver, bi-color or multi-color LEDs will be used to obtain the best color mixing results. However, for the lighting applications where this issue is not critical, separate colored LEDs also can be used. As the light source has separate controllable branches, the LEDs should be placed symmetrically against the SLLS center for the most even light distribution results, as shown in the sample in Figure 8 with the binary-weighted number of LEDs in separate branches (not all combinations are shown: 10 of 15 possible combinations). This segmented module was built as one color/channel module, but it is applicable as a sample of possible implementation.

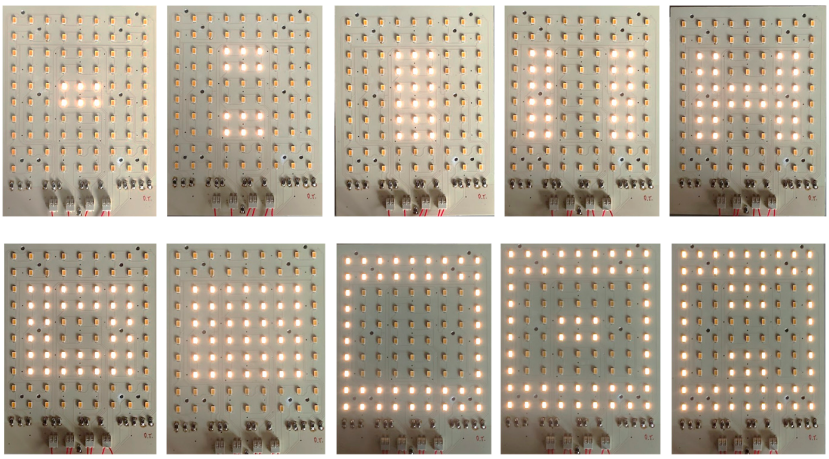

Figure 8. Example of symmetrical placement of LEDs in SLLS with binary-weighted number of LEDs in separate branches.

8. Experimental Validation

For experimental validation, the prototype of the proposed modified SIMO driver was built by combining CCS based on an MP24833 LED driver IC (Figure 3) and one LR stage. The LR for testing purposes was built on two separate stackable PCBs/boards, splitting the power part and control part (these PCBs/boards are shown in Figure 9).

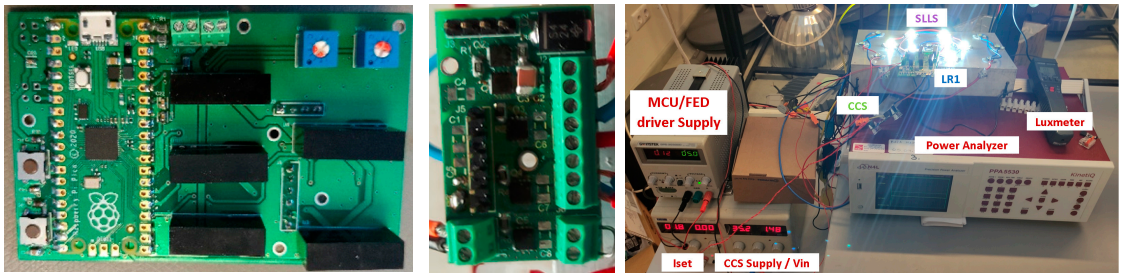

(**a**) (**b**) (**c**)

Figure 9. The prototype of the proposed SIMO driver based on LR: (**a**) control and FET driver board; (**b**) power part board; (**c**) testing setup.

The LR stage (power part, which is shown in Figure 9b) of the prototype is configured as the combination of one current regulator CR1 with four current switches, CS0 . . . CS3. For testing purposes, the most robust FET driving circuit configuration was selected for implementation in the prototype board: isolated gate drivers with an isolated supply for each driver.

As the control system, the core of the proposed LR RP2040 microcontroller was selected. However, it could be any other microcontroller with enough configurable GPIOs: for this prototype, one PWM output and four GPOIs. For testing purposes, two control parameter input methods were implemented: (1) by trimmer and MCU readings of its set value on ADC input and (2) by "increase"/"decrease" push-buttons. A board of the control parts of the prototype is shown in Figure 9a.

The testing setup for the experimental validation of the proposed LR is shown in Figure 9c. Summaries of the initial tests are given in Figures 10 and 11.

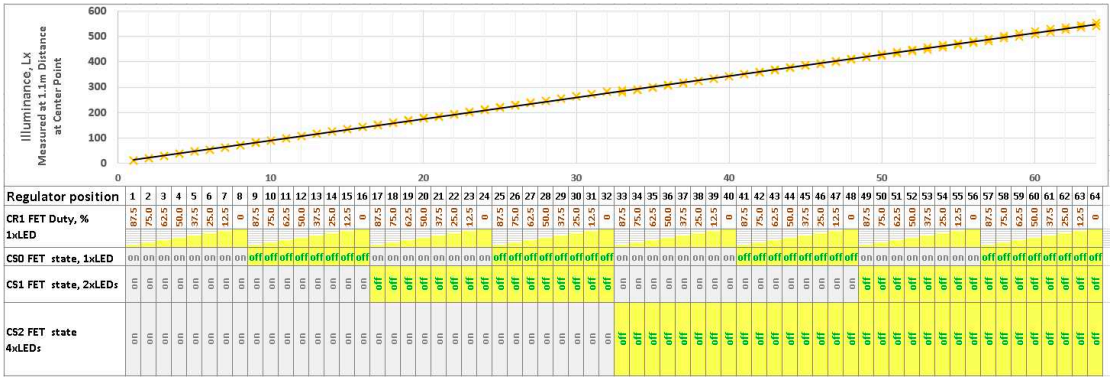

Figure 10. Experimental validation of single LR stage: correspondence of control signals to the illuminance at center point below LED module at 1.1 m distance.

The experimental validation of single LR stage luminous flux regulation is shown in Figure 10. The measurements were made with an indirect method using a luxmeter at the central point below the LED module. Correspondence of the control signals to the illuminance at the center point below the LED module at 1.1 m distance is shown here. The tests were conducted with the quite old (still in good condition), white, high-power LEDs available in the laboratory: Seoul Semiconductor W724C0 LEDs. The V–A and A–lm curves of a single LED of the mentioned type are given in [19]. The configuration of the module was made as shown in Figure 4b, except for the number of CS stages (three stages). The

placement of LEDs is close to each other, but not perfectly symmetrical. Thus, the deviation of the experimental points across a linear interpolation is seen in Figure 10, close to the transition points when switching to the next CS combination state.

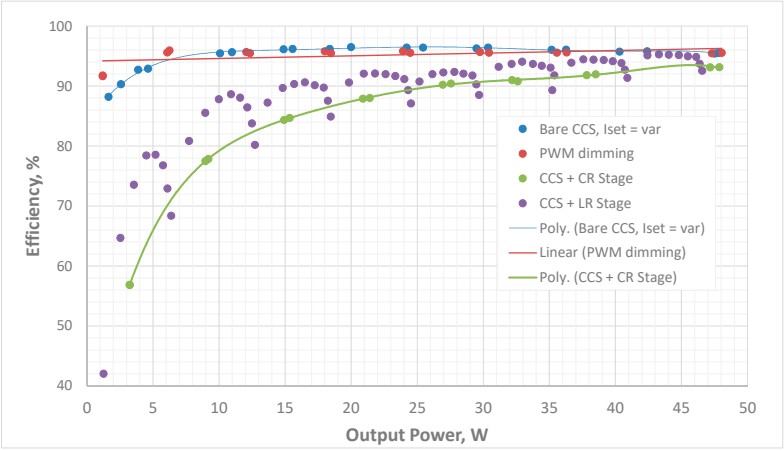

Figure 11. Comparison of the efficiency of different dimmable system configurations by the assessment of experimental data at similar conditions.

The assessment of the efficiency of the proposed system configuration is given in Figure 11. The tests for all dimming options were performed in similar conditions to the LED module mentioned above, with the maximum output power approximately 50 W using eight LEDs in total. Input voltage in all conducted experiments was the same, 35 V. The data obtained using Newtons4th Ltd. (Leicester, UK) PPA5530 precision power analyzer were used for this experimental efficiency validation. It is seen here that the efficiency of the bare CCS part is noticeably better in comparison with the combination of CCS+CR, which is the price for using such a kind of SIMO driver in high-power applications. However, as can be seen from Figure 11, some efficiency improvements can be achieved using the proposed configuration with light regulator stages.

9. Conclusions

The constant current mode SIMO LED driver is a good candidate for the implementation of a color regulation system for LED lamps partly based on existing, well-proven solutions. However, there are some issues with practical implementation: reduced efficiency in the current regulator stages and issues with the additional supply for the control part, as well as the necessity of using specially designed segmented LED light sources in combination with the SIMO driver. This article provides positively working solutions to all these issues described above.

The implementation of LR (Figures 4 and 7) is proposed for improving the efficiency of regulators with theoretical estimation, as shown in Figure 5 and confirmed by experiments (Figure 10).

As the solution for the control part supply issue, it is proposed to use an additional uncontrolled LED branch by implementing this branch in the segmented LED light source.

Also, a feature of this driver that the SLLS with symmetrically arranged binary-weighted LED branches used can be utilized in a lamp as a visual design element, as can be seen from Figure 8.

Author Contributions: Conceptualization, I.G., O.T. and A.B.; methodology, I.G. and O.T.; software, A.B.; validation, O.T., I.G. and A.B.; formal analysis, O.T. and A.B.; investigation, I.G., O.T. and A.B.; resources, O.T. and I.G.; data curation, O.T. and A.B.; writing—original draft preparation, O.T.; writing—review and editing, I.G.; visualization, A.B.; supervision, I.G.; project administration, I.G.; funding acquisition, I.G. All authors have read and agreed to the published version of the manuscript.

Funding: This work was supported in part by the European Regional Development Fund (ERDF) under contract 1.1.1.1/20/A/079 "Research and Development of Two-Phase Thermal Systems Installed in Lighting Equipment for its Functional Improvement" of its Latvian measure 1.1.1.1 "Industry-Driven Research". This work was supported in part by the European Regional Development Fund (ERDF) under contract Nr. 1.1.1.1/16/A/147 "Research and Development of Electrical, Information and Material Technologies for Low Speed Rehabilitation Vehicles for Disabled People" of its Latvian measure 1.1.1.1 "Industry-Driven Research".

Data Availability Statement: All the data presented in this study are summarized in this article.

Conflicts of Interest: The authors declare no conflict of interest.

References

1. Dong, Z.; Tse, C.K.; Hui, S.Y.R. Current-Source-Mode Single-Inductor Multiple-Output LED Driver with Single Closed-Loop Control Achieving Independent Dimming Function. *IEEE J. Emerg. Sel. Top. Power Electron.* **2018**, *6*, 1198–1209. [CrossRef]
2. Galkin, I.A. Simulation of Current Sourced Power Supply Providing Adjustable Currents for Multiple Loads. In Proceedings of the 2019 Electric Power Quality and Supply Reliability Conference (PQ) & 2019 Symposium on Electrical Engineering and Mechatronics (SEEM), Kärdla, Estonia, 12–14 June 2019; pp. 1–6. [CrossRef]
3. Galkin, I.; Tetervjonok, O.; Milashevski, I. Comparative study of steady-state performance of voltage and current fed dimmable LED drivers. In Proceedings of the 2013 International Conference-Workshop Compatibility and Power Electronics, Ljubljana, Slovenia, 5–7 June 2013; pp. 292–297. [CrossRef]
4. Galkin, I.; Tetervenoks, O.; Milashevski, I. Static losses and controllability of current fed dimmable LED drivers. In Proceedings of the 2013 15th European Conference on Power Electronics and Applications (EPE), Lille, France, 2–6 September 2013; pp. 1–10. [CrossRef]
5. Galkin, I.; Tetervenoks, O. Validation of direct current control in LED lamp with non-inverting buck-boost converter. In Proceedings of the IECON 2013—39th Annual Conference of the IEEE Industrial Electronics Society, Vienna, Austria, 10–13 November 2013; pp. 6021–6026. [CrossRef]
6. Dong, Z.; Li, X.L.; Tse, C.K.; Zhang, Z. Application of Current-Source-Mode Converters to Synthesis of Single-Input Dual-Output Regulators with No Cross Regulation. In Proceedings of the 2020 IEEE 9th International Power Electronics and Motion Control Conference (IPEMC2020-ECCE Asia), Nanjing, China, 29 November–2 December 2020; pp. 584–587. [CrossRef]
7. Dong, Z.; Li, X.L.; Tse, C.K.; Zhang, Z. Derivation of Single-Input Dual-Output Converters with Simple Control and No Cross Regulation. *IEEE Trans. Power Electron.* **2020**, *35*, 11930–11941. [CrossRef]
8. Li, X.L.; Dong, Z.; Tse, C.K. Complete Family of Two-Stage Single-Input Multioutput Configurations of Interconnected Power Converters. *IEEE Trans. Power Electron.* **2020**, *35*, 3713–3728. [CrossRef]
9. Li, X.L.; Tse, C.K. Derivation of Complete Family of Multi-Output Configurations Including Voltage-Source-Mode and Current-Source-Mode Converters. In Proceedings of the 2019 IEEE International Symposium on Circuits and Systems (ISCAS), Sapporo, Japan, 26–29 May 2019; pp. 1–5. [CrossRef]
10. Zu, A.; Luo, Q.; Huang, J.; He, Q.; Sun, P.; Du, X. Analysis and design of a multi-channel constant current LED driver based on DC current bus distributed power system structure. *IET Power Electron.* **2020**, *13*, 627–635. [CrossRef]
11. Choi, S.; Kim, T. Symmetric Current-Balancing Circuit for LED Backlight with Dimming. *IEEE Trans. Ind. Electron.* **2012**, *59*, 1698–1707. [CrossRef]
12. Chiu, C.-L.; Chen, K.-H. A high accuracy current-balanced control technique for LED backlight. In Proceedings of the 2008 IEEE Power Electronics Specialists Conference, Rhodes, Greece, 15–19 June 2008; pp. 4202–4206. [CrossRef]
13. Thomas, W.; Pforr, J. Power-transfer of isolated converter with integrated power sharing for LED-lighting system dependent on transformer coupling. In Proceedings of the 2010 IEEE Energy Conversion Congress and Exposition, Atlanta, GA, USA, 12–16 September 2010; pp. 449–456. [CrossRef]
14. Chen, H.; Zhang, Y.; Ma, D. A SIMO Parallel-String Driver IC for Dimmable LED Backlighting with Local Bus Voltage Optimization and Single Time-Shared Regulation Loop. *IEEE Trans. Power Electron.* **2012**, *27*, 452–462. [CrossRef]

15. Li, S.; Guo, Y.; Tan, S.-C.; Hui, S.Y. An Off-line Single-Inductor Multiple-Output LED Driver with High Dimming Precision and Full Dimming Range. *IEEE Trans. Power Electron.* **2017**, *32*, 4716–4727. [CrossRef]
16. Dong, Z.; Li, X.L.; Tse, C.K. Improved-efficiency quasi-two-stage current-source-mode SIMO LED driver. *IET Power Electron.* **2019**, *12*, 3286–3294. [CrossRef]
17. Suganthi, K.; Sundararaman, K.; Nityanarayanan, C.; Thamarai Selvan, M.S.S.; Sudhakar, K.B. A Single-Inductor Multi-Output Current-Mode LED Driver with Soft-Switching. In Proceedings of the 2022 First International Conference on Electrical, Electronics, Information and Communication Technologies (ICEEICT), Trichy, India, 16–18 February 2022; pp. 1–8. [CrossRef]
18. Monolithic Power Systems. MP24833-AGN-Z Datasheet. Available online: https://www.monolithicpower.com/en/documentview/productdocument/index/version/2/document_type/Datasheet/lang/en/sku/MP24833-AGN-Z/document_id/2070/ (accessed on 9 September 2023).
19. Seoul Semiconductors, W724C0 Datasheet. 2008. Available online: https://mm.digikey.com/Volume0/opasdata/d220001/medias/docus/647/W724C0.pdf (accessed on 13 December 2023).

Publication XI

Galkin, I.A.; Saltanovs, R.; **Bubovich, A.**; Blinov, A.; Peftitsis, D. Considerations on Combining Unfolding Inverters with Partial Power Regulators in Battery–Grid Interface Converters. Energies 2024, 17, 893. https://doi.org/10.3390/en17040893.

energies

IMPACT FACTOR 3.0

CITESCORE 6.2

Article

Considerations on Combining Unfolding Inverters with Partial Power Regulators in Battery–Grid Interface Converters

Ilya A. Galkin, Rodions Saltanovs, Alexander Bubovich, Andrei Blinov and Dimosthenis Peftitsis

Special Issue

Power Electronics and Energy Management for Battery Storage Systems 2023

Edited by

Dr. Andrei Blinov and Prof. Dr. Sheldon Williamson

MDPI

https://doi.org/10.3390/en17040893

energies

MDPI

Article

Considerations on Combining Unfolding Inverters with Partial Power Regulators in Battery–Grid Interface Converters

Ilya A. Galkin [1,*], Rodions Saltanovs [1], Alexander Bubovich [1], Andrei Blinov [2] and Dimosthenis Peftitsis [3]

[1] Faculty of Electrical and Environmental Engineering, Riga Technical University, LV-1048 Riga, Latvia
[2] Department of Electrical Power Engineering and Mechatronics, Tallinn University of Technology, 19086 Tallinn, Estonia
[3] Department of Electric Energy, Norwegian University of Science and Technology, 7034 Trondheim, Norway
* Correspondence: gia@eef.rtu.lv

Abstract: The application of electrochemical cells as a source unit of electrical energy is rapidly growing—used in electric vehicles and other electric mobility devices, as well as in energy supply systems—as energy storage, often together with renewable energy sources. The key element of such systems is the power electronic converter used for DC energy storage and AC grid interfacing. It should be bidirectional to charge and discharge the battery when it is necessary. Two-stage battery interface converters are the most common; their DC-DC stage controls the battery current and adjusts voltage, but the DC-AC stage (inverter or frontend) controls the current in the grid. The use of unfolding inverters in two-stage battery interfaces can have some advantages. In this case, the DC-DC converter produces half-sinewave pulsating voltages and currents, but the unfolding circuit changes the polarity of the voltages and currents and produces no switching losses. Another trend of modern power electronics is the principle of partial power processing. In this case, power electronic converters deal only with a part of the total power; therefore, losses in such converters are reduced. This paper considers combining unfolding frontends with partial power DC-DC converters that enable the further reduction in losses. In this paper, it is shown that such implementation of the partial power conversion principle in semi-DC-AC systems is really possible based on the real-time matching of the voltage of the partial-power DC-DC converter, battery voltage (which depends on its state of charge) and the rectified instantaneous voltage of the AC grid.

Keywords: battery energy storage systems; electric vehicles; battery chargers; AC-DC power converters; DC-AC power converters; inverters

Citation: Galkin, I.A.; Saltanovs, R.; Bubovich, A.; Blinov, A.; Peftitsis, D. Considerations on Combining Unfolding Inverters with Partial Power Regulators in Battery–Grid Interface Converters. *Energies* **2024**, *17*, 893. https://doi.org/10.3390/en17040893

Academic Editor: Tek Tjing Lie

Received: 12 December 2023
Revised: 5 February 2024
Accepted: 7 February 2024
Published: 14 February 2024

1. Introduction

Electrochemical cells are historically one of the most known and one of the most widespread devices for the storage of electrical energy [1,2]. This particularly refers to the rechargeable batteries that are the most suitable source of energy for portable electronic equipment, as well as a convenient source of energy for hand tools and household equipment. Nowadays, recent achievements in battery chemistry, in particular those based on Li-Ion technology, accelerate the improvement of the parameters of rechargeable batteries. Overview papers like [3] regularly report a higher specific energy (several hundred Wh/kg) and power (several kW/kg), operation time (several thousand cycles), charge–discharge efficiency (>95%), as well as the more affordable price of Li-Ion batteries. This brings the technology of rechargeable batteries to such application fields like transport (All-Electric Vehicles—EVs or Battery-Powered Electric Vehicles—BEVs) and energy supply (known as battery energy storage systems—BESSs), in particular, to supply systems with renewable energy sources [4]. At the same time, it must be noted that modern rechargeable batteries are not just mechanical combinations/connections of several electrochemical cells. They also often incorporate electronic circuits or battery management systems for cell balancing,

protection and diagnostics [5,6], and, sometimes, thermal management units that stabilize the temperature of these batteries in an intensive charge/discharge process improve their operation parameters even more [7].

The operation of modern batteries occurs in conjunction with dedicated electronic converters controlling the charge and discharge of the batteries. The overviews of BESS usually emphasize two kinds of converters integrated into BESS: isolated and non-isolated [8,9]. The isolated converters are distinguished from the non-isolated ones by the absence/presence of the full power transformer in the converter. The first group typically contains "safe" low-voltage batteries. At the same time, this definition of safety is rather vague. Reference [9] contains a brief analysis of the regulations applicable to BESSs. It has been concluded that these regulations define the constraints for various grid-tied electrical equipment but do not explicitly limit the voltage of batteries. For this reason, in some cases, BESS manufacturers refer to other standards that regard other equipment with batteries, for example, telecom centers [10] and personal mobility vehicles like wheelchairs [11,12]. It is quite typical that these standards separate the parts of the equipment accessible by ordinary users (batteries) from the parts of the equipment accessible only by qualified staff (chargers). While the chargers have quite high AC limitations (for example, 250VAC in [11]), more accessible batteries have much lower DC limitations; ref [10] defines the dangerous level at 60 V while [11] defines it at and 36 V (for lead-acid batteries), and [12] at 50 V (for Li-ion batteries). As a consequence, according to Section 3 of [9], the market-available BESSs typically include a "safe" 48–60 V battery or a battery linked to the ratified grid voltage (300–400 V) or supplied in two configurations with low or high-voltage battery.

The converters of the first type typically include a grid frequency or high-frequency-isolating transformer that galvanically separates the battery component of energy storage from its grid component. For the same safety reasons, the battery interface converters (chargers) of BEVs are also typically isolated. To the same extent, this refers to the converters allocated outside the BEVs—off-board chargers—[13] or those placed inside of them—on-board chargers [14]—as well as the chargers larger [13,14] or smaller [15,16] BEVs.

The converters of the second type, or non-isolated converters, can link to the grid's rather high-voltage batteries. On one hand, the BMS of such batteries is more complex, expensive and less reliable, but on the other hand, this eliminates the need for a full-power-isolating transformer and the corresponding losses. In addition, the same operation power is achieved at lower currents and, therefore, with lower conduction and switching losses. These converters and BESS, therefore, are potentially more energy efficient. Some BESSs available on the market are offered with low and high-voltage battery versions that prove the prospects of this combination of batteries and chargers [17].

When talking about BESS interface converters for high-voltage batteries, it is also necessary to outline their two main topologies: single- and two-stage. The single-stage converters link the floating voltage of the battery and the AC voltage of the grid through a monolithic power converter (grid frontend). They are typically extremely efficient for one operation point with a particular state of charge (SoC) of the battery but not so efficient if SoC is different. Introducing a pre-regulator compensates for the floating of battery voltage and stabilizes the DC voltage of the frontend at the level optimal for its operation. This makes the operation of the frontend more efficient for a wider range of SoC, but it also reduces the efficiency at the best operation point [8,9] due to the extra losses in the pre-regulator.

The final choice of the battery and its interface converter is made based on the trade-off between lower losses and the higher efficiency of BESS on one hand, but on the other, it must consider a safer low-voltage battery, a more simple and reliable battery management system, as well as the simpler installation and maintenance of the BESS.

This work is devoted to a loss reduction in BESSs. Usually, the loss reduction and higher efficiency of BESSs with non-isolated converters refer to two matters: (1) the battery of such a BESS has a higher voltage and, therefore, the interface converter and BESS, on the whole, operate at lower currents leading to lower conduction losses; (2) the absence of the

full-power isolating transformer excludes all the losses associated with this transformer. In addition to these two considerations, this research also utilizes two promising loss reduction techniques. One of them is partial power conversion, but the other one is the use of unfolding inverters. While separate studies on these techniques are frequent, their combination is not studied well. Quite rare reports are devoted to unidirectional coverers, mostly for photovoltaic applications (see Section 2 for details). This paper expands the study to bidirectional systems, namely, to BESSs. Combining these two techniques allows the use of a lower voltage battery without the use of the full-power isolation transformer that causes the above-mentioned trade-off. One part of this research is performed experimentally in order to prove the feasibility of the proposed BESS interface converter. The other part of this work treats a mathematical model of the converter with the goal of determining its losses and the link between its losses and partiality. In both cases, the main research method is data gathering and analysis.

2. Approaches to Loss Reduction

The two-stage interface converter for BESS, considered in this paper, is intended for high-voltage batteries, that allow it to operate with lower currents and, therefore, lower conduction losses. In addition, this converter logically combines and utilizes two trends in the design of power electronic converters, also facilitating loss reduction. The first feature is the use of partial power converters in DC systems which, together with a reduction in processed power, also reduces the losses. In turn, the second feature is related to the operation of the network frontend of the two-stage converters. An alternative to the traditional pulse mode operation of the frontend exists is, in this case, the grid–frequency direct commutation of the DC-link to the grid that requires semi-sinusoidal voltage in the DC-link but allows the almost pure elimination of the switching losses (such converters are known as unfolding inverters or unfolders). Let us consider these two trends in more detail.

In contrast to the full-power DC-DC converters that are subject to full input and output voltages, they conduct a full current and, therefore, process the full system power, and partial-power DC-DC converters (PPC) are connected between system inputs and outputs in such a way that the converter processes only the difference between input and output voltages and currents. For this reason, PPCs deal with only a part of the full system's power while its major part is transmitted from the input of the system to its output without any conversion [18,19].

PPC benefits include the following: (1) a lower converter switching current and voltage, which allows the selection of cheaper and more compact semiconductor switches (transistors and diodes); (2) lower converter losses (determined by lower-rated power) which significantly improves the total energy efficiency and facilitates cooling. The lower the voltage/current difference handled by a PPC, the more pronounced the benefits of the partial power conversion. PPCs are particularly convenient to compensate for the parameter floating of DC energy sources or storages, such as batteries or PVs. For example, voltage reduction in a battery together with its SoC at its discharge may be compensated by a PPC, the input of which is connected to the battery in parallel with its output in a series, thus forming the sum of the battery and PPC voltages. PPC then generates the difference between the maximum battery voltage (at SoC 100%) and its actual voltage. So, by definition, such PPC processes the mentioned difference that is lower than the full battery voltage. For a 100-cell Li-Ion battery, the maximal PPC voltage can conclude $+100 \times (4.2 - 2.5) = +170$ V (where 2.5 V is the cut-off voltage of the cell, but 4.2 V is the maximal open circuit voltage of the fully charged cell) while the full-scale converter deals with 420 V. In this example, the full power is 2.5 times higher than the partial processed power.

Unipolar PPCs can only add (or subtract) their voltage (current) to the base value and bipolar PPCs are capable of both adding and subtracting. The PPCs of the second kind can operate with twice as low voltage/current/power compared to single-polarity PPCs [20]. For example, in the previous battery example, bipolar PPC can operate with

$\pm 100 \times (4.2 - 2.5)/2 = \pm 85$ V while providing, at the same time, the complete compensation of the battery voltage drop at 170 V. In this case, the processed power is five times lower than the actual power.

Schematically, PPC can be a DC-DC converter of any isolated topology. The most versatile implementation of unipolar PPCs is typically based on a Double Active Bridge (DAB), but other schemes are also possible. For example, ref. [21] presents PPCs of flyback and full-bridge phase shift topologies.

Bipolar PPCs include bidirectional or four-quadrant switches at their secondary side. For example, ref. [22] presents a bipolar version of the full-bridge phase shift converter from [21], while [23] describes a PPC with a bipolar DAB. Other schemes utilize resonant chains for better commutation and lower losses; for example, a bipolar DAB with a resonant tank is reported in [24]. It must be noted that all the above-mentioned PPCs [20–24] are intended solely for use in DC-DC systems.

The second trend in the field of power electronic converters, which is utilized in the considered system, refers to the principles of synthesis of the AC voltage in two-stage DC/AC inverters. As has been mentioned, the first stage of such inverters is a DC/DC regulator, while the second stage is a network frontend (rectifier/inverter). These stages are connected through a DC-bus. Traditionally, both stages are pulse mode converters—the first compensates for changes in the battery, and the second forms a sine-form voltage and connects it to the grid. The alternative method of synthesis of the AC voltage/current assumes that the regulator not only compensates for the voltage changes in the battery but also forms a semi-(rectified) sinewave at its output. As a result, the DC-link voltage and current pulsate, while the frontend just unfolds these pulses to the grid with predetermined polarity and with a low network frequency, operating as a commutator or as diodes in a diode rectifier [25,26]. It is clear that the power losses in such a commutator (known as unfolding frontend or unfolder) are lower because they do not include the component of the losses associated with high-frequency switching. This principle of commutation of the pre-shaped semi-sinewave voltage is also applicable to three-phase systems [27,28].

When considering the two-stage battery interface inverters with a pulsating DC-bus, one can notice that, while the frontend produces lower losses, the regulator forms the voltage in the full range from zero to the amplitude of the network voltage that is hardly compatible with partial power principle. On the other hand, if the DC-bus is stabilized, then the regulator can process partial power and may have lower losses, but the frontend is a pulse mode circuit with additional switching losses. It is quite logical that certain attempts were made in order to combine the PPC principle with a pulsating DC-bus and unfolding frontend.

One of the earliest distinct attempts to achieve power partiality with unfolders is reported in [29,30]. The papers present a two-stage two-level voltage-sourced inverter for PVs that adds the variable voltage from the pulse mode circuit to the constant voltage of PV. These works aim to compensate for the voltage reduction over the PV matrix that leads to the operation of the inverter at limited power if the PV voltage is low. Being a unidirectional inverter, it is suitable only for PVs. In addition, the presented inverter is not a truly partial power converter but just operates at reduced parameters (a good explanation of this phenomenon can be found in [19]).

Paper [31] presents a two-stage interface converter for batteries with a mid-point, which combines a specific unipolar two-level inverter with an explicit unfolder. In this case, the converter transforms the constant voltage from one or another DC source (fractions of the battery) into a semi-sine voltage of the DC-bus that is applied to the grid by the unfolder. The inverter rater utilizes the principle of fractional power conversion when partial power is taken from a distinct fraction of the power source (that could lead to the non-even aging of the battery cells). The paper itself is more focused on control matters, particularly, on the problem of voltage zero crossing, but its loss analysis is very brief.

Paper [32] and patent [33] present a two-stage inverter, which combines the true PPC principle with a pulsating DC-bus and unfolding frontend. This work utilizes a series

input–parallel output (SIPO) PPC scheme and, like [29,30], is intended for PV interfacing. These documents provide a feasible study of SIPO PPC with the UF inverter and DC allocation of the current firming inductor. At the same time, they do not pay much attention to the study of the actual partiality and its influence on the losses and parameters of the semiconductor switches. In addition, the proposed technical solutions are not suitable for use with BESS due to their unidirectional nature.

The essence of this work follows from the mismatch of the above-discussed solutions [29–33] from considering the application or principle of the true partiality of power conversion. Its main contribution includes the development of a novel BESS power interface and corresponding control, as well as their evaluation from the point of view of energy efficiency and parameters of the switches. The first novelty, therefore, is a new power electronic converter for BESS that combines a bidirectional unfolder, bidirectional parallel input–series output (PISO) partial power converter and pulsating DC-link. An essential part of this novelty is the method of interfacing, which processes the floating voltage of the BESS battery, forms pulsating semi-sine voltage in the DC-link, and applies it to the AC-grid. The second novelty of this work is a simplified quick methodology of the loss evaluation of the proposed converter based on its actual real-time partiality ratio depending on operation conditions (SoC and grid phase). At last, this work briefly evaluates the positiveness of the proposed BESS interface from the point of view of the voltage and current stress on its switches.

3. Outlines of Proposed Two-Stage BESS Interface Converter

3.1. Structure of Converter

The most explicit configuration of BESS with the proposed two-stage converter is presented in Figure 1a. Apart from the battery and grid, it contains an unfolding grid frontend (UF—inverter, operating at grid's frequency), an isolated bidirectional PPC capable of generating bipolar voltage ($PPC_{chg,dis}$), as well as a "virtual" DC-bus (qDC) with semi-sinewave pulsating voltage. The voltage of the battery is approximately twice as low as the amplitude of the grid voltage. Due to this, the PPC is connected with the battery in series on the DC-bus side and in parallel on the battery side. This configuration (named in [32] as PPC Type II) is analyzed in the present work, in contrast to PPC Type I, which is mostly studied in [32]. Further, this series connection of the battery and PPC is attached in parallel to the UF inverter. This may be an ordinary single-phase H-bridge as in [25] or a three-phase circuit like in [28]. In turn, the PPC can be constructed as any isolated bipolar bidirectional circuit, including the circuits with resonant tanks; for example, a bidirectional DAB is presented in [34].

Another configuration of BESS with the PPC and UF inverter is shown in Figure 1b. It includes an isolated bidirectional unipolar PPC, a "pulsating" DC-bus (qDC+), and an additional unfolding inverter (UF+). The unipolar PPC with the additional inverter UF+ operates as the bipolar PPC of the previous configuration. This reduces number of the switches operating in the high-frequency mode and, therefore, the corresponding switching losses.

One more improvement in the initial BESS configuration assumes the splitting of the bidirectional PPC into two unidirectional PPCs. One of them operates only in the battery charging mode, while another one operates during battery discharge. This means the absence of bidirectional switches that reduce the number of semiconductor elements in each current loop and the corresponding conduction losses. This BESS's configuration is shown in Figure 1c.

Finally, the combining of the two above-mentioned improvements, i.e., the splitting of the bidirectional PPC into two unidirectional ones and the use of unipolar PPC with the extra unfolder instead of the bipolar PPC, provides the achievement of their benefits together. In addition, such configuration enables the fine-tuning of the design of these separated parts of the two-stage BESS interface converter.

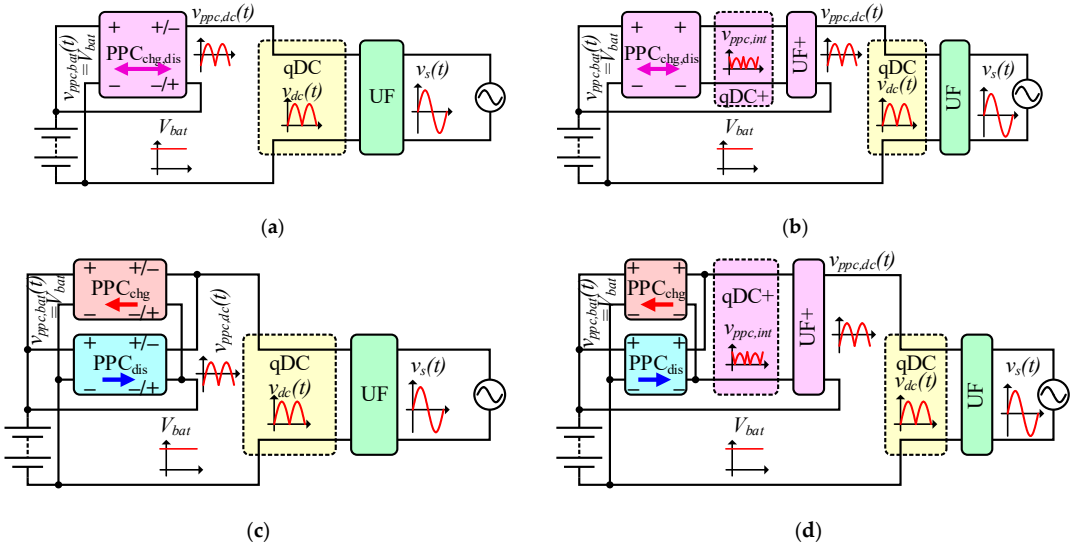

Figure 1. Structural diagrams of a two-stage converter with unfolding frontend and partial power DC/DC converter: (**a**) basic configuration, (**b**) configuration with additional unfolder, (**c**) configuration with two converters dedicated for battery charging and loading and (**d**) configuration with additional unfolder and two converters.

3.2. Topologies and Operation of Frontend

The frontend (Figure 2) is composed of a commutation matrix, switching at grid frequency, and an inductance coil that serves as a current-forming element and can be allocated at the DC or AC port of the frontend.

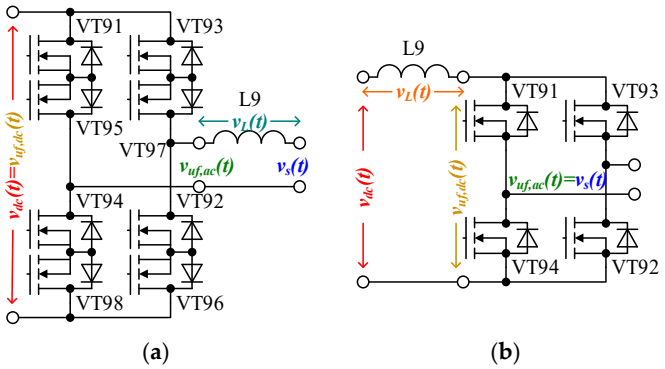

Figure 2. Generalized schematics of unfolding inverters (single phase, basic elements): (**a**) with inductor at AC port and (**b**) with inductor at DC port.

When the coil is allocated at the AC port (Figure 2a), its first contact is fixed at the grid, while the second one is connected through the commutation matrix to the DC-link. The coil then operates with alternating sine current and voltage. Since the voltage in the grid (Figure 3a—blue) must be in line with the grid current (Figure 3b) formed in the coil, the voltage of the coil (Figure 3a—magenta) must have a $\pm 90^\circ$ shift. Therefore, the voltage at the first end of the coil (at the AC port of the commutation matrix) must be slightly leading (for the battery loading mode, as in Figure 3a—green, or lagging, for battery charging mode)

and slightly higher, compared with the grid voltage on the second end of the coil. This, in turn, means that the commutation matrix must be a four-quadrant converter, capable of conducting a current in both directions at both polarities of the voltage. Due to the doubled number of transistors and more complicated control, this case is out of practical interest except for autonomous loads like the motors of larger or smaller vehicles. In a similar way, Figure 3c,d represents the battery charging mode, when the voltage at the AC port of the commutation matrix is lagging, but the current in the coil and grid has a 180° shift (is negative) compared to the grid voltage.

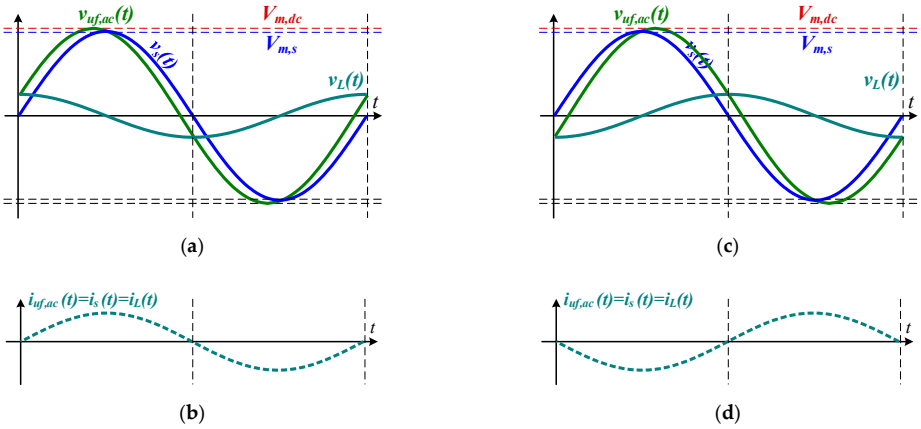

Figure 3. Operation of inductance in unfolding inverter with inductor at AC port: (**a**) voltages and (**b**) current (battery loading mode); (**c**) voltages and (**d**) current (battery charging mode).

The alternative allocation of the current limiting and forming inductance coil is at the DC port of the commutation matrix. Then, the first end of the coil is attached to the DC-link voltage ($v_{dc}(t)$ in Figure 4a), but at the second, the matrix forms a semi-sinusoidal grid voltage ($v_{dc,uf}(t)$ in Figure 4a). Then, the voltage over the coil is semi-sinusoidal with 90° (Figure 4a—orange) as well as its current (Figure 4b). With such a configuration, the polarity of the voltage at the AC port of the frontend always corresponds (must) to the polarity of the current. Therefore, the commutation matrix may be a common transistor H-bridge (Figure 2b). Similarly, Figure 4c,d represents the battery charging mode, when, within any halfwave, the voltage at the DC port of the grid commutation matrix is lagging, but the current in the coil and DC-link is negative.

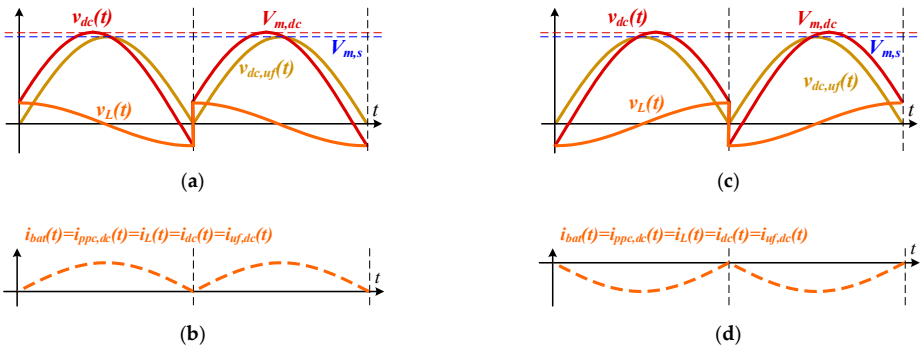

Figure 4. Operation of inductance in unfolding inverter with inductor at DC port: (**a**) voltages and (**b**) current (battery loading mode); (**c**) voltages and (**d**) current (battery charging mode).

In both cases, the DC-link must provide semi-sinewave voltage, composed of sine fragments with a certain small angle from γ to 180 + γ. (for the battery loading mode) and from 180 $-$ γ to $-\gamma$ (for the battery charging mode).

3.3. PPC Topology and Operation

The second part of the considered battery interface system is a DC-DC converter in the partial power processing scheme with one port connected to the battery in parallel and another in series. As has been mentioned above, it may be based on any isolated converter capable of generating bipolar voltage at the port connected to the battery in series. Two options have been considered within this work. The first one is a step-up/down PPC with bipolar DAB (BDAB) that includes a 2 $\times$ 2 matrix of bipolar switches described, for example, that presented in [23] and Figure 5a. Another one is a step-up/down PPC with a standard DAB followed by an extra transistor bridge, serving as a polarity toggler (one more unfolder), as shown in Figure 5b. Due to the twice lower switching losses in the bipolar part, the latter-mentioned configuration is taken as the base for further experimenting and analysis.

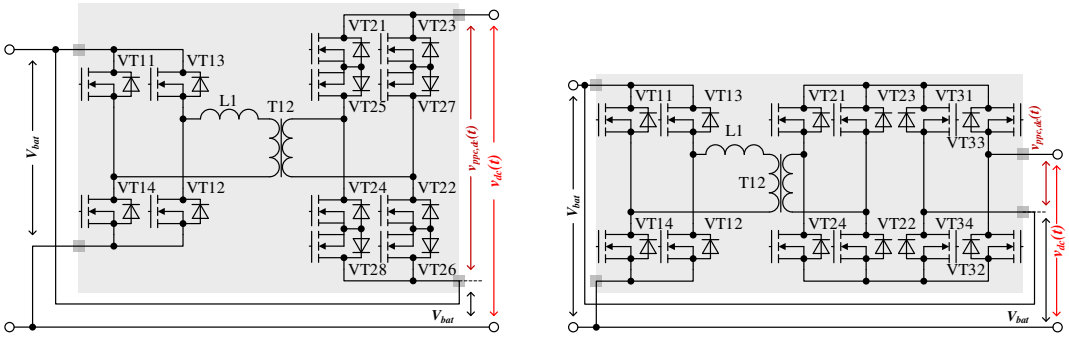

(**a**) (**b**)

Figure 5. Considered configurations of partial power converters: (**a**) with bipolar DAB; (**b**) with bipolar DAB and extra unfolder.

As follows from the previous section, the main function of the DC-DC stage is forming a semi-sine voltage in the DC-link of the converter.

For both configurations of the frontend, this voltage in the battery loading mode is composed of the semi-sine half-waves that are slightly leading compared with the rectified grid voltage, i.e., they start from some small phase γ and continue to the angle 180 + γ. Then, the resulting current is passed to the grid, but the battery of the BESS is loaded.

In contrast, in the battery charging mode, these semi-sinusoidal half-waves of voltage must be lagging compared to the rectified grid half-waves, i.e., they start from 180 $-$ γ and continue to $-\gamma$. Also, in this case, the operation of the DC-DC converter does not depend on the kind of the frontend.

The accurate forming of the current requires a slightly higher amplitude of these half-waves formed by the DC-DC converter. This amplitude can be found from the right triangle of the voltages, the legs of which are the grid voltage and the coil voltage, but the hypotenuse is the voltage of the DC-link. Then,

$$V_{m,dc} = \sqrt{V_{m,s}^2 + (2\pi f \cdot L_s \cdot I_{m,s})^2} \quad (1)$$

$$\text{and } \gamma = arctg(\frac{2\pi f \cdot L_s \cdot I_s}{V_{m,s}}) \quad (2)$$

Here, $V_{m,s}$—the amplitude of the grid voltage, $I_{m,s}$—the requested amplitude of the grid current, and L_s—the inductance of the coil.

The expected operational diagrams of the converter are given in Figure 6 (the BESS discharge or loading mode), Figure 7 (the BESS charge mode) and Figure 8 (the discharge mode to an autonomous load). The "pulsating" DC-link of the interface converter links the unfolding grid frontend VT9x with the series-connected battery and DC port of the PPC. This is why the semi-sinusoidal half-waves (brown curve in these figures), passed to the grid through the unfolding inverter VT9x, are formed as a sum of the battery voltage (black curve) and PPC voltage (red curve). On the other hand, the voltage of the PPC can be found as the difference between the desirable DC-link voltage and battery voltage, i.e., this voltage contains the same semi-sine half-waves with the negative offset, which is equal to the battery voltage. If the PPC operated as a buck converter, the discharged battery (SOC close to 0%) must provide 50% of the voltage span in the DC-link which, in a general case, can be found as follows:

$$V_{span,dc} = V_{\max,dc} - V_{\min,dc} = V_{m,s} + V_{m,s}\sin(\gamma) \quad (3)$$

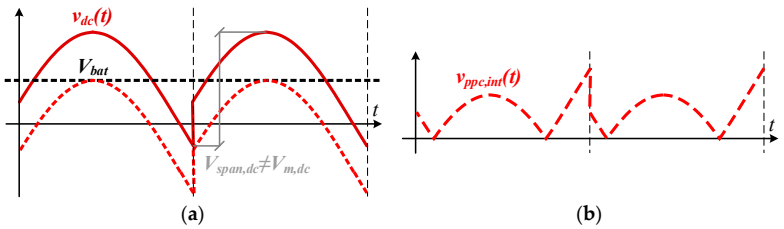

Figure 6. Voltage diagrams in BESS discharge mode: (**a**) voltages, typical for DC-link (black—battery voltage, red—PPC voltage at DC-link, brown—DC-link voltage); (**b**) internal voltage of PPC before extra unfolder.

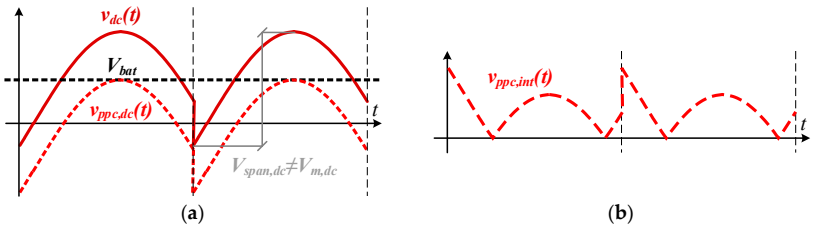

Figure 7. Voltage diagrams in BESS charge mode: (**a**) voltages typical for DC-link (black—battery voltage, red—PPC voltage at DC-link, brown—DC-link voltage); (**b**) internal voltage of PPC before extra unfolder.

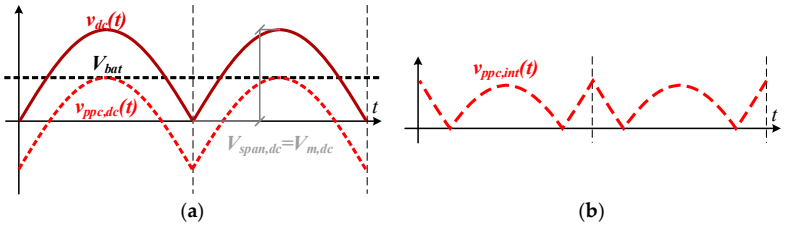

Figure 8. Voltage diagrams in BESS discharge mode for an autonomous ohmic load: (**a**) voltages, typical for DC-link (black—battery voltage, red—PPC voltage at DC-link, brown—DC-link voltage); (**b**) internal voltage of PPC before extra unfolder.

If the PPC is built as a DAB with an extra unfolder (Figure 5b), then, (1) firstly, the DAB generates the rectified form of this voltage (Figures 6b–8b) and then (2) the extra unfolder VT3x applies it to the DC port of the PPC with the required polarity. Meanwhile, the current through the PPC and the battery remains semi-sinusoidal, as shown in Figure 4b.

4. Experimental Validation of Converter

In order to verify the proposed concept, an experimental setup with a rated power of 250 W watts was assembled. Its schematic is given in Figure 9 and the experimental prototype is depicted in Figure 10. The main components of the prototype are listed in Table 1.

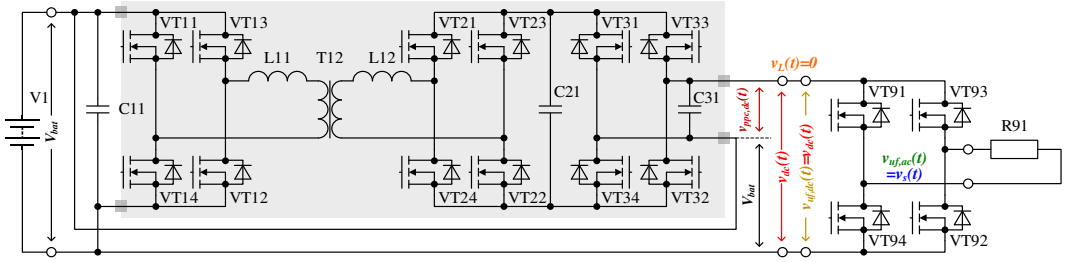

Figure 9. Schematic of the experimental setup with unfolding grid frontend, bipolar DAB and extra unfolder.

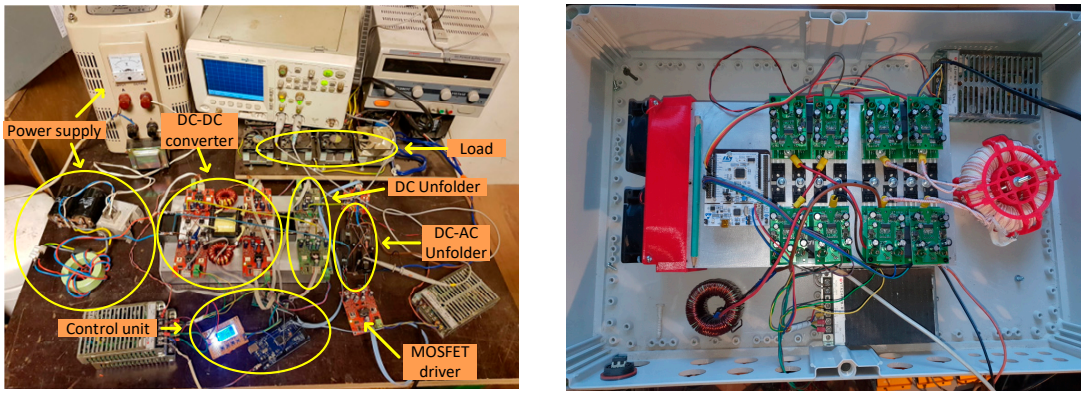

(**a**) (**b**)

Figure 10. Layout of the initial (**a**) and final (**b**) experimental setups.

The main switching elements (IPP60R040C7) are mounted on an aluminum heatsink with natural convection. The isolation transformer T12 of the partial power DC-DC converter (PPC) utilizes the turn ratio of the primary and secondary windings as 1:1. The primary and secondary windings of the transformer contain 25 turns of the CLI 120 × 0.1 face wire. Two E-shaped ferrite profiles ETD59 made of 3C94 with permeability μ = 2300 were used as the transformer core. Chokes L1 and L2 (the split inductor of the DAB) were wound on powder iron rings with the same CLI 120 × 0.1 face wire and had an inductance of 60 μH. At the input, the output and in the middle of the PPC 30 μF film capacitors are located. MOSFET drivers based on the ACPL-333J microcircuit provide the opening and closing of power transistors using a digital signal from the microcontroller through an optocoupler. The drivers have current protection. The control unit of the converter is based on ATmega2560 MCU, which has been selected due to its 12-channel, 16-bit PWM module. A power supply was applied as a battery for the quick imitation of different SOCs. The

load of the converter is an autonomous AC load, represented by a 210 Ω resistor that results in 250 W of the output power generated at 230 VAC. The setup refers to the operation principles given in 0.

Table 1. Components of the experimental setup.

Symbol	Component	Manufacturer, City and Country	Remark
VTxx	IPP60R040C7	Infineon Technologies AG, Neubiberg, Germany	nMOSFET, Si, 650 V, 40 mΩ
T12	Custom		1:1, windings—25 turns of CLI 120 × 0.1 face wire, 2 ETD59-3C94 with μ = 2300
L11, L12	Custom		60 μH, core—powder iron rings, 17 turns of CLI 120 × 0.1 face wire
C11, C21, C31	MKP1848S	Vishay Intertechnology Inc., Malvern, USA	Metallized Polypropylene Film Capacitor, 30 μF, 1000 V
-	ACPL-333J	Broadcom Inc., San Jose, USA	2.5 Amp Output Current IGBT Gate Driver with Integrated Desaturation Detection, Miller Clamp and Fault Status Feedback
-	ATmega2560	Microchip Technology Inc., Chandler, USA	MCU with 12-channel of 16-bit PWM module.
R91	4 × SLN175J230E, 230 Ω, 1 A	Ohmite, Warrenville, USA	High Power Resistor

The measurements obtained from the setup are presented in Figure 11. When considering these diagrams, it must be taken into account that the voltage sensors utilize 1:50 resistive dividers. In turn, all currents were taken from a 1 Ω resistor providing a current scale of 1 V per 1 A. The results given generally correspond to the expected operational diagrams given in Figure 11. Therefore, the general idea of the operation of the proposed converter was confirmed.

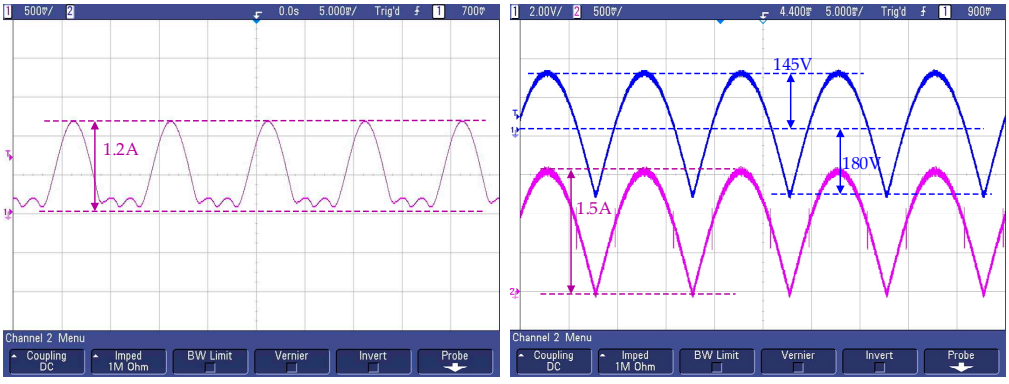

(**a**) (**d**)

Figure 11. *Cont.*

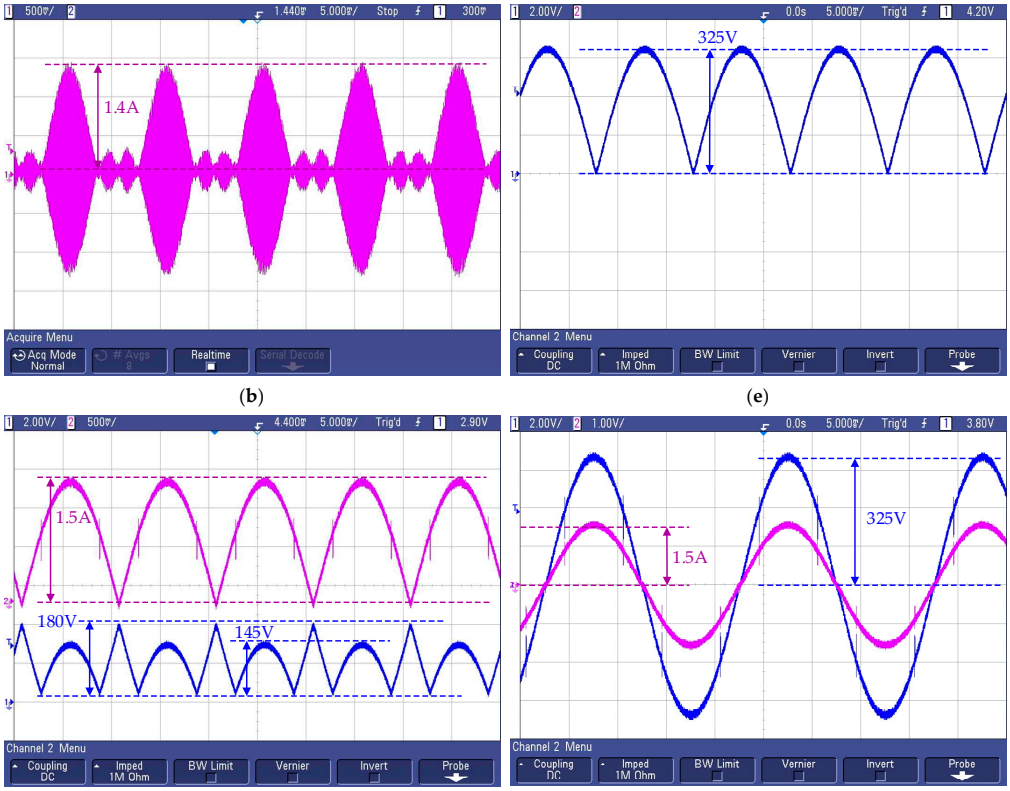

Figure 11. Test results of the proposed BESS interface: (**a**) PPC current at the battery side $i_{ppc,bat}(t)$; (**b**) PPC current in the transformer $i_{ppc,tr}(t)$; (**c**) PPC internal voltage $v_{ppc,int}(t)$ and current $i_{ppc,int}(t)$ before the extra unfolder; (**d**) PPC voltage $v_{ppc,dc}(t)$ and current $i_{ppc,dc}(t)$ at the side of the DC-link; (**e**) DC-link voltage $v_{dc}(t)$; and (**f**) voltage $v_s(t)$ and current $i_s(t)$ in the grid (load).

5. Considerations on Partiality and Its Actual Influence

5.1. Evaluation of Partiality

When evaluating the partial power converters, it is important to determine which part of the total power is actually processed by the converter. The lower the part is, the higher the potential energy efficiency. This part sometimes is expressed in % relative to the full power—as a power partiality ratio:

$$PPR = \frac{P_{PPC}}{P_{\Sigma}} \cdot 100\% \tag{4}$$

Here, P_{PPC} is the active power of the PPC and P_{Σ} is the total power of the system. In contrast to the DC systems, these parameters of the proposed BESS interface converter are integral values. The full system's power can be calculated at the grid side of the converter. With proper control (i.e., without harmonic distortions and reactive power), the full power is found as a product of the RMS grid voltage V_s and grid current I_s. In turn, the active power of the DC-DC converter can be found as a form of average instantaneous power at any port of the converter—either $p(t)_{ppc,bat}$, $p(t)_{ppc,int}$ or $p(t)_{ppc,dc}$. The power at the DC port ($p(t)_{ppc,dc}$) is easy to express because, in the case of the proper control, the current $i_{ppc,dc}(t)$ is a rectified sine-wave (Figures 4b and 11f). In turn, $v_{ppc,dc}(t)$ is the difference of the DC-link

voltage $v_{dc}(t)$ and battery voltage V_{bat}. Considering the above-mentioned and applying the network voltage $v_s(t) = V_{s,\max}\cdot\sin(\omega t)$ with the network current $i_s(t) = I_{s,\max}\cdot\sin(\omega t)$ the instantaneous power is defined as

$$p_{ppc}(t) = I_{s,\max}\sin(\omega t)\cdot(V_{s,\max}\sin(\omega t) - V_{bat}) \tag{5}$$

but its average value (active power through the DC-DC converter) is described as

$$P_{ppc} = \frac{1}{T}\int_0^T I_{s,\max}\sin(\omega t)\cdot(V_{s,\max}\sin(\omega t) - V_{bat})\,dt \tag{6}$$

One part of this integral (minuend) is the network power $P_s = I_s \cdot V_s$, but another part (subtrahend) can be found as the integral of a half-sine.

$$\frac{1}{\pi}\int_0^\pi I_{s,m}\sin(\theta)\cdot V_{bat}d\theta = \frac{2}{\pi}\sqrt{2}I_s V_{bat} \tag{7}$$

Then, the PPR is reversely proportional to the battery voltage:

$$PPR = \left(1 - \frac{2\sqrt{2}V_{BAT}}{\pi V_{s,rms}}\right)\cdot 100\% \tag{8}$$

Let us calculate the PPR for the step-down DC-DC converter and battery providing at least half of the grid voltage amplitude (about 160 VDC) when it is discharged (64 Li-Ion cells with voltage 160–230 VDC). These numbers are given in Table 2. It is seen that (8) expresses a linear function that shows the diminishing influence of the battery voltage on PPR. At V_{bat} = 255 V, which is possible during battery charging for a fully charged battery, (8) shows no PPC contribution in power transfer. This corresponds to an explicit reduction in PPC power even down to 0 in DC systems at no voltage (or current) difference between the ports of the converter. Moreover, the further increase in the battery voltage and forming of the semi-sine half-waves with the help of the DC-DC converter leads to negative power through the DC-DC converter. Therefore, the above-mentioned value represents the reasonable voltage of the battery.

Table 2. Partiality evaluation.

SOC [%]	V_{bat} **[V]**	**PPR [%]**	**SOC [%]**	V_{bat} **[V]**	**PPR [%]**	**SOC [%]**	V_{bat} **[V]**	**PPR [%]**	**SOC [%]**	V_{bat} **[V]**	**PPR [%]**	**SOC [%]**	V_{bat} **[V]**	**PPR [%]**
0	160	37	30	181	29	60	202	21	90	223	13	>100	244	4
10	167	35	40	188	26	70	209	18	100	230	10	>100	252	2
20	174	32	50	195	24	80	216	15	>100	237	7	>100	256	0

At the same time, the data presented in Table 2 are only the surficial presentation of the actual power transfer processes in the DC-DC converter; like AC active power, reactive and harmonic power is only a representation of the real-time power consumption in the AC grid. Figure 12 shows the instantaneous power of the converter, calculated according to (5) for 1 kW of the system power and different battery voltages. The declinations of the instantaneous power form its averaged value, used in (5)–(7), which are always significant (even with no actual power in the converter). Therefore, the averaged PPR, expressed by (8), is of limited usability and the actual influence of partiality has to be evaluated over a time span for different parameters of the system.

5.2. Influence of Partiality

The influence of partiality is studied in this section based on a mathematical model for a two-stage BESS interface converter with a pulse-mode or unfolding frontend, suitable battery (190–315 V for known configurations and 160–270 V for the proposed combination of UF and PPC) and flyback pre-regulator. The flyback is the simplest isolating DC/DC converter; it is capable of converting voltage in both directions (step-up or step-down) and is more convenient for comparison due to simpler associated calculations.

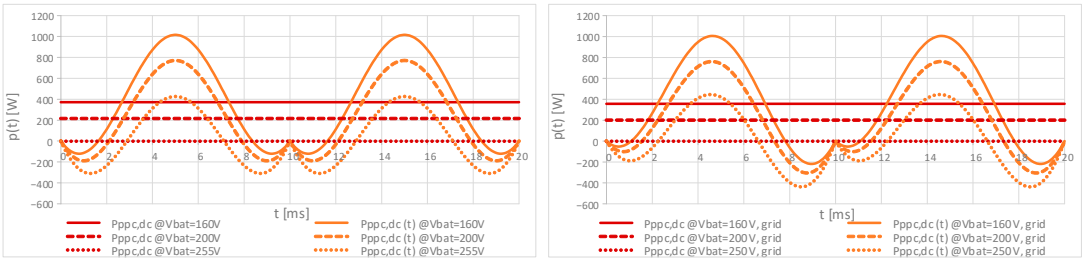

(**a**) (**b**)

Figure 12. Instantaneous power at the DC port of a partial power DC-DC converter (for 1 kW of the total power): (**a**) battery discharge to autonomous load (as considered in Chapter IV); (**b**) battery discharge to the grid.

5.2.1. Brief Loss Evaluation

Typically, the partial power converters are considered a good alternative to the full power systems due to lower voltage and current stress on the switches, as well as due to the lower processing power and, therefore, losses. As shown in Figures 6–8 and 11, the partial power DC-DC converter of the above-proposed BESS interface conducts semi-sine halfwaves of the current with the grid amplitude. As for the commutated voltage of the PPC, it is defined by the battery that, in the following examples, it has a voltage in the range of 160–230 V assuming a step-down DC-DC converter. These values are not much lower than the amplitude of the grid voltage (325 V). Therefore, this typical advantage of the PPC is not so explicit in the case of the considered BESS interface.

In order to evaluate the impact of the proposed configuration on the power losses let us consider a couple of the simplified numerical examples. Firstly, a common BESS interface with a full power pulse-mode frontend and regulator is analyzed.

For the simplified analysis of the switching losses, let us assume the following: (1) the commutated voltage is the voltage of the DC-link that is equal to the amplitude of the grid voltage $V_{s,m}$ = 325 V; (2) voltage rise and fall times tv are equal and proportional to the commutated voltage (i.e., they are constant); (3) current rise and fall times t_i are equal and proportional to the commutated current; (4) voltage/current change times are equal in the middle of the semi-sine current half-wave at maximal current; (5) the switching frequency is chosen so that in the middle of the semi-sine half-wave the length of 1 turn-on or 1 turn-off commutation is 1% of the switching period (Relative Duration of Switching RDS); (6) and, for simplicity, the analysis is provided for the battery discharge mode only.

5.2.2. Losses of Full Power BESS Interface

The most common H-bridge topology operates as a grid-to-battery boost converter with the current path provided by a constantly conducting diode and toggling couple transistor–diode. It is, therefore, possible to conclude that in the continuous current mode,

two switches are always conducting a semi-sine current. Then, assuming for simplicity that both of them are p-n devices, their losses can be defined as

$$\Delta P_{FE1,c} = 2 \cdot \frac{1}{\pi} \int_0^{\pi} \Delta p_c(t) dt = 2 \cdot \frac{1}{\pi} \int_0^{\pi} V_0 I_{s,m} \sin(\theta) d\theta = \frac{4 V_0 I_{s,m}}{\pi} \tag{9}$$

where V_0 is the rated voltage drop over the switch (assumed as a constant for simplicity reasons and equal to 2 V).

The switching losses can be calculated assuming the triangular shape of instantaneous power on the switches during the commutation. Then, the maximal energy loss of turn-on and turn-off commutations is achieved at grid phase 90° when its voltage and current are maximal.

$$E_{FE1,sw,m} = 2 \cdot \frac{V_{s,m} I_{s,m} (t_{i,m} + t_{v,m})}{2} = V_{s,m} I_{s,m} (t_{i,m} + t_v) \tag{10}$$

Then, the maximal equivalent power losses are as follows:

$$\Delta P_{FE1,sw,m} = \frac{V_{s,m} I_{s,m} (t_{i,m} + t_v)}{T_{sw}} = V_{s,m} I_{s,m} RDS = A \tag{11}$$

Since the current change times are considered proportional to the current that is semi-sinusoidal for the other points, the equivalent switching losses are as follows:

$$\begin{aligned} \Delta P_{FE1,sw,k} &= \frac{1}{T_{sw}} \cdot 2 \cdot \frac{V_{sw,k} \cdot I_{sw,k} \cdot (t_{i,k} + t_{v,k})}{2} = \\ &= \frac{V_{s,m} \cdot I_{s,m} \sin\theta_k \cdot (t_{i,m} \frac{I_{s,k}}{I_{s,m}} + t_v \frac{V_{s,k}}{V_{s,m}})}{T_{sw}} = \\ &= \frac{V_{s,m} \cdot I_{s,m} \sin\theta_k \cdot (t_{i,m} \sin\theta_k + t_v)}{T_{sw}} = V_{s,m} I_{s,m} \frac{RDS}{2} \sin\theta_k + V_{s,m} I_{s,m} \frac{RDS}{2} \sin_2\theta_k = \\ &= \frac{A}{2} \sin\theta_k + \frac{A}{2} \sin_2\theta_k \end{aligned} \tag{12}$$

The total switching losses of the frontend are

$$\Delta P_{FE1,sw} = \frac{1}{0.5 T_s} \sum_{k=1}^{N} \Delta P_{sw,k} T_{sw} = \frac{2}{T_s} \sum_{k=1}^{N} \Delta P_{sw,k} \Delta t_k \tag{13}$$

that can then be converted to the integral form

$$\Delta P_{FE1,sw} = \frac{1}{\pi} \int_0^{\pi} \Delta P_{sw}(\theta) d\theta \tag{14}$$

Applying (12) gives the follows:

$$\Delta P_{FE1,sw} = \frac{1}{\pi} \int_0^{\pi} (\frac{A}{2} \sin\theta_k + \frac{A}{2} \sin_2\theta_k) d\theta == \frac{A}{\pi} + \frac{A}{4} - 0 = V_{s,m} I_{s,m} RDS \frac{\pi + 4}{4\pi} \tag{15}$$

The above equations for 1 kW of the grid power and with given assumptions produce losses $\Delta P_{FE1,c}$ = 7.8 W and $\Delta P_{FE1,sw}$ = 11.4 W.

As for the (pre)regulator, it is a DC/DC chopper operating with a DC-link voltage on one port and battery voltage on the other. A versatile solution is a buck–boost scheme, which is also comparable with the simplest PPC realization based on the flyback. One port of this chopper handles the DC-link voltage (the amplitude of the grid voltage $V_{s,m}$) and

average current, corresponding to the power transmitted to/from the grid P_s, i.e., $V_sI_s/V_{s,m} = I_s/1.41 = I_{s,m}/2$. This current is delivered with pulses, the value of which can be found in the voltage transfer equation of the buck–boost converter, which, in discharge mode, is

$$V_{s,m} = V_{bat}\frac{D_{bat}}{(1-D_{bat})} \text{ that gives } D_{bat} = \frac{V_{s,m}}{V_{bat}+V_{s,m}} \tag{16}$$

And the power balance of the converter is as follows:

$$V_{s,m}I_{DC} = V_{bat}I_{bat} \tag{17}$$

where D_{bat} is relative to the time of the switch at the battery side. It is also assumed that the fully charged battery produces a voltage slightly lower than the grid voltage amplitude $V_{s,m}$ (with number of cells N_{cell} = 75) and the current in the inductor of the chopper has low ripples (operation in continuous current mode).

Then, the value of the current pulses in the switches, as well as the current of the inductor can be expressed as

$$I_{La} = \frac{I_{s,m}}{2}\frac{1}{1-D_{bat}} = \frac{I_{s,m}}{2}\frac{V_{bat}+V_{s,m}}{V_{bat}} \tag{18}$$

Since, in the discontinuous conduction mode, one of the switches conducts this current, the conduction losses can be calculated as

$$\Delta P_{REG1,c} = V_0 I_{La} \tag{19}$$

Applying the commutated current $I_{sw} = I_{La}$ and commutated voltage $V_{sw} = V_{s,m} + V_{bat}$ in (12),

$$\Delta P_{REG1,sw} = (V_{s,m}+V_{bat})I_{La}(\frac{t_i}{T_{sw}}+\frac{t_v}{T_{sw}}) \tag{20}$$

and it assumed that these parameters affect the corresponding current/voltage changes as follows:

$$\frac{t_i}{T_{sw}} = \frac{t_{i,m}}{T_{sw}}\frac{I_{La}}{I_{s,m}} = \frac{RDS}{2}\frac{I_{La}}{I_{s,m}} \text{ and } \frac{t_v}{T_{sw}} = \frac{t_{v,m}}{T_{sw}}\frac{V_{s,m}+V_{bat}}{V_{s,m}} = \frac{RDS}{2}\frac{V_{s,m}+V_{bat}}{V_{s,m}} \tag{21}$$

It becomes possible to calculate the corresponding switching losses of the regulator and the total losses of the reference converter (Table 3). The losses of the regulator are more than twice as high as those of the frontend—mostly due to the almost doubled commutated voltage of the buck–boost regulator. The power losses of other regulators are potentially lower.

Table 3. Power losses in case of full power switch mode regulator and inverter.

SOC [%]	0	13	25	38	50	63	75	88	100
V_{bat}, **[V]**	188	203	219	235	251	267	283	299	315
$V_{sw} = V_{s,m} + V_{bat}$, **[V]**	513	529	545	561	577	592	608	624	640
$I_{sw} = I_{La}$, **[A]**	8.41	7.99	7.63	7.32	7.05	6.82	6.61	6.42	6.25
t_i/T_{sw} **[%]**	0.68	0.65	0.62	0.60	0.57	0.55	0.54	0.52	0.51
t_v/T_{sw} **[%]**	0.29	0.31	0.34	0.36	0.39	0.41	0.44	0.46	0.48
$\Delta P_{REG1,c}$ **[W]**	16.8	16.0	15.3	14.6	14.1	13.6	13.2	12.8	12.5
$\Delta P_{REG1,sw}$ **[W]**	41.9	40.7	39.8	39.3	39.0	39.0	39.1	39.3	39.7
ΔP_1 **[W]**	77.9	75.8	74.3	73.1	72.3	71.8	71.5	71.4	71.4
ΔP_1 **[%]**	7.8	7.6	7.4	7.3	7.2	7.2	7.1	7.1	7.1

5.2.3. Losses in Case of Partial Power Regulator

Let us now consider the losses of the BESS interface with a partial power (pre)regulator. The applied converter topology is flyback—a version of buck–boost equipped with split

coil (transformer). Therefore, its static voltage equation remains, but, due to the series connection at the DC-link side, can be rewritten as

$$V_{s,m} - V_{bat} = V_{bat}\frac{D_{bat}}{(1 - D_{bat})} \tag{22}$$

which produces

$$D_{bat} = \frac{V_{s,m} - V_{bat}}{V_{s,m}} \tag{23}$$

With this configuration, the commutated voltage (the sum of the input and output voltages of the converter) is fixed at the level $V_{DC} = V_{s,m}$, i.e., the lower the battery voltage the larger the part that is added by the DC-DC converter. In turn, the commutated current can still be expressed by (20). However, in this configuration, it does not flow explicitly in an inductor but is formed as the sum of two currents of primary and secondary windings that in explicit form can be measured in the battery.

As for the frontend, since the schematic and operation remain unchanged, its losses also remain on the previously calculated level of $\Delta P_{FE2,c}$ = 7.8 W and $\Delta P_{FE2,sw}$ = 11.4 W. The power losses corresponding to the partial power regulator are given in Table 4. The positive effect of the operation with reduced voltage and current is clear, even in the case of the considered flyback converter.

Table 4. Power losses in case of switch mode inverter and partial power regulator.

SOC [%]	0	13	25	38	50	63	75	88	100
V_{bat}, **[V]**	188	203	219	235	251	267	283	299	315
$V_{sw} = V_{s,m}$, **[V]**	325	325	325	325	325	325	325	325	325
$I_{sw} = I_{bat}$, **[A]**	5.33	4.92	4.56	4.25	3.98	3.74	3.53	3.34	3.17
t_i/T_{sw} **[%]**	0.43	0.40	0.37	0.35	0.32	0.30	0.29	0.27	0.26
t_v/T_{sw} **[%]**	0.29	0.31	0.34	0.36	0.39	0.41	0.44	0.46	0.48
$\Delta P_{REG2,c}$ **[W]**	10.7	9.8	9.1	8.5	8.0	7.5	7.1	6.7	6.3
$\Delta P_{REG2,sw}$ **[W]**	12.5	11.4	10.5	9.8	9.2	8.7	8.3	8.0	7.7
ΔP_2 **[W]**	42.39	40.42	38.81	37.47	36.35	35.39	34.56	33.84	33.21
ΔP_2 **[%]**	4.2	4.0	3.9	3.7	3.6	3.5	3.5	3.4	3.3

5.2.4. Losses in Case of Unfolding Frontend

In the case of the unfolding frontend, the grid current in each half-period constantly flows through the couple of the frontend switches. For this reason, the frontend produces only conduction losses that can still be calculated with (9) as $\Delta P_{FE3,c}$ = 7.8 W while $\Delta P_{FE3,sw}$ = 0 W.

For such a frontend, the (pre)regulator forms semi-sine voltage half-waves in the "virtual" DC-link (which includes a small capacitor, capable of reducing only high-frequency voltage ripples). This is why most of the basic parameters are functions of the grid phase:

$$\text{voltage } V_{s,k} = V_{s,m}\sin\theta_k$$

$$\text{and current in virtual DC} - \text{link } I_{sw,k} = I_{s,k} = I_{s,m}\sin\theta_k \tag{24}$$

commutated voltage

$$V_{sw,k} = V_{bat} + V_{s,k} = V_{bat} + V_{s,m}\sin\theta_k \tag{25}$$

$$\text{static equation } V_{s,m}\sin(\theta_k) = V_{bat}\frac{D_{bat,k}}{1 - D_{bat,k}} \tag{26}$$

$$\text{and duty cycle } D_{bat,k} = \frac{V_{s,m}\sin\theta_k}{V_{bat} + V_{s,m}\sin\theta_k} \tag{27}$$

Other parameters, therefore, are also expressed as such functions. The commutated (inductor) current can be found in the DC-link capacitor balance which requires

$$I_{La,k}(1 - D_{bat,k}) = I_{s,k} \text{ giving } I_{sw,k} = I_{La,k} = \frac{I_{s,m} \sin \theta_k}{1 - D_{bat,k}} \tag{28}$$

The conduction losses, dissipated in two switches (one of which is conducting), can then be expressed as

$$\Delta P_{REG3,c,k} = \frac{V_0 I_{s,k}}{1 - D_{bat,k}} \tag{29}$$

$$\text{but applying (27)}^{-}\text{as} \Delta P_{REG3,c,k} = \frac{V_{s,k} V_0 I_{s,k}}{V_{bat}} + V_0 I_{s,k}$$

$$\Delta P_{REG3,c,k} = \frac{V_{s,m} V_0 I_{s,m} \sin_2 \theta_k}{V_{bat}} + V_0 I_{s,m} \sin \theta_k \tag{30}$$

Applying (29) into the equation of averaged (active) power

$$\Delta P_{REG3,c} = \frac{1}{0.5 T_s} \sum_{k=1}^{N} \Delta P_{REG3,c,k} T_{sw} = \frac{1}{\pi} \int_0^{\pi} \Delta P_{REG3,c}(\theta) d\theta \tag{31}$$

after simplifications produces

$$\Delta P_{REG3,c} = \frac{1}{2} \frac{V_0}{V_{bat}} V_{s,m} I_{s,m} + \frac{2}{\pi} \frac{V_0}{V_{s,m}} V_{s,m} I_{s,m} = \frac{V_0}{V_{bat}} P_s + \frac{4}{\pi} \frac{V_0}{V_{s,m}} P_s \tag{32}$$

The switching losses of the pulse mode regulator can still be calculated by (12) utilizing the commutated current (24) and commutated voltage (25). The analytical solution of the corresponding formula refers to a sine-form signal in power 3 or even 4. For this reason, the switching losses are calculated numerically in general form. Then, (12) can be rewritten as

$$\Delta P_{REG3,sw,k} = \frac{1}{T_{sw}} \cdot 2 \cdot \frac{V_{sw,k} \cdot I_{sw,k} \cdot (t_{i,k} + t_{v,k})}{2} = \frac{1}{T_{sw}} \cdot 2 \cdot \frac{(V_{bat} + V_{s,k}) \frac{I_{s,k}}{1 - D_{bat,k}} \cdot (t_{i,k} + t_{v,k})}{2}$$

$$\text{with } \frac{t_{i,k}}{T_{sw}} = \frac{t_{i,m}}{T_{sw}} \frac{I_{La,k}}{I_{s,m}} = \frac{RDS}{2} \frac{I_{s,k}}{1 - D_{bat,k}} \frac{1}{I_{s,m}} \tag{33}$$

$$\text{and } \frac{t_{v,k}}{T_{sw}} = \frac{t_{v,m}}{T_{sw}} \frac{V_{bat} + V_{s,k}}{V_{s,m}} = \frac{RDS}{2} \frac{V_{bat} + V_{s,k}}{V_{s,m}}$$

The results of the conduction loss calculation with (29), their verification with (32) and switching loss calculation with (33) are presented in Table 5. The number of switching cycles in these calculations is 100 which corresponds to a switching frequency at 10 kHz. It is seen that the general level of the losses is comparable with the reference design (pulse mode frontend, pulse mode full power regulator), but some parts of the switching losses "moved" from the frontend to the regulator.

5.2.5. Losses in Case of Unfolding Inverter and Partial Power Regulator

Let us apply the above-scribed loss calculation procedure to the proposed battery interface still assuming that the DC-DC converter is a classical inverting buck–boost chopper.

Like in the previous case the frontend is an unfolding inverter, where the grid current in each half-period constantly flows through two switches and the frontend losses are purely conduction losses calculated with (9) as $\Delta P_{FE4} = \Delta P_{FE4,c} = 7.8$ W.

In addition, the proposed and evaluated configuration utilizes an extra unfolding inverter (Figures 1b,d and 9). Like a grid inverter, this unfolder conducts semi-sine half-waves (although the commutations occur not only at grid phases 0° and 180°). This

means that at the applied assumptions, this inverter produces the same conduction losses $\Delta P_{UF+} = \Delta P_{UF+,c} = 7.8$ W (without significant switching losses).

Table 5. Power losses in case of unfolding inverter and full power regulator.

SOC [%]	0	13	25	38	50	63	75	88	100
V_{bat}, **[V]**	188	203	219	235	251	267	283	299	315
$V_{sw,\,max}$, **[V]**	513	529	545	561	576	592	608	624	640
$V_{sw,\,min}$, **[V]**	193	209	224	240	256	272	288	304	320
D_{max} **[%]**	63	62	60	58	56	55	53	52	51
D_{min} **[%]**	3	2	2	2	2	2	2	2	2
$\Delta P_{REG3,c,\,discrete}$ **[W]**	18.5	17.7	16.9	16.3	15.8	15.3	14.9	14.5	14.2
$\Delta P_{REG3,c,\,exact}$ **[W]**	18.5	17.7	16.9	16.3	15.8	15.3	14.9	14.5	14.2
$\Delta P_{REG3,sw}$ **[W]**	75.3	73.1	71.5	70.5	69.8	69.5	69.4	69.5	69.9
ΔP_3 **[W]**	101.6	98.6	96.3	94.6	93.4	92.6	92.1	91.9	91.9
ΔP_3 **[%]**	10.2	9.9	9.6	9.5	9.3	9.3	9.2	9.2	9.2

The main considerations applied to the calculation of losses of the regulator, connected to the unfolding inverter, can also be expanded to this configuration with some corrections.

In static Equation (26), the rectified grid voltage $V_{s,k}$ has to be changed to the rectified difference of $V_{s,k}$ and battery voltage $V_{s,k}$ (as in Figures 6b–8b). Then, the static equation and expression for the duty cycle calculation is as follows:

$$\left|V_{s,k} - V_{bat}\right| = V_{bat}\frac{D_{bat,k}}{1 - D_{bat,k}} \tag{34}$$

$$\text{and } D_{bat,k} = \frac{\left|V_{s,k} - V_{bat}\right|}{V_{bat} + \left|V_{s,k} - V_{bat}\right|},$$

$$\text{which can be } D_{bat,k} = \frac{V_{s,k} - V_{bat}}{V_{s,k}} \text{ or } D_{bat,k} = \frac{V_{bat} - V_{s,k}}{2V_{bat} - V_{s,k}} \tag{35}$$

depending on the grid phase.

The static current balance (28) for determining the commutated current remains, but has to be composed for internal capacitor C21 and utilized (35) for the duty cycle.

Finally, the commutated voltage also refers to the rectified difference of $V_{s,k}$ and battery voltage $V_{s,k}$

$$V_{sw,k} = V_{bat} + \left|V_{s,k} - V_{bat}\right| \text{that can be } V_{sw,k} = V_{s,k} \text{ or } V_{sw,k} = 2V_{bat} - V_{s,k} \tag{36}$$

The analytical calculation of the losses requires applying (28), (35), (36) to (29) and (33) and a further complicated integration. These equations, therefore, have been used numerically. The calculations for a 64 cells battery, providing a voltage of 160–270 V are presented in Table 6.

Table 6. Power losses in case of unfolding inverter and partial power regulator (battery is composed of 64 cells).

SOC [%]	0	13	25	38	50	63	75	88	100
V_{bat}, **[V]**	160	174	187	201	214	228	242	255	269
$V_{sw,\,max}$, **[V]**	325	342	369	396	424	451	478	505	532
$V_{sw,\,min}$, **[V]**	161	177	187	203	218	230	243	257	272
D_{max} **[%]**	51	49	49	49	49	49	49	49	50
D_{min} **[%]**	1	2	0	1	1	1	0	1	1
$\Delta P_{REG4,c}$ **[W]**	13.2	12.3	11.6	11.0	10.5	10.2	9.9	9.6	9.5
$\Delta P_{REG4,sw}$ **[W]**	22.3	19.8	18.0	16.6	15.6	15.0	14.7	14.7	15.1
ΔP_4 **[W]**	51.1	47.8	45.2	43.3	41.8	40.8	40.2	40.0	40.2
ΔP_4 **[%]**	5.1	4.8	4.5	4.3	4.2	4.1	4.0	4.0	4.0

Additional calculations (Tables 7 and 8) have also been made for batteries with 50 and 75 cells. These calculations in conjunction with the previously obtained data are graphically compared in Figure 13. This diagram proves that the considered BESS interface still has the advantages of partial power converters though they are not so visible as in the case of DC systems. The graphics also show that the highest efficiency can be achieved at a battery voltage of about 255 V (at which there is no circulating power flow through the DC-DC regulator). Therefore, the battery with this voltage in the middle of its operation range can be considered as optimal.

Table 7. Power losses in case of unfolding inverter and partial power regulator (battery made of 50 cells).

SOC [%]	0	13	25	38	50	63	75	88	100
V_{bat}, **[V]**	125	136	146	157	168	178	189	199	210
ΔP_4 **[%]**	6.5	6.0	5.5	5.2	4.9	4.7	4.5	4.3	4.2

Table 8. Power losses in case of unfolding inverter and partial power regulator (battery made of 75 cells).

SOC [%]	0	13	25	38	50	63	75	88	100
V_{bat}, **[V]**	188	203	219	235	251	267	283	299	315
ΔP_4 **[%]**	4.5	4.3	4.1	4.0	4.0	4.0	4.1	4.2	4.4

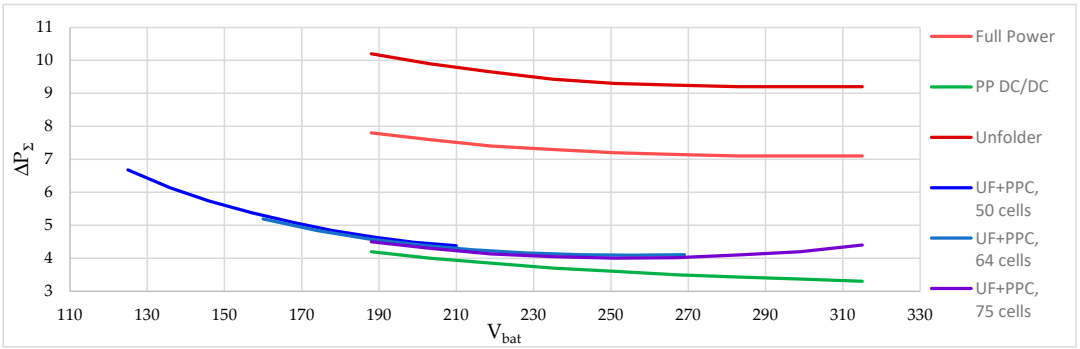

Figure 13. Comparison of power losses in the considered systems.

5.2.6. General Considerations on Calculation of Converter Losses

The battery interface converter with a flyback pre-regulator, considered in Section 5.2, is derived from the inverting buck–boost chopper that calculates the sum of its input and output voltages. So, the flyback converter on the primary side calculates the sum of the primary voltage and "reflected" secondary voltage, but on the secondary side, the sum of the secondary voltage and "reflected" primary voltage is obtained. The unity ratio of turns for the primary and secondary windings of the transformer on both ends converter's switches commutate the sum of voltages. In the case of BESS, one of these voltages is the battery voltage, but the other is the full or partial DC-link voltage. Therefore, the commutated voltage directly depends on the battery.

In turn, the commutated voltage, with the selected loss calculation methodology has a direct influence on the switching losses in the pre-regulator; this voltage is placed in the numerator of the corresponding formula. It has also an indirect influence on these losses because this voltage defines the voltage rise/fall times. For this reason, the switching losses with such a configuration are unreasonably higher compared to the case of other topologies of the pre-regulator that typically calculate the maximal input/output voltage. This voltage

overrating can be evaluated as follows: (190–315 + 315)/315 = 1.6–2 for the full-power full-switching interface converter and interface with an unfolder, 315/(190–315) = 1–1.7 for the partial-power full-switching BESS interface and (190–315 + 315/2)/190–315 = 1.5–1.8 for the proposed converter.

6. Conclusions

After the experimental verification and analysis of the mathematical model for the loss calculation, the proposed battery interface converter that combines an unfolding inverter as the grid frontend with a partial power DC-DC converter as (pre)regulator was found operational. A more detailed explanation of this matter includes the following considerations:

(1) The described series configuration of the utilized battery and output port of the applied DC-DC converter is capable of generating the semi-sine voltage halfwaves that can be transformed by unfolding the inverter into a sine voltage at the grid port of the interface converter. This consideration is valid for multiple configurations of the battery.

(2) The proposed configuration keeps the advantage of the BESS interface with an unfolding inverter—the absence of bulky and less reliable DC-link electrolytic capacitors, calculated for grid frequency.

(3) From an efficiency point of view, the proposed configuration behaves as PPC. Its losses are lower than those of the reference full-power converters, but not as low as the losses in the case of a DC-DC PPC. This can be explained by a larger voltage, to be compensated by the PPC (pre)regulator, as well as by the dynamic nature of this compensation—even at no average power transfer through PPC (at 255 V), there is always some instantaneous power through the regulator that leads to losses. From this point of view, preferences should be given to the batteries with voltages around 255 V (assuming grid voltage of 230 V_{AC}) and battery chemistries that provide lower voltage difference vs. SOC. The level of the losses obtained in this work is rather high. However, it is obtained for inverting buck–boost and flyback regulators, which are more convenient for comparison, but calculate the sum of input and output voltages which leads to higher switching losses (with the considered model).

(4) From the point of view of the current ratings of the switches of the proposed configuration, it is not very advantageous. There are instances in time when the regulator conducts a full grid current. On the other hand, the commutated voltage depends on the battery. At the lowest level, the battery and regulator voltages are equal and are twice as low as the grid voltage amplitude.

The above-mentioned considerations allow us to conclude that the proposed BESS interface keeps the major advantages of the applied loss minimization techniques (PPC and UF). On one hand, compared to the full-power BESS interface with the unfolding inverters, the proposed interface converter provides lower conduction and commutation losses in the voltage pre-regulator (in addition to its smaller size, lower weight and higher reliability due to a twice lower voltage stress on the switches). On the other hand, compared to the switching mode BESS interface with a partial power regulator, the proposed converter provides lower losses in the frontend stage (in addition to the higher reliability of the entire interface converter due to the absence of high-capacity electrolytic capacitors).

Further improvement of this research may include the experimental study of the converter with real grid and multiple configurations of the battery, an experimental evaluation of its efficiency and losses in various operation modes and considering the losses in passive components, as well as the selection of the optimal battery chemistry and its configuration for the proposed battery interface. Particular attention should be paid to the improvement of the proposed and studied BESS interface converter by means of the better choice of the pre-regulator. As has been mentioned, the flyback regulator is not optimal from the point of view of the commutated voltage and switching losses and an alternative has to be chosen. The choice, already mentioned in this paper—DAB with an extra unfolder—due to the

doubled number of transistors in current paths, seems imperfect from the point of view of the conduction losses.

Another potential option—a bidirectional and bipolar push-pull converter—looks more promising. Another way of improvement is splitting the bidirectional regulator into battery charging and battery discharging parts (Figure 1c,d). This could potentially reduce the number of conducting switches and the corresponding switching losses. However, its use may make the trade-off between converter cost and losses more significant. Finally, the performance of the converter can be improved by the reasonable combining of traditional Si semiconductor devices with wide bandgap (SiC and GaN) switches. The proposed BESS interface may have quite distinct allocations of the switching and conduction losses and, therefore, the wise use of SiC and GaN switches looks promising.

The last, but not least, consideration is the influence of the proposed BESS interface converter on the operation parameters of the battery: temperature, state of health and overall lifetime. From this point of view, the most significant factor is the shape of battery charge/discharge currents. It can be guessed that independently of the functional structure (Figure 1) and with particular implementation (Figures 2–5, 9 or other), this current can be constructed as the sum of the currents of the DC/DC converter at its DC-link and battery ports. The first one (Figure 11d) has a semi-sine shape, but the second one can be derived from the instantaneous power of the DC-DC converter (Figure 12) taking into account the DC voltage that finally gives the current at the battery port, shown in Figure 11a. It is clear that this current is not a DC current, comfortable for batteries, but at the same time, it is not a pulse mode current—the most difficult for them. The current is constructed of several sine pieces. The influence of such a current on the battery is not clear and its determination requires multidisciplinary (electrical, chemical and heat exchange) research, dedicated to this topic. Such research is also planned as future work.

Author Contributions: Conceptualization, I.A.G. and A.B. (Andrei Blinov); methodology, I.A.G. and R.S.; validation, R.S, A.B. (Alexander Bubovich) and I.A.G.; formal analysis, D.P.; investigation, I.A.G.; writing—original draft preparation, I.A.G.; writing—review and editing, A.B. (Alexander Bubovich) and I.A.G.; visualization, I.A.G.; supervision, I.A.G.; project administration, A.B. (Andrei Blinov); funding acquisition, A.B. (Andrei Blinov). All authors have read and agreed to the published version of the manuscript.

Funding: This work was supported in part by the European Economic Area (EEA) and Norway Financial Mechanism 2014–2021 under grant EMP474 "Optimized Residential Energy Storage Systems". This work was supported in part by the European Regional Development Fund (ERDF) under contract 1.1.1.1/20/A/079 "Research and Development of Two-Phase Thermal Systems Installed in Lighting Equipment for its Functional Improvement" and contract Nr. 1.1.1.1/16/A/147 "Research and Development of Electrical, Information and Material Technologies for Low Speed Rehabilitation Vehicles for Disabled People" of its Latvian measure 1.1.1.1 "Industry-Driven Research".

Data Availability Statement: Data are contained within the article.

Conflicts of Interest: The authors declare no conflicts of interest.

References

1. Meyer, H.W. *A History Electricity and Magnetism*; The MIT Press: Cambridge, MA, USA, 1971.
2. Spotnitz, R. *Introduction to Batteries—An IEEE Course*; IEEE: New York, NY, USA, 2013.
3. Hu, X.; Zou, C.; Zhang, C.; Li, Y. Technological Developments in Batteries: A Survey of Principal Roles, Types, and Management Needs. *IEEE Power Energy Mag.* **2017**, *15*, 20–31. [CrossRef]
4. Luo, W.; Stynski, S.; Chub, A.; Franquelo, L.G.; Malinowski, M.; Vinnikov, D. Utility-Scale Energy Storage Systems: A Comprehensive Review of Their Applications, Challenges, and Future Directions. *IEEE Ind. Electron. Mag.* **2021**, *15*, 17–27. [CrossRef]
5. Ferreira, B. Batteries, the New Kids on the Block. *IEEE Power Electron. Mag.* **2019**, *6*, 32–34. [CrossRef]
6. Cao, J.; Emadi, A. Batteries Need Electronics. *IEEE Ind. Electron. Mag.* **2011**, *5*, 27–35. [CrossRef]
7. Chen, C.; Plunkett, S.; Salameh, M.; Stoyanov, S.; Al-Hallaj, S.; Krishnamurthy, M. Enhancing the Fast Charging Capability of High-Energy-Density Lithium-Ion Batteries: A Pack Design Perspective. *IEEE Electrif. Mag.* **2020**, *8*, 62–69. [CrossRef]
8. Stynski, S.; Luo, W.; Chub, A.; Franquelo, L.G.; Malinowski, M.; Vinnikov, D. Utility-Scale Energy Storage Systems: Converters and Control. *IEEE Ind. Electron. Mag.* **2020**, *14*, 32–52. [CrossRef]

9. Galkin, I.A.; Blinov, A.; Vorobyov, M.; Bubovich, A.; Saltanovs, R.; Peftitsis, D. Interface Converters for Residential Battery Energy Storage Systems: Practices, Difficulties and Prospects. *Energies* **2021**, *14*, 3365. [CrossRef]
10. The EMerge Alliance Data/Telecom Center Standard Creates an Integrated, Open Platform for Power, Infrastructure, Peripheral Device and Control Applications to Facilitate the Hybrid Use of AC and DC Power within Data Centers and Telecom Central Offices. Available online: https://www.emergealliance.org/standards/data-telecom/standard-faqs/ (accessed on 10 January 2024).
11. International Standard ISO7176: Wheelchairs. Part 25: Lead-Acid Batteries and Chargers for Powered Wheelchairs. Available online: https://www.iso.org/standard/79042.html (accessed on 10 January 2024).
12. International Standard ISO7176: Wheelchairs. Part 31: Lithium-Ion Battery Systems and Chargers for Powered Wheelchairs. Available online: https://www.iso.org/standard/75903.html (accessed on 10 January 2024).
13. Blinov, A.; Zinchenko, D.; Rabkowski, J.; Wrona, G.; Vinnikov, D. Quasi Single-Stage Three-Phase Filterless Converter for EV Charging Applications. *IEEE Open J. Power Electron.* **2022**, *3*, 51–60. [CrossRef]
14. Zinchenko, D.; Blinov, A.; Chub, A.; Vinnikov, D.; Verbytskyi, I.; Bayhan, S. High-Efficiency Single-Stage On-Board Charger for Electrical Vehicles. *IEEE Trans. Veh. Technol.* **2021**, *70*, 12581–12592. [CrossRef]
15. Galkin, I.; Blinov, A.; Verbytskyi, I.; Zinchenko, D. Modular Self-Balancing Battery Charger Concept for Cost-Effective Power-Assist Wheelchairs. *Energies* **2019**, *12*, 1526. [CrossRef]
16. Blinov, A.; Verbytskyi, I.; Zinchenko, D.; Vinnikov, D.; Galkin, I. Modular Battery Charger for Light Electric Vehicles. *Energies* **2020**, *13*, 774. [CrossRef]
17. LG Chem RESU Battery @ Solartopstore.com. Available online: https://www.solartopstore.com/collections/lg-chem-resu-battery (accessed on 20 July 2023).
18. Zapata, J.W.; Kouro, S.; Carrasco, G.; Renaudineau, H.; Meynard, T.A. Analysis of Partial Power DC–DC Converters for Two-Stage Photovoltaic Systems. *IEEE J. Emerg. Sel. Top. Power Electron.* **2019**, *7*, 591–603. [CrossRef]
19. Anzola, J.; Aizpuru, I.; Romero, A.A.; Loiti, A.A.; Lopez-Erauskin, R.; Artal-Sevil, J.S.; Bernal, C. Review of Architectures Based on Partial Power Processing for DC-DC Applications. *IEEE Access* **2020**, *8*, 103405–103418. [CrossRef]
20. Zientarski, J.R.R.; da Silva Martins, M.L.; Pinheiro, J.R.; Hey, H.L. Series-Connected Partial-Power Converters Applied to PV Systems: A Design Approach Based on Step-Up/Down Voltage Regulation Range. *IEEE Trans. Power Electron.* **2018**, *33*, 7622–7633. [CrossRef]
21. Zientarski, J.R.R.; da Silva Martins, M.L.; Pinheiro, J.R.; Hey, H.L. Evaluation of Power Processing in Series-Connected Partial-Power Converters. *IEEE J. Emerg. Sel. Top. Power Electron.* **2019**, *7*, 343–352. [CrossRef]
22. Elasser, A.; Agamy, M.; Huh, K.K. System and Method for a DC/DC Converter. U.S. Patent US9960687, 1 May 2018.
23. Iwaya, K.; Miyazaki, T.; Shoji, K. Series Compensating Electric Power Transmission System. U.S. Patent US10116221B2, 30 October 2018.
24. Blinov, A.; Chub, A.; Korkh, O.; Vinnikov, D.; Galkins, I.; Peftitsis, D. System and Method for Transmitting Power Between Two DC Sources. EE202000020. 2020. Available online: https://www1.epa.ee/patent/kirjeldus/P202000020.pdf (accessed on 2 October 2023).
25. Husev, O.; Matiushkin, O.; Roncero-Clemente, C.; Blaabjerg, F.; Vinnikov, D. Novel Family of Single-Stage Buck–Boost Inverters Based on Unfolding Circuit. *IEEE Trans. Power Electron.* **2019**, *34*, 7662–7676. [CrossRef]
26. Zhao, B.; Abramovitz, A.; Liu, C.; Yang, Y.; Huangfu, Y. A Family of Single-Stage, Buck-Boost Inverters for Photovoltaic Applications. *Energies* **2020**, *13*, 1675. [CrossRef]
27. Oguchi, K.; Ikawa, E.; Tsukiori, Y. A three-phase sine wave inverter system using multiple phase-shifted single-phase resonant inverters. In Proceedings of the Conference Record of the 1990 IEEE Industry Applications Society Annual Meeting, Seattle, WA, USA, 7–12 October 1990; pp. 1125–1131. [CrossRef]
28. Rabkowski, J.; Blinov, A.; Zinchenko, D.; Wrona, G.; Zdanowski, M. Grid-frequency Vienna rectifier and isolated current-source DC-DC converters for efficient off-board charging of electric vehicles. In Proceedings of the 2020 22nd European Conference on Power Electronics and Applications (EPE'20 ECCE Europe), Lyon, France, 7–11 September 2020; pp. 1–10.
29. Anurag, A.; Deshmukh, N.; Maguluri, A.; Anand, S. Integrated DC–DC Converter Based Grid-Connected Transformerless Photovoltaic Inverter with Extended Input Voltage Range. *IEEE Trans. Power Electron.* **2018**, *33*, 8322–8330. [CrossRef]
30. Kumar, R.; Rajaput, M.; Deshmukh, N.; More, D.; Anand, S. Partial Unfolding Scheme for Grid Feeding Transformerless PV Inverter. In Proceedings of the 2018 IEEE International Conference on Power Electronics, Drives and Energy Systems (PEDES), Chennai, India, 18–21 December 2018; pp. 1–6. [CrossRef]
31. Miguchi, Y.; Setiadi, H.; Nasu, Y.; Obara, H.; Kawamura, A. Control Scheme for Leading Power Factor Operation of Single-Phase Grid-Connected Inverter Using an Unfolding Circuit. *IEEE Open J. Power Electron.* **2022**, *3*, 468–480. [CrossRef]
32. Renaudineau, H.; Flores-Bahamonde, F.; Kouro, S.; Zapata, J.W. Single-Phase partial power unfolding inverter for photovoltaic string application. In Proceedings of the 2021 IEEE 30th International Symposium on Industrial Electronics (ISIE), Kyoto, Japan, 20–23 June 2021; pp. 1–6. [CrossRef]

33. Renaudineau, H.J.-M.; Bahamonde, F.A.F.; Renaer, S.F.K. Power Inverter. WO2022140874. 2022. Available online: https://patentscope.wipo.int/search/en/detail.jsf?docId=WO2022140874_cid=P22-LSKDAT-98129-1 (accessed on 10 January 2024).
34. Blinov, A.; Korkh, O.; Chub, A.; Vinnikov, D.; Peftitsis, D.; Norrga, S.; Galkin, I. High Gain DC–AC High-Frequency Link Inverter with Improved Quasi-Resonant Modulation. *IEEE Trans. Ind. Electron.* **2022**, *69*, 1465–1476. [CrossRef]

Patents XII

R. Saltanovs, I. Galkins, **A. Bubovičs**, A. Blinov, D. Peftitsis, SISTĒMA UN METODE LĪDZSPRIEGUMA UZKRĀJĒJA UN MAIŅSPRIEGUMA TĪKLA SALĀGOŠANAI. Latvijas patenta pieteikums Nr. LVP2023000064. Patenta pieteikuma datums 12.07.2023.

SISTĒMA UN METODE LĪDZSPRIEGUMA UZKRĀJĒJA UN MAIŅSPRIEGUMA TĪKLA SALĀGOŠANAI

[001] Izgudrojums attiecas uz elektrotehnikas, elektronikas, informācijas un komunikāciju tehnoloģijas nozari un tās energoelektronikas apakšnozari, konkrēti uz līdzsprieguma enerģijas avotu un maiņsprieguma tīkla salāgojošiem pārveidotājiem. Izgudrojums var tikt izmantots akumulatoru bateriju, superkondensatoru un citu līdzsprieguma uzkrājēju pievienošanai pie standarta maiņsprieguma tīkla.

Zināmais tehnikas līmenis

[002] Pastāv divas tendences energoelektronikas pārveidotāju konstruēšanas jomā. Pirmā skar daļējas jaudas pārveidotāju (no angļu valodas *partial power converters*) izmantošanu līdzsprieguma sistēmās, bet otrā – divu posmu līdzsprieguma-maiņsprieguma pārveidotāju tīkla interfeisa iedarbināšanu zemfrekvences režīmā pārnesot augstfrekvences komutācijas pārveidotāja regulatorā (no angļu valodas *unfolding inverters*).

[003] Atšķirībā no pilnas jaudas līdzsprieguma pārveidotajiem, kas ir pieslēgti pie pilna ieejas/izejas sprieguma un kuri vada pilnu strāvu un pārveido pilnu sistēmas jaudu, daļējas jaudas pārveidotāji (DJP) ir pieslēgti starp sistēmas ieeju un izeju tā, ka pārveidotājs apstrādā tikai ieejas un izejas spriegumu (strāvu) starpību un pārveido tikai daļu no pilnas sistēmas jaudas, kamēr tās pārējā daļa tiek pārraidīta bez pārveidotāja starpniecības [1]. DJP priekšrocības ir šādas: 1) zemāka pārveidotāja komutējamā strāva un spriegums, kas ļauj izvēlēties lētākus un kompaktākus pusvadītāju slēdžus (tranzistorus un diodes); 2) zemāki pārveidotāja zudumi (kurus nosaka zemāka pārveidotāja jauda), kas būtiski uzlabo kopējo energoefektivitāti un atvieglo dzesēšanu. Jo mazāku spriegumu/strāvu starpību apstrādā pārveidotājs jo izteiktākas ir minētas priekšrocības. DJP izmanto lai kompensētu kāda enerģijas avota/uzkrājēja, to skaitā, baterijas vai superkondensatora, sprieguma vai strāvas samazināšanu to darbības laikā. Piemēram, baterijas sprieguma samazināšana tai izlādējoties var tikt kompensēta ar DJP, kura ieeja ir pieslēgta pie baterijas paralēli, bet izeja – virknē (tā ir izejas spriegums veidojas kā baterijas un DJP spriegumu summa). Tad DJP ģenerē izejā baterijas maksimālā un tekošā sprieguma starpību, stādā ar samazinātu ieejas strāvu un pārveido daļēju jaudu. Ir zināmi vienpolārie DJP, kas var tikai piesummēt (vai atņemt) savu spriegumu (strāvu)

pie kopējā. Ir zināmi arī bipolārie DJP, kuru izmantošana ļauj samazināt kontrolējamo spriegumu/strāvu/jaudu divreiz salīdzinājumā ar vienpolāro DJP izmantošanu [2]. Bipolāro DJP izmantošana pie tiem pašiem slēdžu un zudumu parametriem ļauj divreiz palielināt kompensējamā sprieguma/strāvas diapazonu. Piemērām, minētajā piemērā ar bateriju, bipolārais DJP kontrolējot pusi no sistēmas jaudas varētu kompensēt baterijas sprieguma samazinājumu līdz pusei. Shematiski DJP ir jebkuras topoloģijas līdzsprieguma pārveidotājs. Vienpolārais DJP tipiski ir divkāršs aktīvais tilts – DAT (no angļu valodas *Dual Active Bridge*), bet zināmas arī citas shēmas. Piemērām, informācijas avotā [3] ir minēts atpakaļgaitas pārveidotājs (no angļu valodas *flyback*) un pārveidotājs ar vienu tiltu un divu taktu shēmu (no angļu valodas *Push-Pull*). Bipolārajos DJP viena pārveidotāja puse ir aprīkota ar divu virzienu slēdžiem. Piemēram, informācijas avotā [4] ir aprakstīts DJP ar bipolāru divu taktu shēmu, bet informācijas avotā [5] – DAT, kur otrais tilts arī ir bipolārs. Ir zināmas arī citas shēmas, piemēram, shēmas ar shēmtehniskiem uzlabojumiem zudumu samazināšanai, to skaitā, DAT ar otro bipolāru tiltu un rezonanses ķēdītēm [6]. Tomēr, visi minētie DJP [2–6] bez papildu komutācijas elementiem vai shēmām, kas nodrošina gala sprieguma polaritātes maiņu, kā arī bez speciālās dinamiskas vadības, kas nodrošina gala sprieguma pareizu fāzi amplitūdu un frekvenci, ir paredzēti izmantošanai tikai līdzsprieguma/līdzstrāvas sistēmās uzkrājēju savienošanai ar līdzsprieguma tīklu, bet nevar tikt lietoti sistēmās ar maiņspriegumu.

[004] Otrā no energoelektronikas attīstības tendencēm izgudrojuma jomā atteicās uz maiņsprieguma/maiņstrāvas formēšanas principiem divu posmu līdzsprieguma-maiņsprieguma pārveidotājos (DPLMP), kur pirmais posms ir līdzsprieguma/līdzstrāvas regulators, bet otrais – tīkla interfeiss (taisngriezis/invertors). Abi posmi ir savienoti caur līdzsprieguma kopni. Tradicionāli līdzsprieguma/līdzstrāvas regulators – impulsa shēma, kas kompensē kāda enerģijas avota līdzsprieguma/līdzstrāvas izmaiņas (to skaitā tas var būt arī DJP). Savukārt tīkla interfeiss no kopnes līdzsprieguma/līdzstrāvas uzformē tīkla maiņspriegumu/maiņstrāvu (sinusoīdu). Tas darbojas kā otrā impulsa shēma ar augstu komutācijas frekvenci, kas lēnam uzformē mainīgo bipolāro izejas spriegumu/strāvu. Alternatīvais maiņsprieguma/maiņstrāvas formēšanas princips paredz, ka regulators ne tikai kompensē enerģijas avota līdzsprieguma/līdzstrāvas izmaiņas, bet arī uzformē pus-sinusoīdu kopnē. Līdz ar to kopnes spriegums/strāva ir pulsējošā, bet tīkla interfeiss tikai komutē šos impulsus pie tīkla ar iepriekš noteiktu polaritāti un tīkla zemu frekvenci, uzformējot tīkla sinusoīdu [7] vai darbojas kā zemfrekvences komutators. Jaudas zudumi šādā zemfrekvences komutatorā tad neietver

komutācijas zudumus un ir daudz zemāki. Šis princips ir attiecināms arī uz trīsfāžu sistēmām [8].

[005] Līdz ar to, ja DPLMP kopne ir pulsējošā, tad regulatoram ir jāformē spriegums/strāva pilnā diapazonā no nulles līdz tīkla sprieguma/strāvas amplitūdai. Tādejādi, ja DPLMP kopne ir pulsējošā, interfeisam ir mazāki zudumi, bet regulators ar pilnas jaudas shēmu saražo vairāk zudumu. Savukārt, ja DPLMP kopne ir stabilizēta, tad otrādi, regulators var būt arī DJP ar mazākiem zudumiem, bet otrajā impulsa shēmā (interfeisā) veidojas papildu (komutācijas) zudumi. Abos gadījumos DPLMP energoefektivitāte nav tik augstā, cik tā varētu būt izmantojot konfigurāciju gan ar pulsējošu kopni, gan ar DJP.

[006] Patentā [9] un rakstā [10] ir aprakstīts invertors ar DJP, pulsējošu kopni un zemfrekvences tīkla interfeisu (1. zīm.) – šīs risinājums ir pieņemts par izgudrojuma prototipu. Šī invertora zemfrekvences tīkla interfeiss vai zemfrekvences komutators (4) iekļauj tikai tranzistoru tiltu (4a), kas sastāv no tranzistoriem (4aa), (4ab), (4ac) un (4ad). Savukārt daļējas jaudas pārveidošanu veic izolējošs vienvirziena vienpolārs līdzsprieguma pārveidotājs (22), kas sastāv no tranzistoru tilta (22a) (tranzistori: (22a), (22b), (22c) un (22d)), diožu tilta (22d) (diodes (22da), (22db), (22dc) un (22dd)) un augstfrekvences transformatora (22n). Līdzsprieguma pārveidotāja diožu tilta (22d) līdzsprieguma kontakti ir pievienoti paralēli (caur strāvas formējošu spoli (4e)) pie tīkla interfeisa vai zemfrekvences komutatora (4), bet tranzistoru tilta (22a) līdzsprieguma kontakti ir savienoti virknē ar enerģijas avotu (6) un ir pieslēgti pie pārveidotāja izejas. Taču šīs invertors ir paredzēts fotoelektrisko pārveidotāju (saules paneļu) pievienošanai pie maiņsprieguma tīkla. Līdz ar to tas nenodrošina divu virzienu darbību un nav izmantojams kopā ar enerģijas uzkrājējiem.

Izgudrojuma mērķis un būtība

[007] Izgudrojuma mērķis ir samazināt jaudas zudumus līdzsprieguma uzkrājēja un maiņsprieguma tīkla salāgojošā pārveidotājā, izmantojot zemfrekvences tīkla interfeisu un daļējas jaudas pārveidošanas principu (atšķirībā no zināmiem salāgojošiem pārveidotājiem ar pilnas jaudas regulatoru), kā arī nodrošināt tā pilnu funkcionālu divu virzienu darbību (atšķirībā no zināmiem alternatīvo enerģijas avotu salāgojošiem pārveidotājiem).

[008] Izgudrojuma mērķis ir sasniegts ar jaunu energoelektronikas pārveidotāju sistēmu, kurā ir apvienots divvirzienu zemfrekvences tīkla interfeiss, divvirzienu bipolārs daļējas jaudas sprieguma regulators un pulsējoša līdzsprieguma kopne ar pus-sinusoidāliem sprieguma

impulsiem, kā arī ar šīs sistēmas jaunu dinamisku vadību, kas nodrošina sistēmas daļu, baterijas un tīkla savstarpēji sinhronizētu darbību.

[009] Tīkla interfeisa zema (tīkla) komutācijas frekvence būtiski samazina šī interfeisa komutācijas zudumus. Regulatora darbība ar nepilnu jaudu būtiski samazina šī regulatora gan vadāmības un gan komutācijas zudumus. Uzlādējot bateriju, patiecoties samazinātiem jaudas zudumiem sistēmas pārveidotājos, lielāka no tīkla patērētas enerģijas daļa nonāk uzkrājējā. Līdzīgi, slogojot bateriju, pateicoties mazākiem jaudas zudumiem sistēmā, lielāka uzkrātas enerģijas daļa atgriežas tīklā. Rezultātā palielinās enerģijas uzkrāšanas sistēmas ar baterijām kopējā energoefektivitāte.

[010] Daļējas jaudas pārveidošanas principa īstenošana maiņsprieguma sistēmā kļūst iespējama kombinējot daļējas jaudas regulatoru ar diviem vai vairākiem zemfrekvences komutatoriem un salāgojot to darbību ņemot vērā gan baterijas uzlādes pakāpi (baterijas spriegumu) gan tīkla fāzi (tīkla momentānu spriegumu), kā arī kombinējot daļējas jaudas regulatoru ar diviem vai vairākiem zemfrekvences komutatoriem. Līdz šim zināmie DJP [1–6] kaut arī ļauj daļējas jaudas posmā ģenerēt gan pozitīvu, gan negatīvu spriegumu, nav paredzēti maiņsprieguma apstrādei, jo salāgo regulatora darbību tikai ar baterijas uzlādes pakāpi.

[011] Līdzsprieguma uzkrājēja un maiņsprieguma tīkla salāgojošās pārveidotāju sistēmas (turpmāk tekstā – izgudrojuma sistēma) primārajā konfigurācijā (2. zīm.) ietilpst līdzsprieguma uzkrājējs (LU) (1), izolējošs daļējas jaudas divvirzienu bipolārs līdzsprieguma pārveidotājs (DBLP) (2), līdzsprieguma kopnes (3) zemfrekvences komutators (ZK) (4) un maiņsprieguma tīkls (MT) (5). Izolējošs daļējas jaudas DBLP (2) ir četrpols, kura ieeja ir savienota ar LU (1) paralēli, bet izeja – virknē. LU (1) un izolējošā daļējas jaudas DBLP (2) virknes savienojums ir paralēli pieslēgts pie zemfrekvences komutatora (4). Izolējošs daļējas jaudas DBLP (2) var tikt uzbūvēts kā jebkura izolētā divu virzienu bipolārā shēma, to skaitā, kā shēma ar atvieglotu komutāciju ar rezonanses komutācijas kontūriem.

[012] Izgudrojuma sistēmas darbībā var izdalīt divus režīmus: LU (1) uzlādes režīms un slogošanas režīms. LU (1) uzlādēs režīmā zemfrekvences komutators (4) darbojas kā diožu taisngriezis un no tīkla sprieguma $v_s(t)$ līdzsprieguma kopnē (3) veido spriegumu $v_{dc}(t)$, kas sastādās no sinusoīdas pozitīviem pusviļņiem. Līdzsprieguma kopnes (3) pulsējošā sprieguma un LU (1) līdzsprieguma starpība $v_{ppc,dc}(t)$ ir tie paši sinusoīdas pusvilni, taču ar negatīvu nobīdi par uzkrājēja sprieguma vērtību. Spriegumu starpība sastādās no sinusoīdas pusvilnu augšējām daļām ar pozitīvu polaritāti un sinusoīdas pusvilnu apakšējām daļām ar negatīvu polaritāti. Šī

spriegumu starpība ar DBLP pārveidotāja palīdzību ir vēlreiz iztaisnotā un paaugstināta virs uzkrājēja sprieguma vērtības V_{bat}.

[013] Savukārt uzkrājēja slogošanas režīmā DBLP pārveidotājs 2 no uzkrājēja sprieguma V_{bat} uzformē pulsējošu spriegumu no sinusoīdas pusviļņiem ar negatīvu nobīdi $v_{ppc,dc}(t)$ (7. zīm.). Šīs spriegums kopā ar LU (1) spriegumu veido sinusoīdas pusviļņus $v_{dc}(t)$ (8. zīm.) kopnē (3), kas ar komutatora (4) palīdzību uzformē tīklā sinusoīdu $v_s(t)$ (10. zīm.). Tādējādi LU (1) slogošanas režīmā viss notiek otrādi salīdzinot ar uzlādes režīmu.

[014] Saskaņā ar izgudrojuma īstenošanas otro variantu (3. zīm.) sistēma ietver izolējošo daļējas jaudas divvirzienu vienpolāro līdzsprieguma pārveidotāju (DVLP) (21), kas var ģenerēt tikai vienas polaritātes spriegumu $v_{ppc,int}(t)$ (6. zīm.) papildu līdzsprieguma kopni (23), un papildu zemfrekvences komutatoru (24), kas nodrošina izolējošā daļējas jaudas DVLP (21) sprieguma polaritātes maiņu sintezējot spriegumu $v_{ppc,dc}(t)$. Pārējie sistēmas elementi (LU (1), līdzsprieguma kopnes komutators (4) un maiņsprieguma tīkls (5)) un to savstarpējie savienojumi paliek bez izmaiņas.

[015] Izgudrojuma īstenošanas otro varianta darbību raksturo tas, ka izolējošs daļējas jaudas DVLP (21), papildu līdzsprieguma kopne (23) un papildu zemfrekvences komutators (24) kopā aizvieto primāras konfigurācijas izolējošo daļējas jaudas DBLP (2). Līdz ar to LU (1) uzlādēs režīmā komutators (24) sākumā papildus iztaisno papildu līdzsprieguma kopnes (23) pulsējošā sprieguma un LU (1) līdzsprieguma starpību $v_{ppc,dc}(t)$ (7. zīm.), iegūstot $v_{ppc,int}(t)$ (6. zīm.). Tad izolējošs daļējas jaudas DVLP (21) sintezē LU (1) spriegumu $V_{BAT}=v_{PPC1}(t)$. Savukārt LU (1) slogošanas režīmā sākumā izolējošs daļējas jaudas DVLP (21) sintēzē $v_{ppc,int}(t)$ (6. zīm.), tad zemfrekvences komutators (24) uzformē no tā $v_{ppc,dc}(t)$ (7. zīm.).

[016] Izgudrojuma īstenošanas trešais un ceturtais variants ietver divus vienvirziena daļējas jaudas pārveidotājus. Variants bez papildu zemfrekvences komutatora (24) un bez papildu līdzsprieguma kopnes (23) (4. zīm.) balstās uz vienvirziena bipolāriem līdzsprieguma pārveidotājiem (26) un (25), bet variants ar papildu komutatoru (24) un papildu līdzsprieguma kopni (23) (5. zīm.) iekļauj vienvirziena vienpolārus līdzsprieguma pārveidotājus (VVLP) (216) un (215). Šo konfigurāciju darbība izceļas ar to, ka vienvirziena bipolārs līdzsprieguma pārveidotājs (26) un VVLP (216) darbojas tikai LU (1) uzlādēs laikā, bet vienvirziena bipolārs līdzsprieguma pārveidotājs (25) un VVLP (215) – tikai LU (1) slogošanas laikā. Tas divreiz samazina pusvadītāju slēdžu skaitu katrā strāvas kontūrā un attiecīgus jaudas zudumus, kā arī ļauj optimizēt šo pārveidotāju ((26) un (25) vai (216) un (215)) konstrukcijas.

[017] Izgudrojums paskaidrots ar šādiem zīmējumiem:

1. zīm. Invertors ar DJP un zemfrekvences tīkla interfeisu (prototips): vienvirziena vienpolārs līdzsprieguma pārveidotājs (22), kas ietver tranzistoru tiltu (22a) (tranzistori (22aa), (22ab), (22ac), (22ad)), diožu tiltu (22d) (diodes (22da), (22db), (22dc), (22dd)) un augstfrekvences transformatoru (22n); zemfrekvences komutators (4) (tranzistori (4aa), (4ab), (4ac), (4ad)); strāvas formējošā spole (4e); enerģijas avots (6) (fotoelektriskais enerģijas pārveidotājs).

2. zīm. Izgudrojuma sistēmas konfigurācija ar vienu zemfrekvences komutatoru: līdzsprieguma uzkrājējs (1); izolējošs daļējas jaudas DBLP (2); līdzsprieguma kopne (3) (līdzsprieguma posms); zemfrekvences komutators (4); maiņsprieguma tīkls (5).

3. zīm. Izgudrojuma sistēmas konfigurācija ar diviem zemfrekvences komutatoriem: līdzsprieguma uzkrājējs (1); izolējošs daļējas jaudas divvirzienu vienpolārs līdzsprieguma pārveidotājs (21); papildu līdzsprieguma kopne (23); zemfrekvences komutators (24); līdzsprieguma kopne (3); zemfrekvences komutators (4); maiņsprieguma tīkls (5).

4. zīm. Izgudrojuma sistēmas konfigurācija ar diviem vienvirziena bipolāriem līdzsprieguma pārveidotājiem un vienu zemfrekvences komutatoru: līdzsprieguma uzkrājējs (1); vienvirziena bipolārs līdzsprieguma pārveidotājs (25) (kas strādā pie baterijas slogošanas); vienvirziena bipolārs līdzsprieguma pārveidotājs (26) (kas strādā pie baterijas izlādes); līdzsprieguma kopne (3) (līdzsprieguma posms); zemfrekvences komutators (4); maiņsprieguma tīkls (5).

5. zīm. Izgudrojuma sistēmas konfigurācija ar diviem vienvirziena vienpolāriem līdzsprieguma pārveidotājiem un diviem zemfrekvences komutatoriem: līdzsprieguma uzkrājējs (1); vienvirziena vienpolārs līdzsprieguma pārveidotājs (215) (kas strādā pie baterijas slogošanas); vienvirziena vienpolārs līdzsprieguma pārveidotājs (216) (kas strādā pie baterijas izlādes); papildu līdzsprieguma kopne (23); zemfrekvences komutators (24); līdzsprieguma kopne (3) (līdzsprieguma posms); zemfrekvences komutators (4); maiņsprieguma tīkls (5).

6. zīm. Spriegums papildu līdzsprieguma posmā, gadījumā ja ir izmantoti divi zemfrekvences pārveidotāji.

7. zīm. Līdzsprieguma pārveidotāja spriegums līdzsprieguma posma pusē.

8. zīm. Līdzsprieguma posma spriegums – pulsējošs kvazi-sinusoidāls spriegums.

9a. zīm. Spriegumi un strāva līdzsprieguma posmā, gadījumā, ja strāvas formējošā spole atrodas pie zemfrekvences komutatora līdzsprieguma kontaktiem, kur: $V_{m,dc}$ – sinusoīdas pusviļņu amplitūda; $V_{m,s}$ – tīkla sprieguma amplitūda; $v_{dc}(t)$ – kvazi-sinusoidāli pulsējošs spriegums; $v_{dc,uf}(t)$ – sinusoīdas pusviļņi, kas atbilst tīkla sprieguma amplitūdai; $v_L(t)$ – spoles spriegums;

$i_{bat}(t)$ – baterijas momentānā strāva; $i_{ppc,dc}(t)$ – DBLP izejas strāva; $i_L(t)$ – spoles strāva; $i_{dc}(t)$ – strāva līdzsprieguma kopnē.

9b. zīm. Spriegums un strāva līdzsprieguma kopnē, gadījumā, ja strāvas formējošā spole atrodas pie zemfrekvences komutatora maiņsprieguma kontaktiem, kur: $V_{m,dc}$ – sinusoīdas pusviļņu amplitūda; $v_{dc}(t)$ – kvazi-sinusoidāli pulsējošs spriegums; $v_{dc,uf}(t)$ – sinusoīdas pusviļņi, kas atbilst tīkla sprieguma amplitūdai; $i_{bat}(t)$ – baterijas momentānā strāva; $i_{ppc,dc}(t)$ – DBLP izejas strāva; $i_{dc}(t)$ – strāva līdzsprieguma kopnē.

10a. zīm. Spriegums un strāva tikla pusē, gadījumā, ja strāvas formējošā spole atrodas pie zemfrekvences komutatora līdzsprieguma kontaktiem, kur: $V_{m,s}$ – tīkla sprieguma amplitūda; $v_{ac}(t)$ – komutatora spriegums tīkla kontaktos; $v_s(t)=v_{ac}(t)$ – tīkla spriegums; $i_{ac}(t)$ – komutatora strāva tīkla kontaktos; $i_s(t)$ – tīkla strāva.

10b. zīm. Spriegumi un strāva tikla pusē, gadījumā, ja strāvas formējošā spole atrodas pie zemfrekvences komutatora maiņsprieguma kontaktiem, kur: $V_{m,s}$ – tīkla sprieguma amplitūda; $V_{m,dc}$ – sinusoīdas pusviļņu amplitūda; $v_{ac}(t)$ – komutatora spriegums tīkla kontaktos; $v_s(t)\neq v_{ac}(t)$ – tīkla spriegums; $v_L(t)$ – spoles spriegums; $i_{ac}(t)$ – komutatora strāva tīkla kontaktos; $i_s(t)$ – tīkla strāva; $i_L(t)$ – spoles strāva.

11. zīm. Izgudrojuma īstenošanas piemērs ar izolējošo daļējās jaudas DBLP (ar bipolāriem slēdžiem līdzsprieguma posma pusē) un zemfrekvences komutatoru (ar bipolāriem slēdžiem) – gadījums, kad strāvas formējošā spole ir līdzsprieguma kopnes pusē: līdzsprieguma uzkrājējs (1); izolējošs daļējas jaudas DBLP (2); DBLP baterijas puses kontakti (2v) un (2w); līdzsprieguma puses kontakti (2y) un (2z); tranzistoru tilts (2a) (tranzistori (2aa), (2ab), (2ac), (2ad)); līdzsprieguma posma puses ir divu virzienu tilts (2x) (tranzistori (2ba), (2ca), (2bb), (2cb), (2bc), (2cc), (2bd) un (2cd)); spole (2m); augstfrekvences transformators (2n); līdzsprieguma kopne (3); zemfrekvences komutators (4); zemfrekvences komutatora kontakti (4v) un (4w) līdzsprieguma kopnes pusē; komutatora kontakti (4y) un (4z) maiņsprieguma kopnes pusē; komutatora divu virzienu elektronisko slēdžu tilts (4a) (tranzistori (4aa), (4ab), (4ac), (4ad)); strāvas formējošā spole (4e); strāvas formējošas spoles kontakts (4u) komutatora pusē; maiņsprieguma tīkls (5).

12. zīm. Izgudrojuma īstenošanas piemērs ar izolējošo daļējās jaudas DBLP (ar bipolāriem slēdžiem līdzsprieguma posma pusē) un zemfrekvences komutatoru (ar bipolāriem slēdžiem) – gadījums, kad strāvas formējošā spole ir MT pusē: līdzsprieguma uzkrājējs (1); izolējošs daļējas jaudas DBLP (2); DBLP baterijas puses kontakti (2v) un (2w); līdzsprieguma puses kontakti

(2y) un (2z); tranzistoru tilts (2a) (tranzistori (2aa), (2ab), (2ac), (2ad)); līdzsprieguma posma puses ir divu virzienu tilts (2x) (tranzistori (2ba), (2ca), (2bb), (2cb), (2bc), (2cc), (2bd) un (2cd)); spole (2m); augstfrekvences transformators (2n); līdzsprieguma kopne (3); zemfrekvences komutators (4); zemfrekvences komutatora kontakti (4v) un (4w) līdzsprieguma kopnes (3) pusē; komutatora kontakti (4y) un (4z) maiņsprieguma kopnes pusē; zemfrekvences komutatora (4) divu virzienu elektronisko slēdžu tilts (4x) (tranzistori (4ba), (4ca), (4bb), (4cb), (4bc), (4cc), (4bd) un (4cd)); strāvas formējošā spole (4e); strāvas formējošas spoles (4e) kontakts (4u) zemfrekvences komutatora (4) pusē; maiņsprieguma tīkls (5).

13. zīm. Izgudrojuma īstenošanas piemērs ar izolējošs daļējas jaudas DVLP diviem un zemfrekvences komutatoriem uz divkāršā aktīvā tilta bāzes: līdzsprieguma uzkrājējs (1); izolējošs daļējas jaudas DVLP (21); DBLP baterijas puses kontakti (21v) un (21w); līdzsprieguma puses kontakti (21y) un (21z); tranzistoru tilts (21a) (tranzistori (21aa), (21ab), (21ac), (21ad)); līdzsprieguma posma puses tranzistoru tilts (21b) (tranzistori (21ba), (21bb), (21bc), (21bd)); spole (21m); augstfrekvences transformators (21n); iekšējā līdzsprieguma kopne (23); papildu zemfrekvences komutators (24) (tranzistoru tilts (24a) ar tranzistoriem (24aa), (24ab), (24ac), (24ad)); papildu zemfrekvences komutatora kontakti (24v), (24w, (24y) un (24z); līdzsprieguma kopne (3); zemfrekvences komutators (4); zemfrekvences komutatora kontakti (4v) un (4w) līdzsprieguma kopnes pusē; komutatora kontakti (4y) un (4z) maiņsprieguma kopnes pusē; komutatora tranzistoru tilts (4a) (tranzistori (4aa), (4ab), (4ac) un (4ad)); strāvas formējošā spole (4e); strāvas formējošas spoles kontakts (4u) komutatora pusē; maiņsprieguma tīkls (5).

14. zīm. Izgudrojuma īstenošanas piemērs ar izolējošo daļējas jaudas DVLP un diviem zemfrekvences komutatoriem uz divvirzienu reversīvās gaitas pārveidotāja bāzes: līdzsprieguma uzkrājējs (1); izolējošs daļējas jaudas DVLP (21); izolējošā daļējas jaudas DVLP baterijas puses kontakti (21v) un (21w); līdzsprieguma puses kontakti (21y) un (21z); divvirzienu reversīvās gaitas pārveidotāja tranzistori (21ax) un (21bx); augstfrekvences transformators (2n); iekšējā līdzsprieguma kopne (23); papildu zemfrekvences komutators (24) (tranzistoru tilts (24a) ar tranzistoriem (24aa), (24ab), (24ac), (24ad)); papildu zemfrekvences komutatora kontakti (24v), (24w), (24y) un (24z); līdzsprieguma kopne (3); zemfrekvences komutators (4); zemfrekvences komutatora kontakti (4v) un (4w) līdzsprieguma kopnes pusē; komutatora kontakti (4y) un (4z) maiņsprieguma kopnes pusē; komutatora tranzistoru tilts (4a)

(tranzistori (4aa), (4ab), (4ac) un (4ad)); strāvas formējošā spole (4e); strāvas formējošas spoles kontakts (4u) komutatora pusē; maiņsprieguma tīkls (5).

Izgudrojuma īstenošanas piemēri

[018] Izgudrojuma īstenošanas piemērs ar daļējas jaudas DBLP atbilstoši funkcionālai shēmai no 2. zīmējuma ir parādīts 11. zīmējumā. Saskaņā ar šo īstenošanas piemēru sistēmas regulatora sastāvā baterijas puse (kontakti (2v) un (2w)) ir tranzistoru tilts (2a), bet līdzsprieguma posma pusē ir divu virzienu elektronisko slēdžu tilts (2x) (tranzistori (2ba), (2ca), (2bb), (2cb), (2bc), (2cc), (2db) un (2dc)). Tranzistoru (2aa), (2ab), (2ac) un (2ad) saskaņota darbība ar tranzistoriem (2ba), (2bb), (2bc) un (2bd) ļauj sintezēt DBLP līdzsprieguma posma pusē sprieguma $v_{ppc,dc}(t)$ pozitīvu daļu. Savukārt, tranzistori (2aa), (2ab), (2ac) un (2ad) strādājot saskaņoti ar (2ca), (2cb), (2cc) un (2dc) ļauj ģenerēt sprieguma $v_{ppc.dc}(t)$ negatīvu daļu. Tādejādi DBLP ar dinamisku vadību līdzsprieguma posma pusē ģenerē spriegumu, kas atbilst iztaisnotam tīkla spriegumam ar negatīvu nobīdi par baterijas sprieguma vērtību (7. zīm.). Sakarā ar to, ka DBLP maiņsprieguma kontakti (2y) un (2z) ir savienoti virknē ar LU (1), to kopējas spriegums ir DBLP un baterijas spriegumu summa, kas atbilst iztaisnotam tīkla spriegumam bez nobīdes – kvazi-sinusoidāli pulsējošam līdzspriegumam $v_{dc}(t)$ (8. zīm.).

[019] Bez izolējošā daļējas jaudas DBLP (2), sistēmas piemēra konfigurācijā ietilpst vēl zemfrekvences komutators (4). Tā tranzistoru tilts ((4a) vai (4x)) savieno vienā kontūrā balasta induktivitātes spoli (4e), līdzsprieguma kopni (3) un maiņsprieguma tīklu (5). Zemfrekvences komutatora (4) darbība atšķiras, atkarībā no induktivitātes spoles (4e) pieslēgšanas vietas – tranzistoru tilta (4a) vai (4x) līdzsprieguma vai maiņsprieguma pusē.

[020] Ja induktivitātes spole (4e) atrodas pie zemfrekvences komutatora (4) līdzsprieguma kontaktiem (4v) un (4w) (11. zīm.), tad tranzistoru tilts (4a) uzformē spoles kontaktā (4u) sinusoīdas pusviļņus $v_{dc,uf}(t)$ atbilstoši iztaisnotam tīkla spriegumam (9a. zīm. – raustīta līkne spriegumu diagrammā). Tikmēr induktivitātes spoles kontaktā (4v) līdzsprieguma pārveidotājs (2) uzformē sinusoīdas pusviļņus $v_{dc}(t)$ ar nobīdi θ un amplitūdu $V_{m,dc} = \sqrt{V_{m,s}^2 + (2\pi f \cdot L_s \cdot I_s)^2}$ kur: L_s – pielietotas balasta spoles induktivitāte, I_s – tīkla strāvas uzdota efektīvā vērtība, $V_{m,s}$ – tīkla sprieguma amplitūda (9a. zīm. – nepārtraukta līkne spriegumu diagrammā). Pie šiem nosacījumiem spoles spriegumam $v_L(t)$ ir $\pm 90^0$ nobīde no iztaisnota tīkla sprieguma (9a. zīm. – svītrpunktu līkne spriegumu diagrammā). Ja izolējošā daļējas jaudas DBLP (2) sinusoīdas

pusviļņu nobīde θ ir pozitīva, tad arī induktivitātes spoles (4e) sprieguma nobīde ir pozitīvā ($+90^0$), tad induktivitātes spoles (4e) strāvas impulsi ir ar pozitīvu polaritāti (9a. zīm. – strāvu diagramma). Šis gadījums atbilst līdzsprieguma uzkrājēja (1) slogošanai jeb enerģijas patēriņam no uzkrājēja (šis gadījums ir attēlots 9a. zīm.). Ja izolējošā daļējas jaudas DBLP (2) sinusoīdas pusviļņu nobīde θ ir negatīva, induktivitātes spoles (4e) sprieguma nobīde ir -90^0, tad strāvā arī ir negatīvā, bet gadījums atbilst līdzsprieguma uzkrājēja (1) uzlādei. Šīs konfigurācijas gadījumā zemfrekvences komutatora (4) spriegums maiņsprieguma tiklā (5) kontaktos (4y) un (4z) sakrīt ar maiņsprieguma tīkla (5) spriegumu (10a. zīm.).

[021] Ja induktivitātes spole (4e) atrodas pie zemfrekvences komutatora (4) maiņsprieguma kontaktiem (4y) un (4z) (12. zīm.), tad līdzsprieguma posma spriegums $v_{dc}(t)$ sakrīt ar zemfrekvences komutatora (4) spriegumu tā līdzsprieguma kontaktos (4v) un (4w) (9b. zīm.). Zemfrekvences komutators (4) tad pievieno šos nobīdītus sinusoīdas pusviļņus $v_{dc}(t)$ pie induktivitātes spoles (4e) kontakta (4u) katru pusperiodu ar citu polaritāti sintezējot nobīdītu pilnu sinusoīdu (10b. zīm. – nepārtraukta līkne spriegumu diagrammā). Šī sprieguma un kontakta (4y) tīkla sinusoidāla sprieguma (10b. zīm. – raustīta līkne spriegumu diagrammā) starpība formē spoles spriegumu (10b. zīm. – svītrpunktu līkne spriegumu diagrammā), kas ir nobīdīts par $\pm 90^0$ no tīkla sprieguma. Tas ierosina sinusoidālu strāvu spolē. Ja nobīdes leņķi ir pozitīvi tīkla (spoles) strāva ir fāzē ar spriegumu un notiek uzkrājēja slogošana. Pretējā gadījuma strāva ir pretfāzē ar spriegumu un notiek uzkrājēja uzlāde. Līdz ar to, ka līdzsprieguma posma spriegumam ir arī negatīvas vērtības, šīs konfigurācijas gadījumā zemfrekvences komutators (4) sastāv no divu virzienu/divu tranzistoru slēdžiem (tranzistoru tilts (4x) (tranzistori: (4ba), (4bb), (4bc), (4bd) un (4ca), (4cb), (4cc), (4cd)), kas vadāmi atsevišķi katrai sprieguma polaritātei.

[022] DBLP var tikt izveidots uz izolējoša daļējas jaudas DVLP (21) pamata ar papildu zemfrekvences komutatora (24) palīdzību (13. zīm.). Šādā konfigurācija izolējošs daļējas jaudas DVLP (21) veido laika manīgu pozitīvu līdzspriegumu (6. zīm.), bet ZK (4) nosaka šī sprieguma zīmi uzformējot sprieguma likni, kas atbilst iztaisnotam tīkla spriegumam ar nobīdi par baterijas sprieguma vērtību (7. zīm.). Izolējošs daļējas jaudas DVLP, kas ir parādīts 13. zīmējumā, ir divkāršu aktīvais tranzistoru tilts, taču tā vietā varētu tikt izmantota jebkura divvirzienu līdzsprieguma pārveidotāja shēma ar izolējošo elementu (transformatoru), piemēram, divvirzienu reversīvas gaitas pārveidotājs (14. zīm.) vai divu taktu shēma ar transformatoru.

Informācijas avoti

1. J. Anzola et al., “Review of Architectures Based on Partial Power Processing for DC-DC Applications,” IEEE Access, vol. 8, pp. 103405–103418, 2020, doi: 10.1109/ACCESS.2020.2999062.

2. J. R. R. Zientarski, M. L. Da Silva Martins, J. R. Pinheiro, and H. L. Hey, “Series-Connected Partial-Power Converters Applied to PV Systems: A Design Approach Based on Step-Up/Down Voltage Regulation Range,” IEEE Trans. Power Electron., vol. 33, no. 9, pp. 7622–7633, 2018, doi: 10.1109/TPEL.2017.2765928.

3. J. R. R. Zientarski, M. L. da Silva Martins, J. R. Pinheiro, and H. L. Hey, “Evaluation of Power Processing in Series-Connected Partial-Power Converters,” IEEE J. Emerg. Sel. Top. Power Electron., vol. 7, no. 1, pp. 343–352, Mar. 2019, doi: 10.1109/JESTPE.2018.2869370.

4. A. Elasser, M. Agamy, and K. K. Huh, “System and Method for a DC/DC Converter,” US9960687B2, 2018

5. K. Iwaya, T. Miyazaki, and K. Shoji, “Series Compensating Electric Power Transmission System,” US10116221, 2016

6. A. Blinov, A. Chub, O. Korkh, D. Vinnikov, I. Galkins, and D. Peftitsis, “System and Method for Transmitting Power Between Two DC Sources,” EE202000020A, 2020 [Online]. Available: https://www1.epa.ee/patent/kirjeldus/P202000020.pdf

7. O. Husev, O. Matiushkin, C. Roncero-Clemente, F. Blaabjerg, and D. Vinnikov, “Novel Family of Single-Stage Buck–Boost Inverters Based on Unfolding Circuit,” IEEE Trans. Power Electron., vol. 34, no. 8, pp. 7662–7676, Aug. 2019, doi: 10.1109/TPEL.2018.2879776.

8. J. Rabkowski, A. Blinov, D. Zinchenko, G. Wrona, and M. Zdanowski, “Grid-frequency Vienna rectifier and isolated current-source DC-DC converters for efficient off-board charging of electric vehicles,” in 2020 22nd European Conference on Power Electronics and Applications (EPE’20 ECCE Europe), Sep. 2020, p. P.1-P.10. doi: 10.23919/EPE20ECCEEurope43536.2020.9215772.

9. H. J.-M. Renaudineau, F. A. Flores Bahamonde, and S. F. Kouro Renaer, “Power Inverter,” WO2022140874A1, 2022

10. H. Renaudineau, F. Flores-Bahamonde, S. Kouro, and J. W. Zapata, “Single-Phase partial power unfolding inverter for photovoltaic string application,” in 2021 IEEE 30th International Symposium on Industrial Electronics (ISIE), Jun. 2021, pp. 1–6. doi: 10.1109/ISIE45552.2021.9576479.

PRETENZIJAS

1. Līdzsprieguma uzkrājēja (1) un maiņsprieguma tīkla (5) salāgošanas sistēma, kas ir balstīta uz daļējas jaudas pārveidošanas principa un uz maiņsprieguma tīkla (5) interfeisa pārveidotāja zemfrekvences komutācijas, kas sistēmas daļu apvienošanai izmanto līdzsprieguma posmu ar nestabilizēto pulsējošo spriegumu, kas bez salāgojama līdzsprieguma uzkrājēja (1) un maiņsprieguma tīkla (5) ietver izolējošo daļējas jaudas DBLP (2), kurš vienā pusē ir savienots ar līdzsprieguma uzkrājēju (1) paralēli, bet otrā pusē ir savienots ar līdzsprieguma uzkrājēju (1) virknē, un zemfrekvences komutatoru (4) ar tranzistoru tiltu (4a) vai (4x), ja ir izmantoti divvirzienu slēdži, un balasta induktivitātes spoli (4e), kuri savieno maiņsprieguma tīklu (5) ar zemas kapacitātes līdzsprieguma kopni (3), kas atšķiras ar to, ka izolējošs daļējas jaudas DBLP (2) ir divu strāvas virzienu elektroniska spēka shēma, kura ģenerē abu polaritāšu spriegumu līdzsprieguma kopnes (3) pusē, turklāt pie sistēmas līdzsprieguma kopnes (3) ir pieslēgts līdzsprieguma uzkrājēja (1) un izolējošā daļējas jaudas DBLP (2) virknes savienojums.

2. Sistēma saskaņā ar 1. pretenziju, kas atšķiras ar to, ka izolējošs daļējas jaudas DBLP (2) ietver izolējošo daļējas jaudas DVLP (21), kurš ģenerē pozitīvas polaritātes spriegumu papildu līdzsprieguma kopnē (23), un papildu zemfrekvences komutatoru (24), kurš pieslēdz šo pozitīvas polaritātes spriegumu pie līdzsprieguma kopnes (3) abos virzienos.

3. Sistēma saskaņā ar 1. pretenziju, kas atšķiras ar to, ka izolējošs daļējas jaudas DBLP (2) ietver divas bipolāras spēka shēmas – ar pozitīvu strāvas virzienu (25) un ar negatīvu strāvas virzienu (26).

4. Sistēma saskaņā ar 2. pretenziju, kas atšķiras ar to, ka izolējošs daļējas jaudas DVLP (21) ietver divas vienpolāras spēka shēmas: ar pozitīvu strāvas virzienu (215) un ar negatīvu strāvas virzienu (216).

5. Līdzsprieguma uzkrājēja (1) un maiņsprieguma tīkla (5) salāgošanas metode, kuru realizē sistēma saskaņā ar jebkuru no 1. līdz 4. pretenzijai, kas ietver šādus secīgus soļus:

i) spriegums $v_{dc}(t)$ līdzsprieguma kopnē (3) ir uzformēts kā pulsējošs ar divkāršu tīkla frekvenci enerģijas līdzsprieguma uzkrājēja (1) slogošanas režīmā mainoties saskaņa ar sinusoidālu likni no vērtības $V_1 = V_{m,dc} \cdot \sin\theta$ līdz vērtībai $V_2 = V_{m,dc} \cdot \sin(\theta + \pi)$, kur $V_{m,dc} = \sqrt{V_{m,s}^2 + (2\pi f \cdot L_s \cdot I_s)^2}$ ir līdzsprieguma posma maksimāls spriegums, L_s –lietotas balasta spoles induktivitāte un I_s – tīkla strāvas uzdota efektīvā vērtība, $V_{m,s}$ – tīkla sprieguma amplitūda;

ii) spriegums $v_{dc}(t)$ līdzsprieguma kopnē (3) ir uzformēts kā pulsējošs ar divkāršu tīkla frekvenci enerģijas līdzsprieguma uzkrājēja (1) uzlādes režīmā mainoties saskaņa ar sinusoidālu likni no vērtības $V_1 = V_{m,dc} \cdot \sin(-\theta)$ līdz vērtībai $V_2 = V_{m,dc} \cdot \sin(\pi - \theta)$;

iii) spriegums papildu līdzsprieguma kopnē (23), ja tā ir, ir uzformēts kā pulsējošs ar četrkāršu tīkla frekvenci un sastādās no īsākiem sinusoīdas fragmentiem tā, kā tie kopā, komutējot tos pie līdzsprieguma posma pozitīvā vai negatīvā virziena sastāda spriegumu $v_{ppc,dc}(t)=v_{dc}(t)-V_{bat}$;

iv) zemfrekvences komutators (4) nodrošina līdzsprieguma kopnes (3) pieslēgšanu pie maiņsprieguma tīkla (5) pozitīvā vai negatīvā virzienā, pārveidojot līdzsprieguma kopnes (3) pulsējošo spriegumu (strāvu) par maiņsprieguma tīkla (5) maiņspriegumu (maiņstrāvu) un šī zemfrekvences komutatora (4) slēdži darbojas ar maiņsprieguma tīkla (5) frekvenci, kas samazina šī zemfrekvences komutatora (4) komutācijas zudumus;

v) papildu zemfrekvences komutators (24), ja tas ir, nodrošina papildus līdzsprieguma posma (23) pieslēgšanu pie līdzsprieguma posma (3) pozitīvā vai negatīvā virzienā formējot vēlamu spriegumu $v_{ppc,dc}(t)=v_{dc}(t)-V_{bat}$ un šī zemfrekvences komutatora (4) slēdži darbojas ar maiņsprieguma tīkla (5) frekvenci, kas samazina šī papildu zemfrekvences komutatora (24) komutācijas zudumus;

vi) sistēmu līdzsprieguma pārveidotāji (2) vai (21) ar (24) vai (25) ar (26) vai arī (215) un (216) ar (24) līdzsprieguma kopnes (3) pusē strādā ar nepilnu sistēmas spriegumu, bet līdzsprieguma uzkrājēja (1) pusē – ar nepilnu sistēmas strāvu.

KOPSAVILKUMS

Izgudrojums attiecas uz līdzsprieguma enerģijas avotu un maiņsprieguma tīkla salāgojošiem pārveidotājiem. Izgudrojums piemērots akumulatoru bateriju, superkondensatoru un citu līdzsprieguma uzkrājēju pievienošanai.

Izgudrojuma mērķis ir samazināt jaudas zudumus līdzsprieguma uzkrājēja (1) un maiņsprieguma tīkla (5) salāgojošā pārveidotājā, izmantojot zemfrekvences tīkla komutācijas un daļējās jaudas pārveidošanas principus nodrošināt to pilnu funkcionālu divvirzienu darbību. Izgudrojuma mērķis ir sasniegts ar jaunu energoelektronikas pārveidotāju sistēmu, kas apvieno divvirzienu zemfrekvences komutatoru (4), daļējas jaudas divvirzienu bipolāru sprieguma pārveidotāju (2) un pulsējošu līdzsprieguma kopni (3). Izgudrojumā ietilpst arī līdzsprieguma uzkrājēja (1) un maiņsprieguma tīkla (5) salāgošanas metode, kas uzformē līdzsprieguma posmā (3) pulsējošu spriegumu ar divkāršu tīkla frekvenci, kā arī zemfrekvences komutatora (4) vadība, kas nodrošina līdzsprieguma kopnes (3) pieslēgšanu pie maiņsprieguma tīkla (5).

Tīkla komutatora (4) zema darbības frekvence samazina šī interfeisa komutācijas zudumus. Daļējās jaudas divvirzienu bipolāra sprieguma pārveidotāja (2) darbība ar nepilnu jaudu samazina tā vadāmības un komutācijas zudumus, palielinot enerģijas uzkrāšanas sistēmas energoefektivitāti.

SYSTEM AND METHOD FOR TRANSMITTING POWER BETWEEN DC AND AC SOURCES

The invention regards interface converters for DC energy storages to AC-grid. The invention can be used with batteries, supercapacitors and similar storages.

The aim of the invention is reduction of losses in the interface converter that links a DC energy storage (1) and AC-grid (5) applying the principles of bidirectional unfolding and partial power conversion. This aim is achieved with a new system of power electronic converters that combines bidirectional unfolder (4), bidirectional partial power converter (2) and pulsating DC-link (3). Essential part of the invention is the method of interfacing, which processes floating voltage of the DC energy storage (1), forms pulsating semi-sine voltage in the DC-link (3) and applies it to the AC-grid (5).

Low operation frequency of the unfolder (4) reduces its switching losses. Limited power of the bidirectional partial power converter (2) reduces its conduction and switching losses. This increases the overall efficiency of the system.

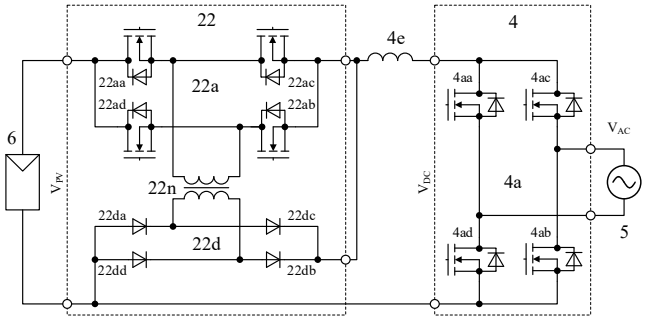

1. zīm.

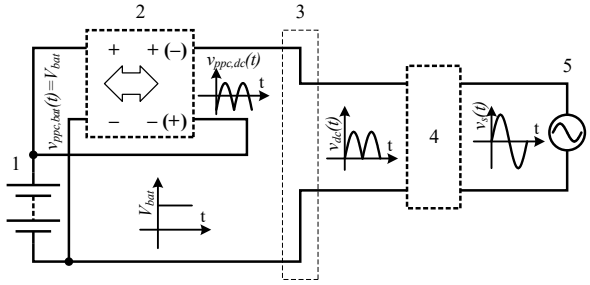

2. zīm.

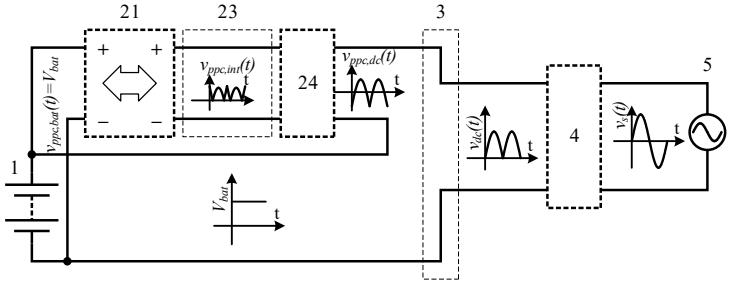

3. zīm.

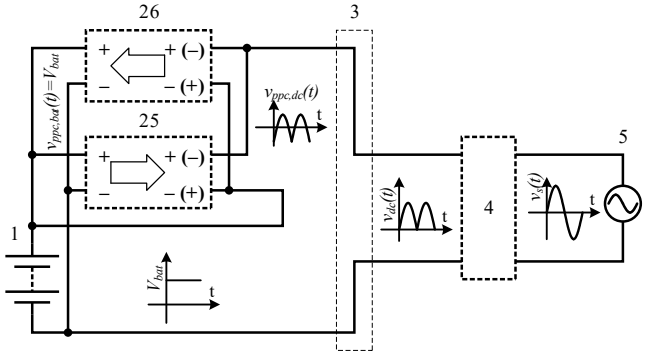

4. zīm.

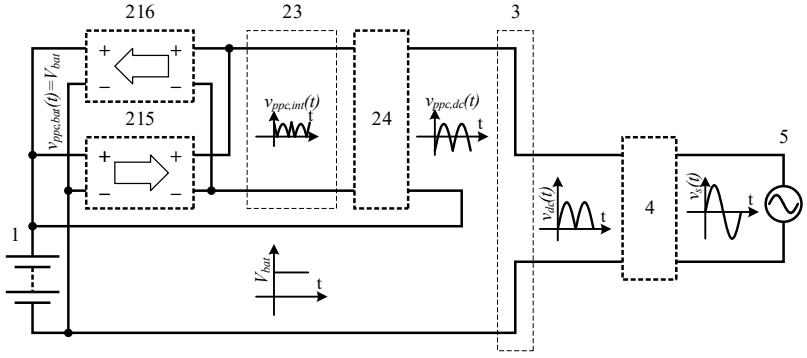

5. zīm.

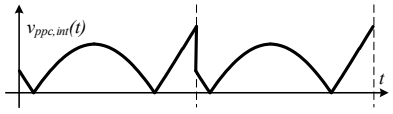

6. zīm.

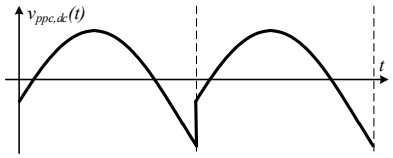

7. zīm.

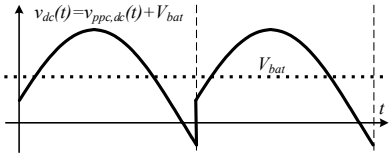

8. zīm.

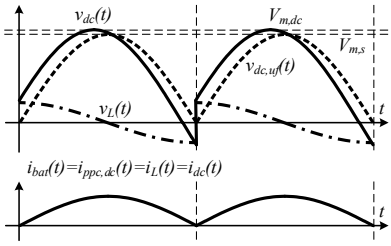

9a. zīm.

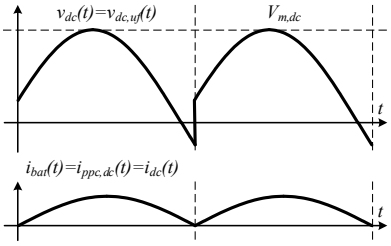

9b. zīm.

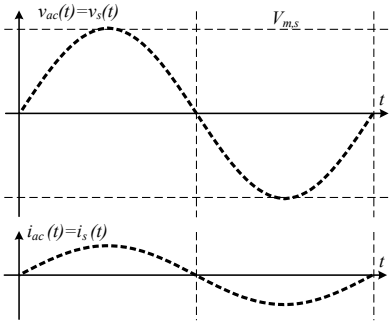

10a. zīm.

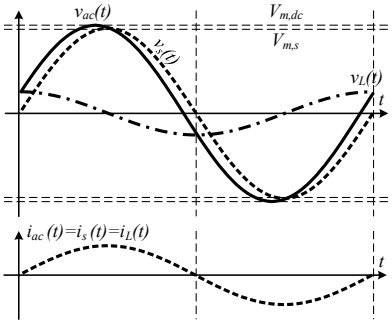

10b. zīm.

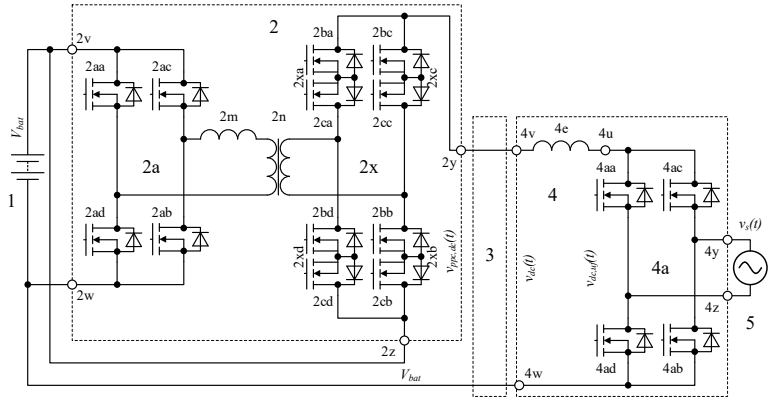
2
2v
2aa
2ac
2ba
2bc
2xa
2xc
2m
2n
2ca
2cc
2a
2x
2y
2ad
2ab
2bd
2bb
2xd
2xb
2cd
2cb
2w
2z
1
V_{bat}
3
$v_{pwr\_ac}(t)$
$v_{dc}(t)$
$v_{dc\_diff}(t)$
4v
4e
4u
4
4aa
4ac
4y
4a
4z
4ad
4ab
4w
$v_s(t)$
5

11. zīm.

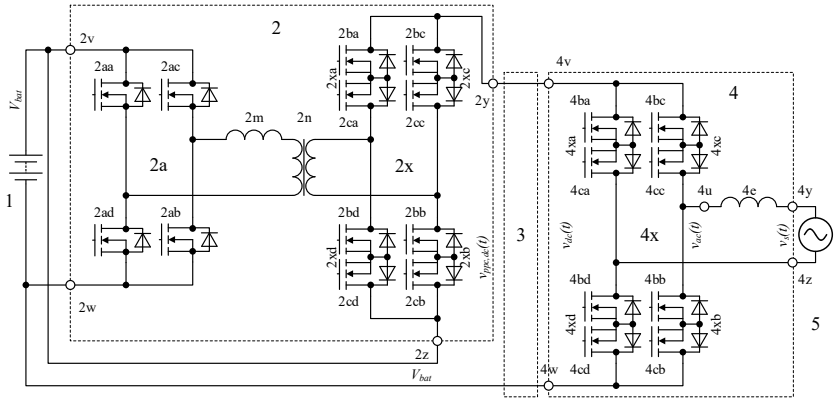
2
2v
2aa
2ac
2ba
2bc
2xa
2xc
2m
2n
2ca
2cc
2a
2x
2y
2ad
2ab
2bd
2bb
2xd
2xb
2cd
2cb
2w
2z
1
V_{bat}
3
$v_{pwr\_ac}(t)$
$v_{dc}(t)$
4v
4
4ba
4bc
4xa
4xc
4ca
4cc
4u
4e
4y
4x
$v_{ac}(t)$
$v_s(t)$
4bd
4bb
4xd
4xb
4z
4w
4cd
4cb
5

12. zīm.

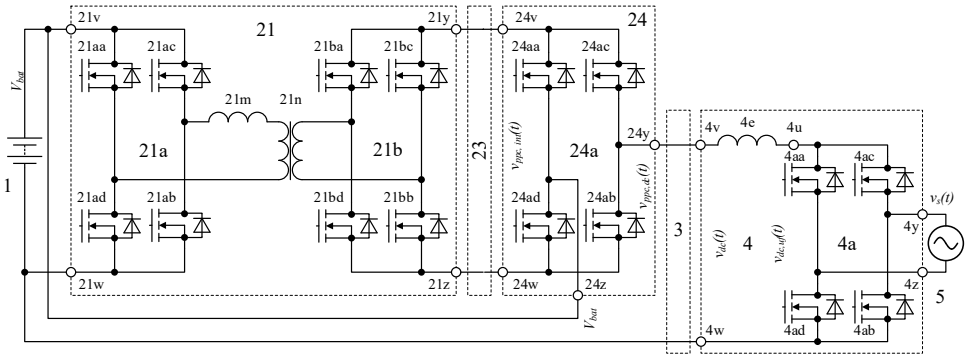
21v
21y
21
24v
24
21aa
21ac
21ba
21bc
24aa
24ac
21m
21n
21a
21b
23
24a
24y
4v
4e
4u
4aa
4ac
21ad
21ab
21bd
21bb
24ad
24ab
3
4
4a
4y
4z
5
21w
21z
24w
24z
4w
4ad
4ab
1

13. zīm.

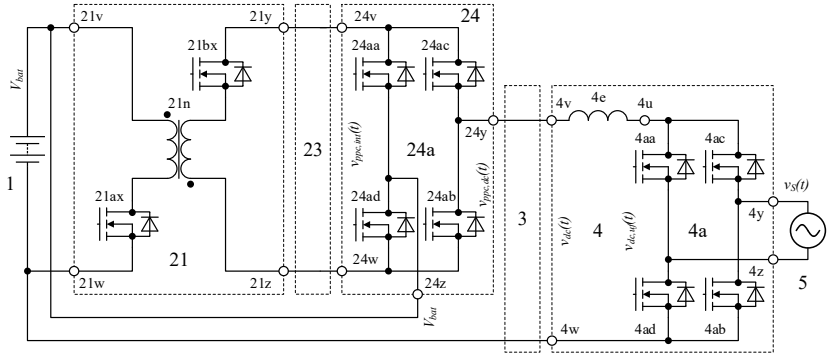
21v
21y
24v
24
21bx
24aa
24ac
21n
23
24a
24y
4v
4e
4u
4aa
4ac
21ax
24ad
24ab
3
4
4a
4y
4z
5
21
21w
21z
24w
24z
4w
4ad
4ab
1

14. zīm.

Patents XIII

O. Tetervenoks, I. Galkins, **A. Bubovičs**, REGULĒJAMA LED GAISMEKĻA INDUKTĪVA ELEMENTA VAIRĀKU IZEJU DRAIVERIS. Latvijas patenta pieteikums Nr. LVP2023000103. Patenta pieteikuma datums 27.10.2023.

REGULĒJAMA LED GAISMEKĻA INDUKTĪVA ELEMENTA VAIRĀKU IZEJU DRAIVERIS

[001] Izgudrojums attiecas uz elektrotehnikas, elektronikas, informācijas un komunikāciju tehnoloģijas nozari un tās energoelektronikas apakšnozari, konkrēti uz regulējamiem stabilizētas strāvas pārveidotājiem, kuri paredzēti darbībai ar strāvas patērētājiem. Izgudrojums var tikt izmantots gaismas diožu (no angļu valodas *light-emitting diode* – LED) segmentēta gaismas avota atsevišķu zaru neatkarīgai laidenai gaismas plūsmas regulēšanai, LED gaismas avotu gaismas toņa/krāsas regulēšanai.

Zināmais tehnikas līmenis

[002] Ir zināms, ka tādus strāvas patērētājus kā gaismas diodes, ar sprieguma avotu savieno caur salāgojošo pasīvo elementu vai specializēto elektriskās enerģijas komutējamo pārveidotāju.
[003] Kā pasīvo salāgojošo elementu starp strāvas patērētāju un sprieguma avotu līdzsprieguma gadījumā izmanto rezistīvo elementu, maiņsprieguma gadījumā – kapacitīvo vai induktīvo. Pasīvo salāgojošo elementu izmantošanai ir šādi trūkumi: papildus zudumi rezistīvajā elementā; pievadītas enerģijas pulsācijas, ja ir izmantots induktīvais vai kapacitatīvais elements; strāvas nobīdes attiecībā pret spriegumu.
[004] Lai novērstu augstāk aprakstītos trūkumus vai mazinātu to sekas, energoelektronikā par salāgojošo elementu starp sprieguma avotu un strāvas patērētāju izmanto augstfrekvences komutējamo pārveidotāju ar noslēgtu vadības kontūru. Piemēram, augstfrekvences komutējamais pārveidotājs ar noslēgtu vadības kontūru izmantots virknē slēgto gaismas diožu no (1.16) līdz (1.17) salāgošanai ar sprieguma avotu (1.0) (1. zīm.), tad to sauc par LED draiveri. Augstfrekvences komutējamajam pārveidotājam ar noslēgtu vadības kontūru stabilizētu strāvu formē induktīvā elementā – droselē (1.6). Atgriezenisko saiti pēc strāvas veido cilpa no strāvas sensora (1.5), kas mēra faktisko droselē (1.6) plūstošu strāvu *I_L1*, summējoša elementa (1.8), kas aprēķina kļūdu starp droselē (1.6) uzdoto strāvas vērtību *I_set* un faktisko strāvu *I_L1*, SSA (1) vadības bloka (1.4), kurš ietver regulatoru un impulsu platuma modulētāju (IPM). Atbilstoši saņemtajam kļūdas signālam no summējošā elementa (1.8), SSA vadības bloks (1.4) formē vadības signālu tranzistoram (1.1). Šādi augstfrekvences komutējamajam pārveidotājam

ar noslēgtu vadības kontūru pēc strāvas (1.1, 1.4, 1.8, 1.5, 1.6) izejā panak stabilizētas strāvas avota SSA (1) uzvedību. Ir zināms, ka strāvas avots teorētiski spej ģenerēt bezgalīgi lielu spriegumu, tāpēc augstfrekvences komutējamajam pārveidotājam ar noslēgtu vadības kontūru pēc strāvas izmanto izejas sprieguma ierobežotāju. Tas veidots no komparatora (1.14), kas spriegumu no dalītāja (1.10) salīdzina ar uzdoto izejas sprieguma ierobežošanas vērtību *Vref* (1.15). Komparators (1.14) padod signālu atslēgšanas blokam (1.7), ja dalītāja (1.10) spriegums pārsniedz augstfrekvences komutējamā pārveidotāja ar noslēgtu vadības kontūru pēc strāvas uzdoto izejas sprieguma ierobežošanas vērtību *Vref* (1.15), tā pasargājot pārveidotāja izejas kondensatoru (1.11) no bojāšanas ar augstu spriegumu. Tad pārveidotājam slēdzamo gaismas diožu skaits ir ierobežots: kopējais sprieguma kritums *V_LED* uz visām virknē slēgtām gaismas diodēm no (1.16) līdz (1.17) nedrīkst pārsniegt pārveidotāja izejas sprieguma ierobežošanas vērtību.

[005] Ir zināms LED gaismeklis ar segmentētu LED gaismas avotu SLGA (4), kurā katram segmentam atbilst savs virknē slēgto gaismas diožu zars, un katrs zars ir atsevišķs strāvas patērētājs. Katram zaram vispārīgā gadījumā ir atšķirīgas pēc krāsas/toņa gaismas diodes. Katram gaismas diožu zaram izmanto atsevišķu ar sprieguma avotu salāgojošu elementu –LED draiveri, kas veidots uz augstāk aprakstīta augstfrekvences komutējamā pārveidotāja ar noslēgtu vadības kontūru pēc strāvas bāzes, katram nepieciešama vismaz viena sava specializēta vadības integrēta mikroshēma, kas ietver visus shēmas vadības elementus (1.4), (1.7), (1.8), (1.14). Katram LED draiverim uzdod savu noregulētu strāvas vērtību *I_set*, tā panāk savstarpēji neatkarīgu laidenu strāvas regulēšanu atsevišķos zaros, bet ar strāvas vērtību attiecības maiņu atsevišķos zaros panāk segmentētā LED gaismas avota SLGA (4) rezultējošās gaismas krāsas/ toņa iestatīšanu. Jo lielāks segmentētā LED gaismas avota SLGA (4) zaru skaits, jo lielāks salāgojošo elementu skaits, līdz ar to sarežģītāka uzbūve un izmaksas.

[006] Par izgudrojuma prototipu izvelēts cita veida augstfrekvences komutējamais pārveidotājs (LED draiveris) segmentēta LED gaismas avota SLGA (4) salāgošanai ar sprieguma avotu (1.0) vai (1.0.0) un savstarpēji neatkarīgu laidenu strāvas regulēšanu atsevišķos zaros [1] – stabilizētās strāvas avota SSA (1) viena induktīva elementa (1.6) vairāku strāvas regulatoru SR (2)/ vairāku regulējamo izeju (no *I_LER_SR1* līdz *I_LED_SRk*) pārveidotājs, kas parādīts 2. zīmējumā. Vispārīgā gadījumā šo prototipa LED draiveri apskata kā salikumu no stabilizētās strāvas avota SSA (1) un vismaz viena strāvas regulatora SR (2) [2–9]. Stabilizētās

strāvas avota SSA (1) viena induktīvā elementa vairāku strāvas regulatoru SR (2) pārveidotāja galvenā īpašība ir tā, ka ievieš tikai vienu noslēgto vadības kontūru pēc strāvas vienam induktīvajam elementam (1.6), kas ir stabilizētās strāvas avota SSA (1) sastāvdaļa. Strāvas regulēšana pārveidotāja atsevišķās izejās (no *I_LER_SR1* līdz *I_LED_SRk*) notiek ar strāvas regulatoriem SR (2) bez noslēgtajiem vadības kontūriem, mainot vadības parametru – aizpildījuma koeficientu (D_Q21, D_Q2k) ar vadāmiem slēdžiem (2.1). Izejas strāvas vērtība strāvas regulatoriem SR (2) ir apgriezti proporcionāla slēdžu (2.1) vadības signālu aizpildījuma koeficientiem.

[007] Stabilizētās strāvas avots SSA (1) ar noslēgtu vadības kontūru pēc strāvas (1.1, 1.4, 1.8, 1.5, 1.6) un tā salikums ar virknē slēgtajiem regulatoriem ir vienāds ar izgudrojuma iekārtu, bet paši regulatori prototipam (2) un izgudrojumam (2.0) ir atšķirīgi.

[008] Prototipa galvenais trūkums ir lieli zudumi strāvas regulatoru (2) diodēs (2.3) pie lielām izejas strāvām, jo īpaši ar izejām pieslēgtu mazu LED skaitu. Kad izejām pieslēdz pa vienai LED, ar diodi (2.3) saistītie zudumi teorētiski neļauj pārveidotājam sasniegt lietderības koeficientu augstāku par 80 %, neņemot vērā zudumus pārējos elementos. Reāla pārveidotāja lietderības koeficients ir vēl zemāks. Ar lielāku LED skaitu lietderība ir augstāka, tomēr to iespējams būtiski uzlabot, izslēdzot strāvas regulatoru (2) diožu (2.3) zudumus, kā parādīts 3. zīmējumā. Otrs būtisks prototipa trūkums ieviešanai reālajā apgaismojuma ierīcē ir tas, ka ir nepieciešams vēl viens atsevišķs līdzsprieguma pazeminošais pārveidotājs LPP (7) prototipa vadības shēmas VSB (5) barošanas sprieguma nodrošināšanai, kas prototipā nav atrunāts, bet ir pats par sevi saprotams (2. zīmējums). Šo problēmu izgudrojumā atrisina ar neregulējama gaismas diožu zara NGDZ (4.1) ieviešanu segmentētam LED gaismas avotam SLGA (4).

Izgudrojuma mērķis un būtība

Tehniskais uzdevums, kuru risina piedāvātais izgudrojums, ir LED gaismekļa gaismas toņa/krāsas regulēšanas sistēmas ieviešanas vienkāršošana, paātrināšana un izmaksu samazināšana, pēc iespējas izmanojot esošo elementu bāzi. Izgudrojuma mērķis ir sasniegts ar jaunu pie segmentētā LED gaismas avota SLGA (4) slēdzamu viena induktīva elementa vairāku izeju LED draiveri ar izeju neatkarīgu regulēšanu, kurā savstarpēji apvienoti stabilizētās strāvas avots SSA (1) ar vairākiem gaismas plūsmas regulatoriem GR (2.0) un vadības sistēmas bloks VSB (5), kā arī segmentētajam LED gaismas avotam SLGA (4) obligāti iekļautu neregulējamo

gaismas diožu zaru NGDZ (4.1), kas nodrošina vadības sistēmas bloku VSB (5) ar barošanas spriegumiem *3V3* un *12V0* bez papildus sprieguma pazeminoša pārveidotāja (7), kā parādīts 6. zīmējumā. Potenciālais izgudrojuma pielietojums ir regulējamā toņa/krāsas LED gaismekļi dažādās pielietojuma jomās, tādās kā dekoratīvs ēku/ielu/iekštelpu apgaismojums, specializēts apgaismojums medicīnas pielietojumiem, dārzkopības apgaismojums, gaismekļi, kuros nepieciešama neatkarīga regulēšana segmentētā LED gaismas avota SLGA (4) atsevišķos zaros, lai iegūtu nepieciešamo gaismas toni/ krāsu.

Izgudrojuma viena induktīvā elementa vairāku izeju LED draivera iekārtas blokshēma un tās pielietojums gaismeklī, slēdzot pie segmentētā LED gaismas avota SLGA (4), ir attēloti 6. zīmējumā. Izgudrojums atšķiras no prototipa (2. zīmejums) ar to, ka draiveris ir izveidots, apvienojot prototipa stabilizētas strāvas avotu SSA (1) un gaismas plsmas regulatorus GR1 – GRk (2.0) prototipa strāvas regulatoru SR1 - SRk (2) vietā. Papildus izgudrojumā segmentētajam LED gaismas avotam SLGA (4) ievieš neregulējamo LED zaru NLGZ (4.1), lai nodrošinātu barošanas spriegumu vadības sistēmas blokam VBS (5) bez papildus līdzsprieguma pazeminošā pārveidotāja (7), kas ir nepieciesams prototipam. Izgudrojuma gaismas plūsmas regulators GR1 –GRk (2.0) veidots kā strāvas regulatora SR1 –SRk (2) salikums ar strāvas slēdžiem SS11 – SSkn (3) ar atzarojumiem SLGA (4) atsevišķu zaru pieslēgšanai. Tas ļauj izveidot vadības algoritmu, ka attēlots 5. zīmējumā, kas regulēšanas diapazona atsevišķās daļās izslēdz diodes (2.3) no strāvas plūšanas ceļa, tādējādi uzlabojot regulatora lietderību raksturlīknes lielāku izejas jaudu daļā. Prototipa strāvas regulatora SR1 – SRk (1) un izgudrojuma gaismas plūsmas regulatoru GR1 – GRk (2.0) teorētiskais lietderības salīdzinājums visā regulēšanas diapazonā ar četrām izejai pieslēgtām gaismas diodēm un 2A maksimālo izejas strāvu ir dots 3. zīmējumā.

Regulējamā LED gaismekļa viena induktīvā elementa vairāku izeju draivera iekārtas ieviešanas paņēmienā apskata gaismas plūsmas regulatora GR1 – GRk (4) tranzistoru Q21 – Q2k (2.1) skaita optimizēšanu, izvēloties bināri svērtu LED skaitu atsevišķos strāvas slēdžu (3) zaros, kā parādīts 4. zīmejumā. Veicot strāvas slēdžu numerāciju pēc principa SSxy, kur x ir srāvas regulatoru un gaismas plūsmas regulatoru numurēšanas indekss un tas sakās ar *1*, bet y ir strāvas slēdža numurēšanas indekss un tas sakās ar 0, un SLGA (4) gaismas diožu numerāciju strāvas slēžu zaros veic pēc principa LED_SSxyz, kur z ir LED numurēšanas indekss, bināri svērto LED skaita principu apraksta pēc izteiksmes $m_{xy} = 2^y$, kur m ir diožu skaits SSxy zarā un,

vienlaicīgi, arī pēdejas SLGA (4) strāvas slēdža gaismas diodes (4.0.6) numurēšanas indekss LED_SSxym, jeb LED_SSxy(y^2)

[009] Izgudrojums paskaidrots ar šādiem zīmējumiem:

1. zīm. Neregulējama LED gaismekļa tipveida draiveris, kas veidots uz pazeminoša augstfrekvences komutējamā pārveidotāja bāzes ar noslēgtu vadības kontūru nesegmentētā LED gaismas avota darbināšanai – tipveida LED draiveris: maiņsprieguma avots MSA (0), līdzsprieguma avots LSA (1.0), maiņsprieguma uz līdzspriegumu pārveidotājs MLP (1.0.1), tipveida LED draiveris TLD (1.0.0), tranzistors Q1 (1.1), ieejas kondensators Cin (1.2), diode VD1 (1.3), SSA vadības bloks U11 (1.4), strāvas sensors I_CS (1.5), drosele L1 (1.6), atslēgšanas bloks AB (1.7), summejošais elements SUM (1.8), uzdota stabilizētas strāvas vērtība *Iset* (1.9), sprieguma dalītājs SD (1.10), izejas kondensators C_LED (1.11), sprieguma dalītāja augšējais rezistors(1.12), sprieguma dalītāja apakšējais rezistors (1.13), komparators U12 (1.14), uzdota izejas sprieguma ierobežošanas vērtība *Vref* (1.15), LED gaismas avots (4.0), LED gaismas avota zara pirmā gaismas diode LED1 (4.0.1), LED gaismas avota zara pēdējā gaismas diode LEDm (4.0.2), stabilizētās strāvas avota ieejas spriegums *Vin*, impulsu platuma modulētājs IPM, droselē L1 plūstošas strāvas vērtība *I_L1*, gaismas diožu strāva *I_LED* un sprieguma kritums uz visām gaismas diodēm *V_LED*.

2. zīm. Regulējama LED gaismekļa vairāku izeju draiveris, kas veidots kā stabilizetās strāvas avota un strāvas regulatoru salikums segmentētā LED gaismas avota darbināšanai – prototips: līdzsprieguma avots LSA (1.0), stabilizētas strāvas avots SSA (1), tranzistors Q1 (1.1), diode VD1 (1.3), drosele L1 (1.6), strāvas regulators SR (2), strāvas regulatora tranzistors Q21, Q2k (2.1), strāvas regulatora izejas kondensators C21, C2k (2.2), strāvas regulatora diode VD21, VD2k (2.3), segmentēts LED gaismas avots SLGA (4), segmentēta LED gaismas avota strāvas regulatora zara pirmā gaismas diode (4.0.3), segmentētā LED gaismas avota strāvas regulatora zara pēdējā gaismas diode (4.0.4), vadības sistēmas bloks VSB (5), mikrokontrolleris MCU (5.1), kondensators mikrokontrollera barošanai *3V3* (5.2), kondensators tranzistoru draiveru barošanai *12V0* (5.3), pirmā strāvas regulatora tranzistora draiveris (5.21), pēdējā strāvas regulatora tranzistora draiveris (5.2k), līdzsprieguma pazeminošais pārveidotājs LPP vadības sistēmas bloka barošanai (7), stabilizētās strāvas avota ieejas spriegums *Vin*, droselē L1 plūstošās strāvas vērtība *I_L1*, gaismas diožu strāva segmentētā LED gaismas avota pirmajā

zarā *I_LED_SR1* un pēdējā zarā *I_LED_SRk*, vadības signāli tranzistoru draiveriem IMP_Q21 – IMP_Q2k, vadības signāli tranzistoru aizvariem D_Q21 – D_Q2k.

3. zīm. Teorētiskais lietderības salīdzinājums prototipa strāvas regulatoram SR ar izgudrojuma gaismas plūsmas regulatoru GR pilnā izejas jaudas diapazonā. Piemērs ar četrām gaismas diodēm zarā.

4. zīm. Regulējama LED gaismekļa vienas izejas draiveris, kas veidots kā stabilizetās strāvas avota un viena gaismas regulatora salikums segmentētā LED gaismas avota ar bināri svērtu LED skaitu zaros darbināšanai – izgudrojuma realizēšanas piemērs: maiņsprieguma avots MSA (0), līdzsprieguma avots LSA (1.0), maiņsprieguma uz līdzspriegumu pārveidotājs MLP (1.0.1), stabilizētās strāvas avots SSA (1), tranzistors Q1 (1.1), diode VD1 (1.3), SSA vadības bloks U11 (1.4), drosele L1 (1.6), summējošais elements SUM (1.8), uzdota stabilizētās strāvas vērtība *Iset* (1.9), gaismas plūsmas regulators GR1 (2.0), strāvas regulators SR1 (2), strāvas regulatora tranzistors Q21 (2.1), strāvas regulatora izejas kondensators C21 (2.2), strāvas regulatora diode VD21 (2.3), strāvas slēdzis SS10, SS11, SS12, SS1n (3), strāvas slēdža tranzistors Q310, Q311, Q312, Q31n (3.1), segmentētais LED gaismas avots SLGA (4), segmentētā LED gaismas avota strāvas regulatora zara pirmā gaismas diode (4.0.3), segmentētā LED gaismas avota gaismas plūsmas regulatora zara pirmā gaismas diode (4.0.5), segmentētā LED gaismas avota gaismas plūsmas regulatora zara pēdējā gaismas diode (4.0.6), stabilizētās strāvas avota ieejas spriegums *Vin*, impulsu platuma modulētājs IPM, droselē L1 plūstošās strāvas vērtība *I_L1*, gaismas diožu strāva segmentētā LED gaismas avota zarā, kas pieslēgts strāvas regulatoram *I_LED_SR1,* gaismas diožu strāva segmentētā LED gaismas avota zarā, kas pieslēgts strāvas slēdzim *I_LED_SS10*, *I_LED_SS11*, *I_LED_SS12*, *I_LED_SS1n*, vadības signāls strāvas regulatora tranzistoram D_Q21, vadības signāls strāvas slēdža tranzistora aizvariem D_Q310, D_Q311, D_Q312, D_Q31n.

5. zīm. Spēka slēdžu vadības signālu diagramma laidenai kopējā gaismas daudzuma regulēšanai gaismas plūsmas regulatoram, kas parādīts 4. zīmējuma, un kas paredzēts segmentētā LED gaismas avota ar bināri svērtu LED skaitu zaros darbināšanai: strāvas regulatora SR1 tranzistora vadības signāls aizpildījuma koeficients D_Q21, strāvas slēdžu SS10, SS11, SS12, SS1n tranzistoru vadības signālu aizpildījuma koeficienti D_Q310, D_Q311, D_Q312, D_Q31n.

6. zīm. Regulējama LED gaismekļa vairāku izeju draiveris, kas veidots kā stabilizetās strāvas avota un vairāku gaismas plūsmas regulatoru salikums segmentētā LED gaismas avota SLGA

darbināšanai, un SLGA papildināts ar neregulējamo LED zaru vadības sistēmas bloka barošanas nodrošināšanai – izgudrojuma papildinātais realizēšanas piemērs: maiņsprieguma avots MSA (0), līdzsprieguma avots LSA (1.0), maiņsprieguma uz līdzspriegumu pārveidotājs MLP (1.0.1), stabilizētās strāvas avots SSA (1), tranzistors Q1 (1.1), diode VD1 (1.3), SSA vadības bloks U11 (1.4), drosele L1 (1.6), summējošais elements SUM (1.8), uzdota stabilizētās strāvas vērtība *Iset* (1.9), gaismas plūsmas regulators GR1, GR2, GRk (2.0), strāvas regulators SR1, SR2, SRk (2), strāvas regulatora tranzistors Q21 (2.1), strāvas regulatora izejas kondensators C21 (2.2), strāvas regulatora diode VD21 (2.3), strāvas slēdzis SS11, SS1n, SS21, SS2n, SSk1, SSkn (3), strāvas slēdža tranzistors Q311, Q31n (3.1), segmentēts LED gaismas avots SLGA (4), segmentēta LED gaismas avota strāvas regulatora zara pirmā gaismas diode (4.0.3), segmentētā LED gaismas avota gaismas plūsmas regulatora zara pirmā gaismas diode (4.0.5), segmentētā LED gaismas avota gaismas plūsmas regulatora zara pēdējā gaismas diode (4.0.6), segmentētā LED gaismas avota neregulējamais gaismas diožu zars NGDZ (4.1), neregulējamā gaismas diožu zara atsevišķas gaismas diodes (4.1.0 – 4.1.3), vadības sistēmas bloks VSB (5), mikrokontrolleris MCU (5.1), kondensators mikrokontrollera barošanai *3V3* (5.2), kondensators tranzistoru draiveru barošanai *12V0* (5.3), strāvas regulatoru tranzistoru draiveri (5.21 – 5.2k), strāvas slēdžu tranzistoru draiveri (5.311- 5.3kn), stabilizētās strāvas avota ieejas spriegums *Vin*, impulsu platuma modulētājs IPM, droselē L1 plūstošas strāvas vērtība *I_L1*, gaismas diožu strāva segmentētā LED gaismas avota zarā, kas pieslēgts strāvas regulatoram *I_LED_SR1,* gaismas diožu strāva segmentētā LED gaismas avota zarā, kas pieslēgts strāvas slēdzim *I_LED_SS11*, *I_LED_SS1n*, vadības signāli strāvas regulatora tranzistoru draiveriem IMP_Q21 – IMP_Q2k, vadības signāli strāvas slēdžu tranzistoru draiveriem IMP_Q311 – IMP_Q3kn vadības signāls strāvas regulatora tranzistora aizvariem D_Q21 – D_Q2k, vadības signāls strāvas slēdža tranzistora aizvariem D_Q311, – D_Q3kn.

Izgudrojuma īstenošanas piemēri

[010] Izgudrojuma realizācijai neregulējama gaismekļa tipveida LED draiveri TLD (1.0.0), kas attēlots 1. zīmējumā, pārveido tā, lai iegūtu stabilizētās strāvas avota SSA (1) īpašības: noņem izejas kondensatoru C_LED (1.11) un noņem izejas sprieguma ierobežotāju (1.10), (1.14), (1.7) vai pamaina sprieguma dalītāja SD (1.10) rezistoru R1 (1.12) un R2 (1.13) attiecību tā, lai izejas sprieguma ierobežošanas vērtība ir lielāka par kopējo sprieguma kritumu uz

slēdzama segmentētā LED gaismas avota (4) visām gaismas diodēm. Pārveidotu TLD (1.0.0) par stabilizētās strāvas avotu SSA (1) saslēdz virknē ar vienu (4. zīmējums) vai vairākiem (6. zīmējums) gaismas plūsmas regulatoriem GR (2.0), un pieliek vadības sistēmas bloku VSB (5), tādejādi iegūst izgudroto regulejamā LED gaismekļa viena vai vairāku izeju draiveri segmentētam LED gaismas avotam SLGA (4).

[011] Katrs gaismas plūsmas regulators GR1 (2.0) ir veidots kā strāvas regulatora SR1 (2) un strāvas slēdžu SS10 – SS1n (3) salikums un nodrošina viena atsevišķa toņa/krāsas LED gaismas plūsmas laidenu regulēšanu. Šāds salikums nodrošina labāku lietderību lielāku izejas jaudu diapazonā salīdzinājumā ar prototipu no 2. zīmējuma: lietderību salīdzinājums gaismas plūsmas regulatoram (2.0) un strāvas regulatoram (2), darbinot vienādu LED skaitu – 4 gaismas diodes ar 2A maksimālo strāvu, ir attēlots 3. zīmējumā.

[012] Gaismas plūsmas regulatora GR1 – GRk (4) tranzistoru Q21 – Q2k (2.1) skaita optimizēšanai, izvēlas bināri svērto LED skaitu atsevišķos strāvas slēdžu (3) zaros, kā parādīts 4. zīmejumā, bet tas nav obligāts nosacījums. Veicot strāvas sledžu numerāciju pēc principa SSxy, kur x ir srāvas regulatoru un gaismas plūsmas regulatoru numurēšanas indekss un tas sakās ar *1*, bet y ir strāvas slēdža numurēšanas indekss un tas sakās ar 0, un SLGA (4) gaismas diožu numerāciju strāvas slēžu zaros veic pēc principa LED_SSxyz, kur z ir LED numurēšanas indekss, bināri svērto LED skaita principu apraksta pēc izteiksmes $m_{xy} = 2^y$, kur m ir diožu skaits SSxy zarā un, vienlaicīgi, arī pēdejas SLGA (4) strāvas slēdža gaismas diodes (4.0.6) numurēšanas indekss LED_SSxym, jeb LED_SSxy(y^2).

[013] Gaismas plūsmas regulatora GR1 (2.0) laidenu gaismas plūsmas regulēšanu nodrošina vadības sistēmas algoritms, kas darbina strāvas regulatoru (2) tranzistorus (2.1) un strāvas slēdžu (3) tranzistorus (3.1) pēc principa, kas attēlots 5. zīmējumā. Šeit gaismas plūsmas regulatoram GR1 (2.0) pieslēgts segmentētais LED gaismas avots SLGA (4) ar bināri svērto LED skaitu strāvas slēdžu zaros (4.0.5, 4.0.6). Kopējais relatīvais LED gaismas daudzums ir proporcionāls uzdotam vadības parametram (augšējā grafika taisne no 5. zīmējuma), arī vadības signāli uz strāvas regulatora (2) tranzistora Q21 (2.1) un strāvas slēdžu (3) tranzistoriem (3.1) Q310…Q31n formējas atbilstoši uzdotā parametra vērtībai. Strāvas regulatora (2) tranzistors Q21 (2.1) vadīts ar signālu D_Q21, kura aizpildījuma koeficients mainās robežās no 0 līdz 100 %, strāvas slēdžu (3) tranzistoriem (3.1) Q310…Q31n vadības signālu D_Q310...DQ31n aizpildījuma koeficients ir tikai 0 % vai 100 % (ieslēgts vai izslēgts). Tranzistoru vadības

signālus IPM_Q21 – IPM_Q2k, IPM_Q311 – IPM_Q3kn padod vadības sistēmas bloka VBS (5) mikrokontrolleris (5.1) caur tranzistoru aizvaru draiveriem (5.21 – 5.2k, 5.311 – 5.3kn).

[014] Segmentētā LED gaismas avota SLGA (4) zaru skaits un struktūra ir saskaņoti ar draivera izeju skaitu un struktūru, kā attēlots 4. un 6. zīmējumos. Maksimāli vienmērīga apgaismotas virsmas toņa/krāsas iegūsanai, SLGA (4) atsevišķu gaismas plūsmas regulatoru (2.0) zaru gaismas diodes izvieto pēc iespejas simetriski. Izgudrojumā uzbūves vienkāršošanai un elementu skaita mazināsanai, izmanto SLGA (4) ar neregulējamo gaismas diožu zaru NGDZ (4.1), kas kalpo par barošanas avotu vadības sistēmas bloka VBS (5) atsevišķām daļām: *3V3* spriegums mikrokontrollera (5.1) barošanai un *12V0* spriegums tranzistoru aizvaru draiveru (5.21 – 5.2k, 5.311 – 5.3kn) barošanai, kā attēlots 6. zīmējumā.

[015] SSA (1) vidēja droseles L1 (1.6) strāva ir vienāda ar uzdoto stabilizētās strāvas vērtību *Iset* (1.9), tā nosaka maksimālo strāvas vērtību draivera izejās un SLGA (4) zaros. Vidējā SRx (2) izejas strāvas vērtība *I_LED_SRx* ir atkarīga no tranzistora Q2x (2.1) impulsu platuma modulētā IPM vadības signāla aizpildījuma koeficienta D_Q2x vērtības un SSA (1) uzdotās stabilizētās strāvas vērtības *Iset*, un ir vienāda ar:

$$I\_LED\_SRx = Iset \cdot (1 - D\_Q2x) \text{ [2],}$$

[016] bet vidēja strāvas slēdžu SSxy (3) izejas stāvas *I_LED_SSxy* vērtība ir vienāda ar 0 vai *Iset*, atkarībā no gaismas regulatora GR1 – GRk (2.0) uzdotās vadības parametra vērtības un attiecīgā tranzistora Q3xy (3.1) vadības signāla D_Q3xy, kā parādīts 5. zīmējumā.

[017] Gaismas toņa / krāsas regulēšanu panāk ar atsevišķu gaismas plūsmas regulatoru GR1 – GRk (2.0) uzdoto vadības parametu attiecības maiņu.

Informācijas avoti

1. Z. Dong, C. K. Tse and S. Y. R. Hui, "Current-Source-Mode Single-Inductor Multiple-Output LED Driver With Single Closed-Loop Control Achieving Independent Dimming Function," in IEEE Journal of Emerging and Selected Topics in Power Electronics, vol. 6, no. 3, pp. 1198-1209, Sept. 2018. doi: 10.1109/JESTPE.2018.2831686

2. I. Galkin, O. Tetervjonok and I. Milashevski, "Comparative study of steady-state performance of voltage and current fed dimmable LED drivers," 2013 International Conference-

Workshop Compatibility And Power Electronics, 2013, pp. 292-297, doi: 10.1109/CPE.2013.6601172.

3. I. Galkin, O. Tetervenoks and I. Milashevski, "Static losses and controllability of current fed dimmable LED drivers," 2013 15th European Conference on Power Electronics and Applications (EPE), 2013, pp. 1-10, doi: 10.1109/EPE.2013.6631863.

4 I. Galkin and O. Tetervenoks, "Validation of direct current control in LED lamp with non-inverting buck-boost converter," IECON 2013 - 39th Annual Conference of the IEEE Industrial Electronics Society, 2013, pp. 6021-6026, doi: 10.1109/IECON.2013.6700123.

5 Z. Dong, X. L. Li, C. K. Tse and Z. Zhang, "Application of Current-Source-Mode Converters to Synthesis of Single-Input Dual-Output Regulators with No Cross Regulation," 2020 IEEE 9th International Power Electronics and Motion Control Conference (IPEMC2020-ECCE Asia), Nanjing, China, 2020, pp. 584-587. doi: 10.1109/IPEMC-ECCEAsia48364.2020.9367708

6 Zu, A., Luo, Q., Huang, J., He, Q., Sun, P. and Du, X. (2020), Analysis and design of a multi-channel constant current LED driver based on DC current bus distributed power system structure. IET Power Electronics, 13: 627-635. https://doi.org/10.1049/iet-pel.2019.0203

7 Z. Dong, X. L. Li, C. K. Tse and Z. Zhang, "Derivation of Single-Input Dual-Output Converters With Simple Control and No Cross Regulation," in IEEE Transactions on Power Electronics, vol. 35, no. 11, pp. 11930-11941, Nov. 2020. doi: 10.1109/TPEL.2020.2983618

8 X. L. Li, Z. Dong and C. K. Tse, "Complete Family of Two-Stage Single-Input Multioutput Configurations of Interconnected Power Converters," in IEEE Transactions on Power Electronics, vol. 35, no. 4, pp. 3713-3728, April 2020. doi: 10.1109/TPEL.2019.2936517

9 X. L. Li and C. K. Tse, "Derivation of Complete Family of Multi-Output Configurations Including Voltage-Source-Mode and Current-Source-Mode Converters," 2019 IEEE International Symposium on Circuits and Systems (ISCAS), Sapporo, Japan, 2019, pp. 1-5. doi: 10.1109/ISCAS.2019.8702218

PRETENZIJAS

1. Regulējamā LED gaismekļa viena induktīva elementa vairāku izeju draivera iekārta satur stabilizētās strāvas avotu SSA (1), gaismas plūsmas regulatorus GR1 – GRk (2.0), kuri ietver strāvas regulatorus SR1- SRk (2) un strāvas slēdžus SS11 – SSkn (3), vadības sistēmas bloku VBS (5), un ir slēdzama pie segmentētā LED gaismas avota SLGA (4) ar obligāti iekļauto neregulējamo gaismas diožu zaru NGDZ (4.1), kas atšķiras ar to, ka strāvas regulatori SR1 – SRk (2) ir aizvietoti ar gaismas plūsmas regulatoriem GR1 – GRk (2.0), kas nodrošina regulatora lietderības pieaugumu līdz 4% lielu izejas jaudu diapazonā.

2. Regulējamā LED gaismekļa viena induktīvā elementa vairāku izeju draivera iekārta saskaņā ar 1. pretenziju, kas atšķiras ar to, ka segmentētā LED gaismas avota SLGA (4) obligāti iekļauj neregulējamo gaismas diožu zaru NGDZ (4.1), bet draivera iekārtā neiekļauj līdzsprieguma pazeminoso pārveidotāju LPP (7), kas nepieciešams vadības sistēmas bloka barošanai VBS (5).

3. Paņēmiens, kuru realizē iekārta saskaņā ar 1. vai 2. pretenziju, kas ietver šādus secīgus soļus:

(i) tipveida LED draivera TLD (1.0.0) pārveidošana par stabilizētās strāvas avotu SSA (1) un nostabilizētās strāvas vertības *Iset* iestatīšana atbilstoši maksimālai SLGA (4) gaismas diožu pieļaujamai strāvas vērtībai;

(ii) gaismas plūsmas regulatoru GR1 – GRk (2.0) ieviešana katrai regulējamai izejai/ SLGA (4) LED krāsai;

(iii) strāvas slēdžu SR1 – SRk (3), to tranzistoru Q311 – Q3kn (3.1) un tranzistoru draiveru (5.311 – 5.3kn) skaita optimizēšana, izvēloties bināri svērto LED skaitu SLGA (4) strāvas slēdžu SSxy (3) zaros pēc principa $m_{xy} = 2^y$, kur m ir LED skaits attiecīgajā zarā, tad SSxy zara pēdēja LED indekss ir LED_SSx(n-1)m (4. zīmējumā);

(iv) neregulējamā gaismas diožu zara NGDZ (4.1) ieviešana segmentētā LED gaismas avotā (4) barošanas sprieguma nodrošināšanai;

(v) vadības sistēmas bloka VBS (5) uz mikrokontrollera (5.1) bāzes ar tranzistoru draiveriem (5.21 – 5.3kn) ieviešana, kas spēj nodrošināt gaismas regulatoru (2.0) tanzistoru (2.1, 3.1) vadību atbilstoši algoritmam, kas parādīts 5. zīmējumā.,

KOPSAVILKUMS

Izgudrojums attiecas uz elektrotehnikas, elektronikas, informācijas un komunikāciju tehnoloģijas nozari un tās energoelektronikas apakšnozari, konkrēti uz regulējamiem konstantas strāvas pārveidotājiem priekš konstantas strāvas patērētājiem. Izgudrojumu var izmantot segmentētā LED gaismas avota atsevišķu segmentu neatkarīgai laidenai gaismas plūsmas regulēšanai, LED gaismas avotu gaismas toņa/krāsas regulēšanai.

Izgudrojuma pieteikuma viena induktīvā elementa vairāku izeju LED draiverim ir augsts pielietojuma potenciāls LED gaismekļu gaismas toņa/krāsas regulēšanas sistēmas ieviešanas vienkāršošanai, paātrināšanai un izmaksu samazināšanai, pēc iespējas izmanojot esošo elementu bāzi.

Izgudrojums spēj nodrošināt viena induktīvā elementa un viena stabilizētās strāvas avota SSA vadības bloka elementu izmantošanu visām draivera izejām, uzlabot regulatora lietderību augstu izejas jaudu diapazonā līdz 4% salīdzinājumā ar prototipu, un izslēgt papildus līzsprieguma pazeminoša pārveidotāja izmantošanas nepieciešamību, kas paredzēts draivera vadības sistēmas bloka VBS barošanai.

Adjustable LED Lamp Single Inductor Multiple Output Driver

The invention relates to the field of electrical engineering, electronics, information and communication technologies and its sub-field of power electronics, specifically to adjustable constant current converters for constant current consumers. The invention can be used for independent dimming of separate segments of segmented LED light source, for adjusting the light tone/color of segmented LED light sources.

The application of the invention has a high potential for simplifying, accelerating, and reducing costs in the implementation of LED light source color/tone control systems by using and combining existing components and solutions.

The invention is capable of utilizing a single inductive element and a single constant current source CSA control block element for all driver outputs, improving the regulator's efficiency in a high output power range of up to 4% in comparison with the prototype, and eliminating the need for an additional voltage buck converter for powering the driver control system block CSB.

ATTĒLI

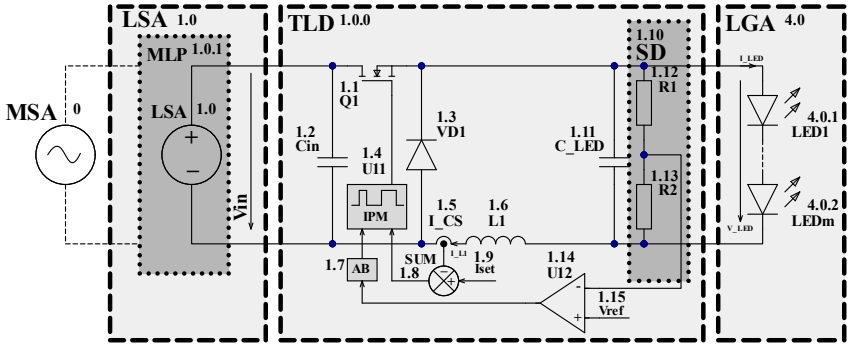

MSA - maiņsprieguma avots
MLP - maiņsprieguma uzlīdzspriegumu pārveidotājs
LSA - līdzsprieguma avots
TLD - tipveida LED draiveris
SD - sprieguma dalītājs
IPM - impulsu platuma modulētājs
SUM - summējošais elements
AB - atslēgšanas bloks
Vin - stabilizētas strāvas avota ieejas spriegums
I_LED - izejas/gaismas diožu vidēja strāva
V_LED - sprieguma kritums uzslodzes: visām izejai pieslēgtam gaismas diodēm
I_L1 - droseles L1 vidēja strāva
LGA - LED gaismas avots

1. zīm.

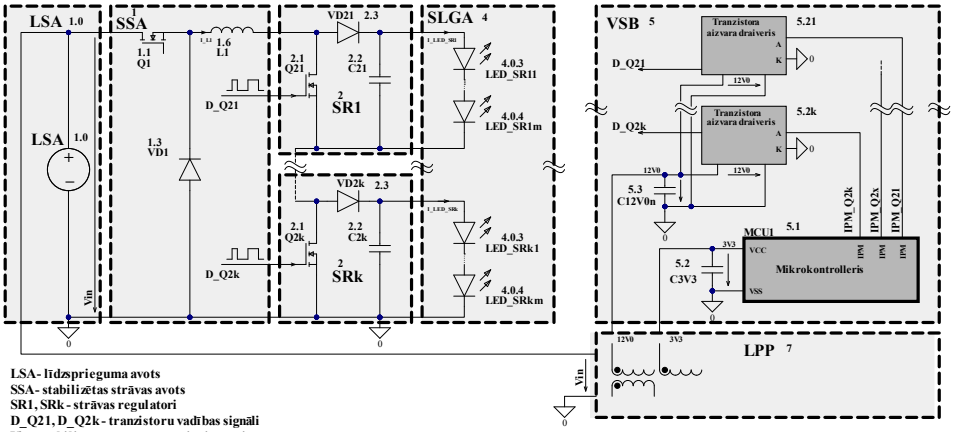

LSA - līdzsprieguma avots
SSA - stabilizētas strāvas avots
SR1, SRk - strāvas regulatori
D_Q21, D_Q2k - tranzistoru vadības signāli
Vin - stabilizētas strāvas avota ieejas spriegums
I_LED_SR1, I_LED_SRk - izeju/gaismas diožu vidēja strāva
I_L1 - droseles L1 vidēja strāva
SLGA - segmentēts LED gaismas avots
LPP - līdzsprieguma pazeminošais pārveidotājs

2. zīm.

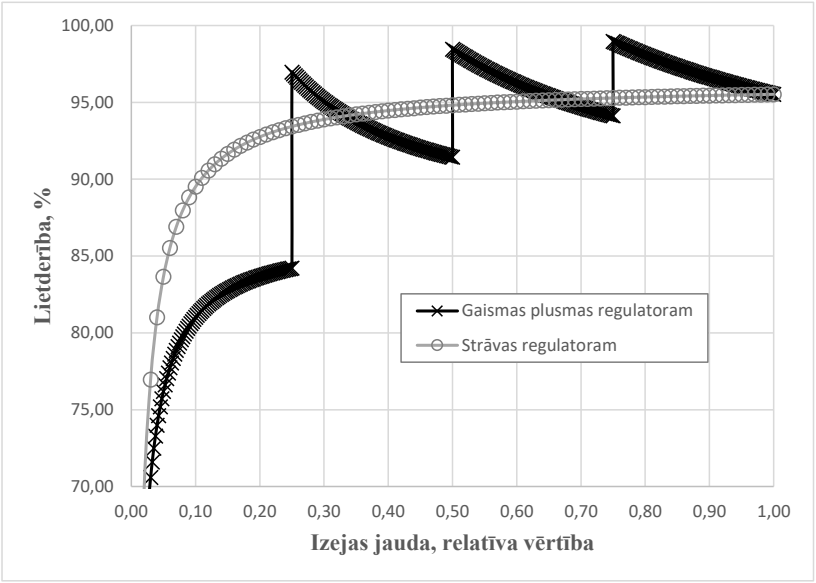
100,00
95,00
90,00
85,00
80,00
75,00
70,00
Lietderība, %
0,00
0,10
0,20
0,30
0,40
0,50
0,60
0,70
0,80
0,90
1,00
Izejas jauda, relatīva vērtība
Gaismas plusmas regulatoram
Strāvas regulatoram

3. zīm.

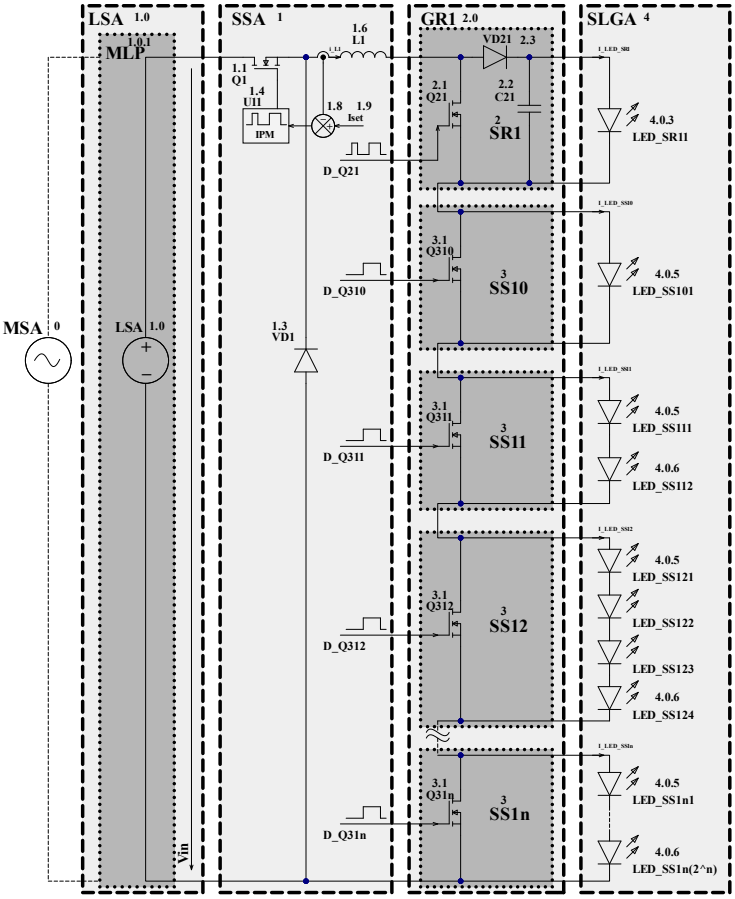

MSA- maiņsprieguma avots
MLP - maiņsprieguma uzlīdzsspriegumu pārveidotājs
LSA- līdzsprieguma avots
SSA- stabilizētas strāvas avots
GR1 - gaismas plūsmas regulators
SR1 - strāvas regulators
SS10, SS11, SS12, SS1n - strāvas slēdži
IPM - impulsu platuma modulētājs
Vin - stabilizētas strāvas avota ieejas spriegums
D_Q21, D_Q310, D_Q311, D_Q312, D_Q31n - tranzistoru vadības signāli
I_LED_SR1 - strāvas regulatora izejas/gaismas diožu vidēja strāva
I_LED_SS0, I_LED_SS1, I_LED_SS2, I_LED_SS1n - strāvas sledžu izeju/gaismas diožu strāva
I_L1 - droseles L1 vidēja strāva
SLGA- segmentēts LED gaismas avots

4. zīm.

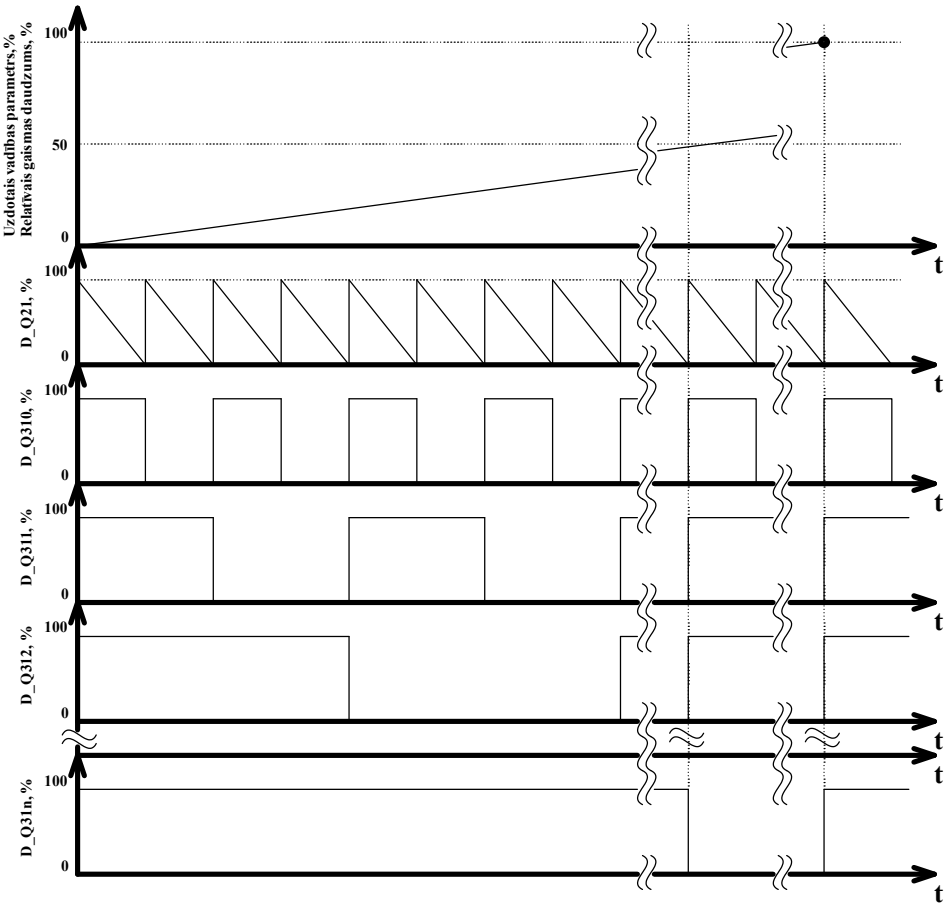

D_Q21- strāvas regulatora SR1 tranzistora vadības signāla aizpildījuma koeficients

D_Q310, D_Q311, D_Q312, D_Q31n - strāvas slēdžu SS10, SS11, SS12, SS1n vadības signāla aizpildījuma koeficienti

5. zīm.

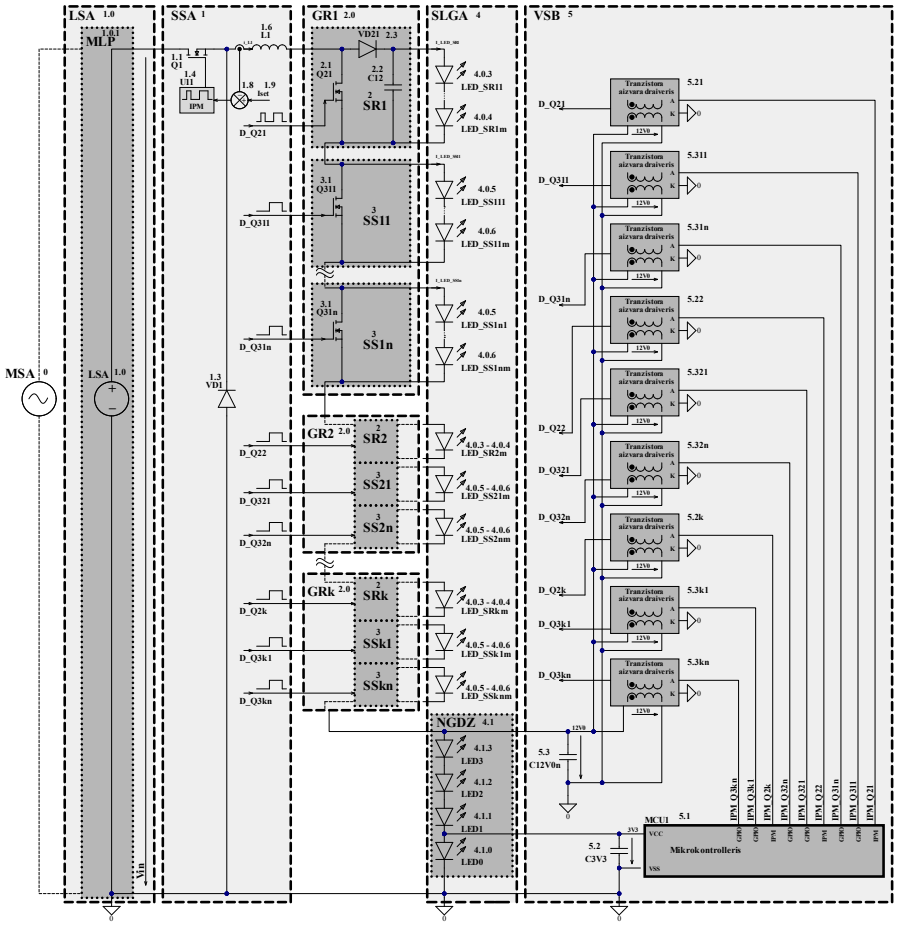

MSA - maiņsprieguma avots
MLP - maiņsprieguma uz līdzspriegumu pārveidotājs
LSA - līdzsprieguma avots
SSA - konstantas strāvas avots

SR1, SR2, SRk - strāvas regulatori
SS11, SS1n, SS21, SS2n, SSk1, SSkn - strāvas slēdži
GR1, GR2, GRk - gaismas regulators
SLGA - segmentēts LED gaismas avots

VSB - vadības sistēmas bloks
NGDZ - neregulējamais gaismas diožu zars
MCU - mikrokontrolleris
Vin - stabilizētas strāvas avota ieejas spriegums

6. zīm.

Aleksandrs Bubovičs was born in 1993 in Riga. He received a Bachelor's degree (2017) and a Master's degree (2018) in Computerised Control of Electrical Technologies from Riga Technical University. Since 2016, he has worked at Riga Technical University, where he is currently a researcher, lecturer and laboratory chief. His research interests include the application of power electronic converters in energy storage systems and medical equipment, as well as thermal management of power electronics.